

INFORMATION TO USERS

This manuscript has been reproduced from the microfilm master. UMI films the text directly from the original or copy submitted. Thus, some thesis and dissertation copies are in typewriter face, while others may be from any type of computer printer.

The quality of this reproduction is dependent upon the quality of the copy submitted. Broken or indistinct print, colored or poor quality illustrations and photographs, print bleedthrough, substandard margins, and improper alignment can adversely affect reproduction.

In the unlikely event that the author did not send UMI a complete manuscript and there are missing pages, these will be noted. Also, if unauthorized copyright material had to be removed, a note will indicate the deletion.

Oversize materials (e.g., maps, drawings, charts) are reproduced by sectioning the original, beginning at the upper left-hand corner and continuing from left to right in equal sections with small overlaps. Each original is also photographed in one exposure and is included in reduced form at the back of the book.

Photographs included in the original manuscript have been reproduced xerographically in this copy. Higher quality 6" x 9" black and white photographic prints are available for any photographs or illustrations appearing in this copy for an additional charge. Contact UMI directly to order.



Bell & Howell Information and Learning
300 North Zeeb Road, Ann Arbor, MI 48106-1346 USA
800-521-0600

**Nonlinear Time-Dependent Analysis of
Externally/Internally
Prestressed Reinforced Concrete Beams**

Bilal M. El-Ariss

A Thesis

in

The Department of Building, Civil, and
Environmental Engineering

Presented in Partial Fulfilment of the Requirements
for the Degree of Doctor of Philosophy at
Concordia University
Montreal, Quebec, Canada

January 1999

© Bilal M. El-Ariss, 1999



National Library
of Canada

Acquisitions and
Bibliographic Services

395 Wellington Street
Ottawa ON K1A 0N4
Canada

Bibliothèque nationale
du Canada

Acquisitions et
services bibliographiques

395, rue Wellington
Ottawa ON K1A 0N4
Canada

Your file Votre référence

Our file Notre référence

The author has granted a non-exclusive licence allowing the National Library of Canada to reproduce, loan, distribute or sell copies of this thesis in microform, paper or electronic formats.

The author retains ownership of the copyright in this thesis. Neither the thesis nor substantial extracts from it may be printed or otherwise reproduced without the author's permission.

L'auteur a accordé une licence non exclusive permettant à la Bibliothèque nationale du Canada de reproduire, prêter, distribuer ou vendre des copies de cette thèse sous la forme de microfiche/film, de reproduction sur papier ou sur format électronique.

L'auteur conserve la propriété du droit d'auteur qui protège cette thèse. Ni la thèse ni des extraits substantiels de celle-ci ne doivent être imprimés ou autrement reproduits sans son autorisation.

0-612-39023-3

ABSTRACT

Nonlinear Time-Dependent Analysis of Externally/Internally Prestressed Reinforced Concrete Beams

Bilal M. El-Ariss, Ph.D.
Concordia University, 1999

A simple procedure for the nonlinear analysis of externally and/or internally prestressed reinforced concrete beams including the time-dependent effects caused by creep and shrinkage of concrete and relaxation of prestressing steel is presented. The procedure is capable of tracing the structural response of these structures through their service load history as well as throughout the elastic, inelastic, and ultimate load ranges.

Sections can change throughout the length of the member and the variation of the material properties within the element is accommodated. The section is divided into concrete parts of different materials and the reinforcement steel is divided into layers of different properties. Each concrete part and steel layer is considered in a uniaxial state of stress.

Time dependent variation of concrete properties is considered. The instantaneous loss in the prestressing force due to friction and anchor setting in posttensioned structures is also recognized. The time domain for which the analysis is required is divided into a number of time intervals. At any instant, the instantaneous changes in stresses and deformations are calculated and added to the existing values. For any time interval, the gradual change in stresses and deformations are determined and added to update the existing values. Also for each time interval, nonlinear equilibrium equations which are valid for the current

material properties are set up and solved using the displacement method. An initial stiffness method combined with the unbalanced load iterations for each load increment or time interval is used for the nonlinear equilibrium.

A series of numerical examples are tested and comparisons are made with other analytical and experimental data. Numerical data from the nonlinear and time-dependent analyses of prestressed posttensioned reinforced concrete simple beams are presented.

In the name of “Allah”, the most gracious, the most merciful

ACKNOWLEDGMENTS

The Author's profound thanks, respect, and gratitude go to his supervisor Dr. H. Poorooshab for his encouragement, help, and support.

Special thanks to Dr. M. M. El-Badry who initiated the author's research, suggested the topic for the thesis, advised through the course of the work, and provided some financial support during a portion of the work.

The author's sincere thanks and respect are due to Dr. R. Bhat for his help and advise.

Also, the author's special thanks and gratitude go to Dr. A. Hanna for his help and encouragement.

Thanks are also extended to my colleagues and friends for their support.

DEDICATION

To the memory of my father, my ideal and my example in life. He will always be in my heart and my mind.

To my mother, sister, brothers, wife, and daughters for their unconditional love, support, and encouragement.

TABLE OF CONTENTS

Table of Contents	i
List of Figures.....	v
List of Tables	ix
Notation	x
1. INTRODUCTION	1
1.1 Background	1
1.2 Combination of Prestressed and Reinforced Concrete	2
1.3 General Overview of the Problem	3
1.4 Needs in The Research on Unbonded Prestressing.....	4
1.5 Objectives.....	5
1.6 Scope.....	6
2. LITERATURE REVIEW.....	7
2.1 Introduction	7
2.2 Previous Work.....	7
3. BASIC MATERIAL PROPERTIES	21
3.1 Introduction	21
3.2 Concrete	23
3.2.1 Instantaneous and Long-Term Strains	23
3.2.2 Concrete Properties	24
3.2.2.1 Compressive Strength.....	24
3.2.2.2 Modulus of Elasticity.....	26
3.2.2.3 Tensile Strength	28
3.2.3 Concrete Short-time Deformations.....	29

3.2.4 Concrete Long-Time Deformations, Creep and Shrinkage	30
3.2.4.1 Creep	30
3.2.4.2 Shrinkage	34
3.3 Steel Reinforcement	37
3.3.1 Reinforcing Steel	37
3.3.2 Prestressing Steel	38
3.4 Comparison Between Prediction Models	41
3.5 Tension Stiffening Effect	41
3.6 Concrete Under Variable Stress	42
3.6.1 Step-by-Step Method	43
3.7 Nonlinear Problems	44
3.8 Basic Nonlinear Solution Techniques	45
3.8.1 Incremental Techniques	45
3.8.2 Iterative Techniques	46
3.8.3 Step-Iterative Techniques	47
3.9 Convergence Criterion	47
 4. SHEAR DEFORMATIONS	 61
4.1 Introduction	61
4.2 Axial and Flexure Deformation Analysis	62
4.3 Axial, Shear, and Flexure Deformation Analysis	62
4.4 Models For Shear Effects	63
4.4.1 Variable Angle Truss Model	63
4.4.2 Compression Field Theory	66
4.4.3 Modified Compression Field Theory	68
4.5 Proposed Model To Include the Effects of Shear Deformations	
in Noncracked Members	70
4.5.1 General Remarks	70
4.5.2 The Methodology	73

4.6	Shear Stresses on a Trapezoidal Cross Section:	
	Reduced Cross Sectional Area.....	76
5.	NONLINEAR ANALYSIS OF PRESTRESSED REINFORCED	
	CONCRETE CROSS SECTIONS	85
5.1	Introduction	85
5.2	Stress-Strain Relationship - Cross Sectional Analysis.....	86
	5.2.1 Concrete	88
	5.2.2 Steel.....	90
5.3	Computation of Internal Forces and Moments - Cross Sectional Analysis	91
	5.3.1 Concrete Compressive Force and Moment.....	91
	5.3.2 Steel Force and Moment	93
	5.3.2.1 Normal steel layers resultant force and moment	93
	5.3.2.2 Internal prestressing steel layers resultant force and moment	94
5.4	Equations of Equilibrium	94
5.5	Derivatives	95
5.6	Time Dependent Stresses and Strains	100
	5.6.1 Free Strain Due to Creep and Shrinkage.....	100
	5.6.2 Variation of Prestressed Steel Stress Due to Relaxation.....	101
5.7	Analysis of cross sections	102
5.8	Verification Examples.....	104
	5.8.1 Example 1	104
	5.8.2 Example 2	106
	5.8.3 Example 3	106
6.	ANALYSIS OF PRESTRESSED REINFORCED	
	CONCRETE STRUCTURES.....	140
6.1	General	140
6.2	Structural Modeling and Discretization	142

6.3	Initial Prestressing Force.....	144
6.3.1	Losses Due to Friction	144
6.3.2	Losses Due to Anchorage Set	145
6.3.3	Effect of stressing Procedure	148
6.4	Member Stiffness Matrix	149
6.5	Fixed-End Forces	154
6.6	Calculation of Deformations of a Member	156
6.7	Imposition of Support Conditions.....	159
6.8	Analysis Procedure	160
6.9	Verification of the Procedure.....	162
6.9.1	Reinforced Concrete Beam Analysis	163
6.9.2	Analysis of Pretensioned Column.....	164
6.9.3	Analysis of Prestressed Simple Beam.....	165
6.9.4	Simply Supported Beams with Internal unbonded Tendons Tested by Harajli and compared with the current study	169
7.	SUMMARY AND CONCLUSIONS.....	213
7.1	Summary	213
7.2	Feature of The Current Study.....	214
7.3	Conclusions.....	215
7.4	Recommendations for future study	217
	REFERENECES	220

LIST OF FIGURES

	Page
Fig. 3.1 Creep and Creep Recovery of Concrete	49
Fig. 3.2 Typical Variation of Shrinkage and Swelling with Time.....	49
Fig. 3.3 Variation of Compressive Strength with Time.....	50
Fig. 3.4(a) Stress-Strain Relationship for Concrete.....	51
Fig. 3.4(b) Stress-Strain Relationship for Reinforcing Steel	51
Fig. 3.4(c) Stress-Strain Relationship for Prestressing Steel	51
Fig. 3.5 Relaxation Reduction Coefficient χ_r	53
Fig. 3.6 Comparison Between the ACI and CEB Models for Variation of Modulus of Elasticity of Concrete with time.....	54
Fig. 3.7 Comparison Between the ACI and CEB Models for Prediction of Creep Coefficient and Shrinkage Strains (Relative Humidity 40%)	55
Fig. 3.8 Distribution of Stresses in a Uniaxial Reinforced Concrete Element	56
Fig. 3.9 Tension Stiffening Models	57
Fig. 3.10 Incremental Techniques.....	58
Fig. 3.11 Iterative Techniques.....	59
Fig. 3.12 Step-Iterative Techniques	60
Fig. 4.1 Curvature Distribution in Beams With and Without Diagonal Tension Cracking	79
Fig. 4.2 Shear Failure Mechanism in a Beam Without Web Reinforcement	80
Fig. 4.3 Shear Failure Mechanism in a Beam With Web Reinforcement.....	80
Fig. 4.4 Shear and Diagonal Compressive Stress Distribution.....	81
Fig. 4.5 Compression Field Theory for Prestressed Beam Subjected to Shear	81
Fig. 4.6 Force Transmission Across Cracks	82
Fig. 4.7 Spacing of Inclined Cracks.....	82
Fig. 4.8 Shearing Stress at any Distance, y_i , Using Either Area A' or A''.....	83
Fig. 4.9 Shear Deformations in a Differential Element	84

Fig. 4.10 Shear Deformations of a Differential Element	84
Fig. 5.1 Typical Cross Sections Treated in the Present Study	108
Fig. 5.2 Division of a Concrete Part into Trapeziums and Rectangles	109
Fig. 5.3 Cross Section and Strain Distribution	110
Fig. 5.4 Idealized Concrete Stress-Strain Relationship	110
Fig. 5.5 Prestressed Concrete T-Section	111
Fig. 5.5(a) to.....	112
Fig. 5.12(b) Stress Distribution and Strain Distribution in Cross Section.....	127
Fig. 5.13 Moment-Curvature Relationship of Mid-span Cross Section (Case of Pure Bending)	128
Fig. 5.14 Moment-Curvature Relationship of Mid-span Cross Section (Case of Fixed Normal Force)	129
Fig. 5.15 Normal Force-Curvature Relationship of Mid-span Cross Section (Case of Fixed Bending Moment).....	130
Fig. 5.16 Comparison Between This Study and Linear Analysis (CRACK).....	131
Fig. 5.17 Comparison Between This Study and Linear Analysis (CRACK).....	132
Fig. 5.18(a) Stress Distribution (Time-Dependent Effects).....	133
Fig. 5.18(b) Strain Distribution (Time-Dependent Effects).....	134
Fig. 5.19 Normal Force-Curvature Relationship of Mid-span Cross Section (Case of Fixed Axial Force).....	135
Fig. 5.20 Normal Force-Curvature Relationship of Mid-span Cross Section (Case of Fixed Axial Force).....	136
Fig. 5.21 Instantaneous and Time-Dependent Stress-Strain Relationship.....	137
Fig. 5.22 Comparison Between This Study and Experimental Work by Priestley, Park, and Lu	138
Fig. 5.23(a) Cross Section of a Single-Tee Beam.....	139
Fig. 5.23(b) Comparison Between this Study and Collins and Mitchell Layer-By-Layer Approach (1987) for M- ψ response	139
Fig. 6.1(a) Typical Reinforced or Prestressed Plane Structure	171

Fig. 6.1(b) Idealization of a Plane Structure	171
Fig. 6.2(a) Displacement Components at a Typical Node	171
Fig. 6.2(b) Local Axes and Positive Directions of Member End Forces and Displacements	171
Fig. 6.3(a) A Plane Frame Member with Internal Tendons	172
Fig. 6.3(b) A Plane Frame Member with External Tendons.....	172
Fig. 6.4 Variation of Prestressing Force Along a Tendon Before and After Anchor Set.....	173
Fig. 6.5 Calculation of Area A (Case of C at Section K).....	173
Fig. 6.6 Calculation of Area A ($L_s >$ Tendon Length).....	174
Fig. 6.7 Typical Variation of Prestressing Force (Jacking from Both Ends).....	174
Fig. 6.8 Displacements $\{D'\}$ and $\{d'\}$ in a Typical Plane Frame Member	175
Fig. 6.9 Normal Force and Bending Moment Diagrams Due to Unit Forces at the Three Coordinates at End O_1	175
Fig. 6.10 Structural Model With Eccentricity at the Ends	176
Fig. 6.11 Division of a Member into Sections and Calculation of Elastic Loads for Calculating the Deformations	177
Fig. 6.12 Original and Deflected Shape of a Typical Plane Frame Member	178
Fig. 6.13 Comparison Between this Study and experiment, Kang (1977), and Lin (1973) for the Midspan Deflection	179
Fig. 6.14 Comparison Between this Study and experiment, Aroni (1968), and Kang (1977) for the Midspan Deflection	180
Fig. 6.15 Pretensioned Partially Prestressed Beam.....	181
Fig. 6.16 Partially Prestressed Beam With External Tendons	182
Fig. 6.17 Deflection Due to Instantaneous, Time-Dependent Effects, and L.L.	183
Fig. 6.18 Deflection Due to Instantaneous, Time-Dependent Effects, and L.L.	184
Fig. 6.19 Deflection Due to Instantaneous, Time-Dependent Effects, and L.L.	185
Fig. 6.20 Deflection Due to Instantaneous, Time-Dependent Effects, and L.L. for 3 Different Span-to-Depth Ratios.....	186

Fig. 6.21 to	187
Fig. 6.29 Deflection Due to Instantaneous, Time-Dependent Effects, and L.L.	195
Fig. 6.30 to	196
Fig. 6.32 Eccentricity Variation along the Span Due to Time-Dependent Effects.....	198
Fig. 6.33 to	199
Fig. 6.35 Eccentricity Variation with Time (Time-Dependent Effects)	201
Fig. 6.36 Midspan Instantaneous and Time-Dependent Deflections	202
Fig. 6.37(a) Load versus Deflection for Beam of Span 10m.....	203
Fig. 6.37(b) Load versus Deflection for Beam of Span 10m.....	203
Fig. 6.38 Moment-Deflection of the Beam (due to prestressing, self weight, and time-dependent effects)	204
Fig. 6.39 Δf_{ps} vs. Deflection (Various Span-to-Depth Ratios)	205
Fig. 6.40(a) Distribution of Top and Bottom Stresses in Concrete Along the Span.....	206
Fig. 6.40(b) Variation of Maximum Compressive Stress in Concrete with Time.....	206
Fig. 6.41 Strain-Deflection Relation at Deviator (due to time-dependent effects)	207
Fig. 6.42 Stress in External Tendons due to Live Loads	207
Fig. 6.43 Variations of the Stress in External Tendons With Different Spans	208
Fig. 6.44 Simple Beam Prestressed with internal unbonded Tendons Tested by Harajli	208
Fig. 6.45 to	209
Fig. 6.48 Comparison Between the Current Study and Experimental Work By Harajli.....	212

LIST OF TABLES

	Page
Table 1: Values of Constants a and b in Equation 3.1	25
Table 2: Relaxation Reduction Coefficient χ_r	52

NOTATION

This is a list of symbols which are common in the thesis. All symbols are defined in the text when they first appear or when they are used in equations.

A	Cross-section area of concrete element
$A, B, \text{ and } I$	Area, first moment, and moment of inertia of the transformed section
A_{ps}	Cross-section area of prestressed tendon
b	Width of rectangular section or width of the flange of a T-section
c	Depth of compression zone in a fully cracked section
D	Displacement
d	Distance between extreme compressive fibre to the bottom reinforcement layer
$\{D'\}, \{D\}$	Vector of local and global displacements
E	Modulus of Elasticity
F	Force
$\{F\}$	Vector of nodal forces
f	Stress related to strength of concrete or steel
$[f]$	Flexibility matrix
f_{ps}	Stress in prestressing tendon
f_y	Yielding strength of normal steel
f_{ct}	Tensile strength of concrete
h	Height of cross-section
h_o	Notional member size
$[H]$	Transformation Matrix
i, j, m, n	Integers
l	Length of member
M	Bending moment, positive moment produces tension at the bottom fiber

N	Normal force, positive when tensile
P	Force
$[S]$	Stiffness Matrix
s_r	Spacing between cracks
t	Time or age
$[T]$	Transformation matrix
T_s	Tension force in stirrups
y	Coordinate defining location of fibre or reinforcement layer, positive when down
α	Modular ratio (ratio of steel modulus of elasticity to concrete modulus of elasticity)
$\beta_c(t-t_o)$	Function describes development of creep with time
β_H	Function to account for the effect of relative humidity and member size on the development of creep with time
Δ	Increment
ε	Normal strain, positive for elongation
η	Dimensionless multiplier for calculation of time-dependent change in axial strain
σ	Normal stress, positive when tensile
τ	Instant of time
$\phi(t, t_o)$	Creep coefficient of concrete
$\chi(t, t_o)$	Aging coefficient of concrete
ψ	Curvature, positive curvature corresponds to positive moment
$\{ \}$	Braces indicate a vector, i.e. a matrix of one column
$[\]$	A rectangular or square matrix

Subscripts

c	Concrete
cs	Shrinkage
ns	Non-prestressing steel
O	Reference point
0	Initial or instantaneous

pr	Relaxation in prestressing steel
ps	Prestressing steel
s	Steel
u	Unit force, unit displacement
ϕ	Creep effect

CHAPTER ONE

INTRODUCTION

1.1 Background

External prestressing technique uses tendons placed completely outside the concrete section. The tendons are used to prestress the structural member longitudinally and they generally represent a portion of the total reinforcement. External prestressing has become a desirable tool for rehabilitation and strengthening existing structures which have insufficient strength and/or excessive deflection and cracking. It is very advantageous in cases where the foundations are fully loaded since external prestressing adds virtually no extra weight to the structure, nor does it change its appearance. It is being increasingly used in the newly erected structures as well, particularly bridges. In addition, some traditionally prestressed bridges were built by incremental launching with the help of some temporary external tendons to increase central prestress during launching without increasing the cross-sectional weight. In the past few years, numerous prestressed concrete bridges have been built in the United States of America and in France using external tendons. This technique has been used recently in Belgium, Switzerland, Venezuela, Germany, and Czechoslovakia. In the United States, the primary objective of the development of the external prestressing technique is to reduce the cost through reducing the web thickness. In France, external prestressing, developed under the influence of the government, is a way to improve quality since it leads to a simple tendon lay-out, small construction deviators, lower frictional losses, and improvement of concreting conditions by eliminating ducts

from webs.

Strengthening by external prestressing is aimed, generally, at reducing the stresses in the reinforced concrete and hence allowing the structure to take over supplementary live loads. The external unbonded tendons are supported at end anchorages, deviators or saddles, and locations of angle changes (at high and low points of draped tendons). This tendon layout is used whenever the profile of the tendons is to match the moment line.

1.2 Combination of Prestressed and Reinforced Concrete

When a combination of prestressed and nonprestressed reinforcement is represented in a concrete member (partially prestressed concrete), the flexural strength is essentially supplied by the tendons, with the nonprestressed steel playing a minor role. For certain types of construction, a full combination of prestressed and reinforced concrete may be the best design, making use of the advantages of both. Reinforced concrete has the advantage of simplicity in construction and lower creep deflection. Prestressing controls deflection and cracking.

Some structural elements will be best designed with a combination of reinforced and prestressed concrete. One occasion for the use of this combination is the case of high live-load to dead-load ratio, when prestressing alone may produce excessive camber. Another is the case of high added dead load requiring prestressing in stages.

Nonprestressed steel does not act until the concrete cracks and it does not contribute significantly toward the precracking strength. Hence, if cracking could result in a primary or secondary failure, nonprestressed steel may be of no help. Consequently, external prestressing will be helpful because corroded prestressing steel can be replaced.

1.3 General Overview of the Problem

Reinforced and prestressed concrete structures are designed to satisfy the requirements of serviceability and safety. The serviceability and the safety requirements of any structure is greatly affected by large deflections, excessive crack widths, and load. Therefore to satisfy these requirements, accurate prediction of displacements, internal forces, and deformations is necessary.

Analytical determination of the displacements, deformations, stresses, and internal forces of reinforced and prestressed reinforced concrete structures throughout their load histories is complicated by a number of factors which include nonhomogeneity of the materials, cracking of the concrete under increasing load, nonlinear material properties of the concrete, reinforcing steel and prestressing tendons, variation of concrete properties with time, time-dependent concrete deformations due to creep and shrinkage, and relaxation of the prestressing steel. Due to these difficulties, engineers in the past have been relying on empirical formulas derived from numerous experiments for the analysis and design of concrete structures. Several investigators have taken advantage of the digital computers to develop analytical solutions for the behaviour of the concrete structures. The present study is one of such continuing efforts and concerns with the flexural behaviour of beams prestressed with unbonded internal or external tendons.

The analysis and design of structures with external tendons is conceptually different from that of structures with internal unbonded tendons. The main difference in behaviour between external and internal unbonded prestressing is the deflected shapes of the beam and the tendons. The deflected shape of internal tendons follows the deflected shape of the beam itself throughout the entire span; however, the deflection of external tendons is

restricted to the deflection of the beam at deviator locations and is different from the deflection of the beam at all other locations. The deflected shape of the beam is nonlinear while the deflected shape of the external tendons is rectilinear leading to changes in eccentricity of the tendons between the points of anchorages and deviators. This is referred to as "second-order effects". Such effects may significantly affect the response of the member and can be more significant in members having high span-to-depth ratios.

The external tendons are not bonded to the concrete or beam, hence the strain compatibility is not applicable at critical and other sections. This makes the stress in the external tendons dependent on the deformations of the whole member; therefore, member dependent and not section dependent. Therefore, proper modeling of the overall beam deformation becomes necessary.

1.4 Needs in The Research on Unbonded Prestressing

There are several research needs in the area of prestressed concrete involving the use of external or internal unbonded tendons. These needs are due to the lack of simple and rational analytical models that are necessary to describe the flexural behaviour of such beams throughout their loading history up to and including the ultimate limit state.

First, several studies attempted to solve the problem of the ultimate limit state using limited experimental test data and lower bound curve fitting. In most of these studies, an equation for the prediction of the stress in the unbonded tendon f_{ps} at ultimate was proposed. Some of these equations were based on one type of loading, others were derived based on one span-to-depth ratio. In a recent study conducted by Naaman and Alkhairi (1991), the authors showed that these equations tend to produce large scatter in the data

when plotted against the experimentally observed results. The scatter was attributed to the failure to include important parameters that affect the value of f_{ps} . These parameters include the relative amount of prestressing and nonprestressing steel, member span-to-depth ratio, type of loading, and the beam cross-section.

Second, predicting the complete response would require not only modeling the flexural deformations, but also the effects of shear deformations on the stress increase Δf_{ps} which is known to be related to the span-to-depth ratio. It should be mentioned that research has been undertaken to model the effect of shear deformations using empirical rather than rational approaches, Harajli and Hijazi (1991).

Third, time-dependent material properties have been ignored in most of the previous work. Elbadry and Ghali (1989) showed that time-dependent effects have proven to be an important parameter in the flexural analysis for serviceability of concrete structures with internal tendons. Therefore, there arises a need to account for the time-dependent effects in the prediction of the flexural response of concrete members with external and/or internal tendons.

1.5 Objectives

The main objective of this study is to develop a numerical model for the flexural analysis of externally and/or internally unbonded prestressed reinforced concrete members throughout their service load history as well as their elastic cracked, inelastic cracked, and ultimate load histories. Another objective is to examine the effects of different design parameters such as span-to-depth ratio and the eccentricity of the external tendons on the flexural behaviour of prestressed concrete members. It is also the objective of this study to

account for the time-dependent effects of creep, shrinkage, and aging of concrete and relaxation of prestressing steel. Shear deformations are also considered in this study for noncracked homogeneous members.

1.6 Scope

The scope of this study will be limited to determining the strains, stresses, displacements, internal forces in the constituent materials for all strength limit states using the displacement method. The analysis will cover simply supported externally prestressed reinforced concrete beams. The analysis will account for the various factors that affect the serviceability and the ultimate limit states such as the time-dependent effects of creep and shrinkage of concrete and relaxation of the prestressing steel, loading and prestressing, the effects of the shear force on the flexural deformations, change in geometry and support conditions, second-order effects due change in tendon eccentricity, span-to-depth ratios, and yielding of the steel. Cracking and tension stiffening of concrete are also considered since it is known from research that the neglect of tensile resistance of concrete, customary in ultimate load calculations, leads to significantly underestimation of deflections.

CHAPTER TWO

LITERATURE REVIEW

2.1 Introduction

One of the major problems associated with prestressed concrete structures is the time-dependent loss of prestressing force due to creep and shrinkage of the concrete as well as relaxation of the prestressing tendons. These phenomena can lead to time-dependent deformations greatly in excess of the initial instantaneous elastic deformations of the structure. It should thus be clear that for structures with long spans such as segmental overhang bridges, these deformations may be very important, especially when consideration is given to the fact that for these bridges the ends of adjacent cantilevers should meet at the correct level, grade, and alignment. In addition, excessive deformations can lead to violation of certain serviceability requirements and are objectionable from an aesthetic point of view. External prestressing is aimed at reducing the stresses in the reinforced concrete and hence allowing the structure to support supplementary live loads. This aim may not be fulfilled if the time-dependent effects are not considered since they tend to reduce the eccentricity of the external tendons. This will lead to a reduced flexural rigidity and therefore lead to a reduced flexural strength of the structure.

2.2 Previous Work

The publications that deal with the topics of the long-time behaviour of prestressed reinforced concrete structures and behaviour of structures with external and/or internal

unbonded tendons are limited in number. In the following sections the available literature, both analytical and experimental investigations, that has a direct bearing on these topics is briefly discussed.

The application of the finite element method for the analysis of concrete structures including the time-dependent effects such as creep, shrinkage, and steel relaxation has been made by a number of investigators. Selna (1967) analyzed planar reinforced concrete frames including cracking, creep, and shrinkage by developing a time-dependent constitutive relations based on linear visco-elasticity. Aas-Jacobsen (1973) studied slender reinforced concrete frames including creep and geometric nonlinearity. Aldstedt (1975) analyzed reinforced concrete frames, including the effects of bond slip, creep, and geometric nonlinearity. Scanlon and Murray (1974) studied the time-dependent deflection of reinforced concrete slabs utilizing Selna's formulation of creep. Rashid (1971) studied two-dimensional problems in concrete creep including the effects of temperature on creep. Sanduh et al (1967) analyzed plain concrete dams including the effects of creep and temperature.

In his book on the limit state design of prestressed concrete structures, Guyon (1960) described the design considerations involved in the design of cantilevered prestressed concrete bridges built in segments.

The long-time behaviour of four prestressed concrete bridges, built by the cantilever method in conjunction with a cast-in-situ technique, was studied by Keijer (1984). For all these bridges, adjacent cantilevers were connected at midspan by means of hinges. Comparison of the results of an extensive parametric study with measurements of the vertical deflections of these structures yielded the following conclusion: Concrete

creep had a dominating influence on the deformations of this type of bridges. Consequently, the creep coefficient as well as the functional form expressing the creep-time relationship was of prime importance in predicting the long-time deformations. A logarithmic creep-time relationship yielded satisfactory agreement between the calculated and the observed deflections.

The shrinkage and creep strains in a prestressed cantilever bridge over the Oise River, in France, were studied by Belmain and Le Bourdelles (1979). According to Danon (1980) that work was primarily aimed at assessing the accuracy of the recommendations of the C.E.B and the French Code in predicting creep and shrinkage.

Ghali et al. (1974) presented a step-by-step procedure to calculate the prestress loss and deformations in multistage prestressed girders. The procedure accounted for effect of elastic and creep recoveries on the prestress loss, as well as the prediction of intrinsic relaxation of the prestressing steel reinforcement due to the varying strain.

An in depth study of the various parameters that affect the time-dependent behaviour of prestressed concrete bridges built by the cantilever method was conducted by Branson and Christian (1971). During the course of that work, a computer program capable of predicting the time-dependent stresses, strains, loss of prestress, and deflections of a segmentally constructed prestressed cantilever bridge was developed.

A computer program capable of analyzing curved segmentally erected concrete box-girder bridges, was developed by Van Zyle and Scordelis (1978). In that work the time-dependent properties of concrete and steel were considered. The stiffness method was used, in conjunction with skew-ended finite elements with eight degrees of freedom at each of the two end nodes, to perform the analysis.

A procedure for the analysis of time-dependent effects in prestressed concrete structures constructed in stages was developed and implemented in a computer program by Khalil (1979). Special attention was paid to the analysis of prestressed concrete cable-stayed systems. Structural concrete members with up to three different concrete layers, each having different time-dependent properties, were included. The stiffness method was used in conjunction with the tangent stiffness method to account for the geometric nonlinearities.

It should be noted that none of the above references presented a work on the externally and/or internally unbonded prestressed reinforced concrete members, nor did they present any significant comparisons between the analytical and experimental data.

Several investigations have been carried out on externally prestressed reinforced concrete members. The most recent ones are discussed briefly.

El-Habr (1988) developed a finite element model to predict the nonlinear behaviour of segmental externally prestressed bridge girders. In that model, the joint stiffness was determined from a parametric study to avoid an ill-conditioned stiffness matrix or an oscillatory solution.

Naaman (1985, 1990, 1992) and Naaman and Alkhairi (1991) have proposed a simplified methodology to compute the stress in unbonded internal tendons of flexural concrete members in the elastic uncracked and cracked range as well as the ultimate or the nominal resistance. The methodology applies to simply supported beams with a symmetrical tendon profile. This methodology introduces the strain reduction coefficients to provide the necessary correlation between member behaviour and the section behaviour, neglecting the effects of diagonal shear cracking and eccentricity variations

(second-order effects). Using the strain reduction coefficients, the analysis of a beam with unbonded tendons is converted to the analysis of a beam with bonded tendons, hence allowing a conventional sectional (fictitious section) analysis to be performed. It should be noted that in the case of elastic cracked range, the strain reduction coefficients are used when only one crack has formed in the beam.

The earliest published application of the finite element method to reinforced concrete structures was by Ngo and Scordelis (1967, 1970) at the University of California, Berkeley in 1967. Simple beams were analyzed in which concrete and steel reinforcements were presented by constant strain triangular elements, and special bond link elements were used to connect the steel to the concrete. A linear elastic analysis was performed on beams with predefined crack patterns to determine principal stresses in the concrete, stresses in the steel reinforcement and bond stresses. Ngo, Scordelis and Franklin (1970) used the same approach to study shear in beams with diagonal tension cracks, considering the effects of stirrups, dowel shear, aggregate interlock and horizontal splitting along reinforcement near the support.

Scordelis (1972, 1984) presented a comprehensive review of the application of the finite element method for the analysis of reinforced concrete structures. He considered plane stress systems, plate bending systems, combined plane stress and plate bending systems, axisymmetric solid systems and general three dimensional solids for both short and long-time loadings. Schnobrich (1974, 1976) and Wegner (1976) presented similar surveys of the application of the finite element method for the study of reinforced concrete structures.

Nilson (1968) introduced nonlinear material properties and nonlinear bond-slip

relationship into the analysis and used an incremental load method to account for these nonlinearities. He analyzed concentric and eccentric reinforced tensile members by using quadrilateral plane stress elements. Cracking was accounted for by stopping the solution when an element indicated a tensile failure, and by redefining a new cracked structure. Franklin (1970) used an iterative procedure with incremental loading technique to trace the response of two dimensional system from initial loading to failure in one continuous computer analysis.

Kang and Scordelis (1980) presented a method of accounting for both nonlinearities of reinforced and prestressed concrete frames. Their method includes the time-dependent effects due to load history, temperature history, creep, shrinkage, aging of concrete, and prestress relaxation. The updated Lagrangian approach was used with load incrementation to trace the behaviour of the structure.

Suidan and Schnobrich (1973) studied beams by using 20-node three-dimensional elements. Elastic-plastic concrete properties and the von Mises yield criterion were utilized. Sarne (1975) analyzed prestressed concrete reactor vessels by using three-dimensional isoparametric elements. He included the time-dependent effects and material nonlinearity in his analysis. Prestressed concrete reactor vessels were analyzed by Rashid (1968), and Wahl and Kasiba (1969) by utilizing axisymmetric elements. Further developments in the analysis of reactor vessels were presented by Zienkiewicz et al. (1977), Argyris et al. (1973), and Connor and Sarne (1975).

Harajli (1990, 1993) presented a theoretical model for the evaluation of the influence of the member span-to-depth ratio on the predicted f_{ps} of unbonded prestressed concrete members at their nominal flexural strength. Strain compatibility approach was

used to compute the prestress f_{ps} . The simply supported unbonded beam was loaded by two equal concentrated loads separated by a given distance. The actual and idealized curvature distribution along the length of the beam were developed at the nominal flexural strength. In this strain compatibility approach, three major simplifying assumptions are adopted: 1) linear strain distribution between the concrete and the ordinary steel which implies that the total elongation of the prestressing steel between anchorage ends can be determined from the conventional curvature distribution along the beam length. This follows from the experimental observation by Mattock, Yamazaki, and Kattula (1971). 2) The total elongation of the prestressing steel between the anchorage ends is due mainly to the plastic deformation occurring in the plastic regions. That is the contribution of the curvature distribution between zero and yield to the total elongation of the tendon is neglected. 3) At the nominal flexural strength of the beam the stress in the unbonded tendons is constant along the length, that is the frictional forces are neglected. Taking the ultimate concrete compressive strain at the beam top fibre according to the ACI Building Code (1983) and using assumptions 1 and 2, the total increase in the tendon elongation between the anchorages and the strain increase in the tendon could be derived. The location of the neutral axis could then be derived and finally the force equilibrium at the critical section yielded an equation for the prestress f_{ps} from the general compatibility equation. It was found that increasing span-to-depth ratio reduced the predicted f_{ps} in magnitude. Beams loaded with single concentrated load encountered the highest reduction in f_{ps} with increasing span-to-depth ratio. It was also noted that proposed equation for f_{ps} is excessively conservative for simply supported beams loaded other than with single concentrated load.

Tan and Naaman (1993) have proposed a model based on the strut-and-tie method to predict the strength of a simply supported beam, externally prestressed with tendons having a single draping point and subjected to a concentrated load at midspan. In this study the beam is divided into B- and D-regions. The B-regions are those in which the strain distribution is reasonably linear across the depth of the cross section. In the D-regions the strain distribution is significantly non-linear over the section. The failure of the beam in the D-region directly under the load is investigated in this study. The analysis of the midspan section uses the classical beam theory (compatibility theory) which may not be strictly correct as the midspan section lies within the D- region below the concentrated load. This ambiguity is deemed to cause some error, as confirmed later in comparing the model with available test data.

Muller and Gauthier (1989) developed a finite element computer program for the ultimate response of simply supported and continuous beams with external tendons. Their model requires information regarding the moment versus rotation relationship.

Alkhairi and Naaman (1993) developed a nonlinear analytical model for the prediction of the complete response of beams prestressed with unbonded tendons. Their model takes into account material nonlinearity, span-to-depth ratios, and eccentricity variations in external tendons. However, their model is applied only for simply supported beams and does not accept segmental construction.

A series of reports, published by the University of Texas at Austin, USA, on the research undertaken by Brown, Burns, and Breen (1974), covered problems related to segmental cantilever bridges. These reports summarized design procedures and criteria and investigated construction problems. A very powerful product of the research effort

was a computerized incremental analysis procedure for segmental construction. The program was verified by Kashima and Breen (1975) who built and tested a model of the Corpus Christi bridge constructed in Texas, USA. Time-dependent deformations were not included in this investigation.

Van Zyl and Scordelis (1978) developed a program for the analysis of curved segmentally erected prestressed concrete box-girder bridges. The structure is idealized as a series of skew-ended box-girder finite element developed by Bazant and El-Nimeri (1973). Such approach eliminates the need for storing the entire stress history and requires the stress information only in the interval preceding the one under consideration.

Khalil (1979) has developed a computer program for the time-dependent analysis of prestressed concrete cable-stayed bridges and other framed structures built in stages. Creep is considered to consist of recoverable and irrecoverable components and a Dirichlet series is used to express the creep function of each of the two components.

Several researchers (1985, 1989) discussed the analysis of prestressed bridges. Detailed comparisons were made between the computed response and that measured in an actual structure made of precast segments. Good agreement was found, but the time-dependent effects were minimum because of the advanced age of the segments. the agreement was very sensitive to the material properties specified in the analysis.

Several other investigations on the behaviour of segmentally erected bridges include those by Ketchum et al. (1986). These investigations were limited to the linear stage of structural behaviour. No significant differences between them can be highlighted, except for the one by Kim (1990) where a parabolistic study was conducted to predict confidence limits for long-term deflections and internal forces.

It should be noted that all of the above mentioned models do not consider time-dependent effects, namely creep, shrinkage, aging of concrete, and relaxation of prestressing tendons.

Several experimental studies have been carried out on externally/internally unbonded prestressed reinforced concrete members. A few are discussed briefly.

Harajli (1993) examined the use of external prestressing as a means of strengthening flexural members. He tested sixteen simply supported beam specimens with rectangular cross section. All specimens were loaded in four-point bending using two symmetrical concentrated loads applied at one-third the span length. To simulate actual conditions of concrete flexural members, large fatigue deformation were induced in the specimens by cyclic loading before external prestressing was applied. The specimens were subjected to 5 to 10 thousand cycles of large amplitude fatigue loading at a constant load range. The load range varied between minimum load P_{\min} and maximum load P_{\max} equal to 30 and 80 percent, respectively, of the calculated ultimate flexural load resistance of the specimens. At the end of cyclic fatigue loading the specimens were externally prestressed while loaded with P_{\min} and then subjected to monotonically increasing load to failure. Test results showed that as a result of external prestressing, the nominal flexural strengths of the beams were increased up to 146 percent without significant reduction in ductility and the induced fatigue deflections were reduced by up to 75 percent. He showed that external tendons using a draped profile were relatively more effective in increasing the flexural strength than tendons with straight profile. The stress ranges and mean stress levels in the internal bonded tension reinforcement decreased considerably leading to improvement in the fatigue life of the strengthened beams.

Harajli and Kanj (1991) tested 26 simply supported concrete beams with rectangular sections prestressed with unbonded tendons and reinforced with and without ordinary reinforcing steel to study the effects of several parameters on the magnitude of stress in the prestressing steel f_{ps} . These parameters included three different contents of tension reinforcing (reinforcing index), two different amounts of ordinary reinforcing steel relative to the prestressing steel (fully prestressed and partially prestressed), and three different member span-to-depth ratios (20, 13, and 8). For each set of input parameters, two beams were tested, one beam under single concentrated load at midspan, and the other beam under two symmetrical third-point loads. The stresses in the prestressing steel and the ordinary steel were measured using the electrical resistance gages attached to the surface of the wires and reinforcing bars at midspan location. The average strain in the prestressing steel was also measured from the elongation of the tendons between the anchorage ends. The corresponding tendon elongation was measured using a wire transducer LVDT attached on either side of the beam and at the same level as the prestressing steel. The results of their tests seemed to indicate that the type of load application has no significant influence on f_{ps} . The results showed that Δf_{ps} for members tested under single concentrated load are of the same order of magnitude as the members tested under two third-point loads. The result of this investigation are in contradiction with the analytical observations made earlier by the writers and by Loov (1987) where beams loaded under single concentrated load reported to mobilize the least Δf_{ps} at nominal flexural resistance of unbonded members.

Saeki, Horiguchi, and Hata (1980) conducted an experimental study on the plastic deformation properties of rectangular and T-sectional beams strengthened by externally

prestressed cables to increase the ultimate shear and flexural strengths. The external prestressing was applied after repair of cracks. Saeki et al. (1980) examined the effects of the effective prestress level of the external cables on the plastic deformation capacity of the beams. They found that the behaviour of the beams could be ductile when the initial prestress was controlled at a reasonable stress level. They also compared the experimental results of the ultimate strength and deformation with the numerical values obtained based on Pannel's analysis (1977). The comparison was used in modifying the effective depth of external cable at failure.

Seible et al. (1990) conducted tests on four concrete beams pretensioned with steel strand and strengthened externally by external post-tensioned tendons. The beams were tested under four point loading. The external tendons were harped at two points below the point of application of the loads at an angle of 4.8 degrees at each point. The test results showed that the average strength increase of the strengthened members was 115% for the beams with single strand and 46% for beams with double steel strands. Midspan deflections at the ultimate load for the strengthened beams were approximately 60% of the corresponding beam deflection. All beam failures were due to the crushing of the concrete.

Burns, Helwig, Tsujimoto (1991) monitored the change in the prestressing force in the internal unbonded tendons of a post-tensioned continuous beam. Their study was limited to the testing of two continuous post-tensioned beams with unbonded tendons. The two specimens that were tested had rectangular cross sections and one with greater span/depth ratio than the other (13.6, 17). The beams were continuous over two spans and supported at the center by a knife edge and by two rollers at the exterior supports. Each beam had one type of concrete, one type of reinforcing steel, and one type of prestressing

strands. The prestressing force was monitored during post-tensioning and before and after the service loads were applied. The tendon force was also monitored during overloading and the ultimate stage of testing of the beams. It was observed that there was no significant change in the tendon force under repeated service loads up to the $12\sqrt{f'_c}$ compressive stress level (extreme fiber of the critical section). During single-span overloads, the tendons slipped into the loaded span which caused the tendons stress to decrease on the end of the beam with the loaded span and to increase on the end with the unloaded span. During two-span overloads, the tendon did not experience a significant change in the distribution of stress. They also observed that for a given deflection, the increase in tendon stress for a beam with severe drape is larger than the corresponding increase experienced by a beam with a less severe drape.

It should be noted that all of the above mentioned experiments do not consider the time-dependent effects. They are also restricted to one type of concrete and one or two types of loads.

All of the literature cited above lack the nonlinear analysis of prestressed reinforced concrete members considering 1) the time-dependent effects of creep and shrinkage of concrete and relaxation of prestressing tendons, 2) the external/internal unbonded tendons, 3) the shear deformations, and 4) the comparison of the analytical data combining 1, 2, and 3 with available experimental observations. It can also be seen from the above literature that two important factors that affect the behaviour of the prestressed concrete structures, namely, the partial prestressing ratio and the span-to-depth ratio of concrete members, were not considered in previous research. Therefore as part of the present research, an investigation has been conducted into the effects of these two

important parameters on the behaviour of prestressed reinforced concrete members.

CHAPTER THREE

BASIC MATERIAL PROPERTIES

3.1 Introduction

Any structural analysis basically involves the simultaneous satisfaction of the equations of equilibrium, compatibility relations, and constitutive relations. The equations of equilibrium and the compatibility relations do not involve the material properties. The constitutive relations, on the other hand, relate the stresses to strains and are consequently dependent on the material properties. The material behaviour of the concrete is strongly time-dependent. Thus, for the overall structural analysis to be adequate, it is essential that the instantaneous as well as the time-dependent material properties of the concrete and steel be estimated reasonably accurately. Reinforcing and prestressing steel are considered homogeneous materials and their properties are generally well defined. On the other hand, concrete is a composite material of complex nature and its properties depend on many variables, i.e. water/cement ratio, aggregates, cement type, humidity, curing, age, time, and therefore very difficult to define accurately.

Both concrete and steel exhibit various nonlinear material properties. The stress-strain relation of concrete is not only nonlinear, but also differs in compression and tension due to the microcracks in the transition zone between the aggregates and the hydrated cement paste. Tensile cracking is one of the most important factor which contributes to the nonlinear behaviour of reinforced concrete structures. Reinforcing steel generally exhibits symmetrical stress-strain relation in tension and compression and its properties are

generally independent of time. Prestressing steel is used exclusively in tension and its stress-strain relation is also nonlinear and its shape is different from that for the reinforcing steel. If a tendon is subjected to a stress of 0.5-0.8 its ultimate strength, the stress will decrease gradually with time due to relaxation. This relaxation in tension is of concern in calculation of the time-dependent prestress loss and the associated deformations. Concrete is unique among structural materials in that it experiences complex physical and chemical changes (creep and shrinkage) over time, which result in properties and deformations that are time-dependent. The characteristics of bond between steel and concrete is of fundamental importance to the behaviour of many reinforced concrete structures whose stiffnesses are directly related to the bond characteristics. In this study, it is assumed that perfect bond exists between concrete and reinforcing steel and concrete and prestressing steel in bonded prestressed concrete members after the transfer of prestress as in pre-tensioned and post-tensioned beams. For post-tensioned unbonded beams in which the tendons are not bonded to the concrete, an iterative method with gradual convergence to the solution, is utilized.

Predicted stresses and deformations in a structure can be considerably in error if the effects of creep and shrinkage of concrete and relaxation of steel are neglected. For the analysis of time-dependent stresses and deformations, it is necessary to employ time functions for strain or stress in the materials involved. Analytical expressions for the prediction of the magnitude of the concrete and steel properties are given in the subsequent sections.

3.2 Concrete

The variation with time of properties such as the concrete strength, its modulus of elasticity, and creep and shrinkage properties as influenced by the concrete mix, the size and shape of the concrete member, the age at first loading and the duration of load and the humidity and temperature of the surrounding atmosphere. The development of prestressing steel relaxation with time is also required. Reliable methods and equations for prediction of the aforementioned properties of concrete and prestressed steel are available in the literature and are suitable for incorporation in computer programs for the required analysis. The most commonly used sources for prediction of these properties are the CEB-FIP Model Code (1990) and the ACI Committee 209 recommendations (1992).

3.2.1 Instantaneous and Long-Term Strains

One of the most important assumptions in studying the deformations of concrete is the total strain of concrete at any time may be composed of strains caused by different phenomena. Davis and Davis (1930, 1937), Glanville (1930), and Troxell et al. (1958) provided the experimental verification of this commonly accepted assumption in their studies of creep and shrinkage of concrete. This assumption is used by many investigators to study the behaviour of concrete structures.

For the present investigation, the total strain $\epsilon(t)$ at any time is assumed to be composed of two components: instantaneous strain and time-dependent strain. The instantaneous strain is caused by a short time loading while the time dependent strain is of two types: creep which is stress-dependent and shrinkage which is stress-independent.

3.2.2 Concrete Properties

Material parameters can be estimated by using empirical expressions derived from experimental observations and from data available in literature. The ACI Committee 209 (1992) has proposed approximate equations for predicting the variation over time of the concrete properties from data related to variables such as the composition mix, the member size, and the environmental conditions. The European practice embodied in the CEB-FIP Model Code for concrete structures, 1990 (MC-90) uses tables and graphs for the same purpose, based on the method developed by Rüsch, Jungwirth, and Hilsdraff (1973). The recommendations of both the ACI Committee 209 and the CEB-FIP Code have been widely applied in bridge design.

3.2.2.1 Compressive strength

The compressive strength of concrete is one of its important properties. Many other properties such as the modulus of elasticity and the tensile strength can be approximately related to the compressive strength which is influenced by many factors, among which the water/cement ratio, mix proportions, size of aggregates, admixtures, type of cement, curing and ambient conditions and the age of concrete are often mentioned.

For an estimate of the compressive strength, $f_c'(t)$, at any time t , the ACI Committee 209 (1982) recommends the following equation:

$$f_c'(t) = \frac{t}{a + bt} f_c'(28) \quad (3.1)$$

where $f_c'(28)$ is the strength at the age of 28 days, t is the time in days after casting of

concrete, and a and b are constants. The values of a and b depend on the type of cement and the curing conditions, see the following table:

Table 1: Values of Constants a and b in Equation 3.1

Cement type*	Curing Condition	a	b
I	Moist	4.00	0.85
	Steam	1.00	0.95
III	Moist	3.30	0.92
	Steam	0.70	0.98

* Type I is normal cement, Type III is high-early strength cement.

According to the CEB-FIP Model Code (1978), the variation of the compressive strength with time is as shown in Fig. 3.3. This graph is for concrete of normal cement and moist cured up to an age of 7 days at approximately 20°C and for the influence of different types of cement, the actual age of concrete must be adjusted as follows:

$$t = \frac{k_{ce}}{30} \sum [(T + 10) \Delta T] \quad (3.2)$$

In this formula, T is the average ambient temperature (in °C) and ΔT is the number of days during which the average ambient temperature is T . The coefficient k_{ce} depends on the type of cement and assumes the following values:

$k_{ce} = 1$ for normal or slow-hardening cements;

$k_{ce} = 2$ for rapid-hardening cements;

$k_{ce} = 3$ for rapid-hardening high strength cements.

An expression reported by Ghali and Favre (1986) to approximate the graph in Fig.

3.3 and another expression by Neville et al. (1983) and takes the form:

$$\frac{f'_c(t)}{f'_c(28)} = \frac{1}{1.276} \left(\frac{t}{4.2 + 0.85t} \right)^{3/2} \quad (3.3)$$

3.2.2.2 Modulus of Elasticity

The modulus of elasticity of concrete is defined as the ratio between the stress and strain in the elastic zone. It is dependent on several factors, notably the strength of concrete and its age, the properties of the aggregates and cement, and the rate of load application. Numerous empirical formula for the evaluation of E_c are available in the literature (Aldstedt, 1975).

(a) *ACI 318 (1989) Code:*

The value of the modulus of elasticity is estimated by the ACI 318(1989) Code equation:

$$E_c = w_c^{1.5} 33 \sqrt{f'_c} \quad (3.4)$$

where E_c (psi) and f'_c (psi) are the modulus of elasticity of concrete and its specified compressive strength; w_c (lb per cu ft) is the unit weight of concrete. For normal weight concrete, E_c (psi) may be taken as $57000 \sqrt{f'_c}$. Equation (3.4) may be rewritten using SI units:

$$E_c = w_c^{1.5} 0.043 \sqrt{f'_c} \quad (3.5)$$

with E_c (MPa), and f'_c (MPa) and w_c (kg/m³); the corresponding value of E_c (MPa) for normal weight concrete is $4730 \sqrt{f'_c}$ (MPa).

Equation (3.4) or (3.5) gives the secant modulus of elasticity, which is the slope of the secant drawn from the origin to a point corresponding to $0.40f'_c$ on the stress-strain curve.

Use of Equation (3.4) or (3.5) will overestimate E_c when f'_c is higher than 6000 psi (40 MPa), in which case the following equation is suggested for normal weight concrete:

$$\begin{aligned} E_c &= 40000 \sqrt{f'_c} + 10^6 \text{ psi} \\ E_c &= 3300 \sqrt{f'_c} + 7000 \text{ MPa} \end{aligned} \quad (3.6)$$

(b) *CEB-FIP Model Code 1990 (MC-90)*:

The modulus of elasticity of concrete, $E_c(28)$ (MPa), at age 28 days, for normal-weight concrete can be estimated by:

$$E_c(28) = 21500 (f_{cm}/f_{cmo})^{\frac{1}{3}} \quad (\text{MPa}) \quad (3.7)$$

where $f_{cmo} = 10 \text{ MPa}$.

When the mean compressive strength f_{cm} MPa is not known, $E_c(28)$ may be estimated from the characteristic compressive strength, f_{ck} (for MPa) at 28 days by the equation:

$$E_c(28) = 21500 [(f_{ck} + \Delta f)/f_{cmo}]^{1/3} \quad (3.8)$$

where $\Delta f = 8 \text{ MPa}$.

Equations (3.7) and (3.8) apply when quartzie aggregates are used. For other aggregates, multiply by a factor varying between 0.7 and 1.2. Equations (3.9) and (3.10)

give the tangent modulus of elasticity, which is equal to the slope of the stress-strain diagram at the origin. When the modulus of elasticity is for use in an elastic analysis, without considering creep, the value of $E_c(28)$ should be reduced by a factor of 0.85 to account for the quasi-instantaneous strain (Hognestad, 1951), which occurs shortly (within one day) after loading.

The modulus of elasticity of concrete at age t may be estimated by:

$$E_c(t) = \beta_E(t)E_c(28) \quad (3.9)$$

with

$$\beta_E = \sqrt{\beta_{cc}(t)} \quad (3.10)$$

where

$$\beta_{cc}(t) = \exp[s(1 - \sqrt{28/t})] \quad (3.11)$$

with s being a coefficient depending on type of cement; s is equal to 0.2, 0.25, and 0.38, respectively, for rapidly hardening high-strength cements, for normal and rapidly hardening cements, and for slowly hardening cements.

3.2.2.3 Tensile Strength

Cracking is a major factor contributing to the nonlinear behaviour of reinforced concrete structures with or without prestressing. The tensile strength of concrete can be determined from a direct tension test. There are, however, some considerable experimental difficulties in conducting such a test and the tensile strength is usually measured by indirect tests such as flexural or cylinder splitting tests. The strength determined from

flexural test, usually referred to as the *modulus of rupture*, f_r , is greater than the direct tensile strength, f_{ct} because of the biaxial compressive and tensile stresses.

A number of empirical expressions for predicting the tensile strength of concrete have been suggested. The ACI Committee 209 (1982) recommends the following equations. For the axial tensile strength,

$$f_{ct} = 0.0069 \sqrt{\gamma_c f_c'} \quad (3.12)$$

and for the modulus of rupture,

$$f_r = a \sqrt{f_c'} \quad (3.13)$$

where γ_c is in kg/m, f_{ct} , f_r and f_c' are in MPa and $a = 0.62$ for normal weight concrete and 0.47 for light weight concrete. The CEB-FIP Model Code (1978) suggests the following expressions:

$$\begin{aligned} f_{ct} &= 0.3(f_c')^{2/3} \\ f_r &= \left(0.6 + \frac{0.4}{\sqrt[4]{h}}\right) f_{ct} \geq f_{ct} \end{aligned} \quad (3.14)$$

where h is the member depth in m.

3.2.3 Concrete Short-Time Deformations

As the stress is applied to the concrete an instantaneous strain will take place. The stress-strain relation for the concrete is shown in Fig. 3.4(a).

3.2.4 Concrete Long-Time Deformations, Creep and Shrinkage

Concrete exhibits two main phenomenon of volume change which may cause stresses, cracking, or deflections. These are creep (or creep recovery) and shrinkage (or swelling) and both are time-dependent phenomena. In short, both creep and shrinkage strains in concrete are assumed to be related mainly to the removal of adsorbed water from the hydrated cement paste. The difference is that in one case a sustained applied stress is the driving force, creep, while in the other it is a differential relative humidity between the concrete and the environment, shrinkage. Therefore, one of the most important assumptions in studying the deformations of concrete is that the total uniaxial strain in concrete under sustained stress at any time may be considered as being composed of instantaneous strain and time-dependent strain.

3.2.4.1 Creep

Creep is defined as the increase in strain under a sustained stress, Fig. 3.1. After the application of load the strain increases with time due to creep at a decreasing rate. There are many factors influencing the creep of concrete, some of these factors are: 1) age at loading, creep in a member loaded at an early age is higher than creep in a member loaded at a later age, 2) intensity of stress, creep increases with an increase in applied stress, 3) compressive strength, gain of strength with time causes decrease in creep, 4) time under loading, longer time under loading causes higher creep, 5) member size, creep decreases with an increase in the volume/surface ratio, 6) aggregate content, creep decreases with an increase in the modulus of elasticity of the aggregate, 7) relative humidity, creep is higher for lower relative humidity, and 8) ambient temperature, creep

increases proportionally to the temperature ranging from 10°C to 60°C (Johansen and Best, 1962). A typical strain-time relationship for a specimen subjected to a sustained stress (Fig. 3.1a) is shown in Fig. 3.1b.

The creep at time t due to a stress $\sigma_c(t_o)$ applied at time t_o is given by:

$$\epsilon_{cr}(t, t_o) = \phi(t, t_o) \frac{\sigma_c(t_o)}{E_c(t_o)} \quad (3.15)$$

In this study, the creep at time t due to a stress $\sigma_c(t_o)$ applied at time t_o is expressed, based on the stress-strain equation by Hognestad (1951), as follows:

$$\epsilon(t) = \frac{\left(\frac{1.7f'_c(t_o)}{\epsilon_o(t_o)} \right) - \sqrt{\left(\frac{1.7f'_c(t_o)}{\epsilon_o(t_o)} \right)^2 - \left(\frac{3.4f'_c(t_o)}{\epsilon_o^2(t_o)} \right) \sigma(t_o)}}{\left(\frac{1.7f'_c(t_o)}{\epsilon_o^2(t_o)} \right)} \phi(t, t_o) \quad (3.16)$$

and

$$\epsilon(t) = \left(\epsilon_o(t_o) + \left(\frac{\epsilon_{cu} - \epsilon_o(t_o)}{0.15} \right) \left(1 - \frac{\sigma(t_o)}{0.85(f'_c(t_o))} \right) \right) \phi(t, t_o) \quad (3.17)$$

where $\phi(t, t_o)$ is the creep coefficient, defined as the ratio of the creep during the period ($t - t_o$) to the instantaneous strain at t_o .

The relationships recommended by the ACI Committee 209 and the CEB-FIP Code for predicting the creep coefficient ϕ are briefly described below.

(a) *ACI Committee 209 (1992):*

For the prediction of the creep coefficient ϕ at any time t for age at loading t_o , the ACI Committee 209 recommends the following equation to be used:

$$\phi(t, t_o) = \frac{(t - t_o)^{0.6}}{10 + (t - t_o)^{0.6}} \phi_u \quad (3.18)$$

where $\phi = \phi(t_\infty, t_o)$ is the ultimate creep coefficient defined as the ratio of creep after a very long time (10 000 days) for age t_o at loading. The value ϕ_u is given by:

$$\phi_u = 2.35\gamma_c \quad (3.19)$$

where γ_c is a correction factor, the product of several multipliers depending upon ambient relative humidity, average thickness of the member or its volume-to-surface ratio, and on the temperature. For relative humidity of 40%, average thickness 6 in (0.15m) or volume-to-surface ratio of 1.5 in and temperature 70 °F (21 °C), all the multipliers are equal to unity. In this case, γ_c may be calculated as a function of the age at loading t_o :

$$\begin{aligned} \gamma_c &= 1.25t_o^{-0.118} \\ \gamma_c &= 1.113t_o^{-0.094} \end{aligned} \quad (3.20)$$

These two equations are applicable for moist-cured concrete and for 1-3 days steam-cured concrete, respectively. The two equations give $\gamma_c \cong 1.0$ when $t_o=7$ and 3 days, respectively.

(b) *CEB-FIP Model Code 1990 (MC-90)*:

The creep coefficient ϕ_{CEB} adopted by MC-90 is given as: $\phi_{\text{CEB}} = \phi_o \beta_c (t - t_o)$ where β_c is a coefficient describing the development of creep with time after loading; ϕ_o is a notional creep coefficient given by:

$$\phi_o = \phi_{RH} \beta(f_{cm}) \beta(t_o)$$

$$\phi_{RH} = 1 + \frac{1 - (RH/100)}{0.46(h_o/h_{ref})^{1/3}} \quad (3.21)$$

where $h_{ref} = 100\text{mm}$.

$$\beta(f_{cm}) = \frac{5.3}{\sqrt{f_{cm}/f_{cmo}}} \quad (3.22)$$

where $f_{cmo} = 10\text{MPa}$ and f_{cm} (MPa) is the mean strength of concrete at age 28 days. The value f_{cm} may be estimated by: $f_{cm} = f_{ck} + 8\text{MPa}$, f_{ck} (MPa) is characteristic compressive strength of cylinders, 150 mm in diameter and 300 mm in height stored in water at 20 °C, and tested at the age of 28 days.

$$\beta(t_o) = \frac{1}{0.1 + t_o^{0.2}} \quad (3.23)$$

The symbol h_o (mm) is the notional size of member defined by:

$$h_o = \frac{2A_c}{u} \quad (3.24)$$

where A_c and u are the area and perimeter in contact with the atmosphere of the cross-section of the considered member.

Development of creep with time is expressed by:

$$\beta_c(t - t_o) = \left(\frac{t - t_o}{\beta_H + t - t_o} \right)^{0.3} \quad (3.25)$$

β_H (mm) is a function of the notional size h_o (mm) and the relative humidity, RH (per cent):

$$\beta_H = \frac{150h_o}{h_{ref}} \left[1 + (0.012RH)^{18} \right]^{0.3} + 250 \leq 1500\text{mm} \quad (3.26)$$

where $h_{ref} = 100\text{mm}$.

The CEB-FIP (1990) recommendations give additional functions to account for the effect of both elevated and reduced temperature and the effect of the type of cement used. When prevailing temperature is higher than 20° C, the effect of temperature on the maturity of concrete is accounted for by using adjusted age t_T in lieu of t_o or t in all the equations presented above. The adjusted age is given by:

$$t_T = \sum_{i=1}^n \left[\Delta t_i \exp \left(13.65 - \frac{4000}{273 + T(\Delta T_i)} \right) \right] \quad (3.27)$$

where Δt_i is the number of days in which a temperature $T(\Delta t_i)$ prevails for period i .

For the effect of concrete type, the age of concrete at loading t_o , should also be adjusted and given by:

$$t_0 = t_{o,T} \left(\frac{9}{2 + (t_{o,T})^{1.2}} + 1 \right)^\alpha \quad (3.28)$$

where $t_{o,T}$ is the adjusted age of concrete according to Equation 3.27 and α is a coefficient depending on the type of cement and equals to -1, 0, and 0.1 for slowly hardening cement, for normally or rapid hardening cement, and for rapid hardening high strength cement respectively.

3.2.4.2 Shrinkage

Shrinkage of concrete is defined as non-stress and non-thermal produced time-

dependent volume change, Fig. 3.2. Shrinkage is generally considered to arise from loss of water and volume changes or carbonation. Shrinkage is influenced by several factors. The major factors are water/cement ratio, volume of cement, aggregate content, relative humidity, ambient temperature, and member size. Shrinkage generally increases with the increase of water/cement ratio, and decreases with the increase of aggregate volume, size of the member, and ambient relative humidity.

A typical variation of shrinkage with time in an unloaded specimen is shown in Fig. 3.2. As Fig. 3.2 indicates, the shrinkage strain, $\epsilon_{cs}(t)$ increases with time, with the highest rate at early ages, and tends asymptotically towards a final maximum value called ultimate shrinkage strain $(\epsilon_{cs})_u$. The shrinkage strain $\epsilon_{cs}(t)$ at any time t is generally related to the ultimate shrinkage strain $(\epsilon_{cs})_u$ by a time function.

The recommendations of the ACI Committee 209 and of the CEB-FIP Code for predicting the magnitude of shrinkage and its variation with time are summarized below.

(a) *ACI Committee 209 (1992)*:

The free shrinkage which occurs between the end of the curing period, t_0 , and any time t is given by:

$$\epsilon_{cs}(t, t_0) = \frac{t - t_0}{a + (t - t_0)} (\epsilon_{cs})_u \quad (3.29)$$

where a is a constant depending on the type of curing; $a = 35$ for moist-cured concrete and $a = 55$ for steam-cured concrete; $(\epsilon_{cs})_u$ is the ultimate free shrinkage occurring after a long time (say 10 000 days) and is given by:

$$(\epsilon_{cs})_u = -780 \times 10^{-6} \gamma_{cs} \quad (3.30)$$

where γ_{cs} is a correction factor, the product of a number of multipliers which depends upon the same factors mentioned above for γ_{cs} . The correction factor $\gamma_{cs} = 1.0$ when the period of initial moist curing is 7 days, the relative humidity of the ambient air is 40%, the average thickness is 6 in (0.15 m) or the volume-to-surface ratio is 1.5 in.

The free shrinkage between any two ages t_0 and t can be calculated as the difference of shrinkage for the periods $(t, 7)$ and $(t_0, 7)$:

$$\varepsilon_{cs}(t, t_0) = \varepsilon_{cs}(t, 7) - \varepsilon_{cs}(t_0, 7) \quad (3.31)$$

(b) *CEB-FIP Model Code 1990 (MC-90)*:

Shrinkage starts at time t_s (days) when curing is stopped. On the other hand, concrete immersed in water at time t_s starts to swell. The shrinkage or swelling at any time t (days) may be estimated by:

$$\varepsilon_{cs}(t, t_s) = \varepsilon_{cso} \beta_s(t, t_s) \quad (3.32)$$

where $\beta_s(t, t_s)$ is a function describing the development of shrinkage/swelling with time, given by:

$$\beta_s(t, t_s) = \left(\frac{t - t_s}{350(h_o/h_{ref})^2 + t - t_s} \right) \quad (3.33)$$

where h_o (mm) is the notional size defined by Equation 3.24 and $h_{ref} = 100\text{mm}$. ε_{cso} is the notional shrinkage given by:

$$\varepsilon_{cso} = \varepsilon_c(f_{cm}) \beta_{RH} \quad (3.34)$$

where

$$\varepsilon_c(f_{cm}) = 10^{-6} [160 + 10\beta_{sc}(9 - f_{cm}/f_{cmo})] \quad (3.35)$$

with β_{sc} equalling 4, 5, or 8, respectively, for slowly hardening cements, for normal or rapidly hardening high-strength cements; $f_{cmo} = 10$ MPa.

$$\beta_{RH} = -1.55 \left[1 - \left(\frac{RH}{100} \right)^3 \right] \quad \text{for } 40\% \leq RH < 99\% \quad (3.36)$$

$$\beta_{RH} = +0.25 \text{ for } RH \geq 99\% \text{ (soaked in water)}. \quad (3.37)$$

Positive β_{RH} indicates swelling and RH (per cent) is relative humidity.

3.3 Steel Reinforcement

The properties of prestressed and nonprestressed steels that are of direct use in design are the yield strength, f_{py} or f_y and the modulus of elasticity, E_{ps} or E_{ns} . The tensile strength, f_{pu} of the prestressed steel is also required in the design. The yield strength of prestressing steel is usually in the range of 0.85-0.9 f_{pu} . The modulus of elasticity of the nonprestressing steel varies little and is generally taken as 200 GPa for all steel types, whereas for the prestressing steel, the modulus varies depending on the type of steel, e.g. wires versus bars, and may be as low as 180 GPa.

3.3.1 Reinforcing Steel

The stress-strain relationship of structural steel is well established and easily

reproducible. Structural steel has the same stress-strain relationship in compression and tension. In general, the stress-strain curve exhibits a marked yield point, a plastic range, and a strain hardening range which is sufficient to define its properties in the analysis of reinforced concrete structures.

In this study, the model used is a bilinear relation as shown in Fig. 3.4 (b) and it is the same for both tension and compression. Two different material states can be identified in the stress-strain curve:

1- Linear elastic, stress and strain are proportional up to the yield stage: $\sigma_s = E_s \varepsilon_s$

where E_s is the modulus of elasticity in the primary tension or compression.

2- Yielded: $\sigma_s = \sigma_y + E_{sh}(\varepsilon_s - \varepsilon_y)$

where E_{sh} is the strain hardening modulus after yielding, σ_y and ε_y are yielding stress and yielding strain respectively.

3.3.2 Prestressing Steel

Besides a large difference in the magnitude of the tensile strength, the stress-strain curve of prestressing steel is different from that of reinforcing steel in that there is no definite yield plateau for prestressing steel. To accommodate this different shape, the stress-strain relationship given by Naaman (1990) is adopted for prestressing steel in this study, Fig. 3.4 (c). Since prestressing steel is never subjected to compressive stress, the compressive stress-strain is not considered.

An important characteristics of prestressed steel and which is of concern in the analysis of the time-dependent behaviour is the relaxation in stress with time. Relaxation is a phenomenon similar to creep and is defined as the decrease in stress with time under

constant strain. Relaxation of prestressed steel is usually determined experimentally and it is termed as *intrinsic relaxation*. Intrinsic relaxation increases quickly as the initial stress in steel approaches its strength. The amount of intrinsic relaxation depends on the type of steel, temperature, and on the initial stress level in steel. The PCI Committee on Prestressed Losses (1975) recommends the following equation:

$$\Delta\sigma_{pr}(t, t_o) = -\frac{1}{k}\sigma_{ps0}\left(\frac{\sigma_{ps0}}{f_{py}} - 0.55\right)\log\left(\frac{t}{t_o}\right)$$

with $\frac{\sigma_{ps0}}{f_{py}} \geq 0.6$ (3.38)

where $\Delta\sigma_{pr}(t, t_o)$ is the intrinsic relaxation at time t in a tendon initially tensioned at t_o by a stress σ_{ps0} ; the time here is in hours and t_o is not less than 1 hour; f_{py} is the yield strength of steel; k is a constant depending on the type of steel ($=10$ and 45 for stress-relieved and low-relaxation steels, respectively).

Another expression is suggested by Ghali and Treviño (1985) based on experimental values given in *CEB-FIP Model Code (1978)* and the FIP report on prestressing steel (1976). The expression can be written as:

$$\Delta\sigma_{pr}(t, t_o) = -k\eta_t\sigma_{ps0}\left(\frac{\sigma_{ps0}}{f_{py}} - 0.55\right)^2$$

with $\frac{\sigma_{ps0}}{f_{py}} > 0.4$ (3.39)

where k is a constant depending on the steel type ($=1.5$ and $2/3$ for stress-relieved and low-relaxation steels, respectively); η_t is a dimensionless coefficient depending on the length of period $(t-t_o)$ and is given by:

$$\begin{aligned}
\eta_t &= \frac{1}{16} \ln \left(\frac{t-t_o}{10} + 1 \right) & \text{for } 0 \leq (t-t_o) \leq 1000 \\
\eta_t &= \left(\frac{t-t_o}{0.5 \times 10^6} \right)^{0.2} & \text{for } 1000 < (t-t_o) \leq 0.5 \times 10^6 \\
\eta_t &= 1 & \text{for } (t-t_o) > 0.5 \times 10^6
\end{aligned} \tag{3.40}$$

In a prestressed concrete member, the prestressing steel commonly experiences a constantly dropping level of stress and its length shortens continuously with time due to the effects of creep and shrinkage of concrete. Thus, the actual relaxation is expected to be smaller than the intrinsic value. Therefore, a *reduced relaxation* value should be used in design. The reduced relaxation value to be used in the calculation of loss of prestress in concrete structure can be expressed as (Ghali and Treviño, 1985):

$$\Delta \bar{\sigma}_{pr} = \chi_r \Delta \sigma_{pr} \tag{3.41}$$

where $\Delta \sigma_{pr}$ is the intrinsic relaxation and χ_r is a dimensionless coefficient given by:

$$\chi_r = e^{(-6.7 + 5.3\lambda)\Omega} \tag{3.42}$$

with λ being the ratio of the initial stress, σ_{ps0} , in the tendon to its tensile strength, f_{pu} , and:

$$\Omega = -\frac{\Delta \sigma_{ps} - \Delta \sigma_{pr}}{\sigma_{ps0}} \tag{3.43}$$

where $\Delta \sigma_{ps}$ is the change in the stress in the prestressing steel due to the combined effects of creep, shrinkage, and relaxation, and $\Delta \sigma_{pr}$ is the intrinsic relaxation as would occur in a constant-length relaxation test. The value of the total loss is not known a priori because it depends on the reduced relaxation. Iteration is required here: the total loss is calculated

using an estimated value of the reduction factor, $\lambda_r = 0.7$.

The value of the χ_r can be obtained from Table 2 or Fig. 3.5. The graph gives the value of χ_r as a function of λ , the ratio of the initial stress in the tendon to its tensile strength.

3.4 Comparison Between Prediction Models

Fig. 3.6 and 3.7 show a comparison between the CEB-FIP and ACI prediction models for elasticity modulus, creep coefficient, and shrinkage strain. The creep coefficients plotted in Fig. 3.6 for ages at load application of 3, 28, 120, 365, and 1400 days. As Fig. 3.6 indicates, creep and shrinkage values estimated by the two models differ considerably, particularly for concrete loaded at early ages. This difference can have a significant effect on the analytical results of structures constructed in stages. Similar observations were made by El-Badry and Ghali (1989) when comparing the CEB-FIP (1978) model and ACI (1982) model.

3.5 Tension Stiffening Effects

Primary cracks develop when concrete reaches its tensile strength. In the presence of reinforcing steel, the concrete between cracks is still capable of sustaining additional tensile stresses due to the bond between steel and concrete. This phenomenon is known as tension stiffening. As load is increased, the bond between steel and concrete degenerates until concrete can no longer sustain additional tensile stresses. Fig. 3.8 shows the stress distribution in a uniaxial reinforced concrete specimen. At the crack locations the steel resists the entire tensile force while concrete in tension is only effective between cracks.

A method to account for tension stiffening used by Scanlon (1971) and modified by Lin (1973) lumps the tension stiffening in concrete by including an unloading branch for the concrete in tension. This is depicted graphically in Fig. 3.9a and 3.9b. Another method to include the effect of tension stiffening lumps the effect in steel. In this approach, depicted in Fig. 3.9c, the stiffness of the steel is increased after cracking has occurred. This was used by Van Greunen, (1979) and Chan (1982).

In the present study, the tension stiffening is included by a linear branch on the tension side of the concrete stress-strain curve. This is depicted graphically in Fig. 3.9d.

3.6 Concrete Under Variable Stress

Creep of concrete under variable stress conditions makes the time-dependent analysis more complex. Several approximate methods have been suggested to simplify the analysis. The most commonly used methods are the effective modulus method by Faber (1927), the rate of creep method by Glanville (1930), the method of superposition by McHenry (1943), the rate of flow method by England and Illiston (1965) where creep was divided first into three components, namely, elastic creep, delayed elastic and flow creep, and Trost's approach (1967) of strain history which was later modified by Bazant (1972) in his method known as the "age-adjusted effective modulus method". All methods are based on the assumption that creep is proportional to the applied stress.

Among the various methods, the superposition of creep (the step-by-step method) and the age-adjusted effective modulus method have been shown to predict creep of concrete most closely. The two methods will be utilized in the analysis of time-dependent stresses and strains; therefore, a brief discussion of them is given below.

3.6.1 Step-by-Step Method

For the analysis under varying stress, numerical solutions are desirable. Step-by-step method proved to be the most efficient. Such a procedure is completely general and can be used with any creep function and any prescribed stress and strain relationship that vary in an arbitrary fashion. The step-by-step analysis can be used to calculate the strain at any time when the stress history is prescribed or to predict the stress if the variation of strain is known.

Assume that the stress in concrete varies over a period of time between t_o and t . For the purpose of the analysis, the period $(t-t_o)$ is divided into a number of time intervals whose length should increase with the age of concrete. For best results, under continuously varying stress, the time intervals Δt_i should be chosen such that their lengths are approximately equal on the log-time scale (Bazant, 1972). Assume that the stress is divided into increments introduced simultaneously at the middle of the intervals. Then the strain at time $t_{i+0.5}$ is expressed as:

$$\epsilon_c(t_{i+0.5}) = \sum_{j=1}^i \frac{\Delta \sigma_j}{E_c(t_j)} [1 + \phi(t_{i+0.5}, t_j)] \quad (3.44)$$

where t_j is the middle of the interval j and $\Delta \sigma_j$ is the stress increment applied at t_j . Equation 3.44 can be written as:

$$\epsilon_c(t_{i+0.5}) = \frac{\Delta \sigma_i}{E_c(t_i)} [1 + \phi(t_{i+0.5}, t_i)] + \sum_{j=1}^{i-1} \frac{\Delta \sigma_j}{E_c(t_j)} [1 + \phi(t_{i+0.5}, t_j)] \quad (3.45)$$

Thus,

$$\Delta \sigma_i = \frac{E_c(t_i)}{1 + \phi(t_{i+0.5}, t_i)} \left(\epsilon_c(t_{i+0.5}) - \sum_{j=1}^{i-1} \frac{\Delta \sigma_j}{E_c(t_j)} [1 + \phi(t_{i+0.5}, t_j)] \right) \quad (3.46)$$

which can be used when the strain history is known to determine the stress $\sigma_{(t+0.5)}$ at the end of interval i from the stress increments calculated for all the previous intervals, noting that:

$$\sigma_c(t_i + 0.5) = \sigma_c(t_i - 0.5) + \Delta\sigma_i \quad (3.47)$$

where $(t_i - 0.5)$ is the beginning of interval i . Successive applications of Equations 3.45 to 3.47 for each time interval gives the variation of the stress with time.

The step-by-step analysis just described has been the basis of a number of computer programs developed by several researchers to study the behaviour of different structures under the time-dependent effects of creep, shrinkage, and relaxation.

In this study the equations 3.44 to 3.47 are modified to accommodate for the material nonlinearity in a manner similar to the modifications shown in equations 3.16 and 3.17, i.e.:

$$\varepsilon(t_{i+0.5}) = \sum_{j=1}^i \frac{\left(\frac{1.7f'_c(t_o)}{\varepsilon_o(t_o)} \right) - \sqrt{\left(\frac{1.7f'_c(t_o)}{\varepsilon_o(t_o)} \right)^2 - \left(\frac{3.4f'_c(t_o)}{\varepsilon_o^2(t_o)} \right) \sigma(t_o)}}{\left(\frac{1.7f'_c(t_o)}{\varepsilon_o^2(t_o)} \right)} [1 + \phi(t_{i+0.5}, t_j)] \quad (3.48)$$

and

$$\varepsilon(t_{i+0.5}) = \sum_{j=1}^i \left(\varepsilon_o(t_o) + \left(\frac{\varepsilon_{cu} - \varepsilon_o(t_o)}{0.15} \right) \left(1 - \frac{\sigma(t_o)}{0.85(f'_c(t_o))} \right) \right) [1 + \phi(t_{i+0.5}, t_j)] \quad (3.49)$$

3.7 Nonlinear Problems

In reinforced concrete structures nonlinearities occur in two different forms. The first is *material or physical nonlinearity* which results from nonlinear constitutive laws, cracking

of concrete, and/or yielding of steel. The second is *geometric nonlinearity* which derives from large displacements or finite changes in the geometry of the deforming member due to the presence of large axial forces.

3.8 Basic Nonlinear Solution Techniques

The solution of nonlinear problems is usually attempted by one of three basic techniques: *incremental* or *stepwise procedures*, *iterative* or *Newton methods*, and *step-iterative* or *mixed procedures*. The nonlinear equilibrium equation of a member is:

$$[S]\{D\} = \{F\} \quad (3.50)$$

where the nonlinearity occurs in the stiffness matrix $[S]$, which is a function of nonlinear material properties.

3.8.1 Incremental Techniques

The basis of the incremental or stepwise procedure is the subdivision of the load into a number of load increments $\{\Delta F\}_1, \{\Delta F\}_2, \dots, \{\Delta F\}_n$. The total effective load is then given by:

$$\{F\} = \sum_{i=1}^n \{\Delta F\}_i \quad (3.51)$$

In general, these load increments need not be of equal magnitude. The load is applied one increment at a time, and during the increment, the equations are assumed to be linear. $[S]_i$ is assumed fixed throughout each increment but may take different values during different load increments. The solution of the linear equations of the *i*th step of loading is obtained as an increment of the displacement $\{\Delta D\}_i$ where a fixed value of

stiffness matrix $[S]_{i-1}$ evaluated at the end of previous increment ($i-1$) is used:

$$[S]_{i-1} \{\Delta D\}_i = \{\Delta F\}_i \quad (3.52)$$

and where $[S]_0$ is the initial value of the stiffness matrix computed from the material properties at the start of the loading (zero load). The total load and displacement vectors at the end of the i th loading step is given by:

$$\begin{aligned} \{F\}_i &= \sum_{j=1}^i \{\Delta F\}_j \\ \{D\}_i &= \sum_{j=1}^i \{\Delta D\}_j \end{aligned} \quad (3.53)$$

These displacement increments are accumulated to give the total displacements at any stage of loading, and the incremental process is repeated until the total load has been reached. The incremental procedure approximates the nonlinear problem as a series of linear problems so the nonlinearity is treated as *piecewise linear*. The procedure is illustrated schematically in Fig. 3.10 where it can be seen that the results obtained in the successive load steps tend to drift increasingly away from the true solution. To increase the accuracy, smaller load increments may be used.

3.8.2 Iterative Techniques

In iterative techniques, the structure is fully loaded and iterations are performed until equilibrium is satisfied to a certain degree of accuracy. In each iteration, equilibrium is not necessarily satisfied since an approximated constant value of the stiffness matrix is used. Therefore, the portion of the total load that is not balanced, which represents the

discrepancy from equilibrium state, is equal to the difference between the external load and the internal resisting load. After each iteration, the unbalanced load is used in the next iteration to compute an additional increment of the displacements using Equation 3.53. This process is repeated until the unbalanced load or the displacement increments are small enough to ignore. The total displacement at the end of any iteration is given by Equation 3.52.

Based on the type of stiffness used in the iterations, the iterative techniques can be classified into two methods: the *tangent stiffness* method and the *initial stiffness* method as shown in Fig. 3.11. Use of the tangent stiffness method generally results in rapid convergence to the true solution with a minimum number of iterations, but requires that the stiffness matrix be updated in the solution of displacement increments in each iterations. The initial stiffness method, on the other hand, requires the largest number of iterations but has the advantage that the same stiffness matrix which was generated in the first iteration can be used for all iterations.

3.8.3 Step-Iterative Techniques

The step(incremental)-iterative techniques utilize a combination of the incremental and iterative techniques to achieve better accuracy. The total load is divided into increments, and for each load increment one of the two iterative techniques is used to perform the iterations. This technique is shown schematically in Fig. 3.12.

3.9 Convergence Criterion

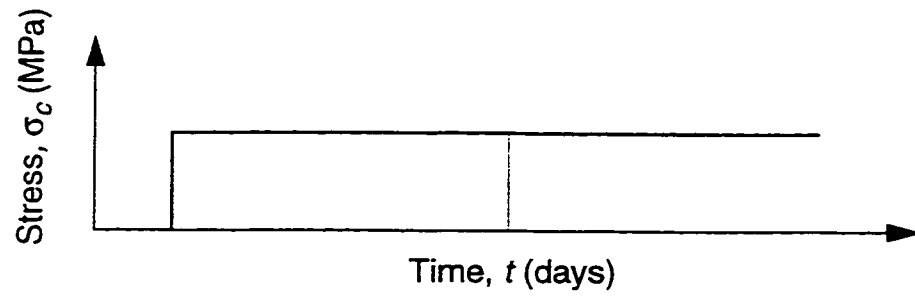
In solving the nonlinear equilibrium equations by iterative methods, the

convergence at the end of an iteration can be measured by two criteria. The first criterion is the magnitude by which equilibrium is violated. This can be measured by the magnitude of the residual (unbalanced) forces. The second criterion is the accuracy of the total displacements. This can be measured by the displacement increments.

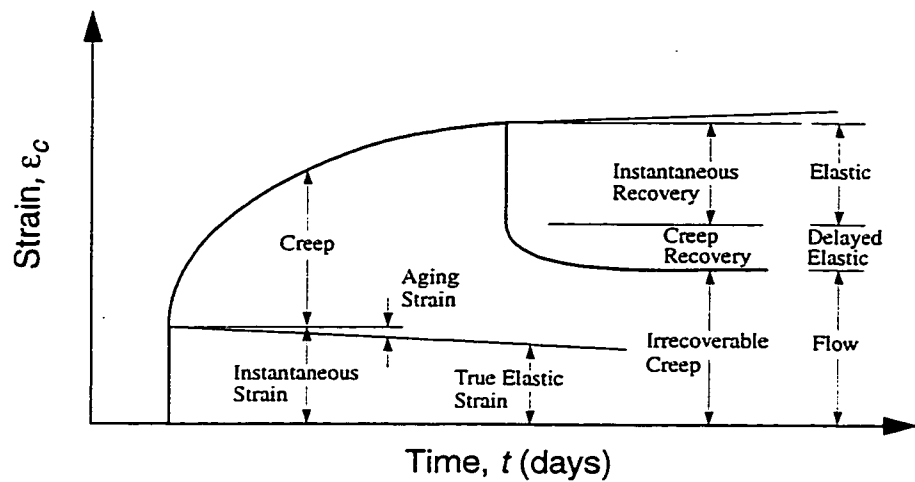
For this study the displacement criterion is used as a primary convergence criterion. But in order to check against equilibrium violation, the unbalanced force criterion is also provided. Two kinds of displacement tolerances are provided for this study. The first is the displacement ratio tolerance and the second is the displacement increment tolerance. A displacement ratio is defined as the ratio between the displacement increment after any iteration and the total displacement after the previous iteration.

In the first procedure, the maximum absolute displacement increments in the global directions at all nodes are determined. In the second procedure, the maximum absolute displacement ratios in the three global directions are determined.

If all components of the displacement increments or ratios are smaller than tolerable value, then convergence is assumed to have occurred and no further iterations are performed. Similar procedure is used in the case of unbalanced force convergence criterion but the force ratios to be used in the second procedure are defined as the ratios of the unbalanced forces after any iteration to the nodal forces applied at the first iteration. It is to be noted that the second procedure is preferable to the first, since it is easier to specify tolerable ratios of displacements or forces than to estimate their absolute values. In addition to the convergence criteria previously described, a maximum number of iterations must also be specified in the input data in order to terminate the iteration procedure in case the specified convergence tolerances are too stringent.



(a) Stress History



(b) Strain-Time Relationship

Fig. 3.1 Creep and Creep Recovery of Concrete

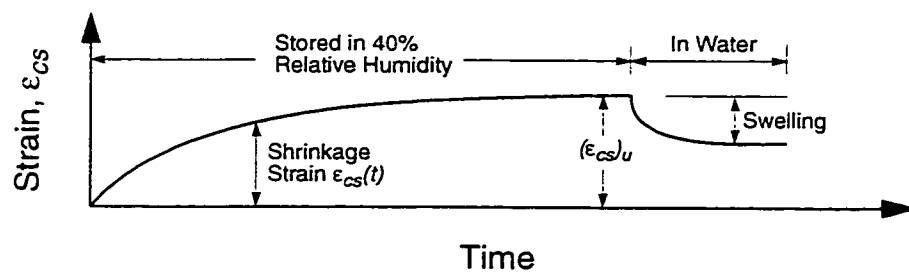


Fig. 3.2 Typical Variation of Shrinkage and Swelling with Time

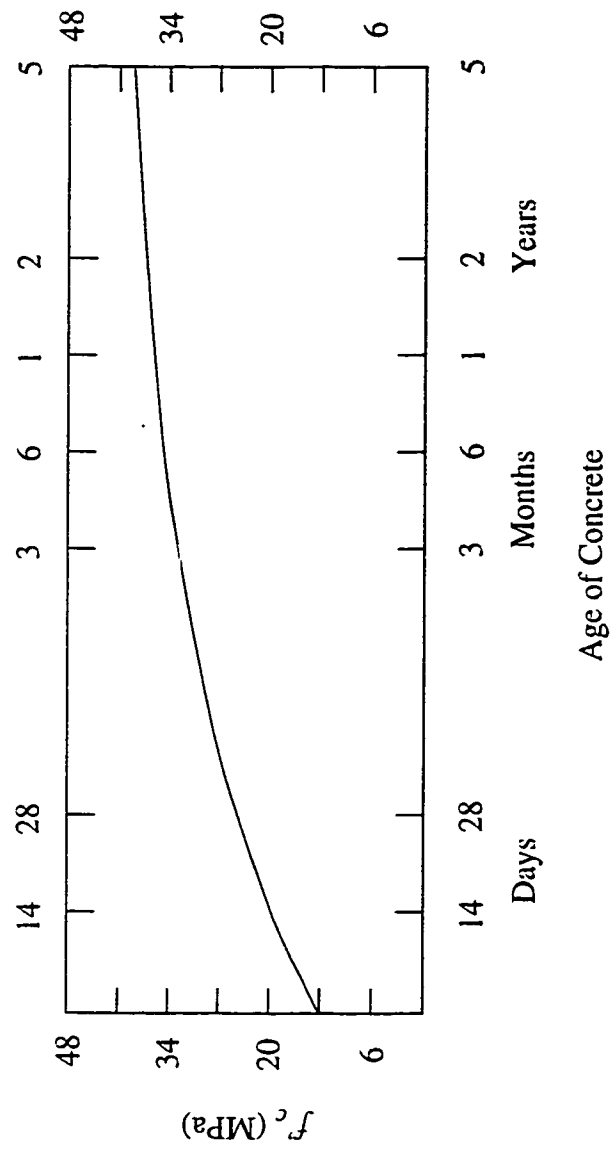


Fig. 3.3 Variation of Compressive Strength With Time

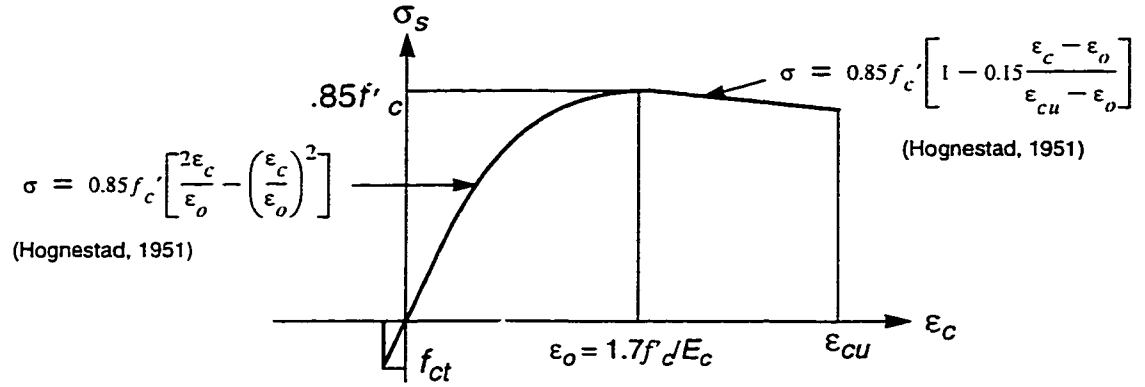


Fig 3.4 (a) Stress-Strain Relationship for Concrete

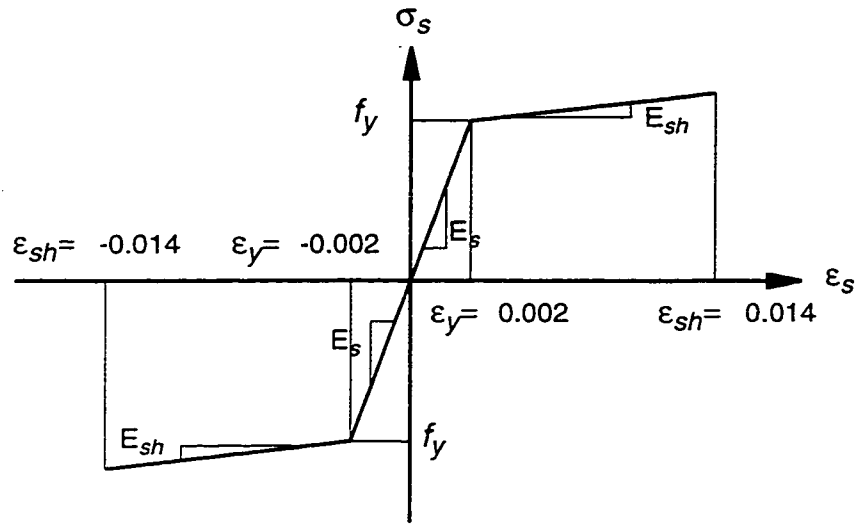


Fig. 3.4 (b) Stress-Strain Relationship for Reinforcing Steel

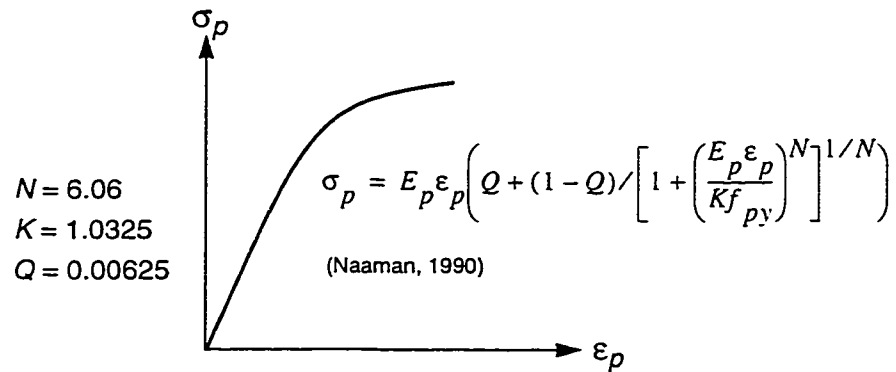


Fig. 3.4 (c) Stress-Strain Relationship for Prestressing Steel

Table 2 Relaxation Reduction Coefficient χ_r

Ω	λ						
	0.55	0.60	0.65	0.70	0.75	0.80	0.80
0.0	1.000	1.000	1.000	1.000	1.000	1.000	1.000
0.1	0.6492	0.6978	0.7282	0.7490	0.7642	0.7757	0.7757
0.2	0.4168	0.4820	0.5259	0.5573	0.5806	0.5987	0.5987
0.3	0.2824	0.3393	0.3832	0.4166	0.4425	0.4630	0.4630
0.4	0.2118	0.2546	0.2897	0.3188	0.3429	0.3627	0.3627
0.5	0.1694	0.2037	0.2318	0.2551	0.2748	0.2917	0.2917

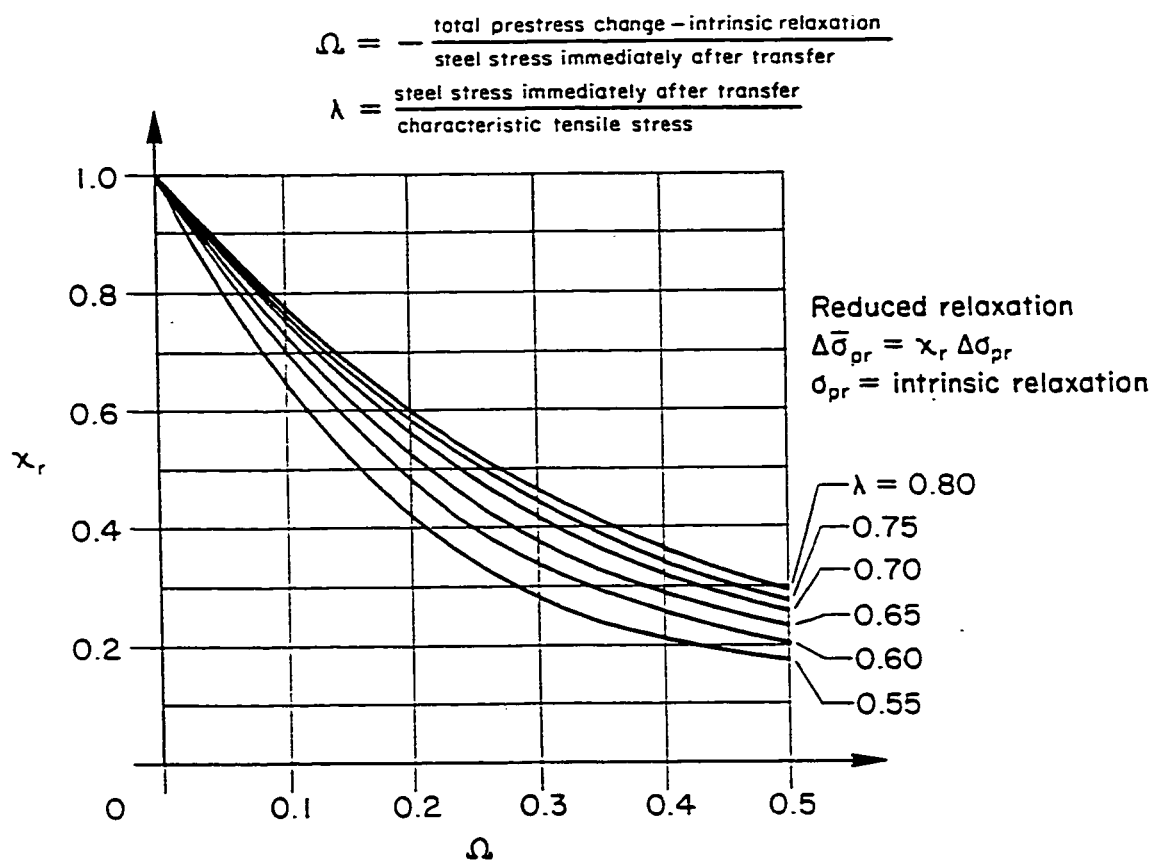


Fig. 3.5 Relaxation Reduction Coefficient χ_r

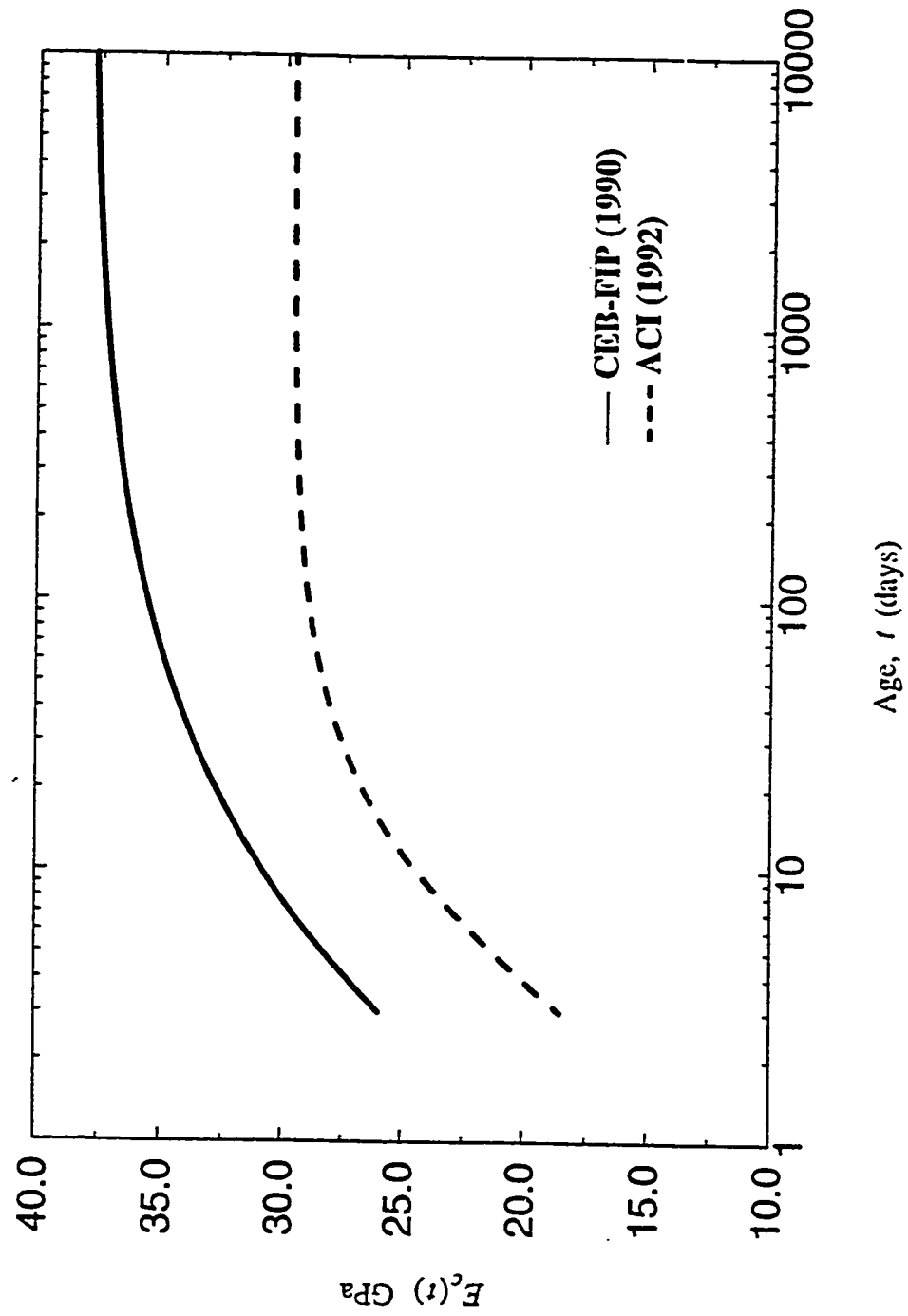
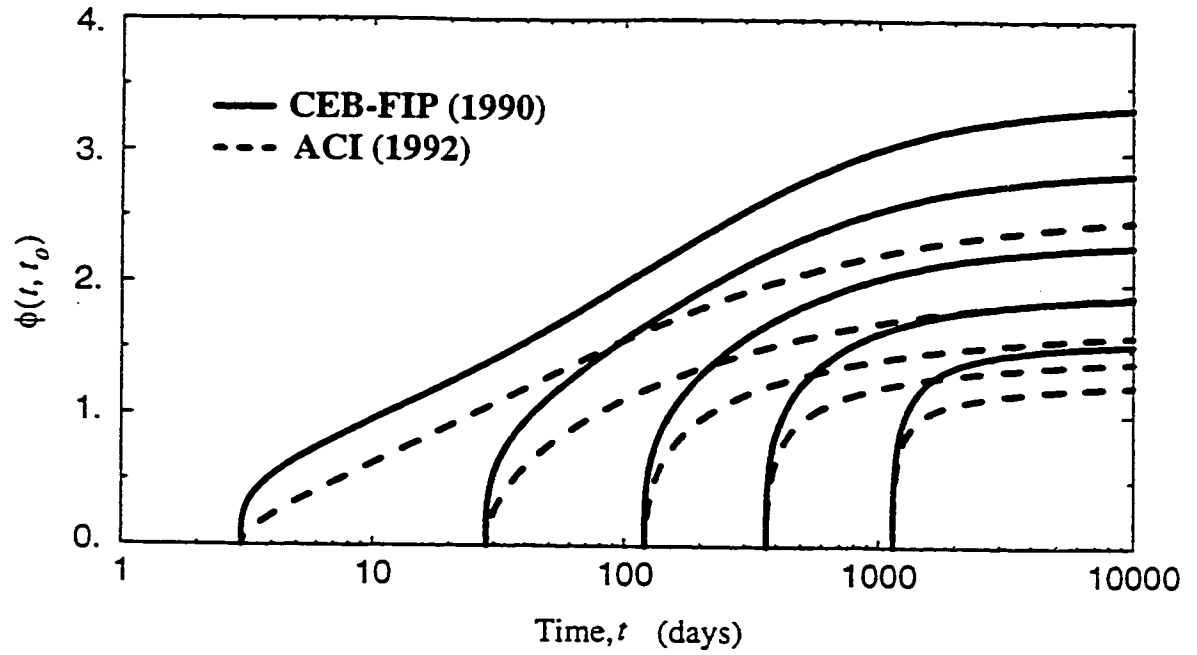
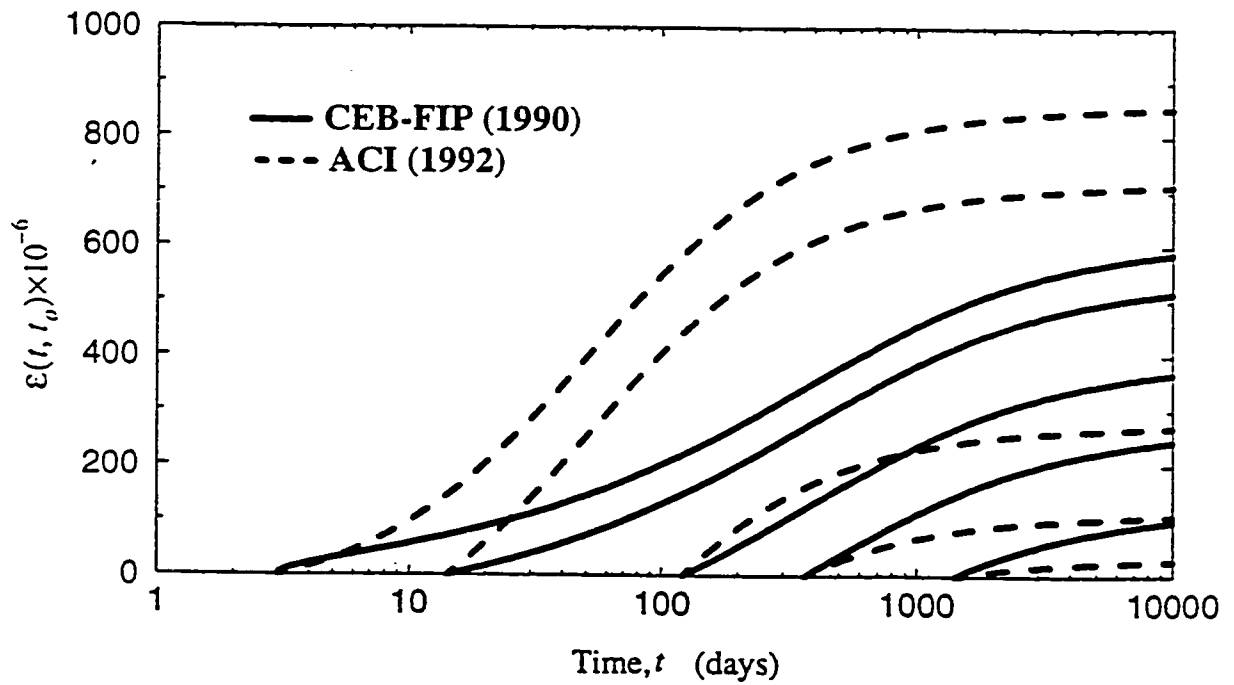


Fig. 3.6 Comparison Between the ACI and CEB Models for Variation of Modulus of Elasticity of Concrete with time



(a) Creep Coefficient



(b) Shrinkage Strain

Fig. 3.7 Comparison Between the ACI and CEB Models for Prediction of Creep Coefficient and Shrinkage Strains (Relative Humidity 40%)

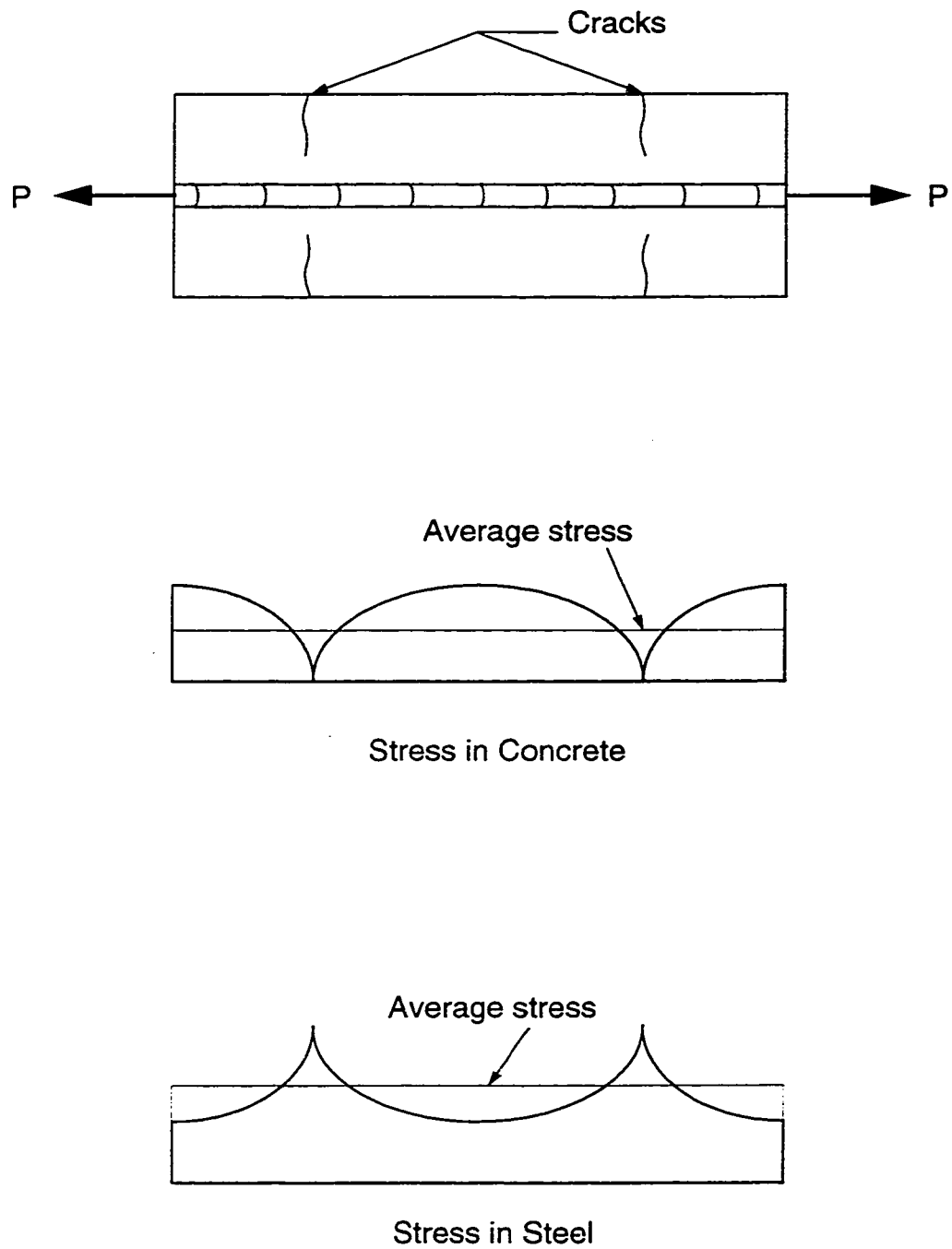


Fig. 3.8 Distribution of Stresses in a Uniaxial Reinforced Concrete Element

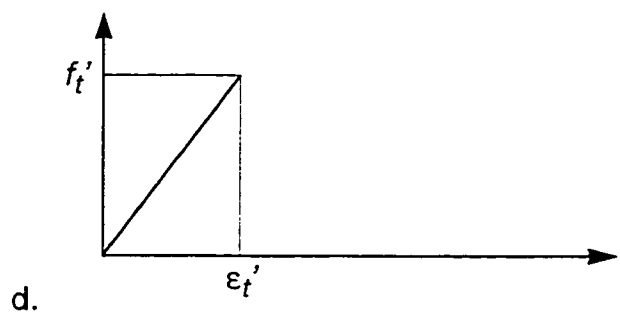
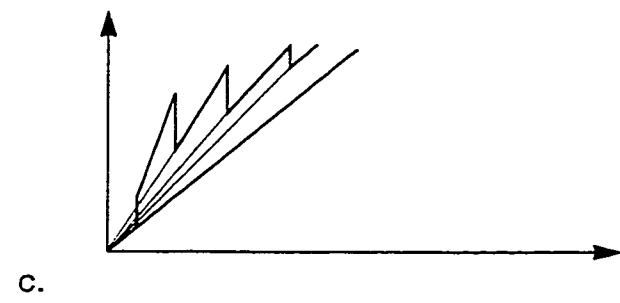
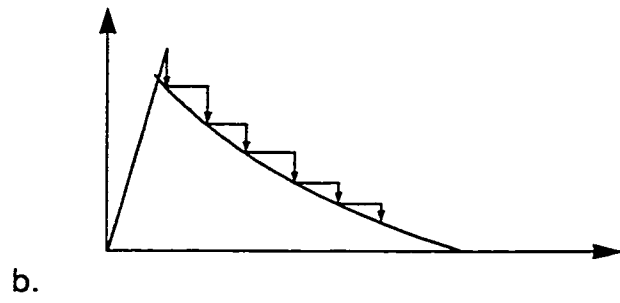
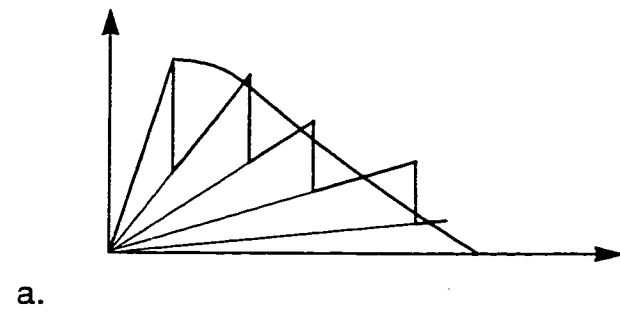


Fig. 3.9 Tension Stiffening Models

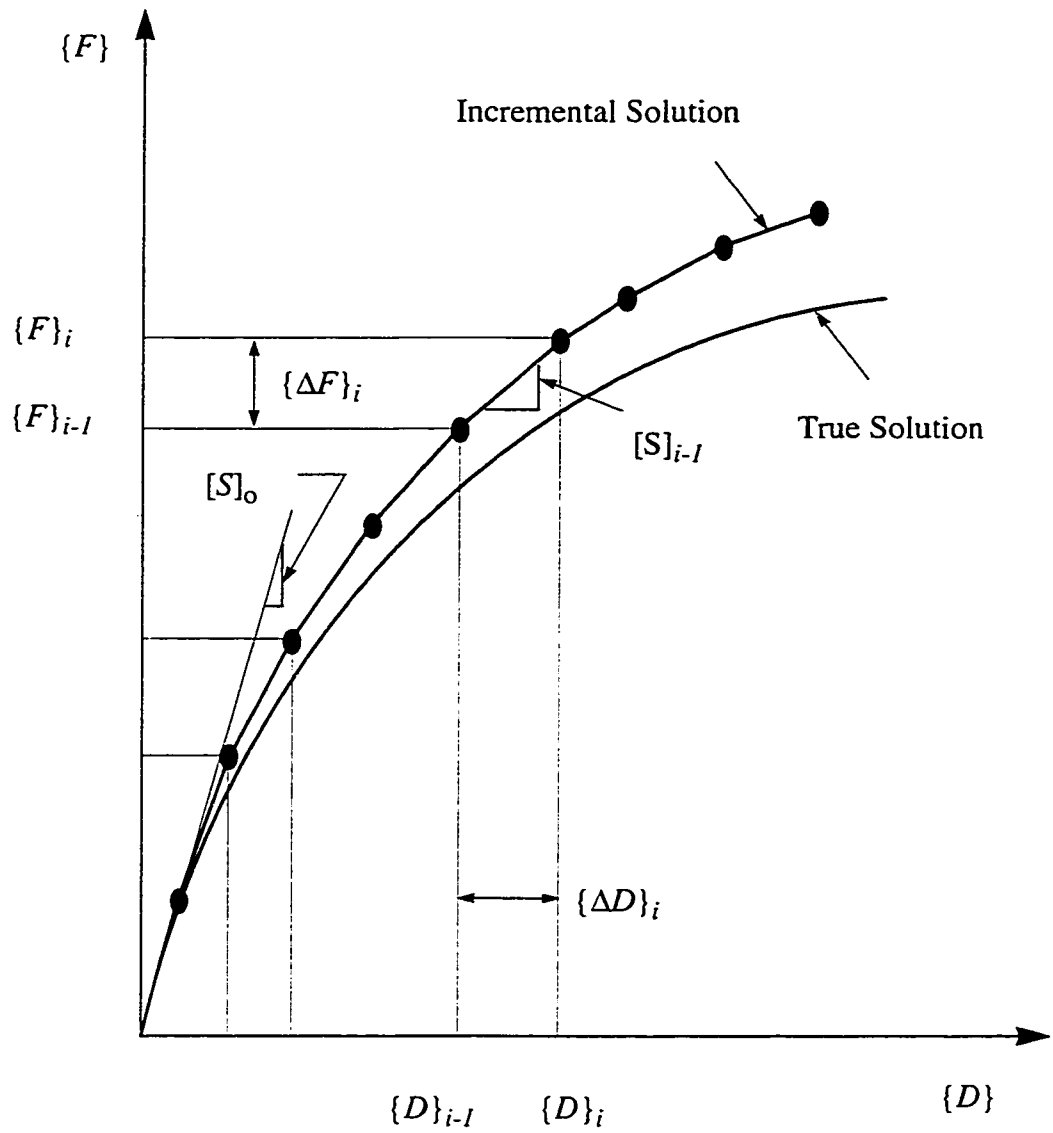


Fig. 3.10 Incremental Techniques

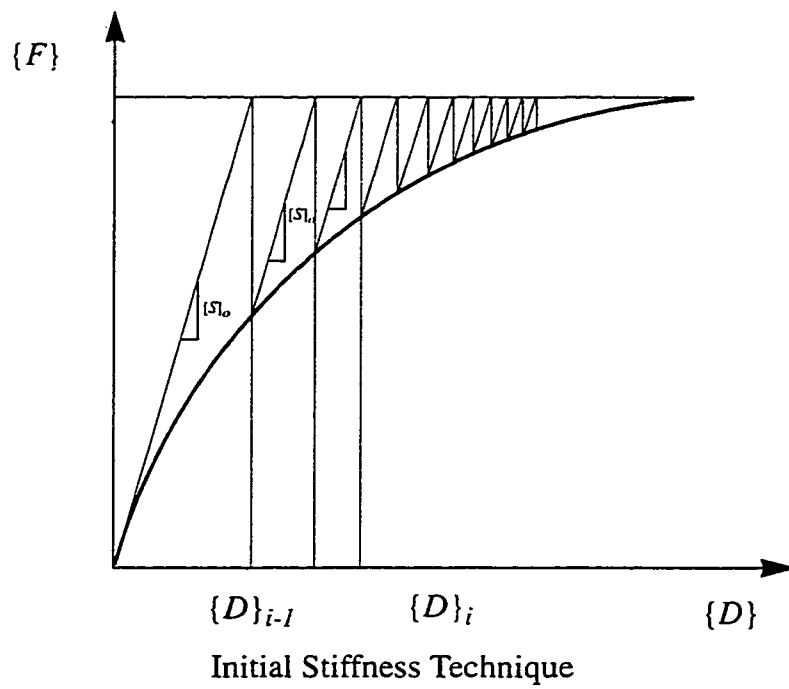
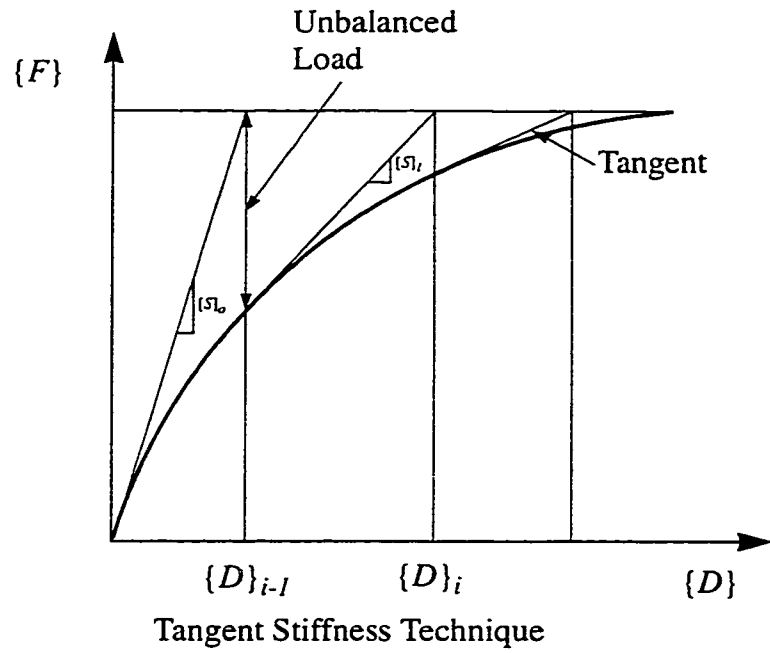


Fig. 3.11 Iterative Techniques

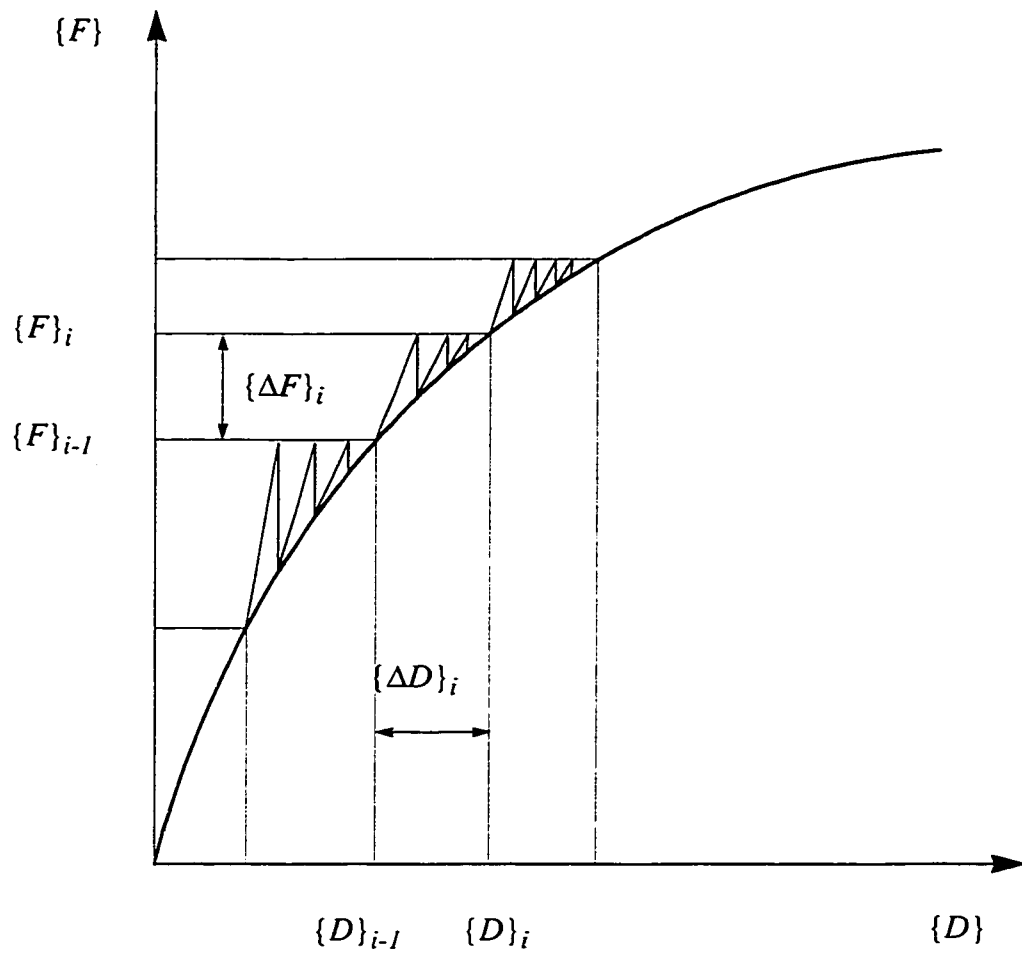


Fig. 3.12 Step-Iterative Techniques

CHAPTER FOUR

SHEAR DEFORMATIONS

4.1. Introduction

Flexure and shear together lead to a biaxial state of stress. This state of stress will produce principal stresses. Cracks will form when the principal tensile stress exceeds the tensile strength of the concrete. The crack will form normal to the direction of the principal tensile stress. In regions of large bending moments and small shear forces (or in the absence of the shear forces), the principal stresses, which are due to flexure, are parallel to the longitudinal axis of the member. The principal stresses at the extreme tensile fibres are responsible for the initiation of flexural cracks perpendicular to the axis of the member. In regions of high shear forces and small bending moments (or in the absence of the bending moments), the principal stresses are inclined to the longitudinal axis of the member. Hence the crack will form in the web and it will be inclined to the member axis. In regions of high moments and high shear forces cracks usually start approximately vertically into the beam due to flexure until a critical combination of flexure and shear stresses develop near the interior end of the cracks. Inclined cracks then develop as an extension of the vertical cracks. After cracking, the entire mechanism of shear resistance is altered drastically and the contributions of the aggregate interlock, dowel action, stirrups, and prestressing steel to the shear resistance of the beam have to be considered. Therefore, when shear stresses are significant, their effects on the flexural deformations must be taken into account.

In this chapter, a simple methodology is described to include the shear effects in the linear analysis of flexural behaviour of uncracked homogenous beams.

4.2. Axial and Flexure Deformation Analysis

The analysis of a reinforced concrete element subjected to axial and flexural loads is founded on the basic assumption of plane sections: A cross section which was plane prior to loading continues to be plane section under loads. This means that the axial, or longitudinal, strains across the section are linearly proportional to the distance from the neutral axis, or any other axis that passes through an arbitrarily chosen reference point within the section. Therefore, the strain distribution can be defined by two variables, i.e. strain at a reference point and curvature. The axial, or longitudinal, stress at any point, which depends on the axial strain at that point, can be computed using the appropriate constitutive relationship of the material. This analysis is used to find the internal forces, namely axial load and bending moment, resulting from a particular axial strain distribution. These loads are the stress resultants which can be determined by integrating the stresses over the cross section.

4.3. Axial, Shear, and Flexure Deformation Analysis

In the previously mentioned analysis, the longitudinal stresses are the principal stresses acting on the cross section. However, when there is a shearing force acting on the section, the principal stresses are no longer parallel to the longitudinal axis of the beam and are inclined to the member axis. The shear stress distribution over the section is not uniform and therefore the principal tensile and compressive stresses change angle of

inclination within the section. To incorporate the effects of shear in the analysis, few models have been developed. The most commonly used models are briefly discussed in the following sections; namely: the *displaced bending moment diagram* using *Variable Angle Truss Model* which was proposed by Park and Paulay (1975), the *Compression Field Theory (CFT)* developed by Mitchell and Collins (1974) and Collins and Mitchell (1978, 1981), and the *Modified Compression Field Theory (MCFT)* introduced by Collins and Mitchell (1985) and Vecchio and Collins (1986)

4.4. Models For Shear Effects

4.4.1 Variable Angle Truss Model

The Variable Angle Truss Model was first introduced by Ritter (1899) who showed that reinforced concrete beam subjected to combined shear and flexure act like a truss with concrete struts in compression and stirrups in tension. Later Morsh (1902) explained the truss mechanism in more detail by implying that the shear is resisted by a continuous field of concrete struts parallel to diagonal cracks, generally at 45° to the beam axis. The flexural concrete compression zone and the flexural reinforcement form the top and bottom chord of the truss. The stirrups form the tension members, neglecting the concrete in tension.

In 1910, the ACI Code adopted the 45° truss model with the assumption that a portion of the total applied shear load is resisted by the tensile strength of the concrete prior to cracking, V_c , while the remainder is resisted by the vertical stirrups, V_s , assuming

that the cracks are inclined at a 45 degree. This model is still used in the current version of the ACI Code with minor modifications.

Park and Paulay (1975) gave a rational methodology to incorporate the effects of shear on the flexural deformations using the *Variable Angle Truss Model*. The authors introduced the concept of the *displaced bending moment diagram*, where they proposed that after the formation of diagonal cracks, the tension force in the flexural reinforcement at sections away from the maximum moment becomes larger than that computed from the bending moment diagram. This increase is largely dependent on the inclination of the cracks, i.e. the inclination of the compressive struts. Based on the Variable Angle Truss Model, Park and Paulay (1975) gave a detailed derivation of the moment increase due to diagonal tensile cracking based on beam action with and without web reinforcement. Figure 4.1 shows the additional moment due to shear for a simply supported beam subjected to a concentrated load at midspan.

To account for the effect of concrete contribution on the force increase in the flexural tensile reinforcement, Park and Pauly (1975) considered beam action of a beam without web reinforcement in which diagonal cracks develop at an angle, α , to the member axis, as shown in Figure 4.2. The moment equilibrium at sections 1 and 2, requires that:

$$M_1 = Tjd = M_2 + V_c jd \cot \alpha \quad (4.1)$$

where M_1 is the moment at section 1, M_2 is the moment at section 2, V_c is the shear force resisted by the concrete, jd is the lever arm between the resultant compressive and tensile forces, and α is the angle of the crack inclination. Solving for T :

$$T = \frac{M_1}{jd} = \frac{M_2}{jd} + V_c \cot \alpha \quad (4.2)$$

this shows that the tension force at section 2, T , is governed by the bending moment at section 1.

Similarly, the tension induced in the flexural reinforcement by the forces associated with a beam with web reinforcement is computed by referring to Figure 4.3.

From the equilibrium of force polygon for joint X , one obtains:

$$V_s = C_d \sin \alpha = T_s \sin \beta \quad (4.3)$$

The spacing between stirrups, s , is:

$$s = jd(\cot \alpha + \cot \beta) \quad (4.4)$$

Taking moment about the compressive force, C' , at section 1 gives the following relation:

$$M'_1 = V_s x = M'_2 + V_s \cot \alpha = T' jd + \frac{s}{2} T_s \sin \beta \quad (4.5)$$

where M'_1 is the moment at section 1, M'_2 is the moment at section 2, V_s is the shear force resisted by the stirrups, T' is the force in the tensile reinforcement, and T_s is the tensile force in the stirrups.

Combining the two mechanisms of the concrete and stirrups at section 2:

$$\begin{aligned} V_x &= V_s + V_c \\ M_x &= M_2 + M'_2 \\ T_x &= T + T' \end{aligned} \quad (4.6)$$

The total tension force in the flexural reinforcement at section 2 is obtained as:

$$T_x = \frac{M_x}{jd} + V_c \cot \alpha + \frac{V_s}{2}(\cot \alpha - \cot \beta) \quad (4.7)$$

$$T_x = \frac{M_x}{jd} + \frac{e_v}{d} V_x$$

where

$$\frac{e_v}{d} = \cot \alpha - \frac{\eta}{2}(\cot \alpha + \cot \beta) \quad (4.8)$$

and

$$\eta = \frac{V_s}{V_x} = \frac{V_x - V_c}{V_x} \quad (4.9)$$

It is evident from Equation (4.7) that after the formation of diagonal cracks, the tension force T_x in the flexural steel becomes greater than that required to resist the external moment at that section.

4.4.2 Compression Field Theory

The compression field theory (CFT) developed by Mitchell and Collins (1974) can be deployed to analyze a beam subjected to shear. In this approach, the shear stresses are assumed to be distributed uniformly over an effective area of b_v wide and d_v deep. The direction of the principal compressive stresses is assumed constant over the entire cross section as shown in Figure 4.4. The CFT also assumes that after cracking the concrete carries no tension and the shear is carried by a field of diagonal compression with angle of inclination to the longitudinal axis given by:

$$(\tan \theta)^2 = \frac{\epsilon_x - \epsilon_2}{\epsilon_t - \epsilon_2} \quad (4.10)$$

where

ϵ_x = longitudinal strain at mid-depth of the web, with tension being considered positive

ϵ_t = transverse strain, with tension being considered positive

ϵ_2 = principal compressive strain, considered to be negative

From Mohr's circle for strain, the principal tensile strain (Fig. 4.5) in the web is determined as:

$$\epsilon_1 = \epsilon_x + \epsilon_t - \epsilon_2 \quad (4.11)$$

and the shear strain in the web:

$$\gamma = 2(\epsilon_x - \epsilon_2) \cot \theta \quad (4.12)$$

If a symmetrically reinforced prestressed concrete beam is subjected to a shear force V , CFT renders a total of five unknowns: the stress in the longitudinal bars, f_x ; the stress in the longitudinal prestressing tendons, f_p ; the stress in the stirrups, f_v , the diagonal compressive stress in the concrete, f_2 ; and the inclination, θ , of the diagonal compressive stresses. These five unknowns can be solved by using three equilibrium equations, two compatibility equations, and the constitutive relationships for the materials with reference to Figure 4.5.

The compressive stress-strain relationship is usually defined from the response of a standard concrete cylinder test. But due to the influence of shear and diagonal cracks, the concrete becomes weaker and softer. The softening of the concrete in the web is accounted

for using the suggested relationship developed by Vecchio and Collins (1986):

$$f_2 = f_{2max} \left[2 \left(\frac{\epsilon_2}{\epsilon'_c} \right) - \left(\frac{\epsilon_2}{\epsilon'_c} \right)^2 \right] \quad (4.13)$$

where

$$\frac{f_{2max}}{f'_c} = \frac{1}{0.8 - 0.34\epsilon_1/\epsilon'_c} \leq 1.0 \quad (4.14)$$

ϵ'_c is the strain at the peak stress f'_c from a standard concrete cylinder compression test and is a negative quantity.

4.4.3 Modified Compression Field Theory

The modified compression field theory (MCFT), developed by Vecchio and Collins (1986), is basically the CFT but with some adjustments. These adjustments are consideration of i) the contribution of the tensile stresses in the concrete between cracks and ii) the contribution of aggregate interlock to shear transfer across the crack.

Vecchio and Collins (1986) recommended that the tensile strength of the cracked concrete be evaluated using the following formula:

$$f_1 = \frac{f_{cr}}{1 + \sqrt{200\epsilon_1}} \quad (4.15)$$

A more conservative expression for f_1 is used by Collins and Mitchell (1987):

$$f_1 = \frac{\alpha_1 \alpha_2 f_{cr}}{1 + \sqrt{500\epsilon}} \quad (4.16)$$

where α_1 and α_2 are factors accounting for the bond characteristics of the reinforcement

and the type of loading. The CFT assumes that the shearing force is transmitted across the crack solely by the reinforcement. In addition to the shear transfer due to the reinforcement, the MCFT accounts for the shear transfer due to aggregate interlock on the crack surface as shown in Figure 4.6. The maximum shear stress on the crack depends on the crack width and the limiting value for the shear that can be transferred across the crack as suggested by Collins and Mitchell (1987) is given by:

$$v_{ci} = \frac{0.18 \sqrt{f'_c}}{0.3 + \frac{24w}{a + 16}} \quad (4.17)$$

where a is the maximum aggregate size. The above expression has been simplified from the expression developed by Vecchio and Collins (1986). The crack width, w , can be taken as the product of the principal tensile strain, ϵ_1 , and the average spacing of the diagonal cracks, $s_{m\theta}$, Fig. 4.7. Thus

$$w = \epsilon_1 s_{m\theta} \quad (4.18)$$

The spacing of the inclined cracks will depend upon the crack control characteristics of both the longitudinal and the transverse reinforcement. It is suggested by Collins and Mitchell (1987) that this spacing be taken as:

$$s_{m\theta} = \frac{1}{\left(\frac{\sin \theta}{s_{mx}} + \frac{\cos \theta}{s_{mv}} \right)} \quad (4.19)$$

where s_{mx} and s_{mv} are the crack spacing indicative of the crack control characteristics of the longitudinal and transverse steel, respectively, see Figure 4.7. Neither s_{mx} or s_{mv} should be taken less than 100 mm.

4.5. Proposed Model to Include the Effects of Shear Deformations in Noncracked Members

4.5.1 General Remarks

The axial and bending deformations are the most commonly considered deformations in finding the deflections. An additional deflection is produced by the effects of shear deformations. When shear deformations are large, their effects must be considered when finding the deflections of the member.

The horizontal shear stresses along any fiber of homogeneous, isotropic, uncracked beam with a rectangular cross section can be easily derived from considerations of internal equilibrium of forces in the axial direction of a free body of an element of length dx , Fig. 4.8. The longitudinal shear stress is:

$$\nu = \frac{VQ}{Ib} \quad (4.20)$$

and

$$Q = \int_{y=y_1}^{y=c} y dA = \frac{1}{2} b (c^2 - y_1^2) \quad (4.21)$$

where V is the total shear force applied at the section, Q is the first moment of area of the segment of the cross-section at which the shear is sought, I is the second moment of inertia of the entire cross-section about the neutral axis, and b is the width of the cross section at which the shear is computed. The horizontal shear stress ν is also the vertical shear stress, because shear stresses on two perpendicular planes must be equal. Substituting Equation (4.21) in Equation (4.20) leads to the following:

$$\nu = \left(\frac{3}{2}\right)\left(\frac{V}{A}\right)\left(1 - \frac{y_1^2}{c^2}\right) \quad (4.22)$$

Equation (4.22) shows that the distribution of shearing stresses in a rectangular cross section is parabolic. As it can be seen from Figure 4.8, the shearing stresses are zero at the top and bottom of the cross section ($y = \pm c$) edges and maximum at the neutral axis ($y = 0$). The shear stress-strain relation for an isotropic material is:

$$\gamma = \frac{1}{G}\nu \quad (4.23)$$

where γ is the shear strain and G is the shear modulus.

Substituting Equation (4.22) into Equation (4.23) results in the following:

$$\gamma = \frac{1}{G}\left(\frac{3}{2}\right)\left(\frac{V}{A}\right)\left(1 - \frac{y_1^2}{c^2}\right) \quad (4.24)$$

Equation (4.24) indicates that the strains due to shearing stresses also change parabolically over the depth of the section. Hence, the shear deformations of a member of rectangular section cause an element of the member of length dx to be deformed as shown in Figure 4.9. The cross sections will become distorted because the shear strains are zero at the top and bottom of the section ($y = \pm c$) edges and maximum at distance $y = 0$. Lines ab and ac in Figure 4.9(a) represents the neutral axis ($y = 0$) of the beam before and after shear deformations have taken place, respectively, and the angle between them, γ_{\max} , is the shear strain. If the vertical sides at points a and b are assumed to remain vertical at points a and c , then the top and bottom edges of the member will be parallel to line ac . The deformation of the element can be easily observed if the shear strain is considered at different levels, y , along the depth and away from the neutral axis. At each level, the shear

stress changes parabolically indicating that the shear strain is less than γ_{\max} . At the outer edges, the shear strain is zero, and hence the edges are at right angles with the sides.

In structural analysis, it is common to consider an average shear stress acting upon the cross section. Therefore, in the current study the shear strain of the a member will be, approximately, considered constant along the depth of the cross section as shown in Figure 4.10. The shear strain is then equal to the average shear stress, v_{ave} , divided by the shear modulus of elasticity, G :

$$\gamma = \frac{1}{G} v_{ave} \quad (4.25)$$

where

$$v_{ave} = \frac{V}{A_r} \quad (4.26)$$

in which V/A_r is the average shear stress obtained by dividing the applied shear force by the reduced cross-sectional area of the member. The reduced area, A_r , is as follows:

$$A_r = \frac{A}{n} \quad (4.27)$$

where A is the cross-sectional area under shear stresses and n is a constant (shear coefficient), which is dependent on the shape of the cross section, to account for the use of an average stress. For a rectangular cross section $n = 1.2$. Substituting Equation (4.27) in Equation (4.26) and Equation (4.26) in Equation (4.25), we get:

$$\gamma = \frac{nV}{GA} \quad (4.28)$$

For an idealized cracked section, the shear flow in the tension zone is constant and

therefore the shear stress in the tension zone is:

$$\nu = \frac{V}{b_w j d} \quad (4.29)$$

4.5.2 The Methodology

A differential element of length dx under the action of a pair of shear forces of magnitude V will experience a shear strain, γ , and deforms as shown in Figure 4.10. The coordinate x and y are the distance along the longitudinal axis of the member and y is the deflection. The shear strain is the angle strain according to the following relationship:

$$\gamma = \frac{dy}{dx} \quad (4.30)$$

Substitution of Equation (4.30) into Equation (4.29) gives:

$$\frac{dy}{dx} = \frac{nV}{GA} \quad (4.31)$$

Recognizing that the shear force varies throughout the length of the member and can be expressed as a function $V(x)$, Equation (4.31) becomes:

$$\frac{dy}{dx} = \frac{nV(x)}{GA} \quad (4.32)$$

Equation (4.32) allows the computation of the slope at any point in a member due to a pure shear force. By integrating Equation (4.32), the deflection at any point in a member can be calculated and as a result, the deflected shape of the member can be obtained as follows:

$$\text{deflection } = y = \int_{x=0}^{x=L} \left(\frac{nV(x)}{GA} \right) dx \quad (4.33)$$

This deflected shape must be superimposed on that produced by any flexural moments applied on the member.

Differentiation of Equation (4.33) once with respect to x , produces the following relationship:

$$\frac{d^2y}{dx^2} = \frac{n}{GA} \frac{dV(x)}{dx} \quad (4.34)$$

From general relationships among varying load, varying shear, and varying flexural moment along the length of the member, it is known that:

$$\begin{aligned} \frac{dM(x)}{dx} &= V(x) \\ \frac{dV(x)}{dx} &= w(x) = \frac{d^2M(x)}{dx^2} \end{aligned} \quad (4.35)$$

where $w(x)$ is the distributed load applied on the member.

Substitution of Equation (4.35) in Equation (4.34) and rearranging terms give:

$$\left(\frac{d^2y}{dx^2} \right)_{shear} = \frac{n}{GA} \frac{d^2M(x)}{dx^2} \quad (4.36)$$

Equation (4.36) is the curvature of any section throughout the length of the member due to pure shear.

It is also known that the curvature due to flexure is given by the following differential equation:

$$\left(\frac{d^2 y}{dx^2}\right)_{flexure} = \frac{M(x)}{EI} \quad (4.37)$$

For the shear deformations to be included in the analysis, the curvature given in Equation (4.37) must be added to the curvature in Equation (4.36). Therefore the total curvature with the shear deformations included is give by:

$$\begin{aligned} \frac{d^2 y}{dx^2} &= \left(\frac{d^2 y}{dx^2}\right)_{flexure} + \left(\frac{d^2 y}{dx^2}\right)_{shear} \\ \frac{d^2 y}{dx^2} &= \frac{M(x)}{EI} + \frac{n}{GA} \frac{d^2 M(x)}{dx^2} \end{aligned} \quad (4.38)$$

For a rectangular cross section of a homogeneous elastic material subjected to a normal force N at an arbitrary reference point and a bending moment M , the analysis can be performed assuming that two parameters, ϵ_o and ψ , define the strain distribution over the section. These two parameters are the longitudinal strain at the reference point and the curvature, respectively. Therefore, the strain at any point in the section is:

$$\epsilon = \epsilon_o + \psi y \quad (4.39)$$

where y is the distance from the reference point to the point at which the strain is required.

Satisfying the equilibrium requirements for N and M in a linear analysis gives the strain, ϵ_o , and the curvature, ψ , as:

$$\epsilon = \frac{IN - BM}{E(A_a I - B^2)} ; \quad \psi = \frac{-BM + A_a M}{E(A_a I - B^2)} \quad (4.40)$$

A_a , B , and I are the transformed area of the cross section under axial strain, its first and second moments about an axis through the reference point. Equations (4.40) can be put in

a matrix format as follows:

$$\begin{bmatrix} \epsilon_o \\ \psi \end{bmatrix} = \frac{1}{E(A_a I - B^2)} \begin{bmatrix} I & -B \\ -B & A_a \end{bmatrix} \begin{bmatrix} N \\ M \end{bmatrix} \quad (4.41)$$

when shear deformations are included in the analysis, Equation (4.41), in accordance with Equation (4.38), becomes:

$$\begin{bmatrix} \epsilon_o \\ \psi \end{bmatrix} = \frac{1}{E(A_a I - B^2)} \begin{bmatrix} I & -B & 0 \\ -B & A_a & \frac{nE(A_a I - B^2)}{GA} \end{bmatrix} \begin{bmatrix} N \\ M \\ \frac{d^2 M(x)}{dx^2} \end{bmatrix} \quad (4.42)$$

For a cracked section, the analysis is the same as before and Equation (4.42) can still be used where now A_a , B , and I are the transformed area of the cracked cross section under axial stresses, its first and second moments about an axis through the reference point and A is the area of the cracked cross section under shear stresses.

4.6 Shear Stresses on a Trapezoidal Cross Section: Reduced Cross Sectional Area

Consider a cross section of trapezoidal shape subjected to nonlinear stress distribution. The constitutive relationship of the material is given by:

$$f_c = 0.85 f'_c \left[\frac{2\epsilon_c}{\epsilon_o} - \left(\frac{\epsilon_c}{\epsilon_o} \right)^2 \right] \quad (4.43)$$

where f'_c is the compressive strength of concrete, ϵ_o is the strain at stress $0.85f'_c$, Hognestad (1951), and ϵ_c is the strain at any stress level f_c . The horizontal shear stresses

along any fiber of homogeneous, isotropic, uncracked beam with a trapezoidal cross section can be easily derived from considerations of internal equilibrium of forces in the axial direction of a free body of an element of length dx . The longitudinal shear stress is:

$$\nu = \frac{1.7 f'_c V Q(y)}{\epsilon_o E_c I b(y)} \quad (4.44)$$

where E_c is the modulus of elasticity of concrete, $Q(y)$ is the first moment of area of the segment of the cross-section at which the shear is sought and it is a function of the cross section depth (y), y is measured from any arbitrary reference point, $b(y)$ is the width of the cross section in terms of (y) where the shear stress is computed, and I is the second moment of inertia of the entire cross-section about an axis through the reference point. $Q(y)$, $b(y)$, and I are given in the following formulae:

$$Q = \int_{y=y}^{y=c} y dA \quad (4.45)$$

$$Q = \frac{1}{d} \left[\frac{b_1 d}{2} (c^2 - y^2) - \frac{b_1 c}{2} (c^2 - y^2) + \frac{b_2 c}{2} (c^2 - y^2) + \frac{b_1}{3} (c^3 - y^3) - \frac{b_2}{3} (c^3 - y^3) \right] \quad (4.46)$$

$$b(y) = \frac{1}{d} (b_1 d - b_1 c + b_2 c + b_1 y - b_2 y) \quad (4.47)$$

$$I = \frac{b_2 d^3}{12} + \frac{(b_1 - b_2) d^3}{36} + d \left[b_2 \left(c - \frac{d}{2} \right)^2 + \left(\frac{b_1 - b_2}{2} \right) \left(c - \frac{d}{3} \right)^2 \right] \quad (4.48)$$

where b_1 and b_2 are the widths of the cross section at the top and bottom respectively, d is the total depth of the cross section, and c is the depth of the reference point from the top.

From the shear strain energy for a differential element of length dl , the reduced

area can be obtained as follows:

$$\Delta U = \frac{1}{2} \int \frac{v^2}{G} dl da$$

$$\Delta U = \frac{1}{2} \int \frac{v^2}{G} dl b(y) dy$$
(4. 49)

Substitution of Equation (4.44) into Equation (4.49) gives:

$$\Delta U = \frac{1}{2G} \int \left(\frac{1.7 f_c V Q(y)}{\epsilon_o E_c I b(y)} \right)^2 dl b(y) dy$$
(4. 50)

and the total shear strain energy is:

$$\Delta U = \frac{1}{2} \int_0^l \frac{V^2}{G A_r} dl$$
(4. 51)

Rearranging Equation (4.50):

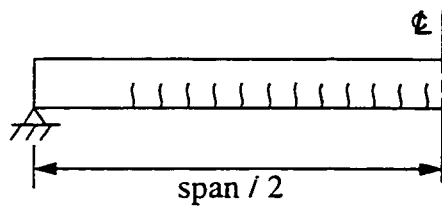
$$\Delta U = \frac{1}{2} \int \frac{V^2}{G} \left(\frac{1.7 f_c Q(y)}{\epsilon_o E_c I b(y)} \right)^2 b(y) dy dl$$

$$\Delta U = \frac{1}{2} \int \frac{V^2}{G} \left(\frac{1.7 f_c Q(y)}{\epsilon_o E_c I} \right)^2 \frac{1}{b(y)} dy dl$$
(4. 52)

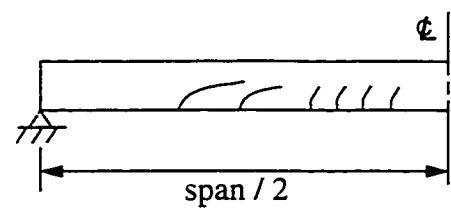
Comparing Equation (4.51) with Equation (4.52) will yield the reduced area as follows:

$$A_r = \int_{y=y_1}^{y=c} \left(\frac{\epsilon_o E_c I}{1.7 f_c Q(y)} \right)^2 b(y) dy$$
(4. 53)

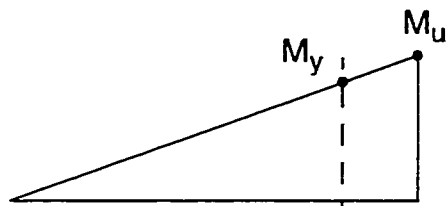
where $Q(y)$, $b(y)$, and I are given in Equations (4.46), (4.47), and (4.48) respectively. For a rectangular cross section, the reduced area A_r is $A/1.2$ where A is the area of the cross section.



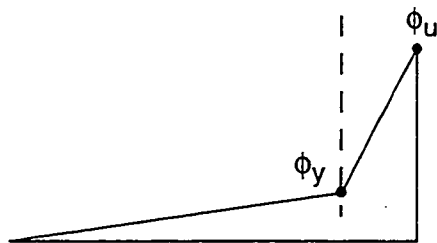
Cracking in beam



Cracking in beam



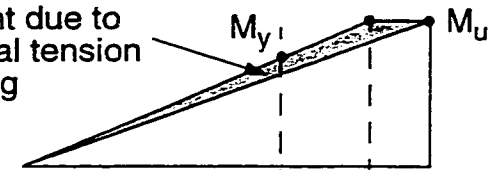
Moment diagram



Curvature distribution

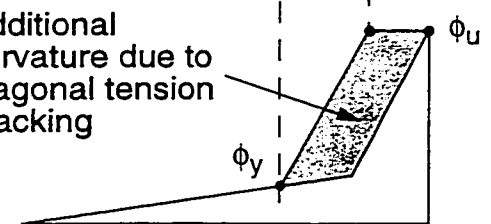
(a) Member without diagonal tension cracking

Additional moment due to diagonal tension cracking



Moment diagram

Additional curvature due to diagonal tension cracking



Curvature distribution

(b) Member with diagonal tension cracking

Fig. 4.1 Curvature Distribution in Beams With and Without Diagonal Tension Cracking (After Park and Paulay 1975)

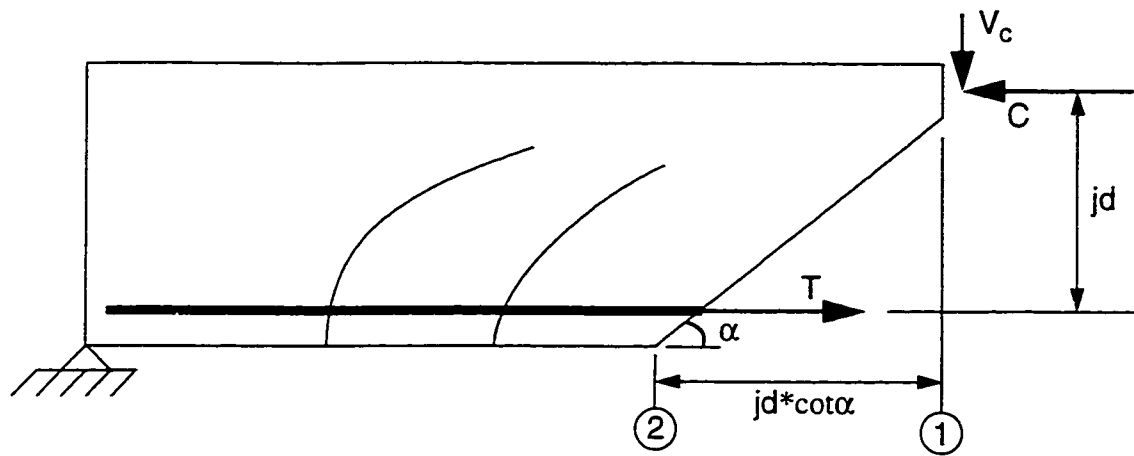


Fig. 4.2 Shear Failure Mechanism in a Beam Without Web Reinforcement

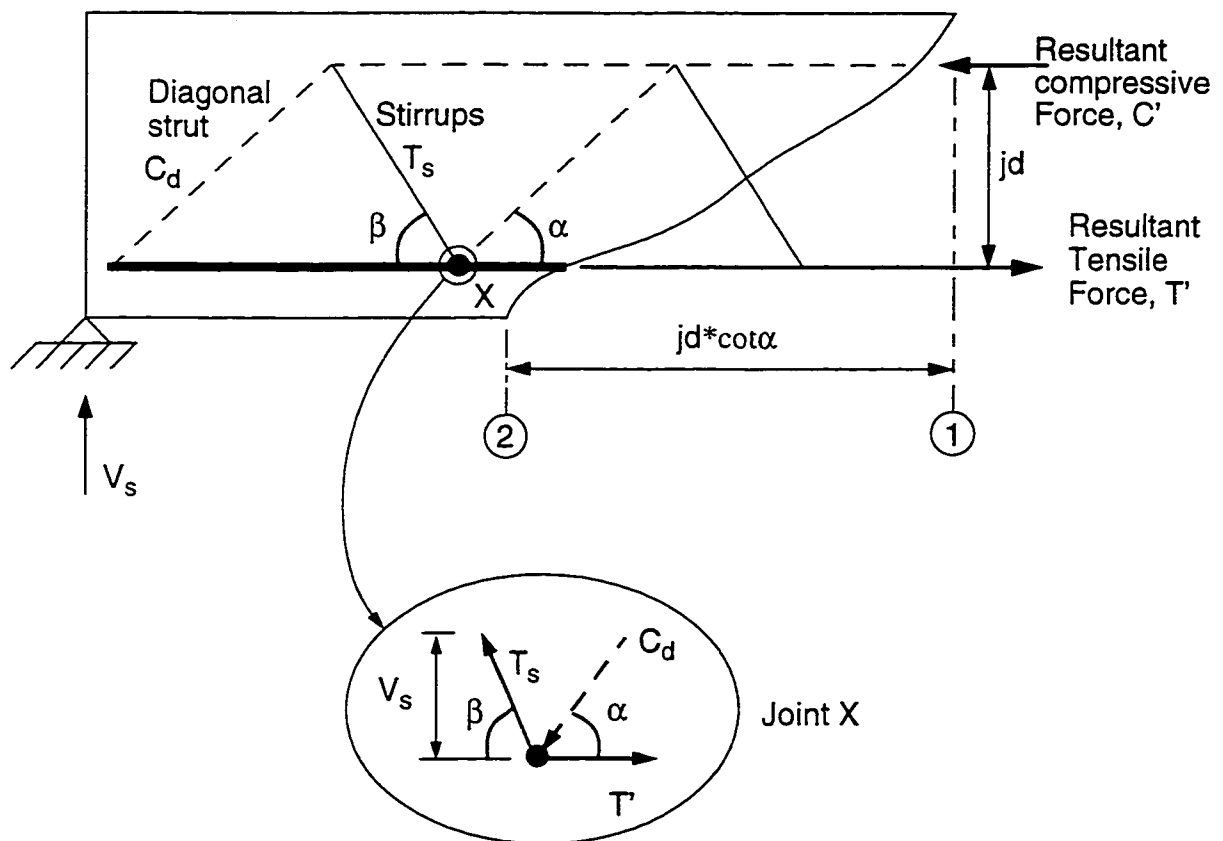


Fig. 4.3 Shear Failure Mechanism in a Beam With Web Reinforcement

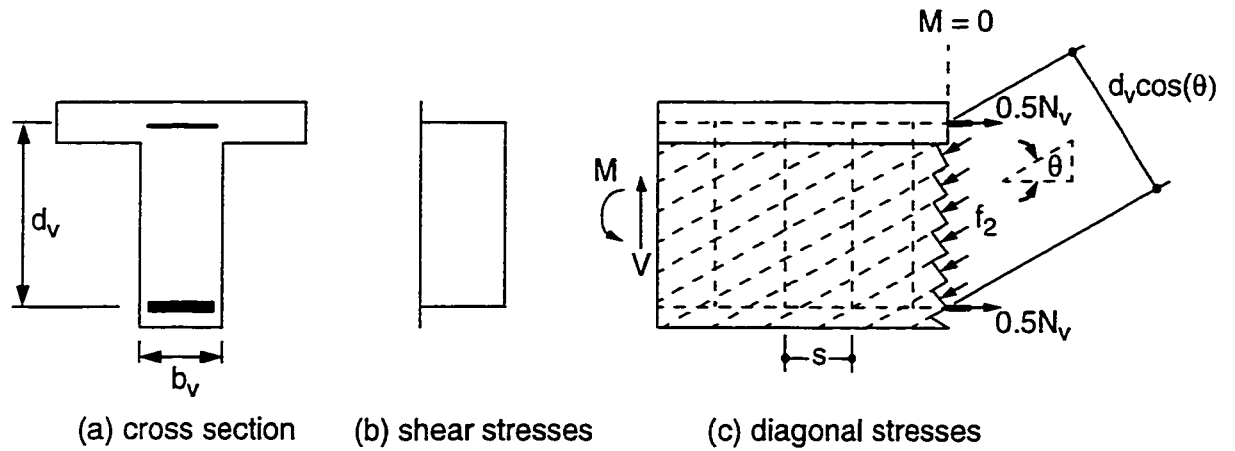


Fig. 4.4 Shear and Diagonal Compressive Stress Distribution

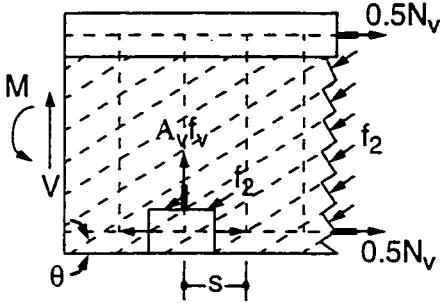
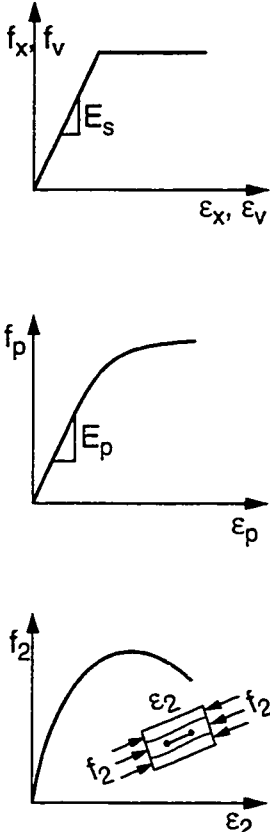
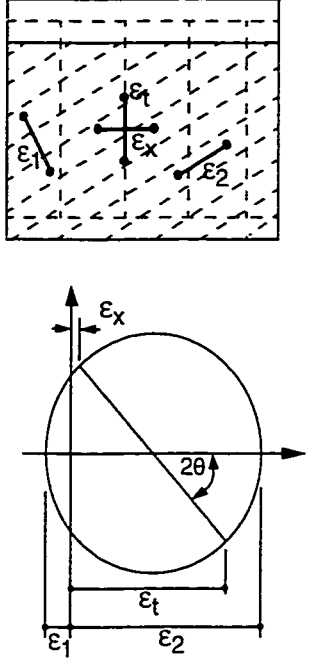
<u>EQUILIBRIUM</u>	<u>STRESS-STRAIN</u>	<u>COMPATIBILITY</u>
 <p> $f_2 = V (\tan\theta + \cot\theta) / (b_w d_w)$ $N_x = A_x f_x + A_p f_p = V \cot\theta$ $A_v f_v / s = V \tan\theta / d_v$ </p>		 <p> $\tan^2\theta = (\epsilon_x - \epsilon_2) / (\epsilon_1 - \epsilon_2)$ $\epsilon_p = \epsilon_x + \Delta\epsilon_p$ </p>

Fig. 4.5 Compression Field Theory for Prestressed Beam Subjected to Shear

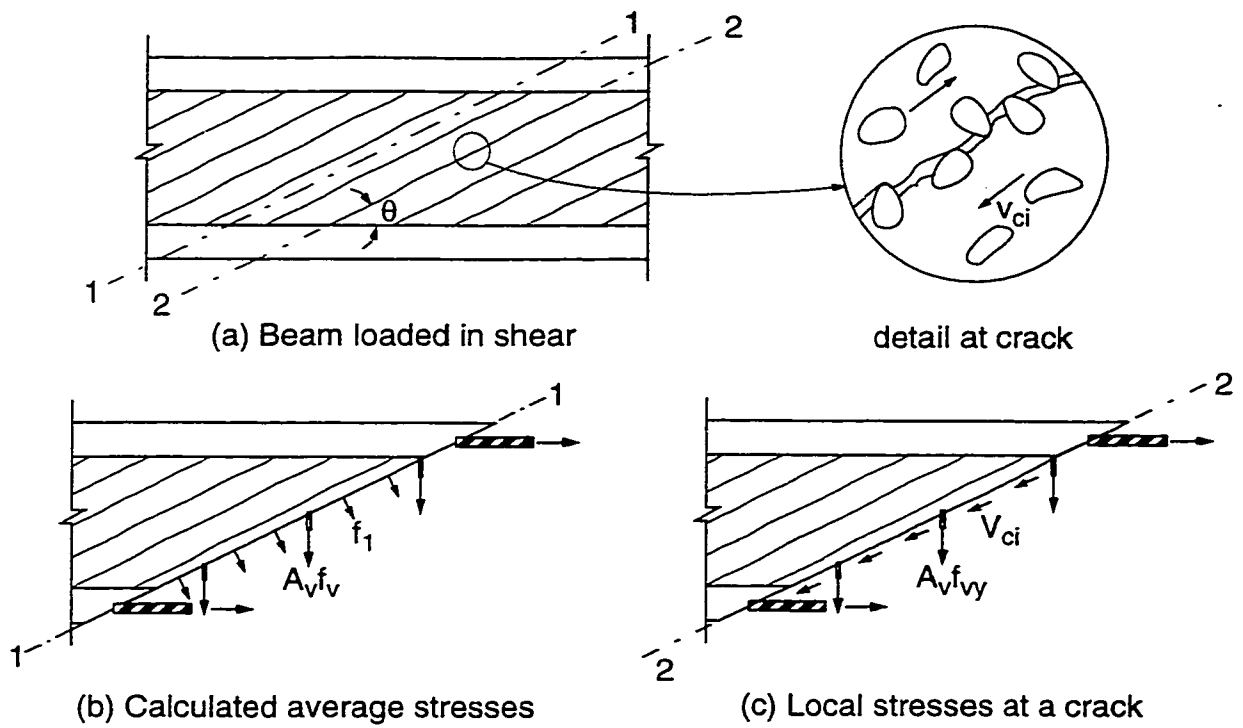


Fig. 4.6 Transmitting Forces Across Cracks

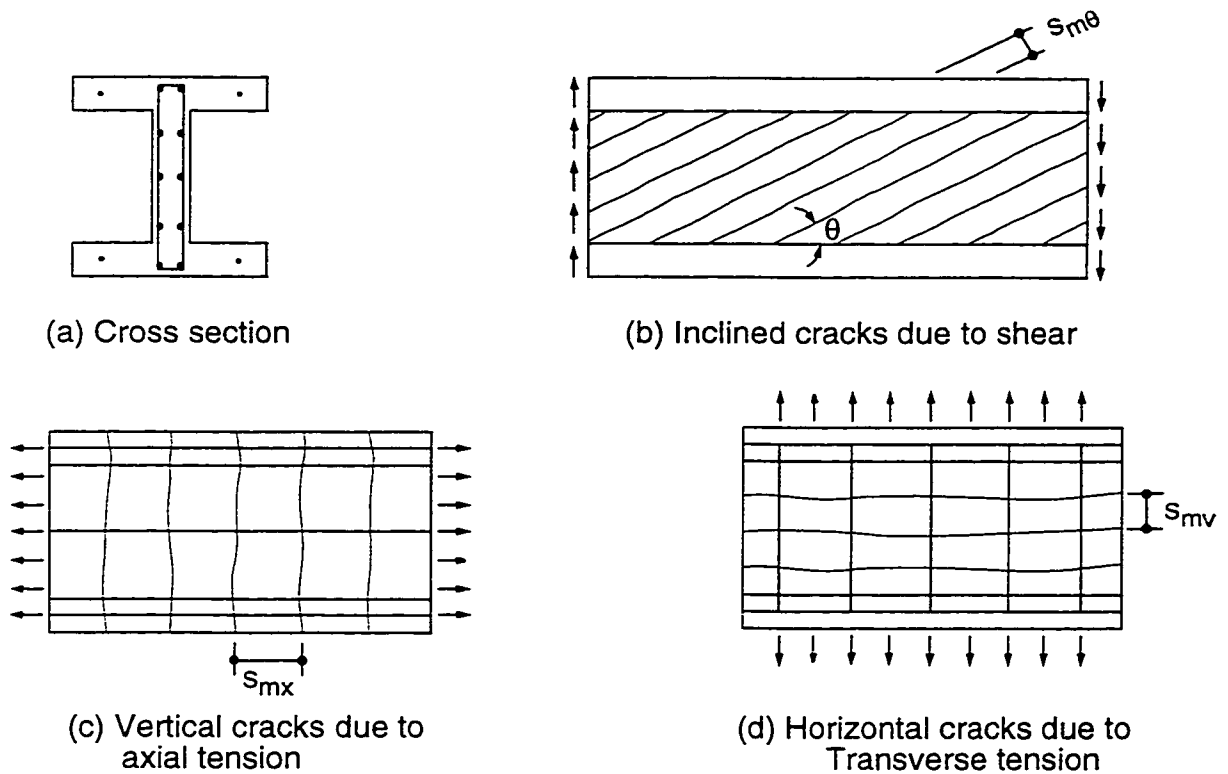


Fig. 4.7 Spacing of Inclined Cracks

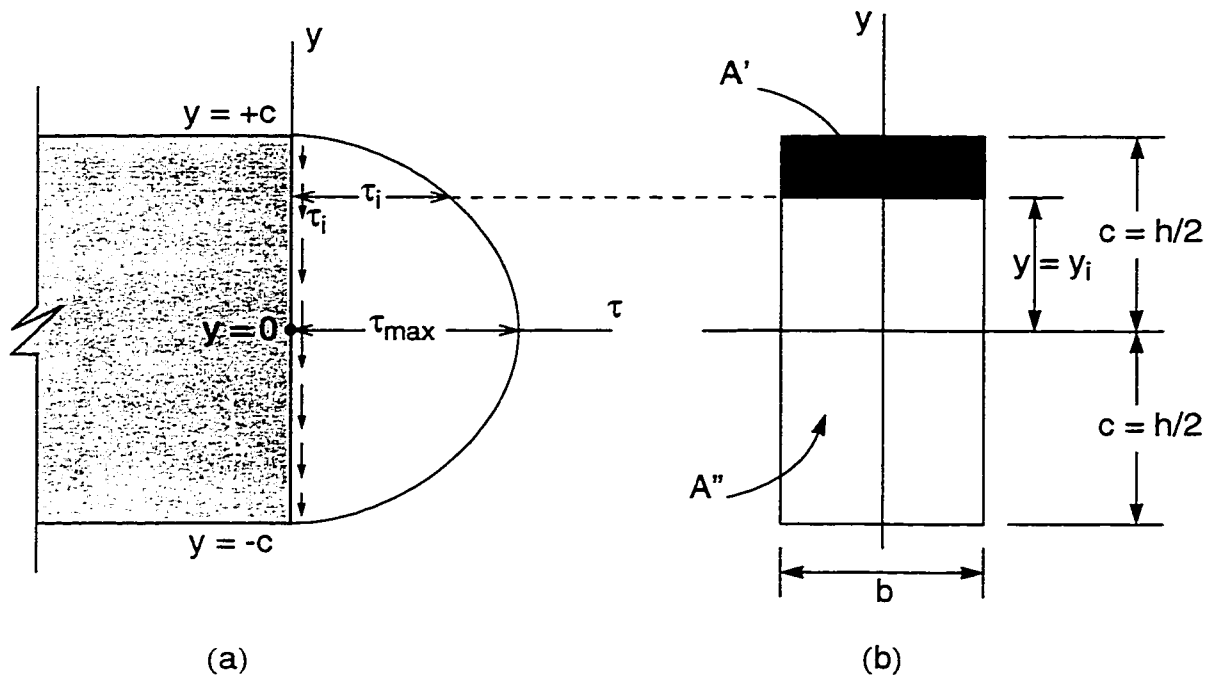


Fig. 4.8 Shearing Stress at any Distance, y_i , Using Either Area A' or A''
 (a) Shear Stress Distribution on Elevation of the Beam and
 (b) Rectangular Cross Section of the Beam.

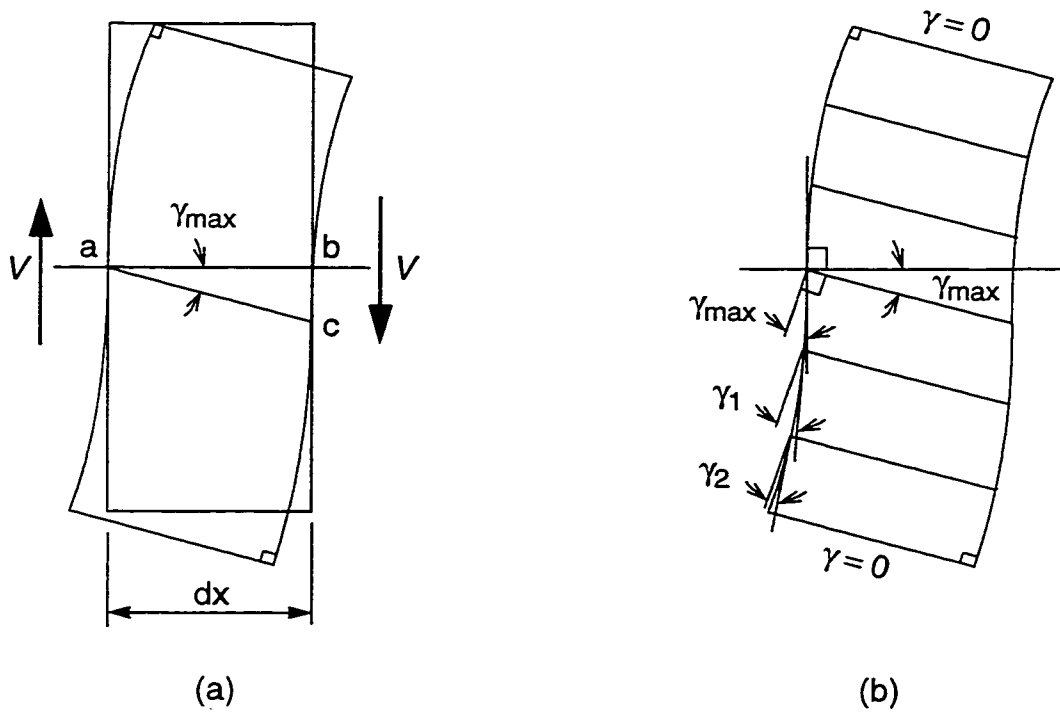


Fig. 4.9 Shear Deformations of a Differential Element

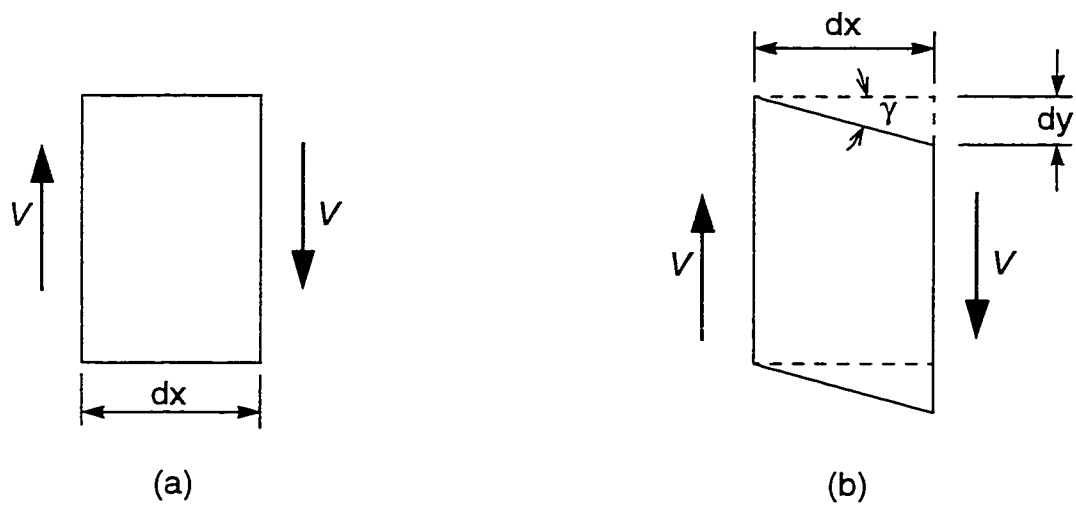


Fig. 4.10 Shear Deformations of a Differential Element
(a) Pair of Shear Force, (b) Shear Deformation.

CHAPTER FIVE

NONLINEAR ANALYSIS OF PRESTRESSED REINFORCED CONCRETE CROSS SECTIONS

5.1 Introduction

The stresses and deformations in a prestressed reinforced concrete member are subject to change due to the changing level of loading and over a long period of time due to creep and shrinkage of concrete and relaxation of prestressing steel. Therefore, the knowledge of the stresses and strains in different sections along the prestressed concrete member is important for the prediction of its behaviour. The cross sections commonly used in prestressed concrete beams are the rectangle, the symmetrical I, the T, the inverted T, and the box. Composite cross sections may also be used in prestressed reinforced beams whose stem is precast and the top is a slab cast in place directly on the stem. If no temporary intermediate support is furnished, the weight of both the slab and the stem will be carried by the stem acting alone. After the slab concrete has hardened, the composite section will carry live or additional dead load.

The cross-section of any reinforced or prestressed concrete frames or beams may be cracked or uncracked depending on the amount of the reinforcing steel, prestressing steel, and the level of loading. The cross sections considered are assumed to have one axis of symmetry and subject to a bending moment and an axial force caused by prestressing or the loading. Perfect bond is assumed between the concrete and the steel; thus at any fiber, the strains in concrete and steel are equal. Plane sections are assumed to remain plane after

deformations. Cracks in concrete occur when the stresses exceed the tensile strength of concrete. The time-dependent properties of creep and shrinkage of concrete and relaxation of prestressing steel result in loss and thus in time-dependent change of the resultant of stresses on the cross section. Generally, the nonprestressing steel is present in the prestressed section. The time dependent effect usually produce a reduction of tension in the prestressed steel and of compression in the concrete and an increase of compression in the nonprestressing steel. The concrete in the tension zone is considered while the tensile stresses are less or equal to the tensile strength of concrete.

This chapter covers the nonlinear analysis of individual reinforced or prestressed concrete sections by using the equilibrium conditions, compatibility conditions that define the linear strain distribution, and the material stress-strain relationships described in Chapter 3. The analysis gives the instantaneous and time-dependent changes in stresses and strains between consecutive construction or loading stages. The results of this analysis of the various cross sections of the member are used to determine the changes in the displacements, reactions, and internal forces in statically indeterminate structures.

5.2 Stress Strain Relationship in Cross Section - Cross-Sectional Analysis

The cross-section of a partially prestressed reinforced concrete member is composed of different materials and having one axis of symmetry along which the external load is applied. The cross section may be composed of several concrete parts of different types. The section may contain more than one layer of prestressed steel and more that one layer of nonprestressed reinforcement. The concrete parts can be of rectangular or trapezoidal shape as shown in Fig. 5.1. The cross section is considered to be constructed,

prestressed, and loaded in stages, therefore, the period of the analysis is divided into time intervals. The start of each interval coincides with the addition of a new part to the section or with the application of loads or prestressing. Thus, at the time t_i , the cross section is assumed to be subjected to increments of a normal force and a bending moment of known magnitude. During the interval i , further changes take place due to the time-dependent effects of creep, shrinkage, and relaxation. The purpose of the analysis is to determine, for each time interval, the instantaneous and time-dependent changes in stress in all concrete parts and prestressing and nonprestressing steel layers.

To analyze any prestressed reinforced concrete cross section, the material properties must be known: the moduli of elasticity of the prestressing and nonprestressing steel, E_{ps} and E_{ns} , the modulus of elasticity of concrete, E_c , the creep and shrinkage coefficients of concrete, ϕ and ϵ_{cs} , the tensile strength of concrete, f_{ct} , and the intrinsic relaxation of the prestressing steel, $\Delta\sigma_{pr}$. These properties can be computed using the mathematical expressions in Chapter 2 based on the American and European practices. Also needed for the analysis are the geometric properties of the section, the magnitude of the internal forces (normal force and bending moment) due to the loads and the initial prestressing force, and the locations of the prestressing and nonprestressing steel layers in the cross section. For accurate description of the cross section geometry, any concrete section of irregular shape can be divided into a set of rectangles and/or trapeziums for which the dimensions are specified, Fig. 5.2.

In the analysis, the actual section is replaced by a transformed section for which the actual area of any part i is replaced by a transformed area given by $(E_i/E_{ref})A_i$ where E_{ref} is an arbitrary chosen value of a reference modulus of elasticity; E_i is the modulus of elasticity

of part i of the section. The member is thus considered to have a modulus of elasticity E_{ref} and cross section properties equal to those of transformed section.

In any prestressed reinforced concrete sections, the reference modulus of elasticity is taken equal to E_c , the modulus of elasticity of one of the parts, and the reinforcement area, prestressing and nonprestressing, is replaced by α times the actual area, where α is the modular ratio (ratio of the modulus of elasticity of steel to the modulus of elasticity of concrete):

$$\alpha = \frac{E_s(E_{ps}, E_{ns})}{E_c(t_o)} \quad (5.1)$$

5.2.1 Concrete

Consider a cross section subjected to a normal force, N , at an arbitrary reference point O and a bending moment, M , Fig. 5.3a. From the assumption that plane sections remain plane after deformations, two parameters ϵ_{ref} and y_n (or curvature, the slope of the strain diagram) can thus be used to find the strain distribution along the depth of the cross section, Fig. 5.3b.

A tensile force, N , a tensile stress, σ , and the corresponding strain, ϵ are positive. A bending moment, M is regarded as positive when producing tension at the bottom fiber. Positive curvature is associated with a positive moment.

The y -coordinate defines the location of any fiber from an arbitrarily chosen reference point O; y is positive for fibers below O. The symbol Δ indicates a change in value, a positive Δ represent an increase. Thus, the free shrinkage, $\Delta\epsilon_{cs}$, and the intrinsic relaxation, $\Delta\sigma_{pr}$ are always negative quantities.

Consider a composite section made up of concrete parts of different properties and reinforced with several layers of prestressing and nonprestressing steel. At the instance which will be considered the start of any time interval i , the cross section is subjected to increments of normal force, ΔN , at a reference point and a bending moment increment, ΔM , given by:

$$\Delta N = \Delta N_{external} - \sum P_j \quad (5.2)$$

$$\Delta M = \Delta M_{external} - \sum P_j y_{psj} \quad (5.3)$$

where $\{\Delta N, \Delta M\}_{external}$ represent the change in internal forces due to external loads and the statically indeterminate effects (if any) on the initial prestressing and other loading applied at the instant considered, The symbol P refers to the absolute value of the prestressing force just before transfer in pretensioned tendons, or the force after deducting the losses due to friction and anchor set in post-tensioned tendons. The subscripts j refers to the j th tendon prestressed at the instant considered and y_{psj} is its distance from point O. After determining the strain distribution, the symbols A , B , and I in the equations below are determined. These symbols are the properties of the transformed section, whether cracked or uncracked.

Assuming the strain in the concrete varies linearly over the depth of the cross-section, the strain in the concrete at any level can be found in terms of the strain at a reference point and the depth of the compression zone (or the curvature):

$$\varepsilon_c = \varepsilon_{ref} \left(1 - \frac{y}{y_n} \right)$$

where

$$y_n = c - d_o$$

For the nonlinear analysis, the parabolic and linear parts of the concrete compression and the tensile stress-strain relations are given respectively as suggested by Hognestad (1951), see Fig. 3.4 (a) and Fig. 5.4:

$$\sigma_c = 0.85f'_c \left[\frac{2\varepsilon_{ref}}{\varepsilon_o} - \left(\frac{\varepsilon_c}{\varepsilon_o} \right)^2 \right] \quad (5.4)$$

$$\sigma_c = 0.85f'_c \left[1 - 0.15 \frac{\varepsilon_{ref} - \varepsilon_o}{\varepsilon_{cu} - \varepsilon_o} \right] \quad (5.5)$$

$$\sigma_{ct} = E_c \varepsilon_{ct} \quad (5.6)$$

substitution of the equation of the strain in Equations (5.2) yields to:

$$\sigma_c = 0.85f'_c \left[\frac{2\varepsilon_{ref}}{\varepsilon_o} - \frac{2\varepsilon_{ref}y}{\varepsilon_o y_n} - \left(\frac{1}{\varepsilon_o} \right) \left(\varepsilon_{ref}^2 - 2\varepsilon_{ref}^2 \left(\frac{y}{y_n} \right) + \varepsilon_{ref}^2 \left(\frac{y^2}{y_n^2} \right) \right) \right]$$

$$\sigma_c = (0.85f'_c) \left[\frac{2\varepsilon_{ref}}{\varepsilon_o} - \frac{\varepsilon_{ref}^2}{\varepsilon_o^2} + \left(\frac{2\varepsilon_{ref}^2}{\varepsilon_o^2 y_n} - \frac{2\varepsilon_{ref}}{\varepsilon_o y_n} \right) y - \frac{\varepsilon_{ref}^2}{\varepsilon_o^2 y_n^2} y^2 \right]$$

Similar substitution of the equation of the strain in Equations (5.3) and (5.4) will yield the stress in terms of the reference strain and the depth of compression zone (or curvature).

5.2.2 Steel

The strain in any steel layer whether it is normal steel or internal prestressing steel

is computed in a manner similar to the concrete strain:

$$\epsilon_s = \epsilon_{ref} \left(1 - \frac{y_s}{y_n} \right) = \epsilon_{ref} \left(\frac{c - d_s}{c - d_o} \right)$$

where

$$y_s = d_s - d_o$$

i) Normal Steel:

A rectilinear stress-strain relationship is used for the normal steel, see Fig. 3.4 (b):

Elastic range:

$$\sigma_s = E_s \epsilon_s \quad (5.7)$$

Inelastic range:

$$\sigma_s = \sigma_y + E_{sh} \epsilon_s \quad (5.8)$$

ii) Prestressing steel:

The following stress-strain relationship given by Naaman (1990) is used:

$$\sigma_p = E_p \epsilon_p \left(Q + (1 - Q) \left[1 + \left(\frac{E_p \epsilon_p}{K f_{py}} \right)^N \right]^{1/N} \right) \quad (5.9)$$

where N , K , and Q are empirical parameters whose values are recommended by Naaman (1990) as 6.06, 1.0325, and 0.00625 respectively, see Fig. 3.4 (c).

5.3 Computation of Internal Forces and Moments - Cross-Sectional Analysis

5.3.1 Concrete Compressive Force and Moment

The compressive force of the concrete is computed by integrating the compression

stress block. For the parabolic part:

$$\int_{-d_0}^{y_n} \sigma_c da = \int_{-d_0}^{y_n} 0.85 f'_c \left[\frac{2\epsilon_{ref}}{\epsilon_o} - \frac{\epsilon_{ref}^2}{\epsilon_o^2} + \left(\frac{2\epsilon_{ref}^2}{\epsilon_o^2 y_n} - \frac{2\epsilon_{ref}}{\epsilon_o y_n} \right) y - \frac{\epsilon_{ref}^2}{\epsilon_o^2 y_n^2} y^2 \right] da$$

$$\int_{-d_0}^{y_n} \sigma_c da = 0.85 f'_c \left[\left(\frac{2\epsilon_{ref}}{\epsilon_o} - \frac{\epsilon_{ref}^2}{\epsilon_o^2} \right) \int_{-d_0}^{y_n} da + \left(\frac{2\epsilon_{ref}^2}{\epsilon_o^2 y_n} - \frac{2\epsilon_{ref}}{\epsilon_o y_n} \right) \int_{-d_0}^{y_n} y da - \frac{\epsilon_{ref}^2}{\epsilon_o^2 y_n^2} \int_{-d_0}^{y_n} y^2 da \right]$$

$$\int_{-d_0}^{y_n} \sigma_c da = 0.85 f'_c \left[\left(\frac{2\epsilon_{ref}}{\epsilon_o} - \frac{\epsilon_{ref}^2}{\epsilon_o^2} \right) A + \left(\frac{2\epsilon_{ref}^2}{\epsilon_o^2 y_n} - \frac{2\epsilon_{ref}}{\epsilon_o y_n} \right) B - \frac{\epsilon_{ref}^2}{\epsilon_o^2 y_n^2} I \right]$$

$$\int_{-d_0}^{(c-d_o)} \sigma_c da = 0.85 f'_c \left[\left(\frac{2\epsilon_{ref}}{\epsilon_o} - \frac{\epsilon_{ref}^2}{\epsilon_o^2} \right) A + \left(\frac{2\epsilon_{ref}^2}{\epsilon_o^2 (c-d_o)} - \frac{2\epsilon_{ref}}{\epsilon_o (c-d_o)} \right) B - \frac{\epsilon_{ref}^2}{\epsilon_o^2 (c-d_o)^2} I \right]$$

Similarly, taking moment of the compressive force of the concrete about the reference point, gives:

$$\int_{-d_0}^{y_n} \sigma_c y da = \int_{-d_0}^{y_n} 0.85 f'_c \left[\frac{2\epsilon_{ref}}{\epsilon_o} - \frac{\epsilon_{ref}^2}{\epsilon_o^2} + \left(\frac{2\epsilon_{ref}^2}{\epsilon_o^2 y_n} - \frac{2\epsilon_{ref}}{\epsilon_o y_n} \right) y - \frac{\epsilon_{ref}^2}{\epsilon_o^2 y_n^2} y^2 \right] y da$$

$$\int_{-d_0}^{y_n} \sigma_c y da = 0.85 f'_c \left[\left(\frac{2\epsilon_{ref}}{\epsilon_o} - \frac{\epsilon_{ref}^2}{\epsilon_o^2} \right) \int_{-d_0}^{y_n} y da + \left(\frac{2\epsilon_{ref}^2}{\epsilon_o^2 y_n} - \frac{2\epsilon_{ref}}{\epsilon_o y_n} \right) \int_{-d_0}^{y_n} y^2 da - \frac{\epsilon_{ref}^2}{\epsilon_o^2 y_n^2} \int_{-d_0}^{y_n} y^3 da \right]$$

$$\int_{-d_0}^{y_n} \sigma_c y da = 0.85 f'_c \left[\left(\frac{2\epsilon_{ref}}{\epsilon_o} - \frac{\epsilon_{ref}^2}{\epsilon_o^2} \right) B + \left(\frac{2\epsilon_{ref}^2}{\epsilon_o^2 y_n} - \frac{2\epsilon_{ref}}{\epsilon_o y_n} \right) I - \frac{\epsilon_{ref}^2}{4\epsilon_o^2 y_n^2} [y_n^4 - (-d_o)^4] \right]$$

$$\int_{-d_o}^{(c-d_o)} \sigma_c y da = 0.85 f'_c \left(\left(\frac{2\varepsilon_{ref}}{\varepsilon_o} - \frac{\varepsilon_{ref}^2}{\varepsilon_o^2} \right) B + \left(\frac{2\varepsilon_{ref}^2}{\varepsilon_o^2 (c-d_o)} - \frac{2\varepsilon_{ref}}{\varepsilon_o (c-d_o)} \right) I - \frac{\varepsilon_{ref}^2}{4\varepsilon_o^2} \times \right. \\ \left. \left((c-d_o)^2 - \frac{(-d_o)^4}{(c-d_o)^2} \right) \right)$$

5.3.2 Steel Force and Moment

5.3.2.1 Normal Steel Layers Resultant Force and Moment

This force is obtained by summing up algebraically the forces in all the normal steel layers:

For elastic behaviour:

$$\sum_{i=1}^n A_{si} \sigma_{si} = \sum_{i=1}^n A_{si} E_{si} \varepsilon_{si}$$

$$\sum_{i=1}^n A_{si} \sigma_{si} = \sum_{i=1}^n A_{si} E_{si} \varepsilon_{ref} \left(\frac{c-d_{si}}{c-d_o} \right)$$

For inelastic behaviour:

$$\sum_{i=1}^n A_{si} \sigma_{si} = \sum_{i=1}^n [A_{si} \sigma_{yi} + A_{si} E_{shi} \varepsilon_{si}]$$

$$\sum_{i=1}^n A_{si} \sigma_{si} = \sum_{i=1}^n \left[A_{si} \sigma_{yi} + A_{si} E_{shi} \varepsilon_{ref} \left(\frac{c-d_{si}}{c-d_o} \right) \right]$$

Similarly for the moment, the total moment is the summation of all the moments:

For elastic behaviour:

$$\sum_{i=1}^n A_{si} \sigma_{si} (d_{si} - d_o) = \sum_{i=1}^n A_{si} E_{si} \epsilon_{si} (d_{si} - d_o)$$

$$\sum_{i=1}^n A_{si} \sigma_{si} (d_{si} - d_o) = \sum_{i=1}^n A_{si} E_{si} \epsilon_{ref} \left(\frac{c - d_{si}}{c - d_o} \right) (d_{si} - d_o)$$

For inelastic behaviour:

$$\sum_{i=1}^n A_{si} \sigma_{si} (d_{si} - d_o) = \sum_{i=1}^n [A_{si} \sigma_{yi} + A_{si} E_{shi} \epsilon_{si}] (d_{si} - d_o)$$

$$\sum_{i=1}^n A_{si} \sigma_{si} (d_{si} - d_o) = \sum_{i=1}^n \left[A_{si} \sigma_{yi} + A_{si} E_{shi} \epsilon_{ref} \left(\frac{c - d_{si}}{c - d_o} \right) \right] (d_{si} - d_o)$$

5.3.2.2 Internal Prestressing Steel Layers Resultant Force and Moment

Similar to the normal steel layers, the force and the total moment are obtained by summing up algebraically the forces and the moments in all the individual prestressing steel layers:

$$\sum_{j=1}^m A_{pj} \sigma_{pj} = \sum_{j=1}^m A_{pj} E_{pj} \epsilon_{pj} \left(Q + (1 - Q) / \left[1 + \left(\frac{E_{pj} \epsilon_{pj}}{K f_{pyj}} \right)^N \right]^{1/N} \right)$$

$$\sum_{j=1}^m A_{pj} \sigma_{pj} = \sum_{j=1}^m A_{pj} E_{pj} \epsilon_{pj} \left(Q + (1 - Q) / \left[1 + \left(\frac{E_{pj} \epsilon_{pj}}{K f_{pyj}} \right)^N \right]^{1/N} \right)$$

5.4 Equations of Equilibrium

There are two equilibrium equations, summation of all axial forces must be zero and

summation of all bending moments about the reference point must also be zero:

$$\sum F = 0$$

$$\Delta N + C + T = 0$$

$$\sum M = 0$$

$$\Delta M + Cy_c + Ty_s = 0$$

5.5 Derivatives

Newton's iteration method is used for the solution of the equations of equilibrium which are a system of nonlinear simultaneous algebraic equations. In this method, partial derivatives of these equations with respect to the unknowns ϵ_{ref} and c are obtained. The problem becomes one of finding the roots of the linear system:

$$\begin{bmatrix} \frac{\partial}{\partial \epsilon_{ref}} \sum F & \frac{\partial}{\partial c} \sum F \\ \frac{\partial}{\partial \epsilon_{ref}} \sum M & \frac{\partial}{\partial c} \sum M \end{bmatrix} \begin{bmatrix} \Delta \epsilon_{ref} \\ \Delta c \end{bmatrix} = \begin{bmatrix} \sum F \\ \sum M \end{bmatrix}$$

It should be mentioned here that in the previous equations and the following ones, the formulation for the linear descending and tension parts of the stress-strain curve of the concrete are not shown. But they are coded and incorporated in the computer programs for this study. The derivatives of the equations of equilibrium are:

$$\frac{\partial}{\partial \epsilon_{ref}} \sum F = \frac{\partial}{\partial \epsilon_{ref}} \left(\int_{-d_o}^{(c-d_o)} \sigma_c b dy + \sum_{i=1}^n A_{nsi} \sigma_{nsi} + \sum_{i=1}^m A_{psi} \sigma_{psi} \right)$$

$$\frac{\partial}{\partial \epsilon_{ref}} \sum F = \frac{\partial}{\partial \epsilon_{ref}} \int_{-d_o}^{(c-d_o)} \sigma_c b dy + \frac{\partial}{\partial \epsilon_{ref}} \sum_{i=1}^n A_{nsi} \sigma_{nsi} + \frac{\partial}{\partial \epsilon_{ref}} \sum_{i=1}^m A_{psi} \sigma_{psi}$$

$$\frac{\partial}{\partial \epsilon_{ref}} \sum F = 0.85 f_c \left[\left(\frac{2}{\epsilon_o} - \frac{2\epsilon_{ref}}{\epsilon_o^2} \right) A + \left(\frac{4\epsilon_{ref}}{\epsilon_o^2 (c-d_o)} - \frac{2}{\epsilon_o (c-d_o)} \right) B - \frac{2\epsilon_{ref}}{\epsilon_o^2 (c-d_o)^2} I \right]$$

$$+ \left(\sum_{i=1}^n A_{nsi} E_{nsi} \left(\frac{c-d_{nsi}}{c-d_o} \right) \right) \\ + \left(\sum_{i=1}^n \left[A_{nsi} E_{nshi} \left(\frac{c-d_{nsi}}{c-d_o} \right) \right] \right)$$

$$+ \sum_{j=1}^m \left(A_{psj} E_{psj} \frac{(c-d_{psj})}{(c-d_o)} Q + A_{psj} E_{psj} \frac{(c-d_{psj})}{(c-d_o)} (1-Q) \times \right.$$

$$\left[1 + \left(\frac{E_{psj} \epsilon_{ref} (c-d_{psj})}{K f_{pyj} (c-d_o)} \right)^N \right]^{-1/N} - \left(\frac{1}{N} \right) A_{psj} E_{psj} \frac{(c-d_{psj})}{(c-d_o)} (1-Q) \times$$

$$\left[1 + \left(\frac{E_{psj} \epsilon_{ref} (c-d_{psj})}{K f_{pyj} (c-d_o)} \right)^N \right]^{-(1+N)/N} (N) \epsilon_{ref}^{(N-1)} \left(\frac{E_{psj} (c-d_{psj})}{K f_{pyj} (c-d_o)} \right)^N$$

$$\frac{\partial}{\partial c} \sum F = \frac{\partial}{\partial c} \int_{-d_0}^{(c-d_o)} \sigma_c b dy + \sum_{i=1}^n A_{nsi} \sigma_{nsi} + \sum_{i=1}^m A_{psi} \sigma_{psi}$$

$$\frac{\partial}{\partial c} \sum F = \frac{\partial}{\partial c} \int_{-d_0}^{(c-d_o)} \sigma_c b dy + \frac{\partial}{\partial c} \sum_{i=1}^n A_{nsi} \sigma_{nsi} + \frac{\partial}{\partial c} \sum_{i=1}^m A_{psi} \sigma_{psi}$$

$$\frac{\partial}{\partial c} \sum F = 0.85 f'_c \left[\left(\frac{-2\epsilon_{ref}^2}{\epsilon_o^2 (c-d_o)^2} + \frac{2\epsilon_{ref}}{\epsilon_o (c-d_o)^2} \right) B + \frac{2\epsilon_{ref}^2}{\epsilon_o^2 (c-d_o)^3} I \right]$$

$$+ \left(\sum_{i=1}^n \left[\frac{A_{nsi} E_{nsi} \epsilon_{ref}}{(c-d_o)} - A_{nsi} E_{nsi} \epsilon_{ref} \frac{(c-d_{nsi})}{(c-d_o)^2} \right] \right)$$

$$+ \left(\sum_{i=1}^n \left[\frac{A_{nsi} E_{nshi} \epsilon_{ref}}{(c-d_o)} - A_{nsi} E_{nshi} \epsilon_{ref} \frac{(c-d_{nsi})}{(c-d_o)^2} \right] \right)$$

$$+ \sum_{j=1}^m \left(A_{psj} E_{psj} \epsilon_{psj} \frac{Q}{(c-d_o)} - A_{psj} E_{psj} \epsilon_{psj} \frac{(c-d_{psj})}{(c-d_o)} Q \right)$$

$$+ A_{psj} E_{psj} \epsilon_{psj} \frac{(1-Q)}{(c-d_o)} \left[1 + \left(\frac{E_{psj} \epsilon_{ref} (c-d_{psj})}{K f_{pyj} (c-d_o)} \right)^N \right]^{-1/N}$$

$$- A_{psj} E_{psj} \epsilon_{psj} \frac{(c-d_{psj})}{(c-d_o)^2} (1-Q) \left[1 + \left(\frac{E_{psj} \epsilon_{ref} (c-d_{psj})}{K f_{pyj} (c-d_o)} \right)^N \right]^{-1/N}$$

$$+ A_{psj} E_{psj} \epsilon_{psj} \frac{(c-d_{psj})}{(c-d_o)} (1-Q) - \left(\frac{1}{N} \right) \left[1 + \left(\frac{E_{psj} \epsilon_{ref} (c-d_{psj})}{K f_{pyj} (c-d_o)} \right)^N \right]^{-\frac{(1+N)}{N}} \times$$

$$\left(N \left(\frac{E_{psj} \epsilon_{ref}}{K f_{pyj} (c-d_o)} \right)^N (c-d_{psj})^{(N-1)} - N \left(\frac{E_{psj} \epsilon_{ref} (c-d_{psj})}{K f_{pyj}} \right)^N \frac{1}{(c-d_o)^{(N+1)}} \right)$$

$$\frac{\partial}{\partial \epsilon_{ref}} \sum M = \frac{\partial}{\partial \epsilon_{ref}} \left(\int_{-d_0}^{(c-d_o)} \sigma_c y b dy + \sum_{i=1}^n A_{nsi} \sigma_{nsi} (d_{sjn} - d_o) + \sum_{j=1}^m A_{psj} \sigma_{psj} (d_{psj} - d_o) \right)$$

$$\frac{\partial}{\partial \epsilon_{ref}} \sum M = \frac{\partial}{\partial \epsilon_{ref}} \int_{-d_0}^{(c-d_o)} \sigma_c y b dy + \frac{\partial}{\partial \epsilon_{ref}} \sum_{i=1}^n A_{nsi} \sigma_{nsi} (d_{sjn} - d_o) +$$

$$\frac{\partial}{\partial \epsilon_{ref}} \sum_{j=1}^m A_{psj} \sigma_{psj} (d_{psj} - d_o)$$

$$\frac{\partial}{\partial \epsilon_{ref}} \sum M = \left(0.85 f_c \left(\frac{2}{\epsilon_o} - \frac{2\epsilon_{ref}}{\epsilon_o^2} \right) B + \left(\frac{4\epsilon_{ref}}{\epsilon_o^2 (c-d_o)} - \frac{2}{\epsilon_o (c-d_o)} \right) I - \right.$$

$$\left. \frac{\epsilon_{ref}}{2\epsilon_o^2} \left((c-d_o)^2 - \frac{(-d_o)^4}{(c-d_o)^2} \right) \right)$$

$$+ \left(\sum_{i=1}^n A_{nsi} E_{nsi} \left(\frac{c-d_{nsi}}{c-d_o} \right) (d_{nsi} - d_o) + \sum_{i=1}^n A_{nsi} E_{nshi} \left(\frac{c-d_{nsi}}{c-d_o} \right) (d_{nsi} - d_o) \right)$$

$$+ \sum_{j=1}^m \left(A_{psj} E_{psj} \frac{(c-d_{psj})}{(c-d_o)} Q + A_{psj} E_{psj} \frac{(c-d_{psj})}{(c-d_o)} (1-Q) \times \right.$$

$$\left[1 + \left(\frac{E_{psj} \epsilon_{ref} (c-d_{psj})}{K f_{pyj} (c-d_o)} \right)^N \right]^{-1/N} - \left(\frac{1}{N} \right) A_{psj} E_{psj} \frac{(c-d_{psj})}{(c-d_o)} (1-Q) \times$$

$$\left[1 + \left(\frac{E_{psj} \epsilon_{ref} (c-d_{psj})}{K f_{pyj} (c-d_o)} \right)^N \right]^{-(1+N)/N} (N) \epsilon_{ref}^{(N-1)} \left(\frac{E_{psj} (c-d_{psj})}{K f_{pyj} (c-d_o)} \right)^N \times$$

$$(d_{psj} - d_o)$$

$$\frac{\partial}{\partial c} \sum M = \frac{\partial}{\partial c} \left(\int_{-d_0}^{(c-d_o)} \sigma_c y b dy + \sum_{i=1}^n A_{nsi} \sigma_{nsi} (d_{sjn} - d_o) + \sum_{j=1}^m A_{psj} \sigma_{psj} (d_{psj} - d_o) \right)$$

$$\frac{\partial}{\partial c} \sum M = \frac{\partial}{\partial c} \int_{-d_0}^{(c-d_o)} \sigma_c y b dy + \frac{\partial}{\partial c} \sum_{i=1}^n A_{nsi} \sigma_{nsi} (d_{sjn} - d_o) + \frac{\partial}{\partial c} \sum_{j=1}^m A_{psj} \sigma_{psj} (d_{psj} - d_o)$$

$$\frac{\partial}{\partial c} \sum M = 0.85 f'_c \left[\left(\frac{(-2) \epsilon_{ref}^2}{\epsilon_o^2 (c-d_o)^2} + \frac{2 \epsilon_{ref}}{\epsilon_o (c-d_o)^2} \right) I - \frac{\epsilon_{ref}^2}{2 \epsilon_o^2} \left((c-d_o) + \frac{(-d_o)^4}{(c-d_o)^3} \right) \right]$$

$$\begin{aligned} & + \left(\sum_{i=1}^n \left[A_{nsi} E_{nsi} \epsilon_{ref} \frac{(d_{nsi} - d_o)}{(c-d_o)} - A_{nsi} E_{nsi} \epsilon_{ref} \frac{(c-d_{nsi})}{(c-d_o)^2} (d_{nsi} - d_o) \right] \right. \\ & \left. + \sum_{i=1}^n \left[A_{nsi} E_{nshi} \epsilon_{ref} \frac{(d_{nsi} - d_o)}{(c-d_o)} - A_{si} E_{nshi} \epsilon_{ref} \frac{(c-d_{nsi})}{(c-d_o)^2} (d_{nsi} - d_o) \right] \right) \\ & + \sum_{j=1}^m \left\{ A_{psj} E_{psj} \epsilon_{psj} \frac{Q}{(c-d_o)} - A_{psj} E_{psj} \epsilon_{psj} \frac{(c-d_{psj})}{(c-d_o)} Q \right. \\ & + A_{psj} E_{psj} \epsilon_{psj} \frac{(1-Q)}{(c-d_o)} \left[1 + \left(\frac{E_{psj} \epsilon_{ref} (c-d_{psj})}{K f_{pyj} (c-d_o)} \right)^N \right]^{-1/N} \\ & - A_{psj} E_{psj} \epsilon_{psj} \frac{(c-d_{psj})}{(c-d_o)^2} (1-Q) \left[1 + \left(\frac{E_{psj} \epsilon_{ref} (c-d_{psj})}{K f_{pyj} (c-d_o)} \right)^N \right]^{-1/N} \\ & + A_{psj} E_{psj} \epsilon_{psj} \frac{(c-d_{psj})}{(c-d_o)} (1-Q) - \left(\frac{1}{N} \right) \left[1 + \left(\frac{E_{psj} \epsilon_{ref} (c-d_{psj})}{K f_{pyj} (c-d_o)} \right)^N \right]^{-\frac{(1+N)}{N}} \times \\ & \left. \left(N \left(\frac{E_{psj} \epsilon_{ref}}{K f_{pyj} (c-d_o)} \right)^N (c-d_{psj})^{(N-1)} - N \left(\frac{E_{psj} \epsilon_{ref} (c-d_{psj})}{K f_{pyj}} \right)^N \frac{1}{(c-d_o)^{(N+1)}} \right) \right\} : \\ & (d_{psj} - d_0) \end{aligned}$$

5.6 Time Dependent Stresses and Strains

The analysis of the time-dependent effects is based on the displacement method in which the free strain due to creep and shrinkage is treated as an initial strain (Zienkiewicz, 1977). In the analysis by the displacement method, initial strains are artificially restrained by forces which are subsequently eliminated by application of equal and opposite forces on the entire cross section. In the present work, the steps of analysis suggested by Ghali and Favre (1986) are used.

5.6.1 Free Strain Due to Creep and Shrinkage

Let t_1, t_2, \dots represent time instants at which external loads or prestressing are applied. The symbol $\Delta\sigma_c(t_j)$ will be used to represent a stress increment introduced at time t_j , and sustained without change in magnitude up to time t . In reinforced and prestressed concrete, the reinforcement restrains the deformation due to creep and shrinkage. The restraint subjects the concrete to stress increments which develop gradually. Let $\Delta\sigma_c(t_{j+1}, t_j)$ represent the stress increment gradually developed between t_j and t_{j+1} . The analysis will be done step-by-step; thus, for any interval i , the stress increments during early intervals will be known from the preceding calculations. Assume that both $\Delta\sigma_c(t_j)$ and $\Delta\sigma_c(t_{j+1}, t_j)$ are known for $j = 1, 2, \dots, i-1$. It is required to calculate the hypothetical free strain which would occur in the absence of the reinforcement during interval t_i to t_{i+1} , with $i > j$. A stress increment $\Delta\sigma_c(t_j)$ produces creep during the interval considered equal to:

$$\frac{\Delta\sigma_c(t_j)}{E_c(t_j)} [\phi(t_{i+1}, t_j) - \phi(t_i, t_j)]$$

and in this study, the creep is:

$$\frac{\left(\frac{1.7f_c'(t_j)}{\epsilon_o(t_j)}\right) - \sqrt{\left(\frac{1.7f_c'(t_j)}{\epsilon_o(t_j)}\right)^2 - \left(\frac{3.4f_c'(t_j)}{\epsilon_o^2(t_j)}\right)\Delta\sigma(t_i)}}{\left(\frac{1.7f_c'(t_j)}{\epsilon_o^2(t_j)}\right)} [\phi(t_{i+1}, t_j) - \phi(t_i, t_j)]$$

and

$$\left(\epsilon_o(t_j) + \left(\frac{\epsilon_{cu} - \epsilon_o(t_j)}{0.15}\right) \left(1 - \frac{\Delta\sigma(t_i)}{0.85(f_c'(t_j))}\right)\right) [\phi(t_{i+1}, t_j) - \phi(t_i, t_j)]$$

Therefore, for the purpose of the present analysis, the two increments $\Delta\sigma_c(t_j)$ and $\Delta\sigma_c(t_{j+1}, t_j)$ are considered lumped together to produce the creep during the interval i .

Shrinkage during the same interval is $\Delta\epsilon_{cs}(t_{i+1}, t_i)$. Thus, the total hypothetical free strain which would occur between t_i and t_{i+1} is the addition of creep and shrinkage.

Stresses will develop in any time interval when the free strain in concrete is not free to occur due to the presence of the reinforcement or due to attachment to other concrete parts having different creep or shrinkage parameters.

5.6.2 Variation of Prestressed Steel Stress Due to Relaxation

As defined in Chapter 3, the intrinsic relaxation, $\Delta\sigma_{pr}$, is the reduction with time in the stress of a prestressing tendon when it is stretched and held at a constant length between two fixed points. The amount of intrinsic relaxation occurring during a given period of time depends to a great extent on the stress level in the steel at the beginning of the period considered. In the absence of relaxation tests, the magnitude of the intrinsic relaxation can

be determined from empirical equations such as those given in Chapter 3.

In a concrete member, creep and shrinkage cause an additional reduction in the steel stress, and therefore, the prestressing steel exhibits smaller relaxation loss as compared to the intrinsic relaxation obtained from a constant-length relaxation test. Ghali, Sisodiya, and Tadros (1974) employed a step-by-step procedure to account for the effect of variation in the prestress level on the magnitude of relaxation. Ghali and Trevino (1985) presented a more accurate reduction coefficient, χ_r . The reduced relaxation, $\Delta\bar{\sigma}_{pr}$, can thus be expressed as

$$\Delta\bar{\sigma}_{pr} = \chi_r \Delta\sigma_{pr} \quad (5.10)$$

where

$$\chi_r = e^{(-6.7 + 5.3\lambda)\Omega} \quad (5.11)$$

with λ being the ratio of the initial stress, σ_{ps0} , in the tendon to its tensile strength, f_{pu} , and

$$\Omega = -\frac{\Delta\sigma_{ps} - \Delta\sigma_{pr}}{\sigma_{ps0}} \quad (5.12)$$

where $\Delta\sigma_{ps}$ is the change in stress in prestressing steel during a given period of time due to the combined effects of creep, shrinkage, and relaxation. This value is generally not known a priori as it depends on the reduced relaxation. Therefore, iteration is necessary; first an assumed value of $\chi_r = 0.7$ is used to calculate $\Delta\sigma_{ps}$ and later adjusted by using Equation (5.11) or Fig. 3.5 if necessary.

5.7 Analysis of cross sections

When the two parameters that define the strain distribution $\{\Delta\epsilon_0(t_{i+1}, t_i), y_n\}_{free}$ of the hypothetical free strain due to creep and shrinkage during the period t_i to t_{i+1} are known,

then the time-dependent changes in stress and strain occurring in each concrete part and steel layer between t_i and t_{i+1} can be determined assuming that the material properties ϕ , χ , ϵ_{cs} , and $\Delta\bar{\sigma}_{pr}$ are known for the time interval considered.

The hypothetical free strain can be prevented by introducing an artificial stress whose distribution over the j th concrete part is defined by the stress at point O:

$$[(\Delta\sigma_c)_{restraint}]_j = 0.85f'_c(t_{i+1}) \left[\frac{2\epsilon_{ref}(t_{i+1}, t_i)}{\epsilon_o(t_{i+1})} - \left(\frac{\epsilon_c(t_{i+1}, t_i)}{\epsilon_o(t_{i+1})} \right)^2 \right]$$

or

$$[(\Delta\sigma_c)_{restraint}]_j = 0.85f'_c(t_{i+1}) \left[1 - 0.15 \frac{\epsilon_{ref}(t_{i+1}, t_i) - \epsilon_o(t_{i+1})}{\epsilon_{cu} - \epsilon_o(t_{i+1})} \right]$$

Integrating the stress block of the concrete part j represent the resultants of the artificial restraining stress, $\Delta N_{c,s}$, $\Delta M_{c,s}$ (as described in the equations above). The integration is preformed for all concrete parts and the A , B , and I are the cross section area, its first and second moments about an axis through the arbitrary reference point O.

Relaxation of the prestressing steel is the reduction in the tension of the tendons and in the compression in the concrete at the same level and thus causes tensile strains in the concrete at the tendon levels. The strain in concrete due to relaxation of prestressing steel can be artificially prevented by the application of the forces:

$$\Delta N_{pr} = \sum_{k=1}^n (\Delta\bar{\sigma}_{pr} A_{ps})_k$$

$$\Delta M_{pr} = \sum_{k=1}^n (\Delta\bar{\sigma}_{pr} A_{ps} y_{ps})_k$$

where the summation is performed for the prestressing steel layers tensioned before or at t_i ; A_{spk} and y_{psk} are the cross section and the y-coordinate of the k th prestressing steel layer.

Addition of all of the forces in the concrete parts as well as the steel layers results in $\{\Delta N, \Delta M\}_{restraint}$, the total force which would artificially prevent creep, shrinkage, and relaxation.

The artificial restraint is eliminated by the application of $\{\Delta N, \Delta M\}_{restraint}$ in a reversed directions on an adjusted transformed section composed of the area of concrete in each part, multiplied by E_c/E_{ref} plus the area of reinforcements, multiplied by E_s/E_{ref} . This produces the change in strain distribution which is used to determine the change in the stresses of the different materials according to their constitutive laws.

5.8 Verification Examples

A computer program was coded in this study for the instantaneous and time-dependent nonlinear analysis of prestressed reinforced concrete sections. This program can be used for the analysis of concrete members with any cross section shape having one axis of symmetry and reinforced with or without prestressing. This program is suitable for the nonlinear analysis of composite members made of concrete parts of different properties and steel layers (prestressing or nonprestressing) of different properties.

5.8.1 Example 1

A midspan cross section of an 80 ft (24.4 m) simple beam, see Fig. 5.5, is analyzed. The section has one layer of tensile nonprestressing steel, $A_s = 10 \text{ in}^2$ (6452 mm²), and one layer of compression nonprestressing steel, $A'_s = 4 \text{ in}^2$ (2581 mm²). The prestressing steel

has an area of $A_{ps} = 3 \text{ in}^2$ (1936 mm²). Given data: $E_c(t_o) = 4000 \text{ ksi}$ (27600 MPa), $E_{ps} = 27000 \text{ ksi}$ (186200 MPa), $E_{ns} = 29000 \text{ ksi}$ (200000 MPa), $\phi(t, t_o) = 1.5$, $c = 0.8$, $\Delta\sigma_{pr}(t, t_o) = -13 \text{ ksi}$ (-89.6 MPa), $\epsilon_{cs} = -300 \times 10^{-6}$, $f_{ct} = 0.5 \text{ ksi}$ (3.45 MPa). Consider a reference point at the top fiber. The section has been analyzed for a variety of loadings and for all behaviour from elastic to the ultimate load. The analysis has been performed for the instantaneous and time-dependent responses. The results of the current study have been compared to the linear analysis of CRACK (El-Badry, M.M., 1985). The following cases were studied:

- 1- Pure bending moment see Figs. 5.5(a) - 5.7(b).
- 2- Constant normal force (prestressing force) and varying bending moment, see Figs. (5.8(a) - 5.10(b).
- 3- Constant bending moment and changing normal force, see Figs. 5.11(a) - 5.12 (b).
- 4- Moment-curvature diagram for the case of pure bending, see Fig. 5.13.
- 5- Moment-curvature diagram for the constant normal force and varying bending moment, see Fig. 5.14.
- 6- Normal force-curvature diagram for the case of constant bending moment and changing normal force, see Fig. 5.15.
- 7- Comparison with CRACK (El-Badry, M.M., 1985), see Figs. 5.16 and 5.17.
- 8- Time-dependent analysis (stress and strain distributions), normal force-curvature diagram, and comparison between instantaneous and time-dependent responses for the case of normal force and bending moment, see Figs. 5.18(a) - 5.20.
- 9- Stress-Strain relationships for the instantaneous and time-dependent effects, se Fig. 5.21.

5.8.2 Example 2

The beam shown in Fig. 5. 22 was one of the pretensioned specimen tested by Priestley, Park, and Lu (1971) and was made from concrete with the following properties: $f'_c = 44.9$ MPa (6.5 ksi), $\epsilon'_c = -0.0025$, and $f_{cr} = 2.9$ MPa (0.42 ksi). The member was pretensioned using two 7mm (0.27 in) diameter wires with a total area of 77 mm^2 (0.12 in^2). The wires had a rounded stress-strain curve which could be represented by the following modified Ramberg-Osgood function:

$$f_{pf} = 200 \times 10^3 \epsilon_{pf} \left\{ 0.032 + \frac{0.968}{[1 + (135 \epsilon_{pf})^6]^{1/6}} \right\}$$

The prestressing of the member was such that $\Delta \epsilon = 4.24 \times 10^{-3}$. This beam has been used in the current nonlinear analysis to verify the short-term moment-curvature response. It can be seen that there is a good agreement between the obtained theoretical results and the experimental data.

5.8.3 Example 3

The analytical results from the current study were compared to the analytical results of the analysis of short and long-term moment-curvature responses of the cross section shown in Fig. 5.23(a) using the layer-by-layer approach by Collins and Mitchell (1987), see Fig. 5.23 (b). The beam is precast pretensioned single-tee beam whose section is shown in Fig. 5.23(a). The low relaxation prestressing strands were tensioned to a stress of 1400 MPa (203 ksi) in the pretensioning bed, prior to casting of the concrete. The stress-strain relationship of the strands is given by the following formula:

$$f_{pf} = 200 \times 10^3 \epsilon_{pf} \left\{ 0.025 + \frac{0.975}{[1 + (118 \epsilon_{pf})^{10}]^{0.10}} \right\}$$

except that the strands are assumed to rupture at a strain of 0.04 (i.e. 4%). Collins and Mitchell (1987) used a computer program (PLANE) to compute the moment-curvature response. In their analysis, the cross section was represented by eight layers and the eight steel layers lumped at their C.G. For the long-term response, the creep coefficient of the concrete is assumed to be equal to 2.7 and that the concrete was first loaded when its compressive strength was 25 MPa (3.6 ksi). The initial tangent modulus of elasticity of the concrete is therefore equal to 7430 MPa (1077 ksi). For the long term application of loading, the compressive strength of concrete will be 35 MPa (5 ksi) and the cracking stress will be 2 MPa (0.29 ksi). It will be assumed that the prestressing strands will lose 3% of their initial stress due to relaxation and will rupture at a strain of 0.054. In addition to the creep and relaxation, it is assumed that a concrete shrinkage strain of -0.48×10^{-3} occurs.

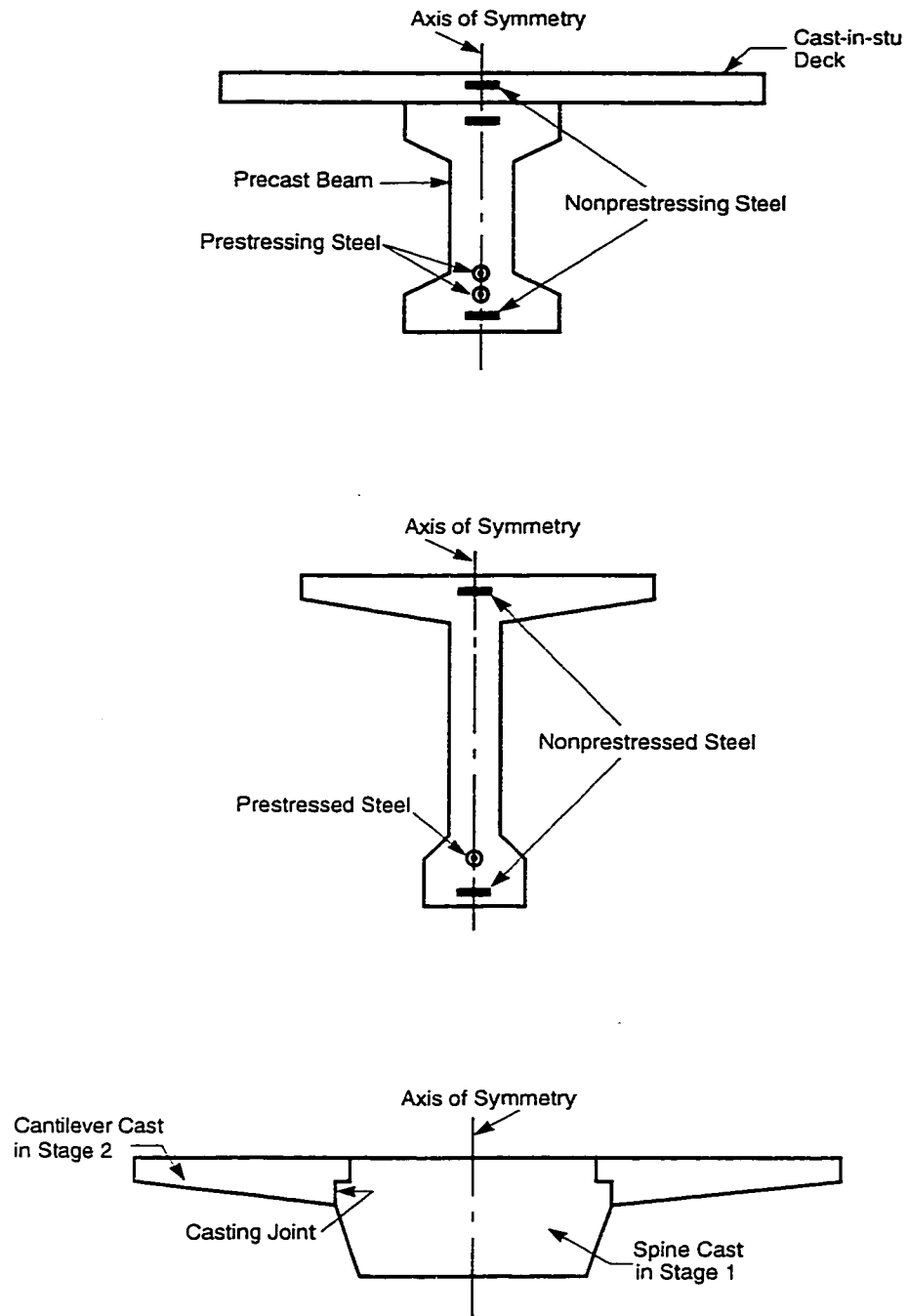


Fig. 5.1 Typical Cross Sections Treated in the Present Study

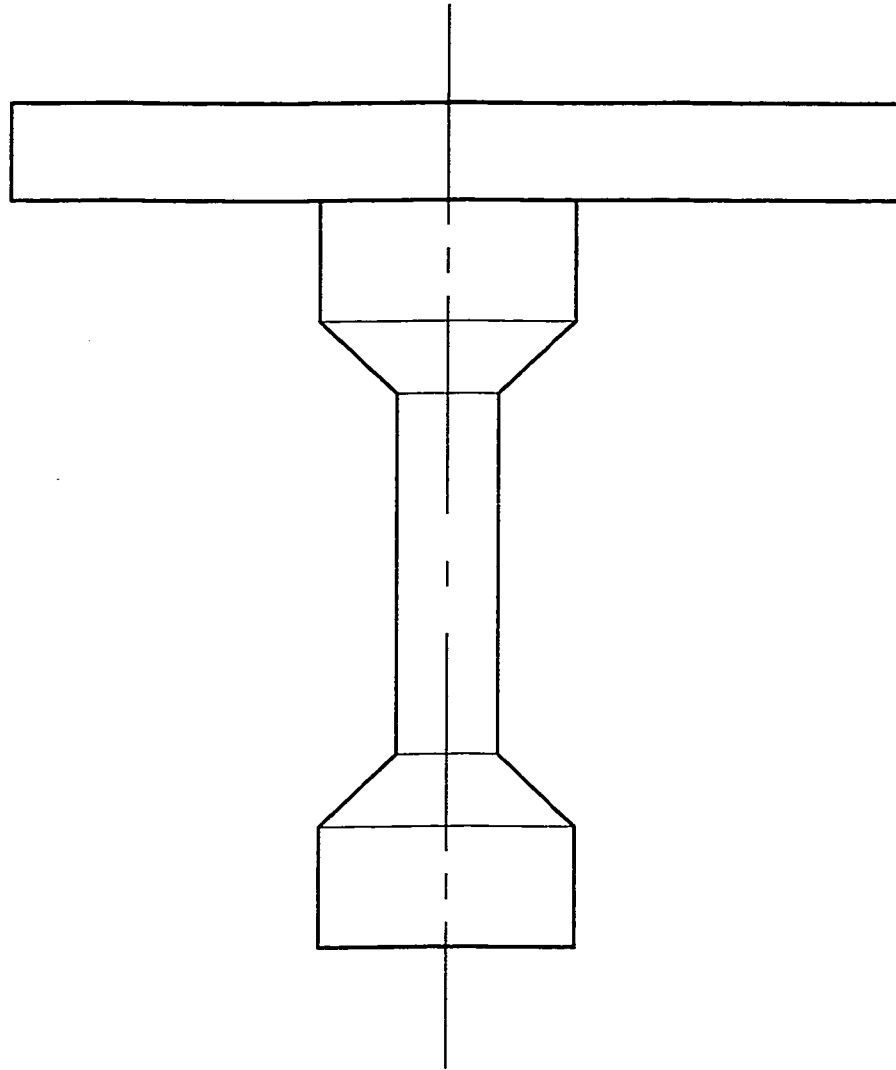


Fig. 5.2 Division of a Concrete Section into Trapeziums and Rectangles

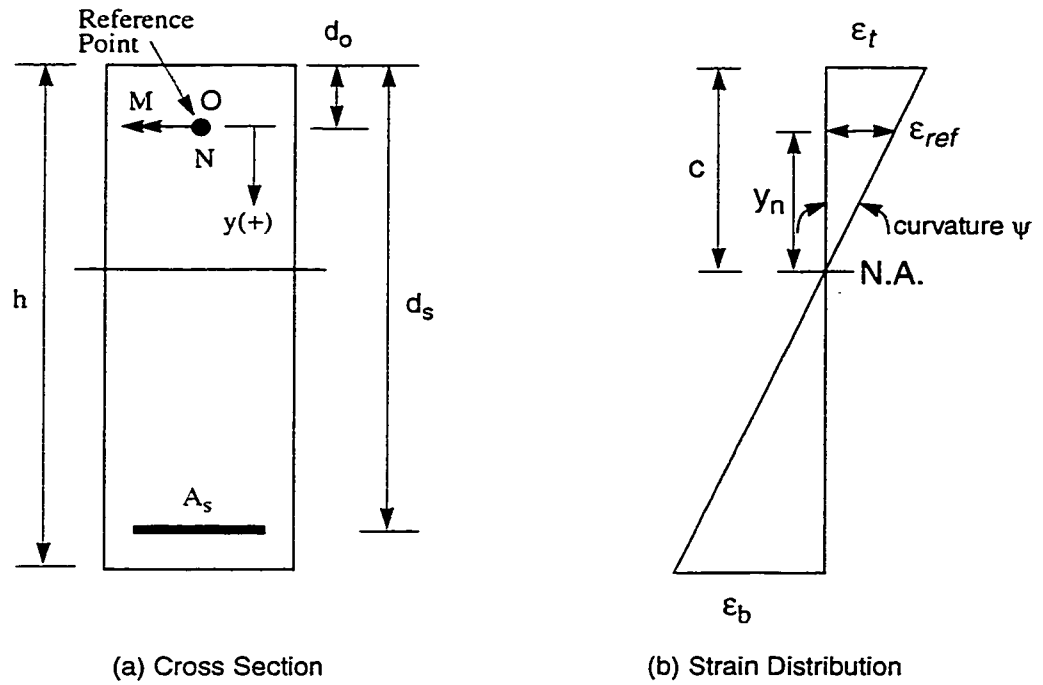


Fig. 5.3 Cross Section and Strain Distribution

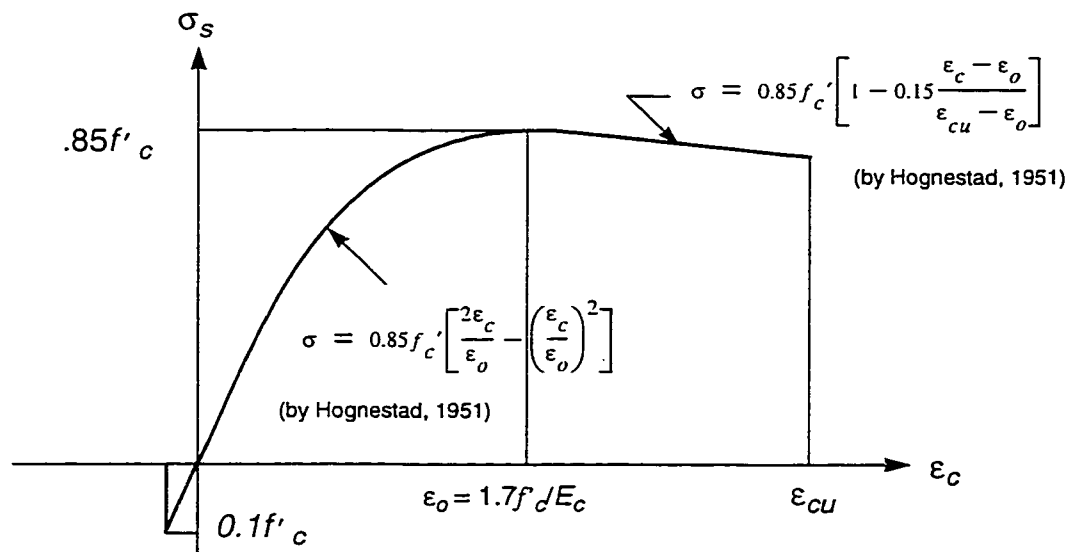


Fig. 5.4 Idealized Concrete Stress-Strain Relationship

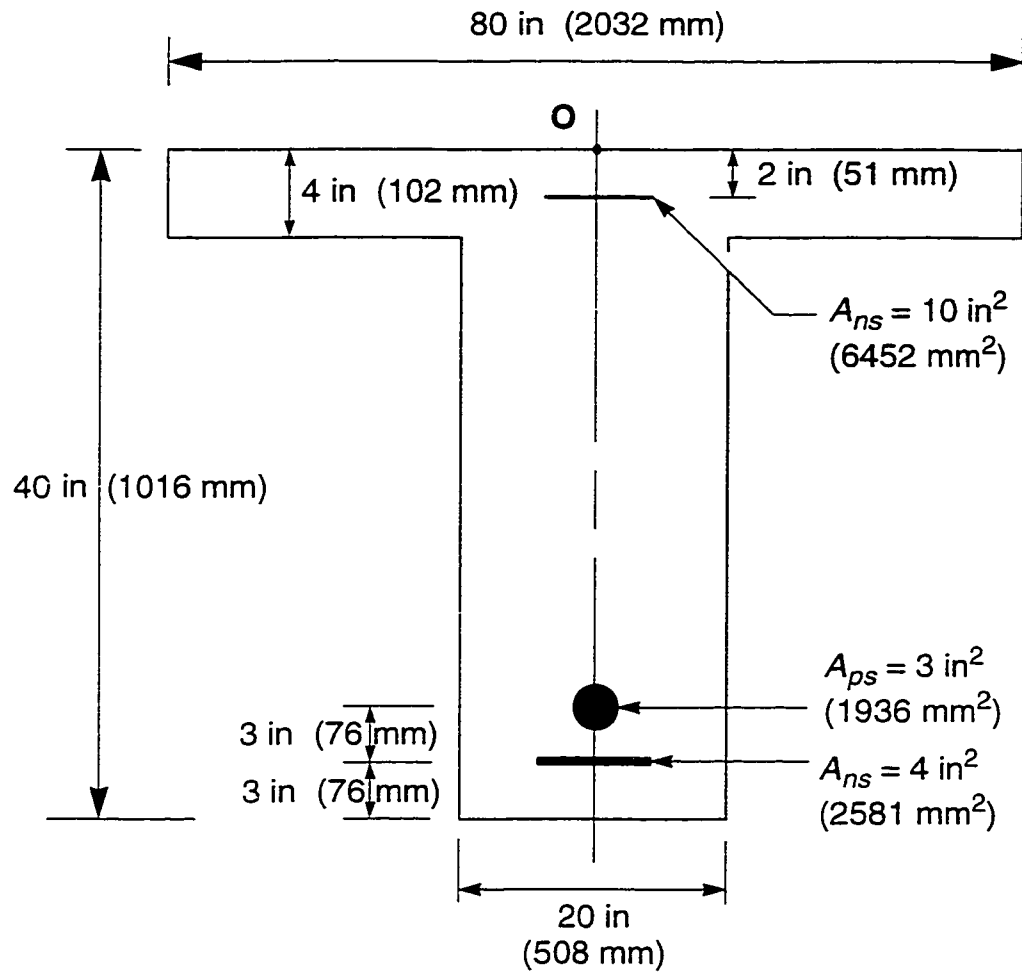


Fig. 5.5 Prestressed Concrete T-Section

$N = 0$
 $M = 1000 \text{ k.in (113 kN.m)}$

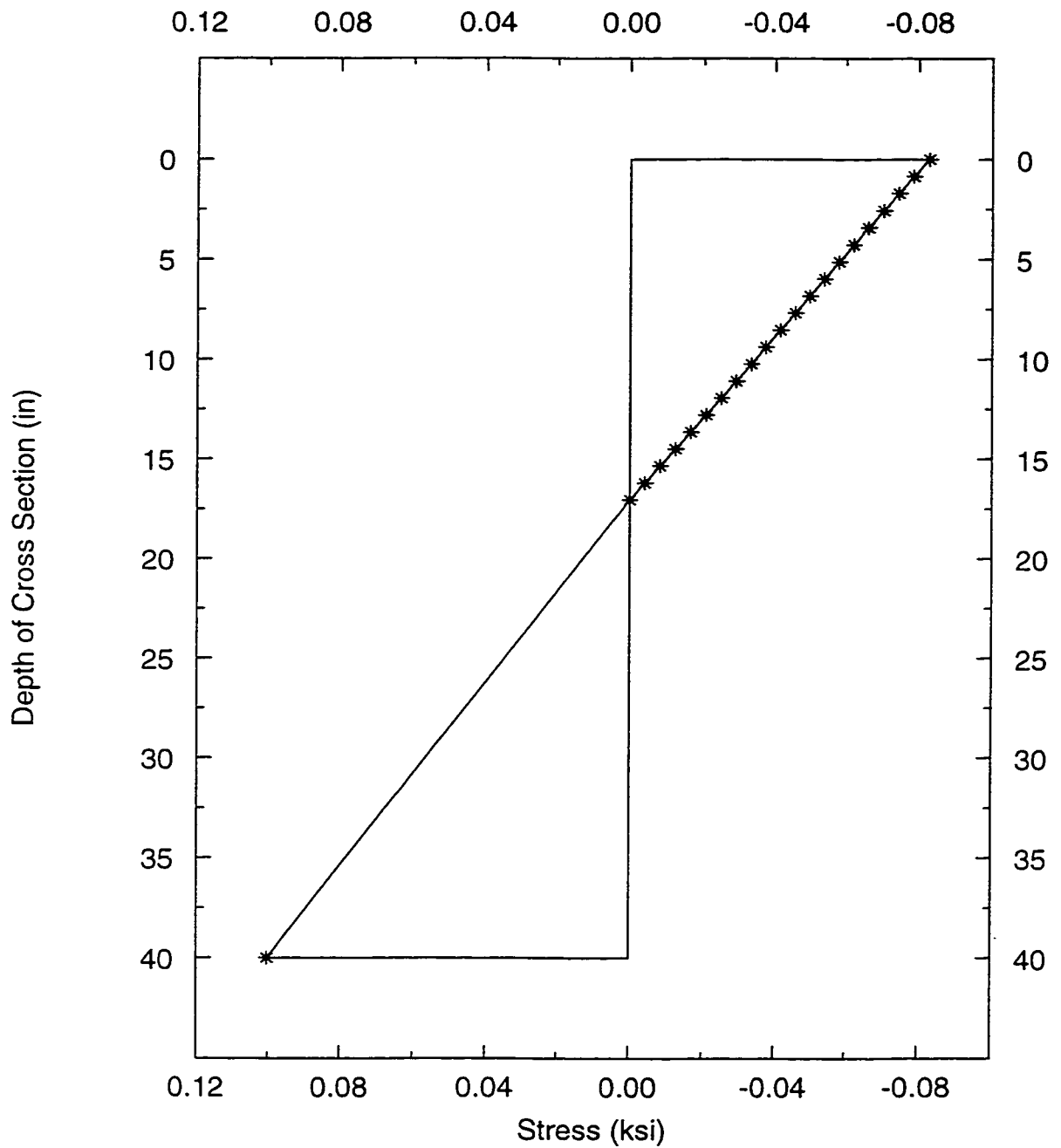


Fig. 5.5(a) Stress Distribution

$N = 0$
 $M = 1000 \text{ k.in (113 kN.m)}$

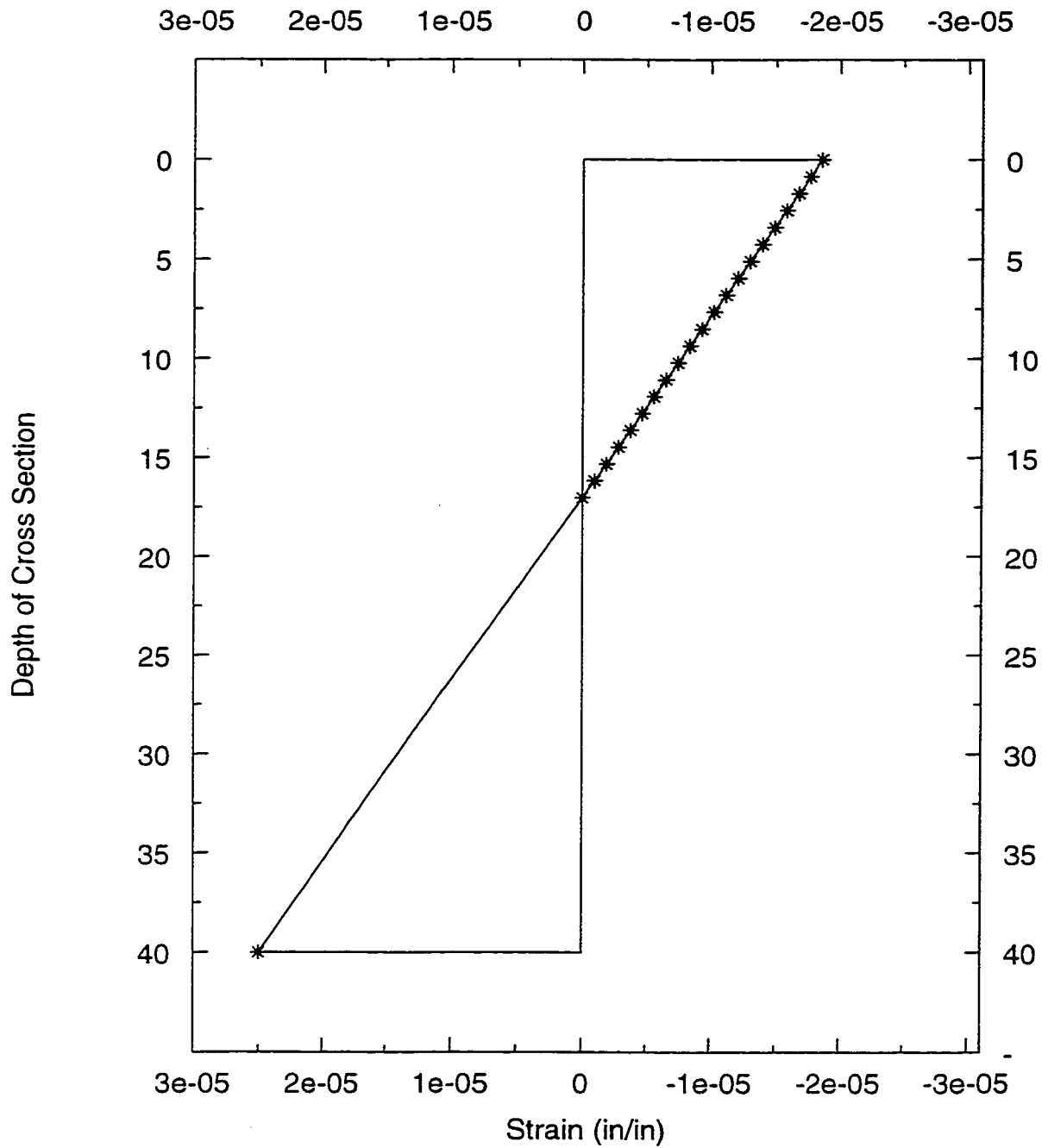


Fig. 5.5(b) Strain Distribution

$N = 0$
 $M = 40000 \text{ k.in (4520 kN.m)}$

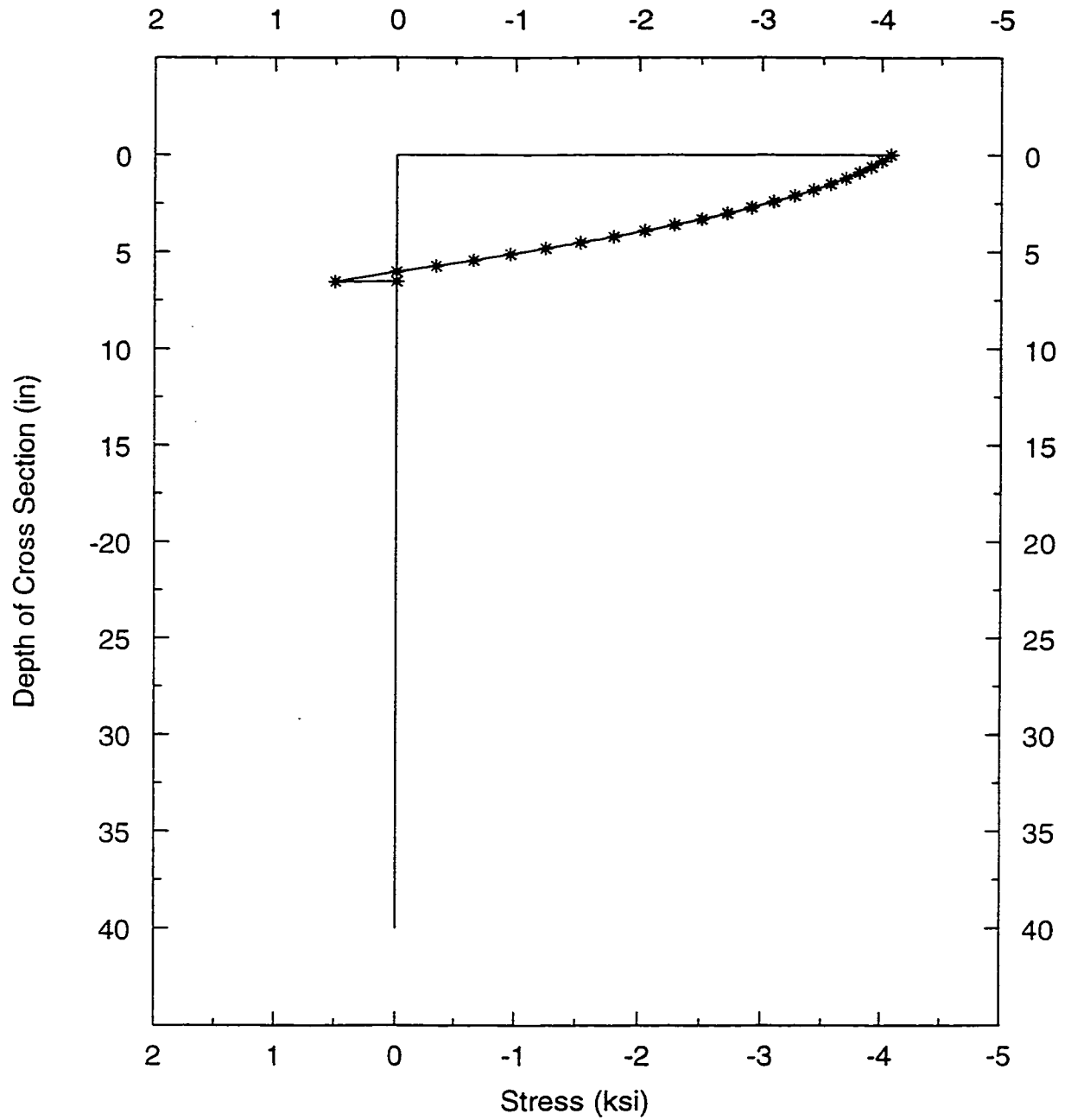


Fig. 5.6(a) Stress Distribution

$N = 0$
 $M = 40000 \text{ k.in (4520 kN.m)}$

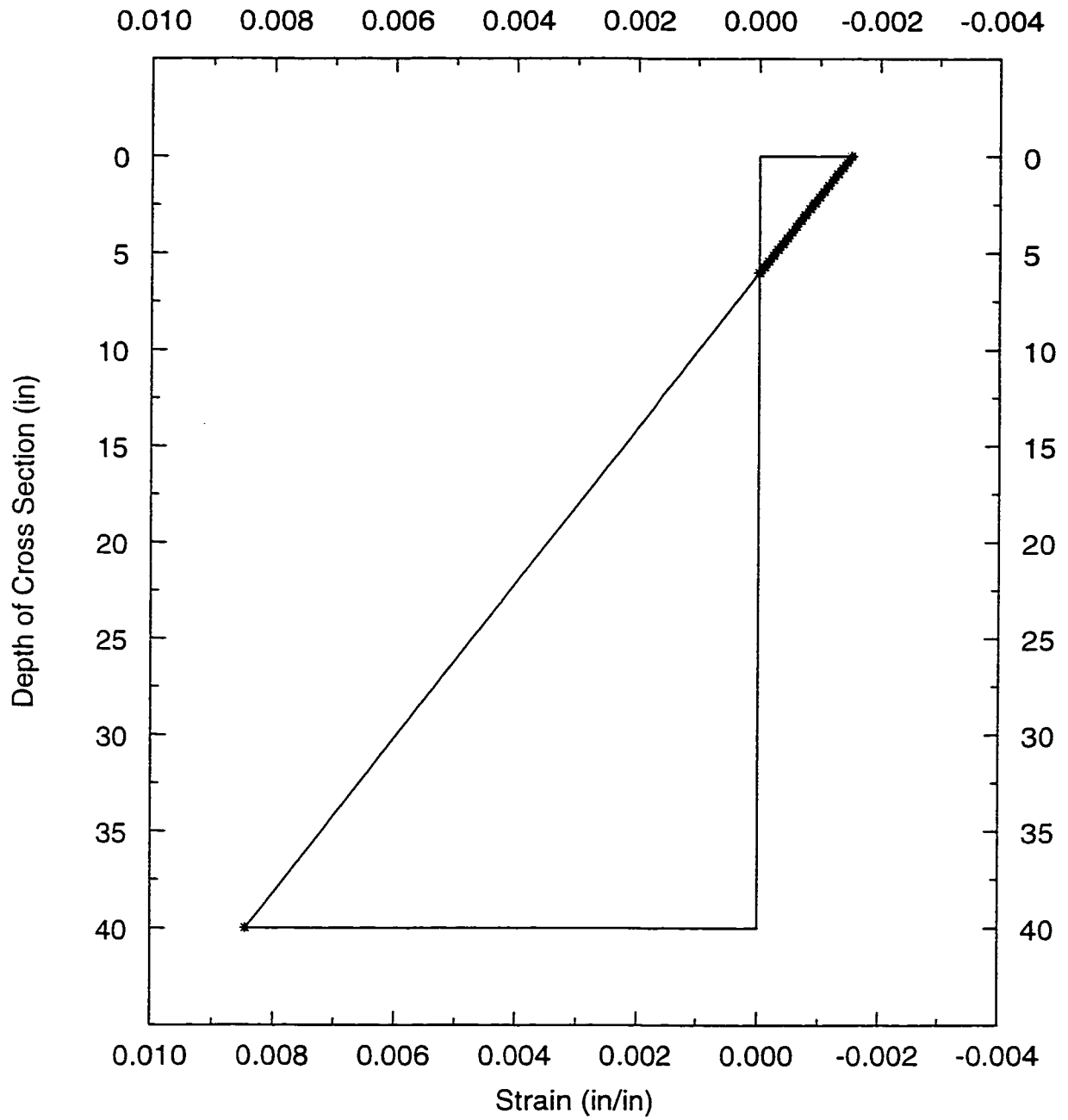


Fig. 5.6(b) Strain Distribution

$N = 0$
 $M = 45000 \text{ k.in (5085 kN.m)}$

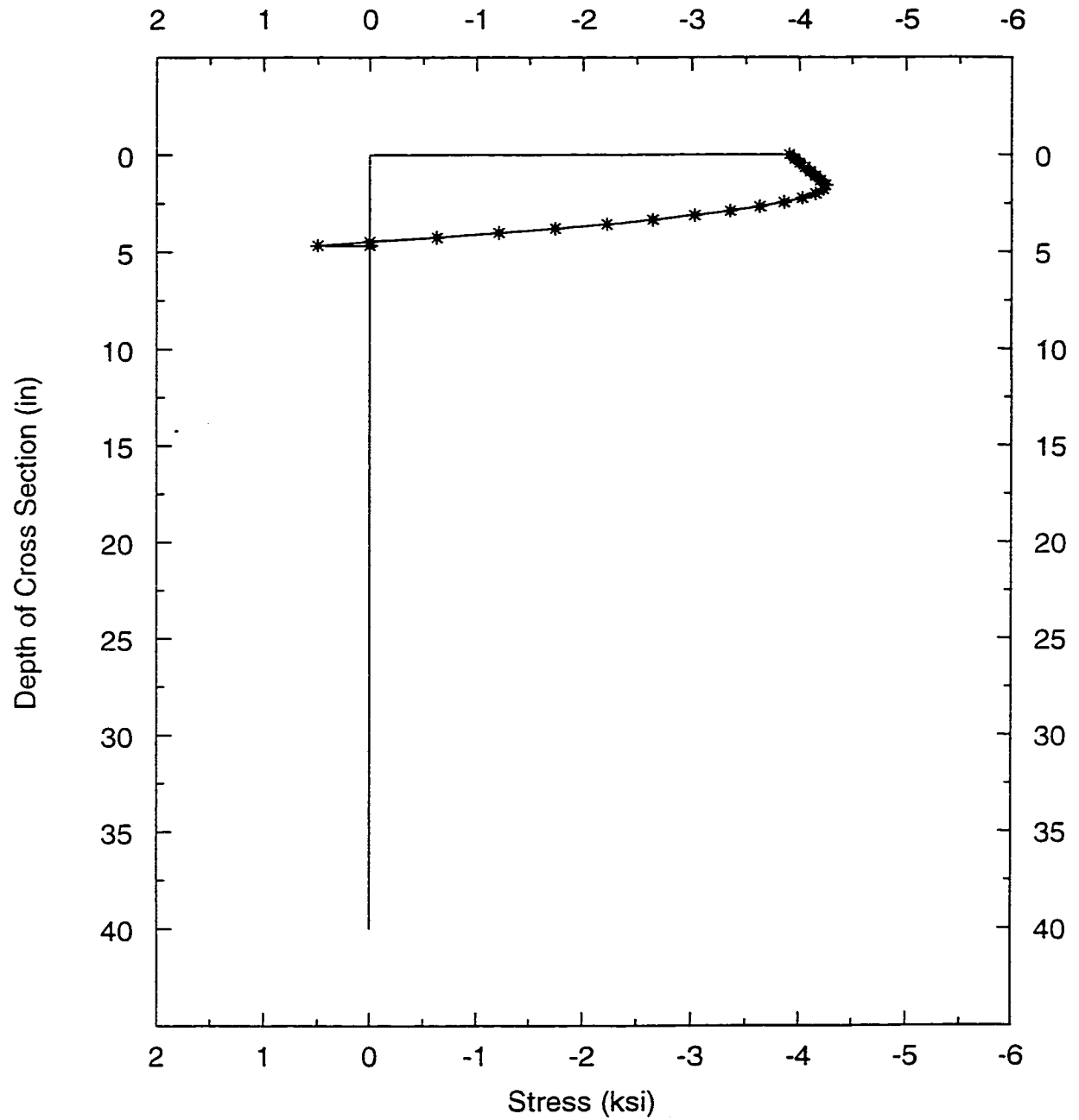


Fig. 5.7(a) Stress Distribution

$N = 0$
 $M = 45000 \text{ k.in (5085 kN.m)}$

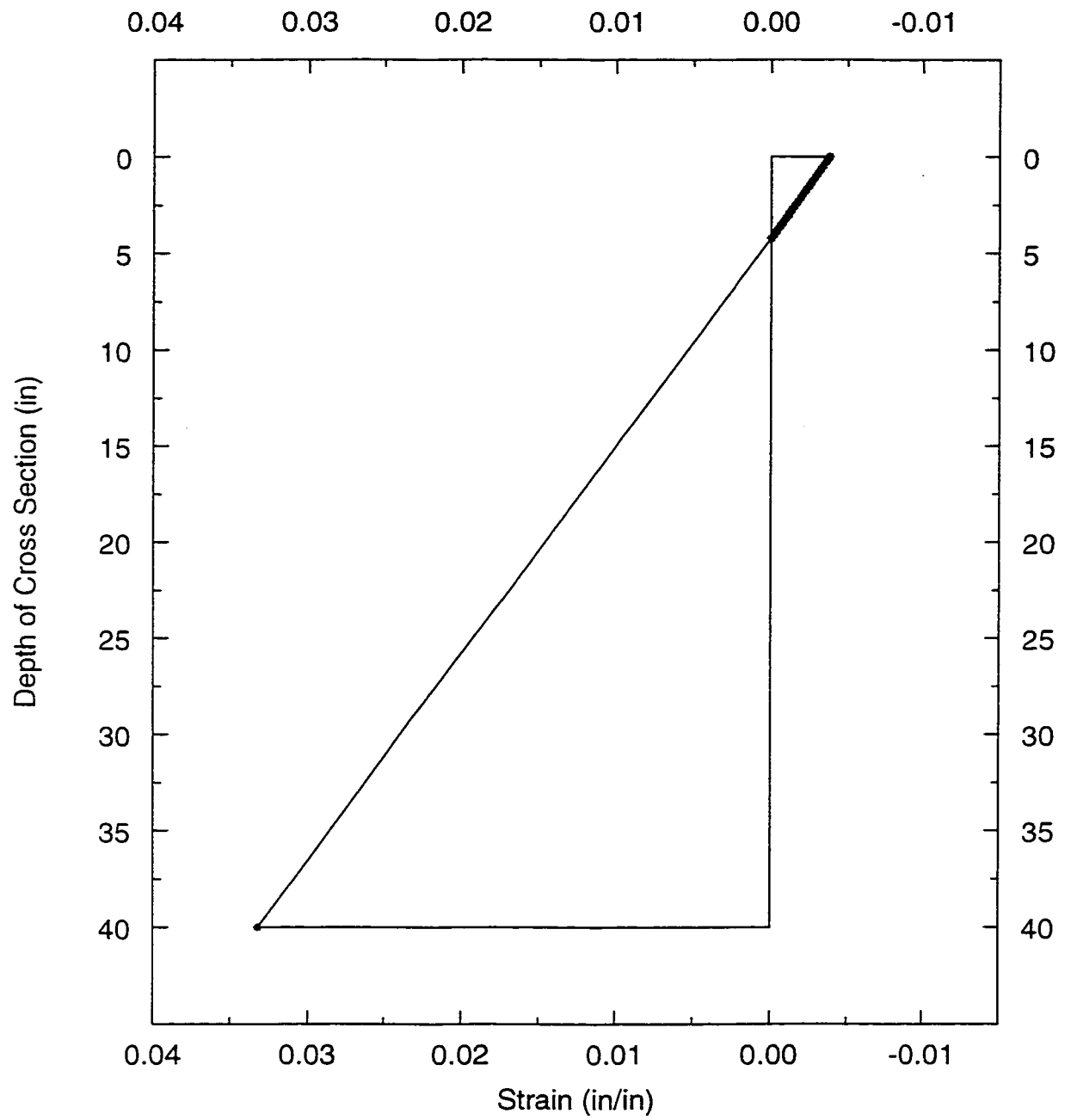


Fig. 5.7(b) Strain Distribution

$N = -600 \text{ k} \text{ } (-2669 \text{ kN})$
 $M = 1000 \text{ k.in} \text{ } (113 \text{ kN.m})$

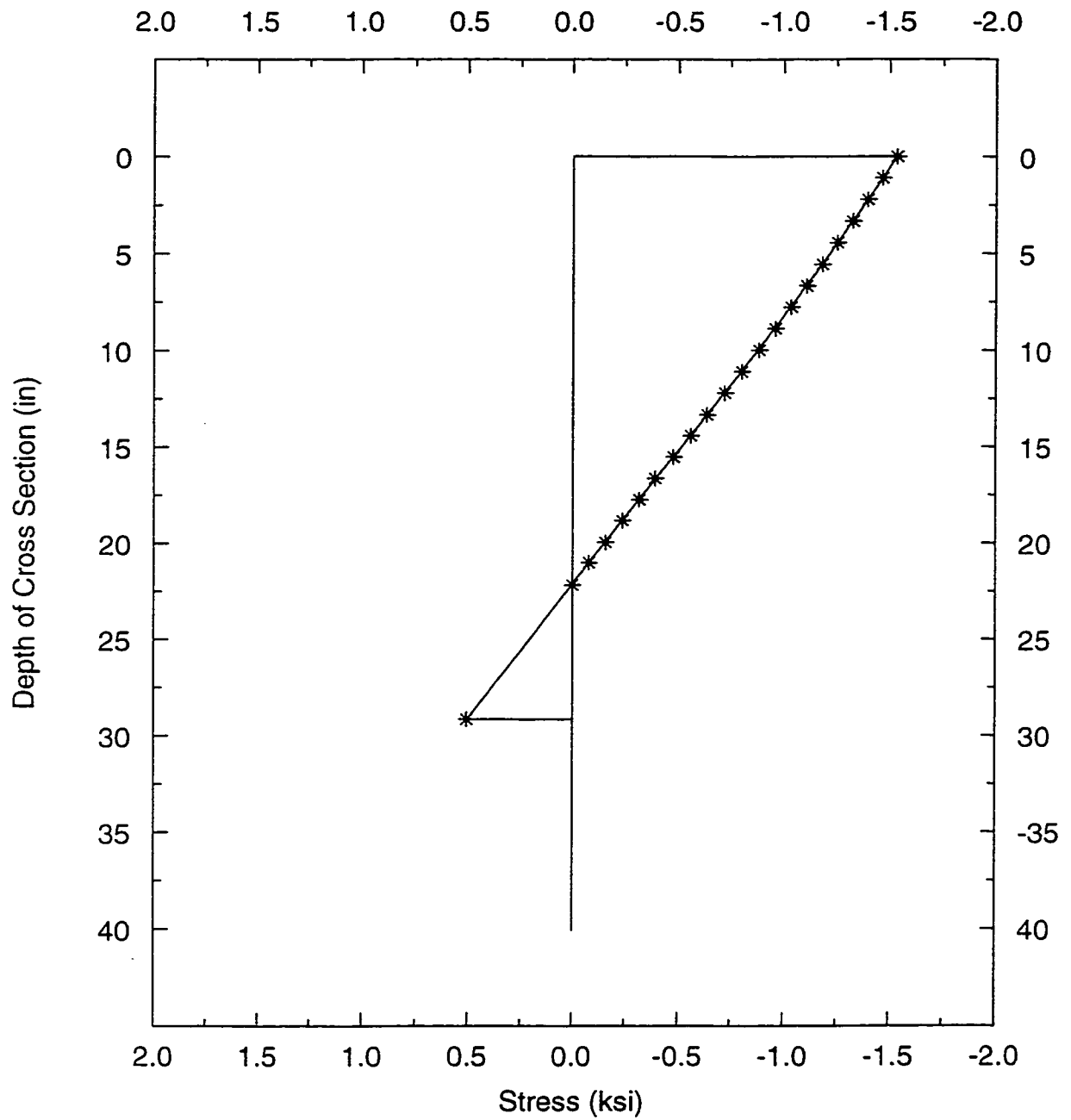


Fig. 5.8(a) Stress Distribution

$N = -600 \text{ k} \text{ } (-2669 \text{ kN})$
 $M = 1000 \text{ k.in} \text{ } (113 \text{ kN.m})$

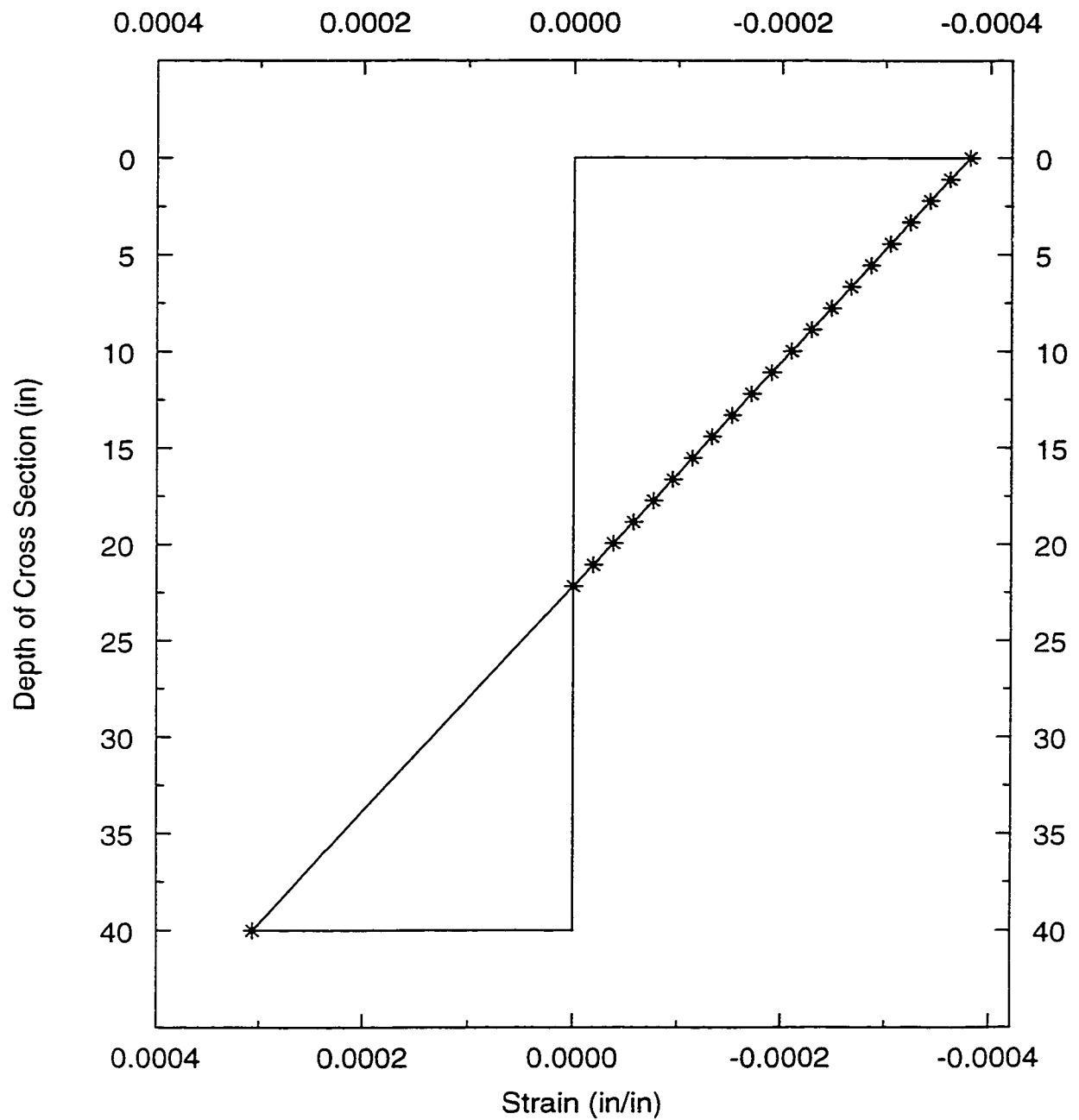


Fig. 5.8(b) Strain Distribution

$N = -600 \text{ k} \text{ } (-2669 \text{ kN})$
 $M = 30000 \text{ k.in} \text{ } (3390 \text{ kN.m})$

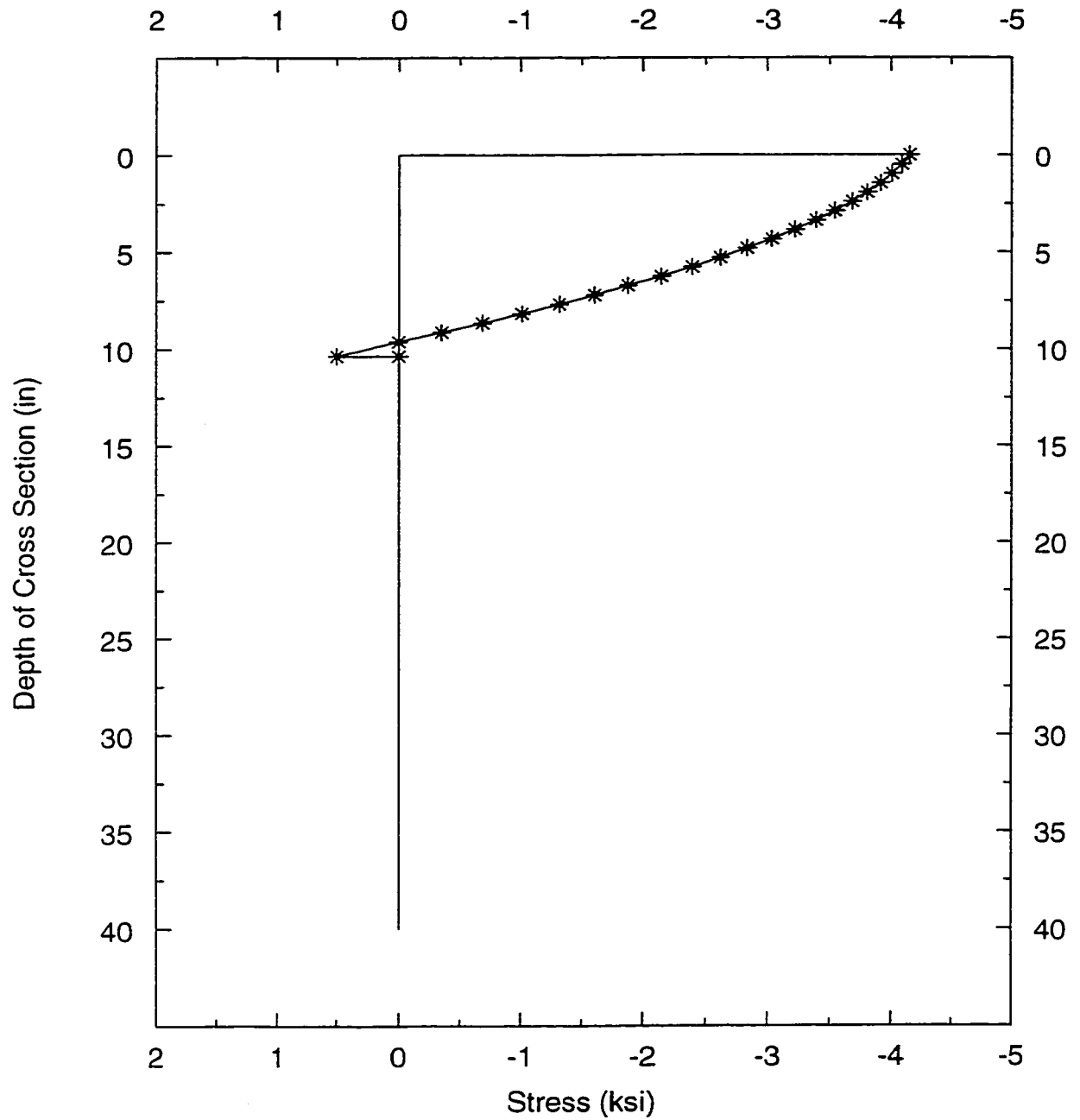


Fig. 5.9(a) Stress Distribution

$N = -600 \text{ k} \text{ } (-2669 \text{ kN})$
 $M = 30000 \text{ k.in} \text{ } (3390 \text{ kN.m})$

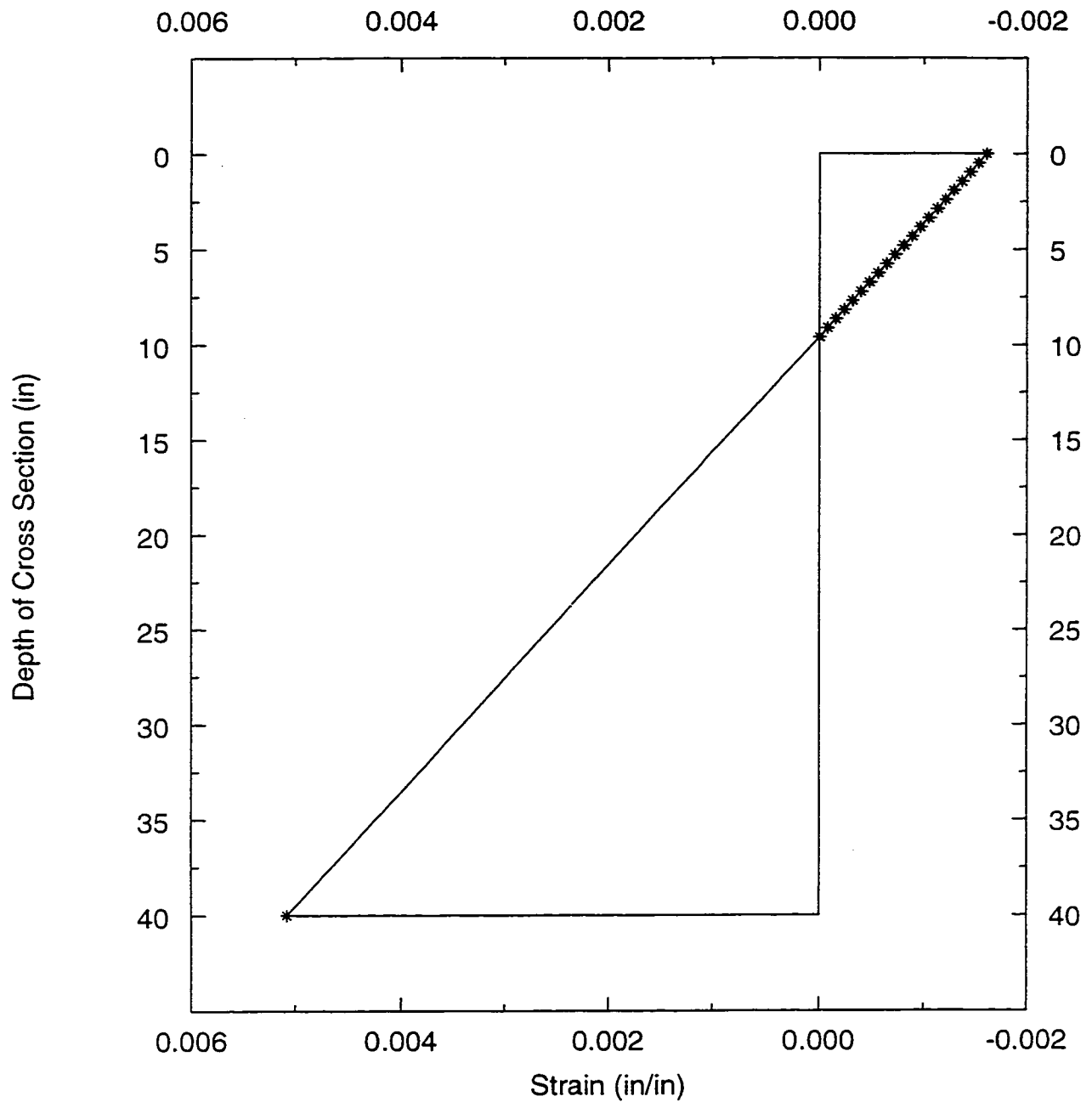


Fig. 5.9(b) Strain Distribution

$N = -600 \text{ k} \text{ } (-2669 \text{ kN})$
 $M = 40000 \text{ k.in} \text{ } (4520 \text{ kN.m})$

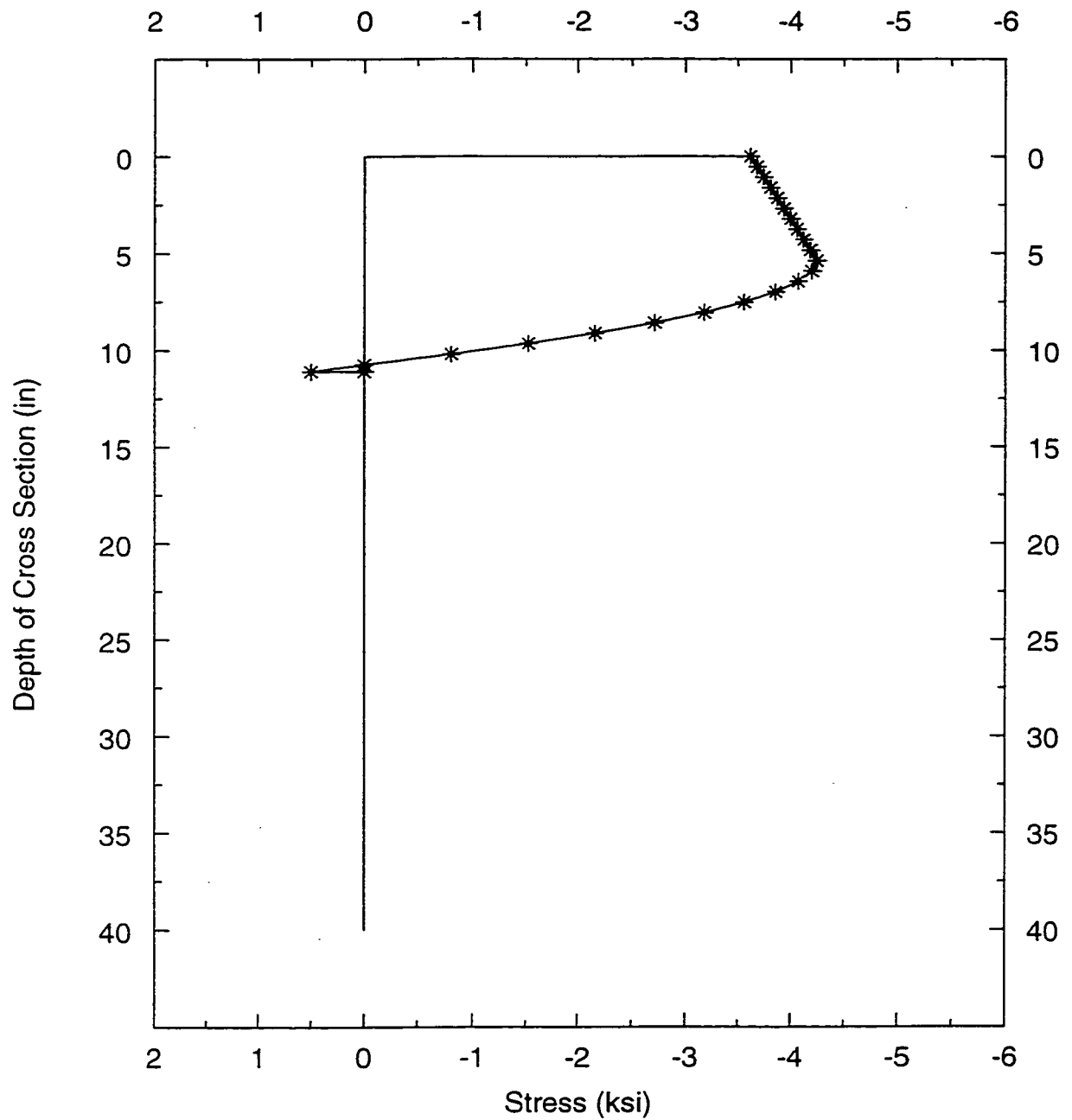


Fig. 5.10(a) Stress Distribution

$N = -600 \text{ k} \text{ } (-2669 \text{ kN})$
 $M = 40000 \text{ k.in} \text{ } (4520 \text{ kN.m})$

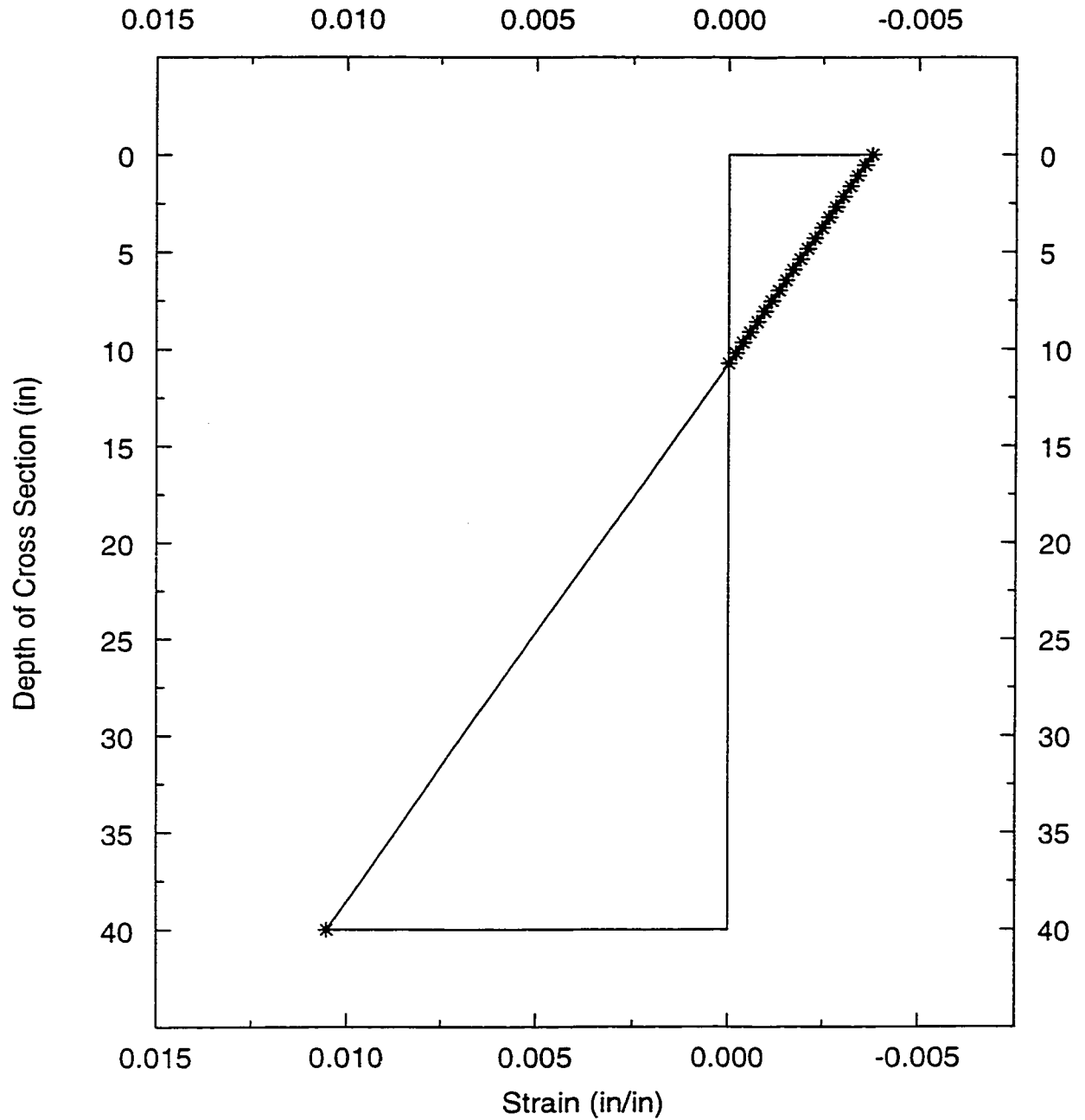


Fig. 5.10(b) Strain Distribution

$N = -2000 \text{ k} \text{ } (-8896 \text{ kN})$
 $M = 1000 \text{ k.in} \text{ } (113 \text{ kN.m})$

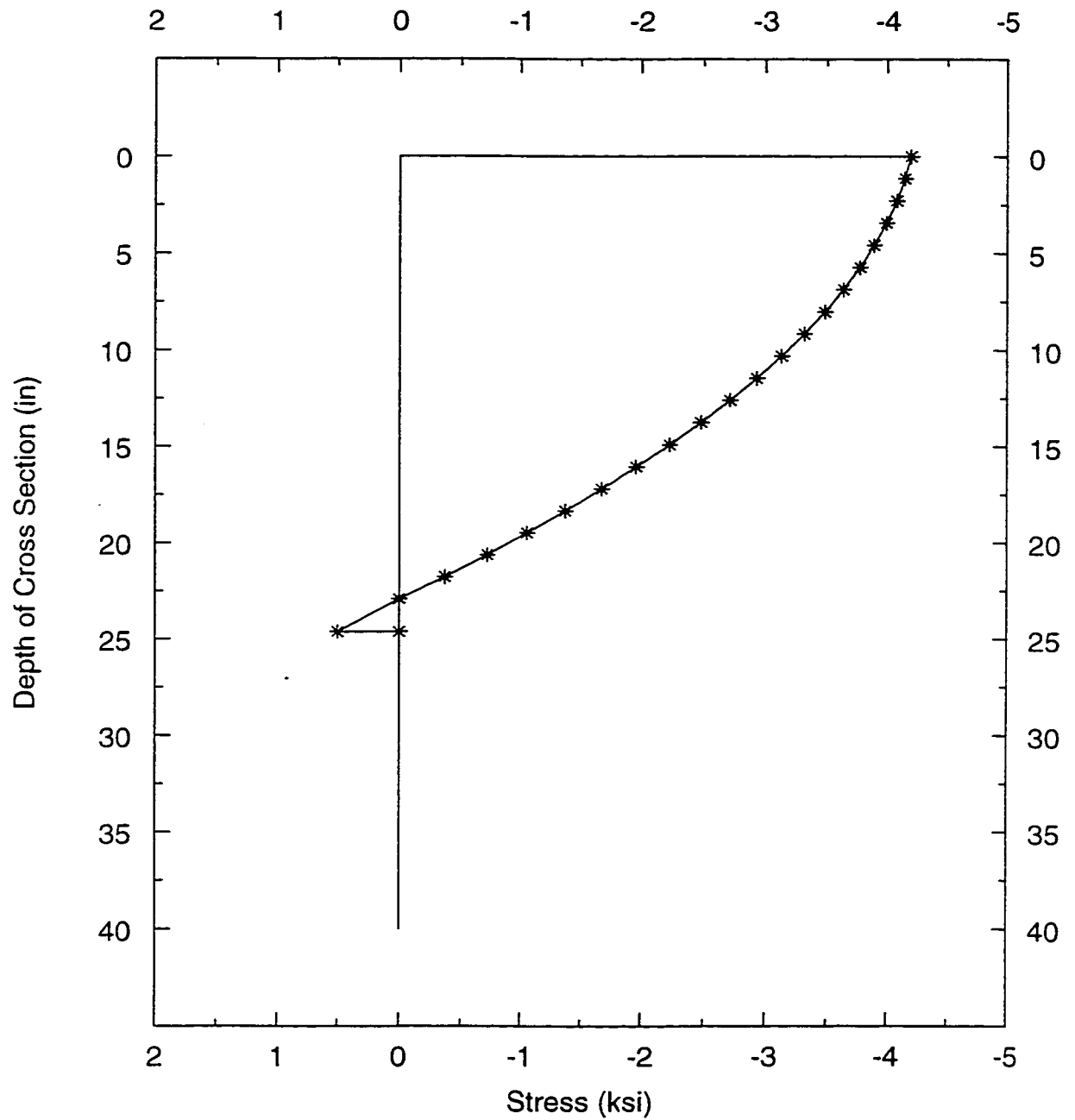


Fig. 5.11(a) Stress Distribution

$N = -2000 \text{ k} \text{ } (-8896 \text{ kN})$
 $M = 1000 \text{ k.in} \text{ } (113 \text{ kN.m})$

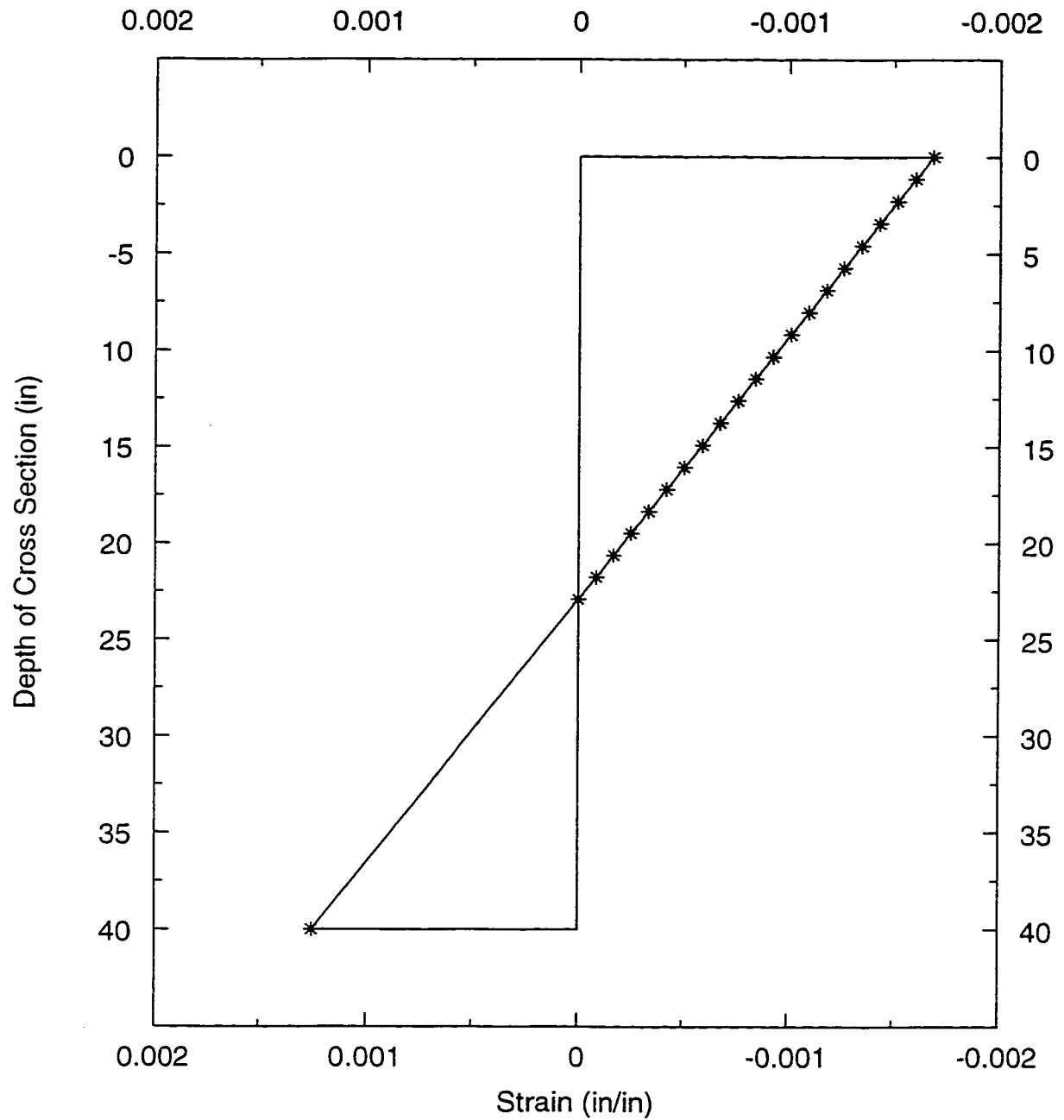


Fig. 5.11(b) Strain Distribution

$N = -2250 \text{ k} \text{ } (-10008 \text{ kN})$
 $M = 1000 \text{ k.in} \text{ } (113 \text{ kN.m})$

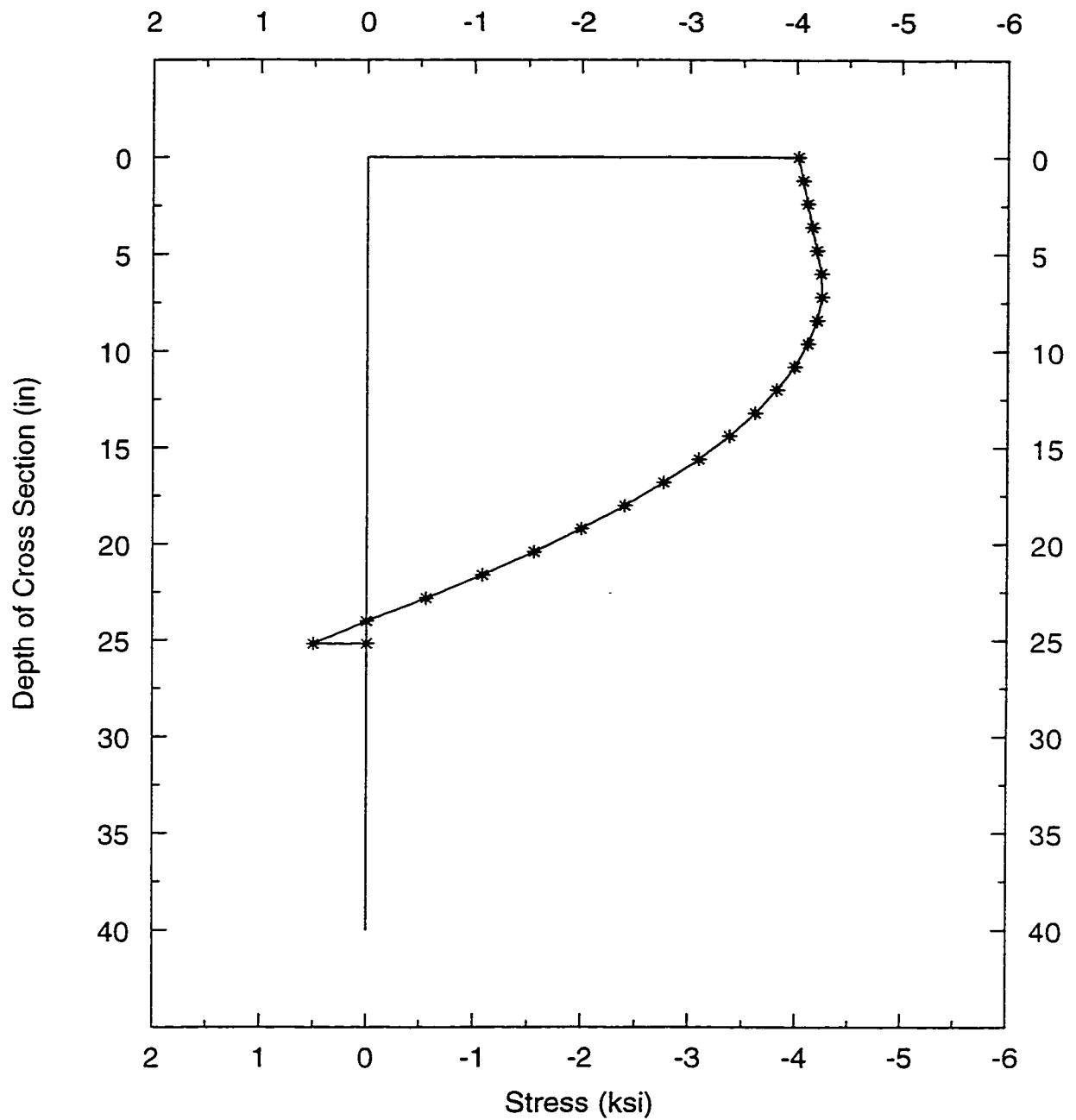


Fig. 5.12(a) Stress Distribution

$N = -2250 \text{ k} \text{ } (-10008 \text{ kN})$
 $M = 1000 \text{ k.in} \text{ } (113 \text{ kN.m})$

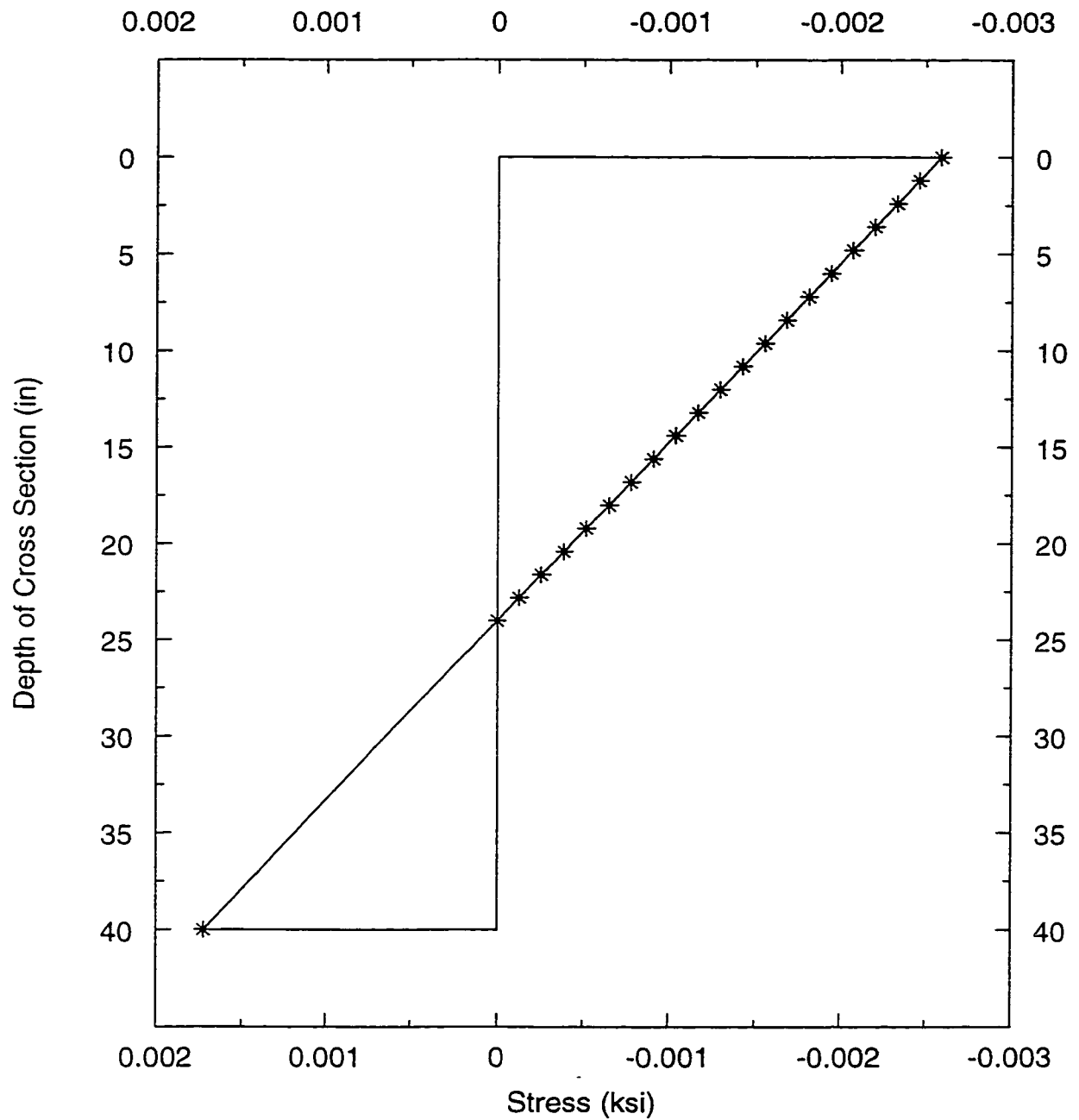


Fig. 5.12(b) Strain Distribution

Pure Bending Moment Case

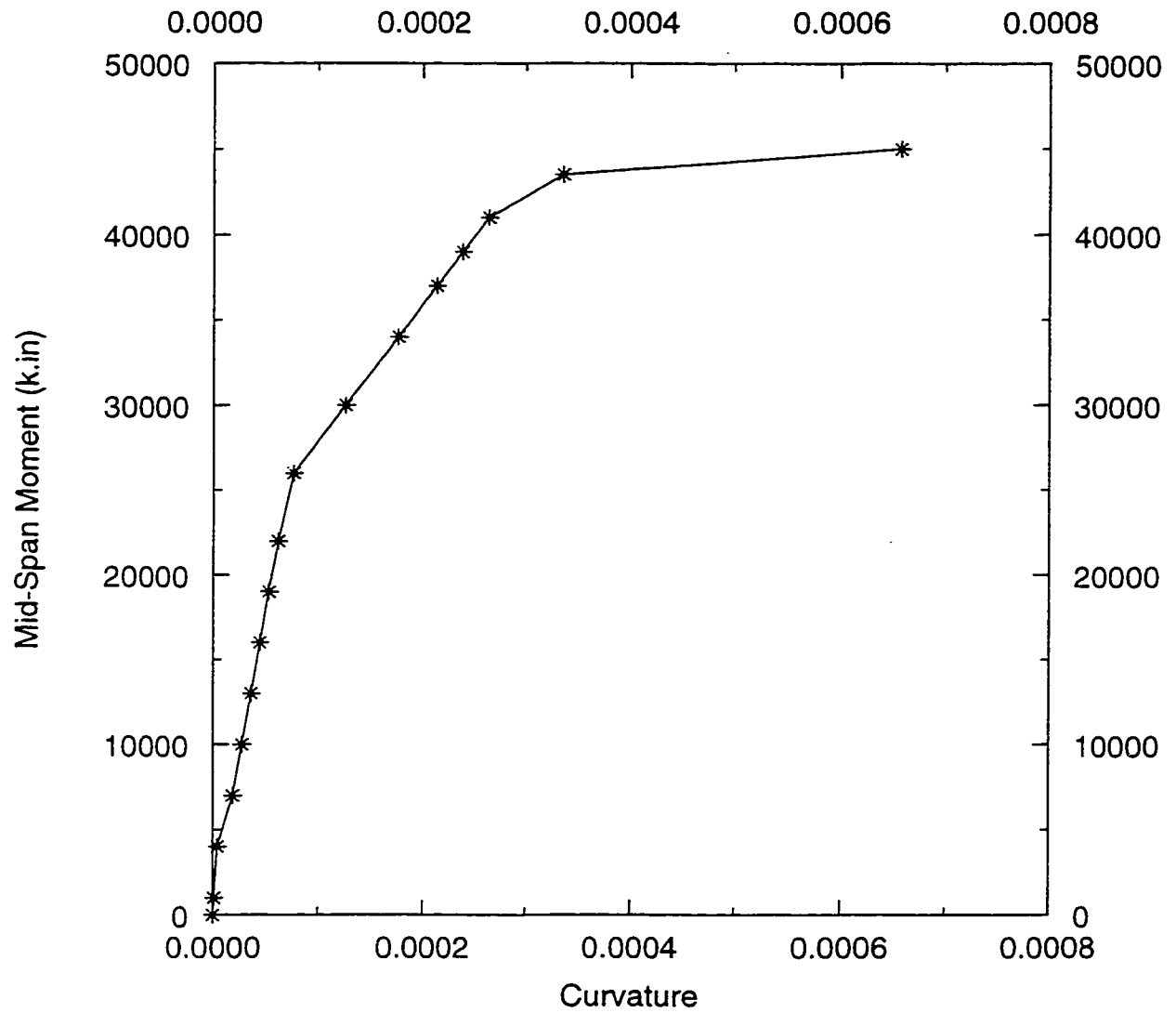


Fig. 5.13 Moment-Curvature Relationship of Mid-span Cross Section
(Case of Pure Bending Moment)

Normal Force is fixed (-600 k) (-2669 kN)

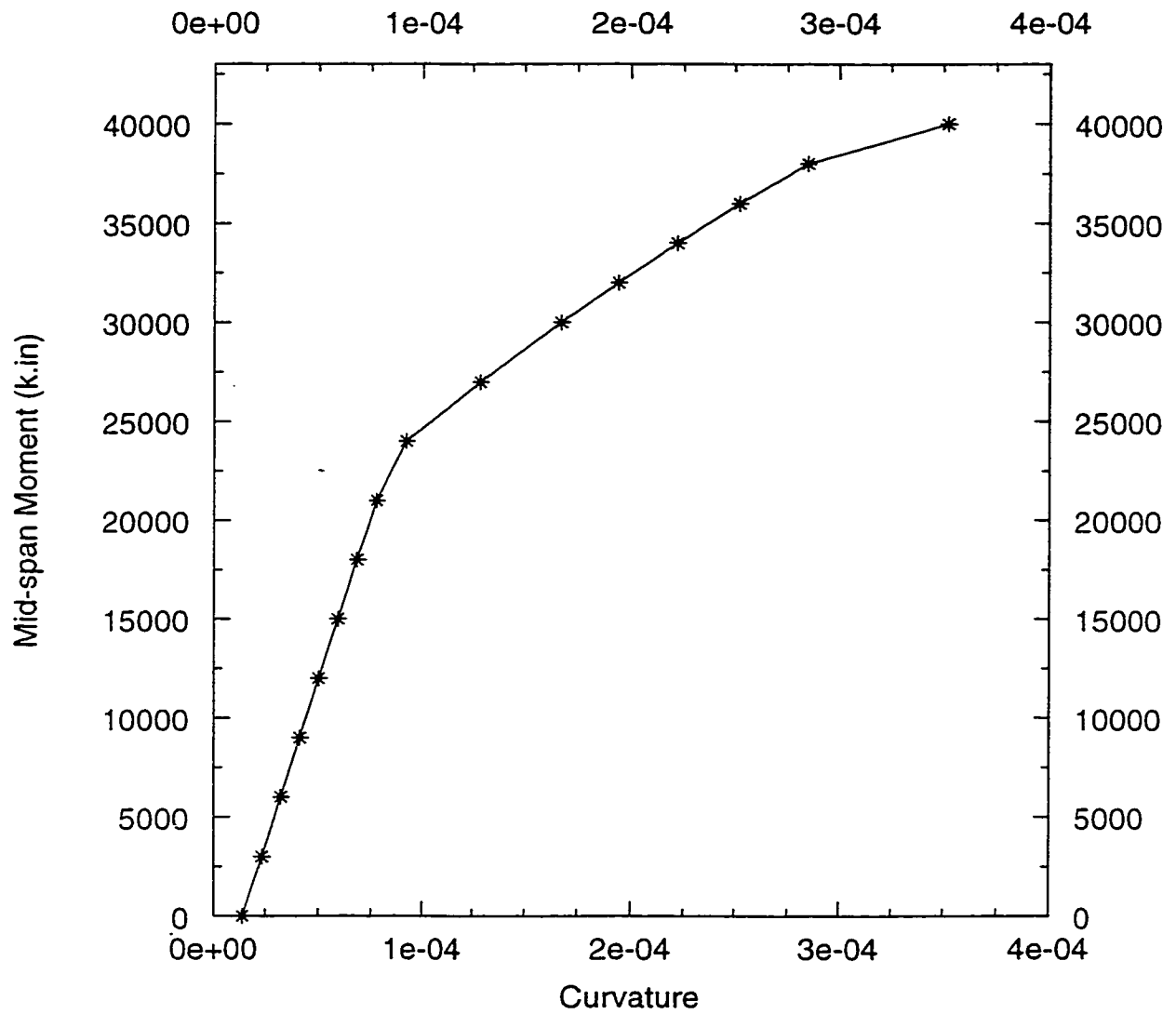


Fig. 5.14 Moment-Curvature Relationship of Mid-span Cross Section
(Case of Fixed Normal Force)

Bending moment is fixed (1000 k.in) (113 kN.m)

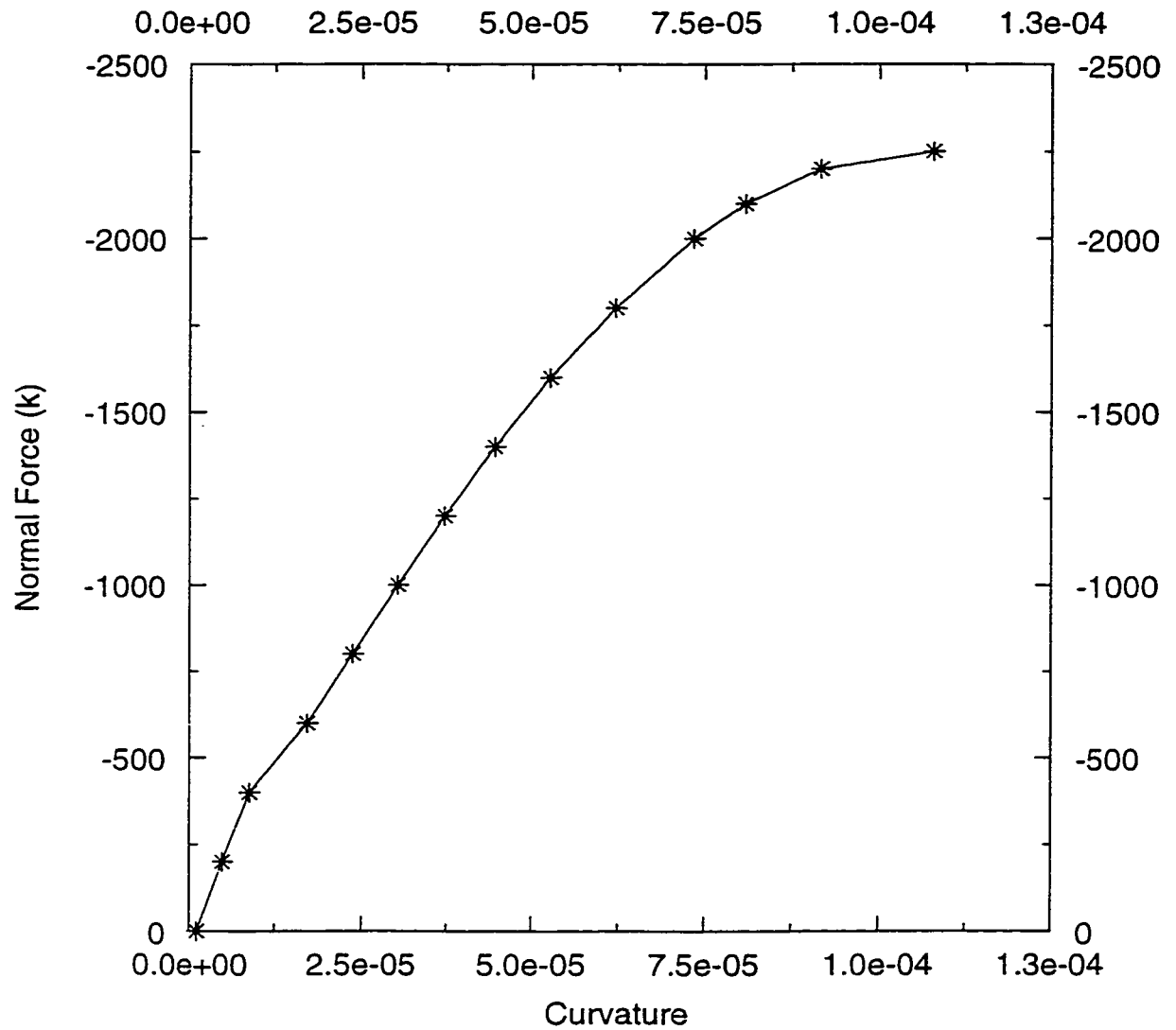


Fig. 5.15 Normal Force-Curvature Relationship of Mid-span Cross Section
(Case of Fixed Bending Moment)

$N = -100 \text{ k} \text{ } (-445 \text{ kN})$
 $M = 500 \text{ k.in} \text{ } (56.5 \text{ kN.m})$

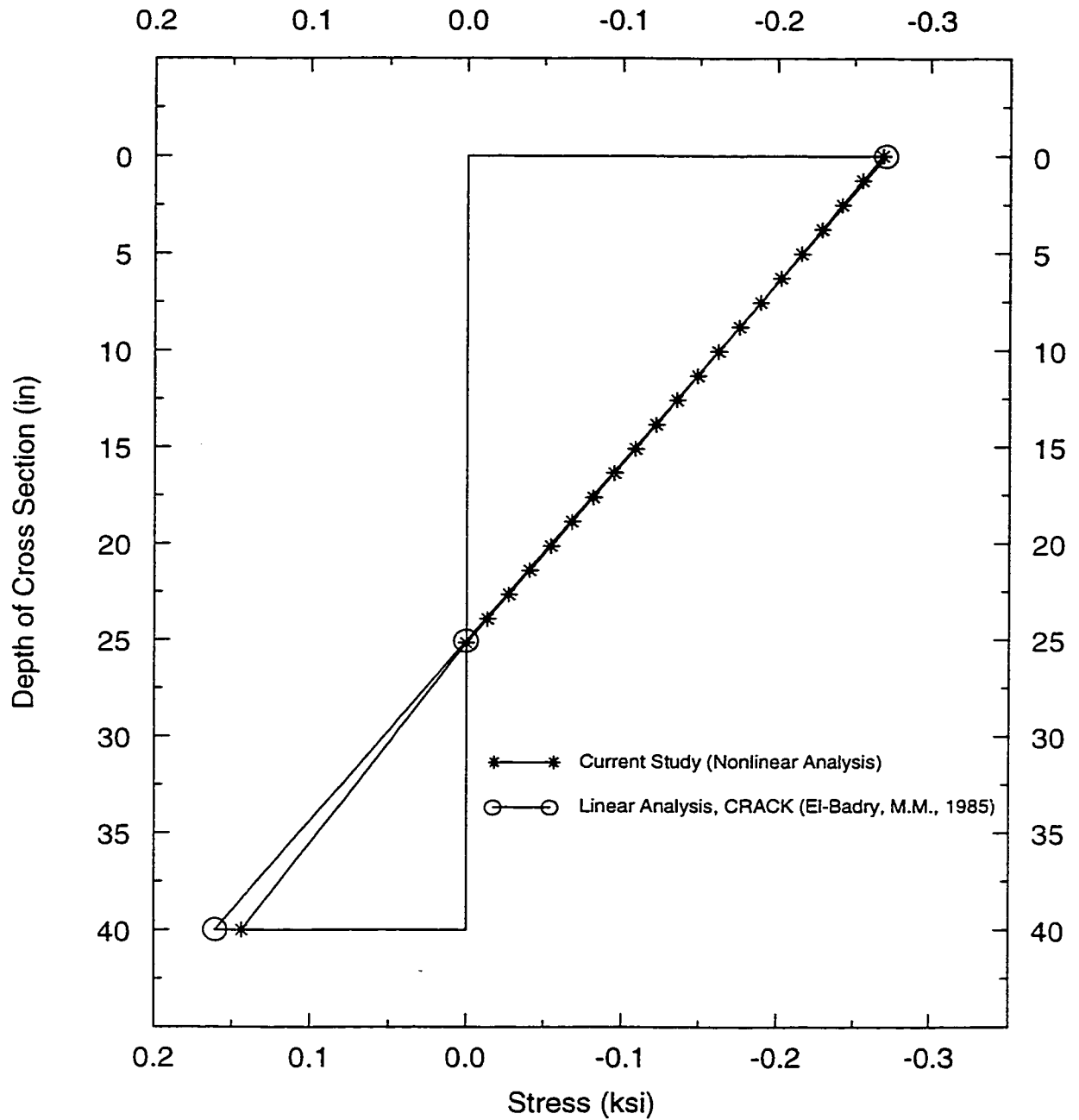


Fig. 5.16 Comparison Between This Study and Linear Analysis, CRACK
 (El-Badry, M.M., 1985)

$N = -600 \text{ k} \text{ } (-2669 \text{ kN})$
 $M = 1000 \text{ k.in} \text{ } (113 \text{ kN.m})$

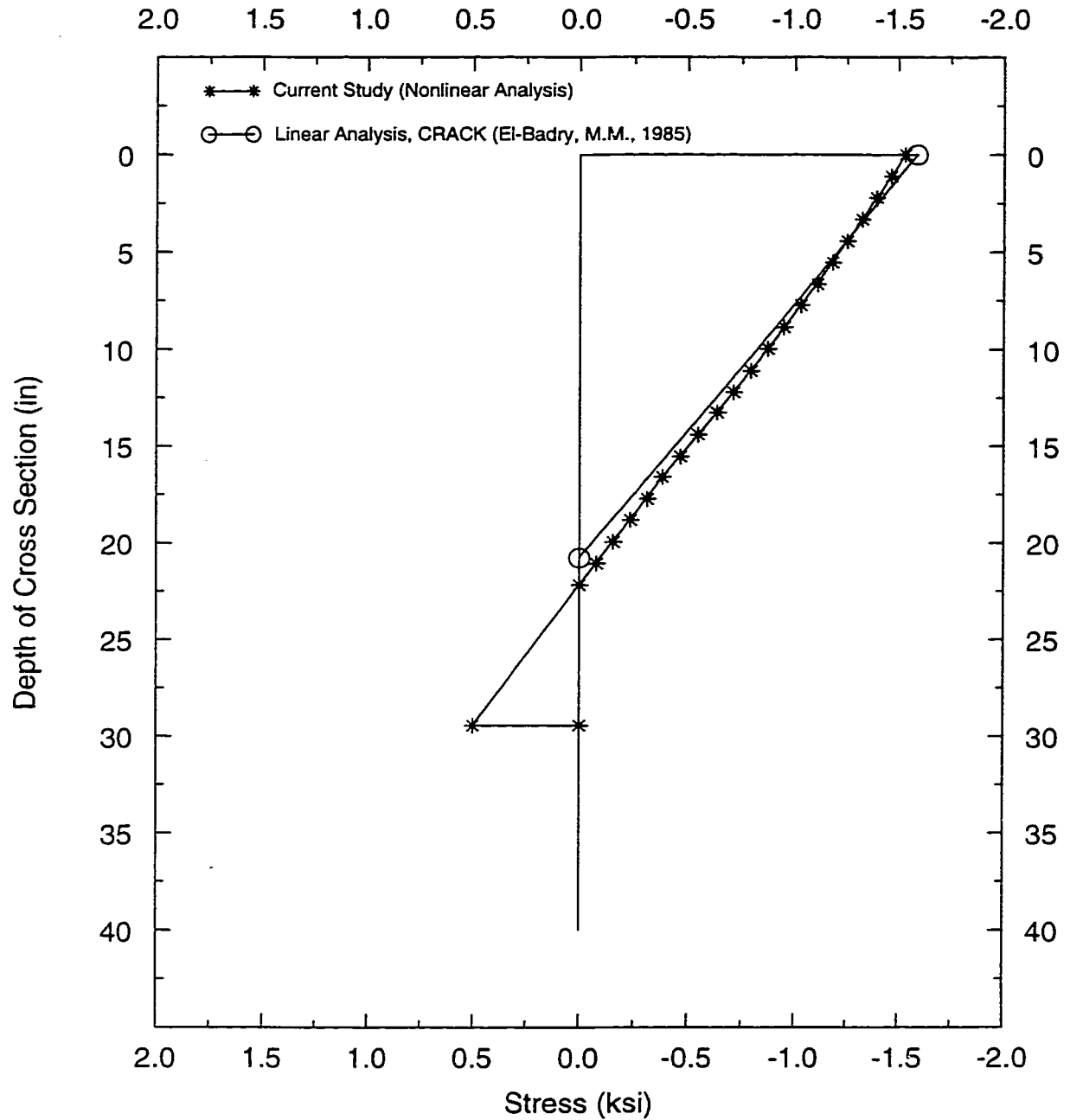


Fig. 5.17 Comparison Between This Study and Linear Analysis, CRACK (El-Badry, M.M., 1985)

Due To Time-Dependent Effects
(If M is increased over 41000 k.in, the tensile steel ruptures)

N = -600 k (-2669 kN)
M = 41000 k.in (4633 kN.m)

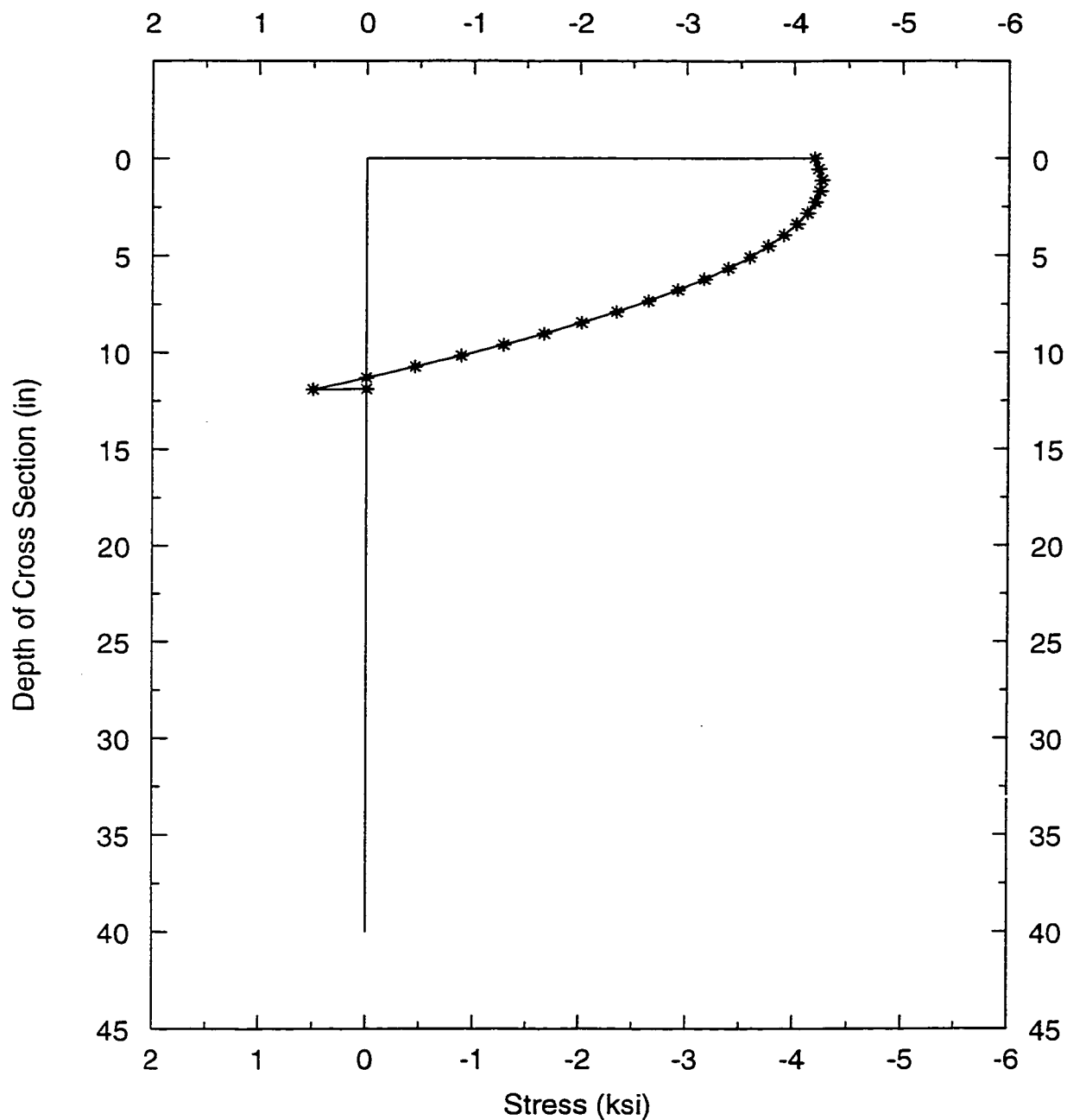


Fig. 5.18(a) Stress Distribution

Due To Time-Dependent Effects
(If M is increased over 41000, the tensile steel ruptures)

N = -600 k (-2669 kN)
M = 41000 k.in (4633 kN.m)

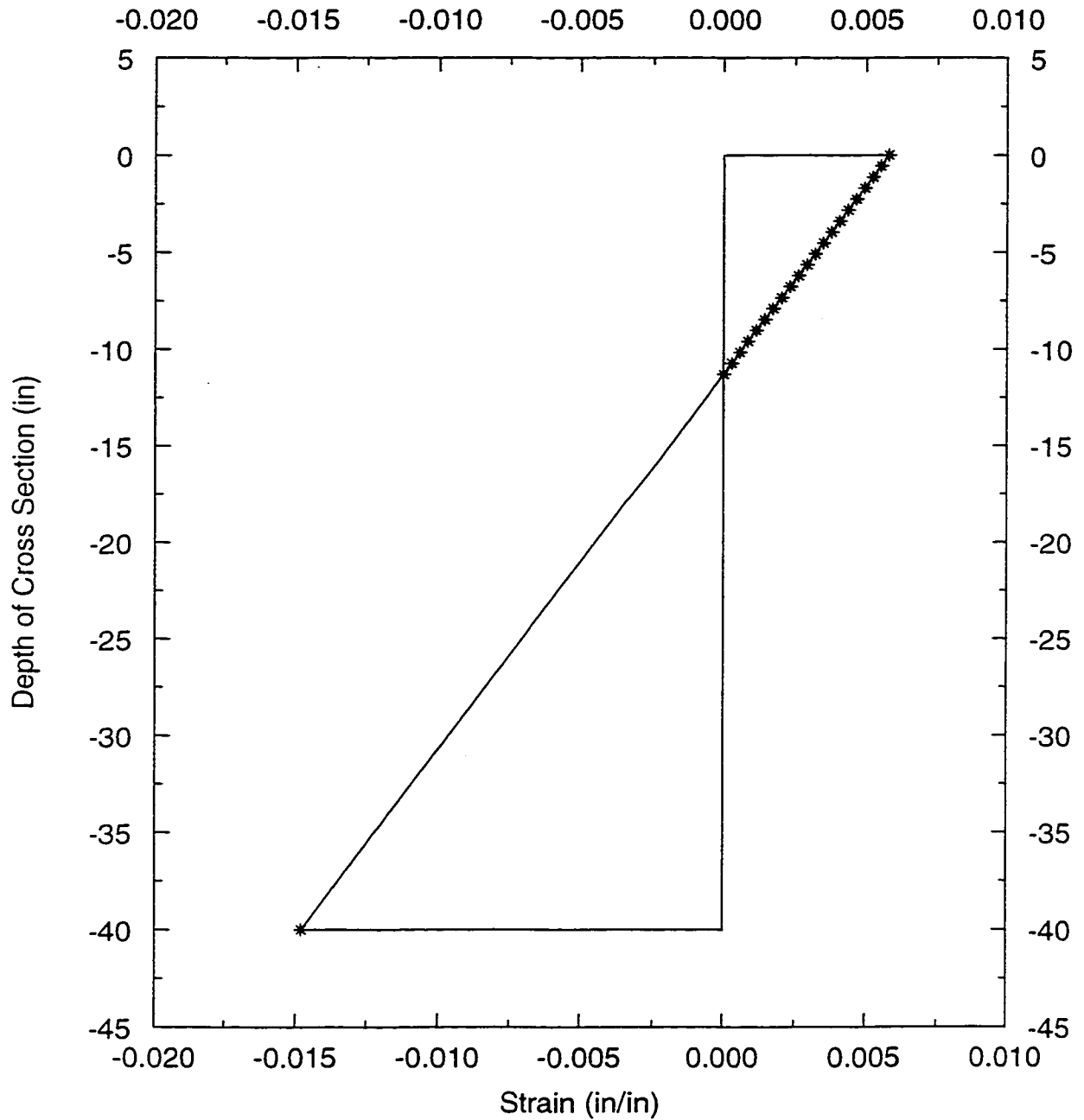


Fig. 5.18(b) Strain Distribution

Due To Time-Dependent Effects

$N = -600 \text{ k}$ (-2669 kN) (constant)

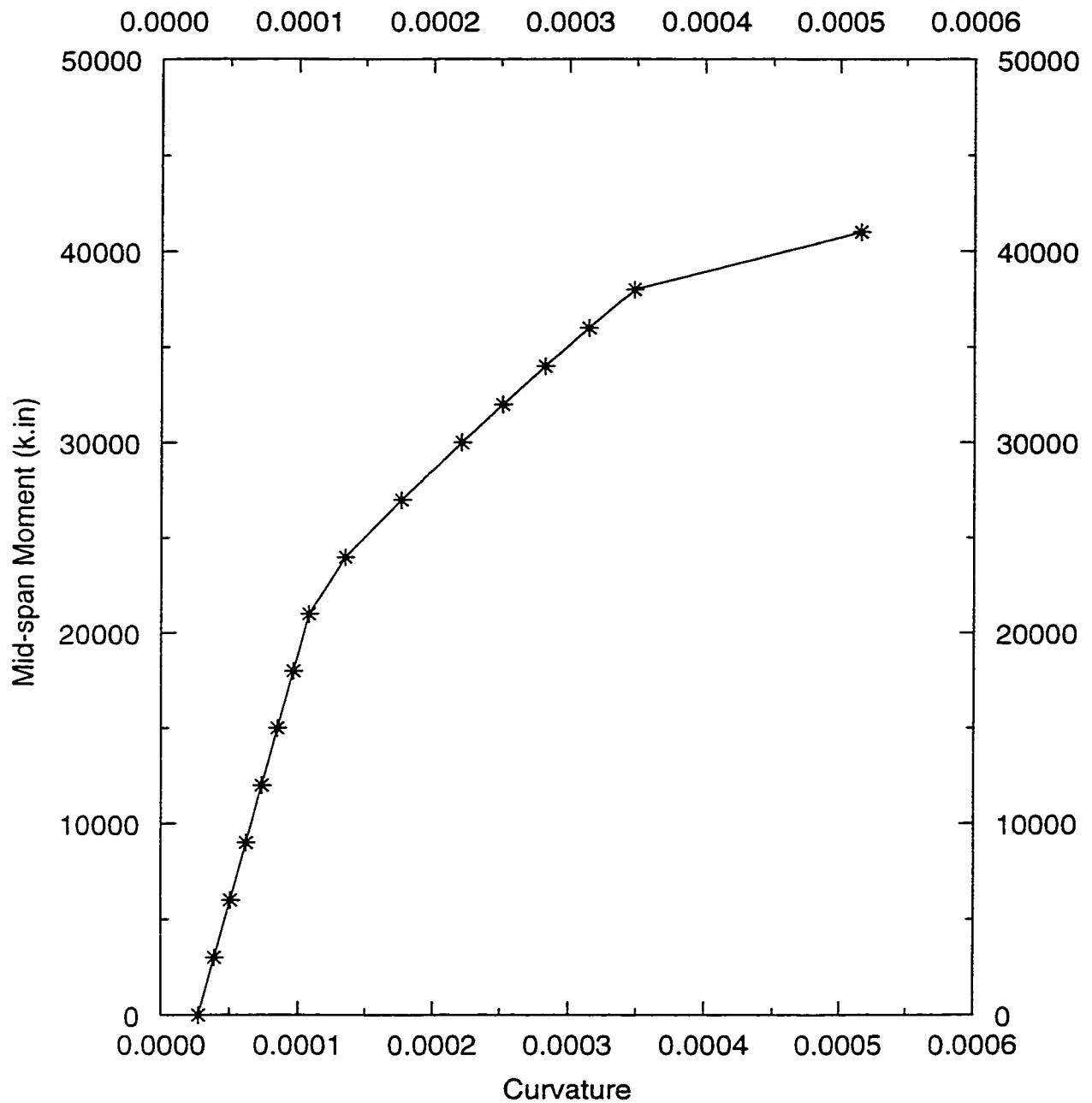


Fig. 5.19 Moment-Curvature Relationship of Mid-span Cross Section
(Case of Fixed Axial Force)

Instantaneous and Time-Dependent Effects

$N = -600 \text{ k} \text{ } (-2669 \text{ kN}) \text{ (constant)}$

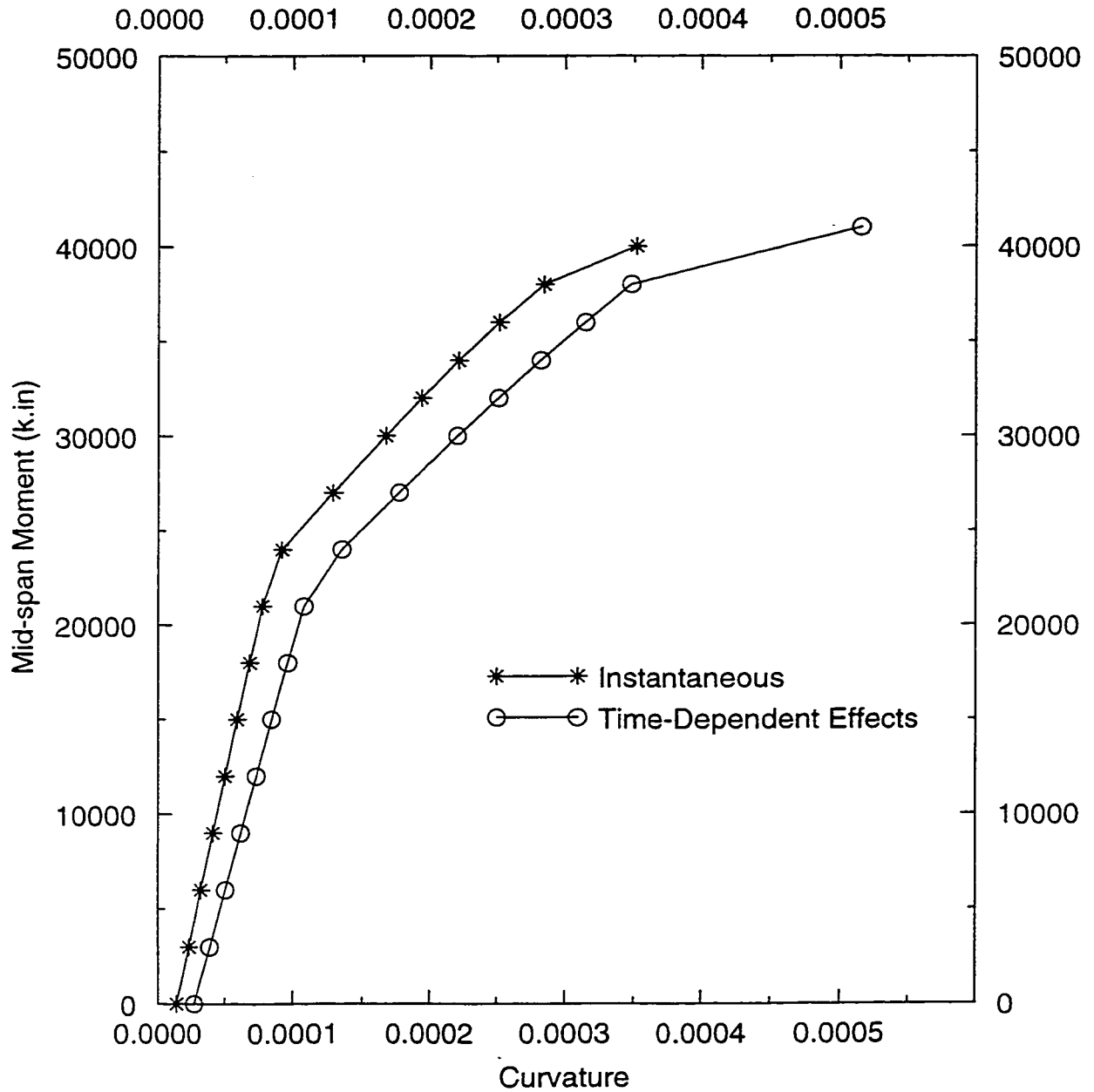
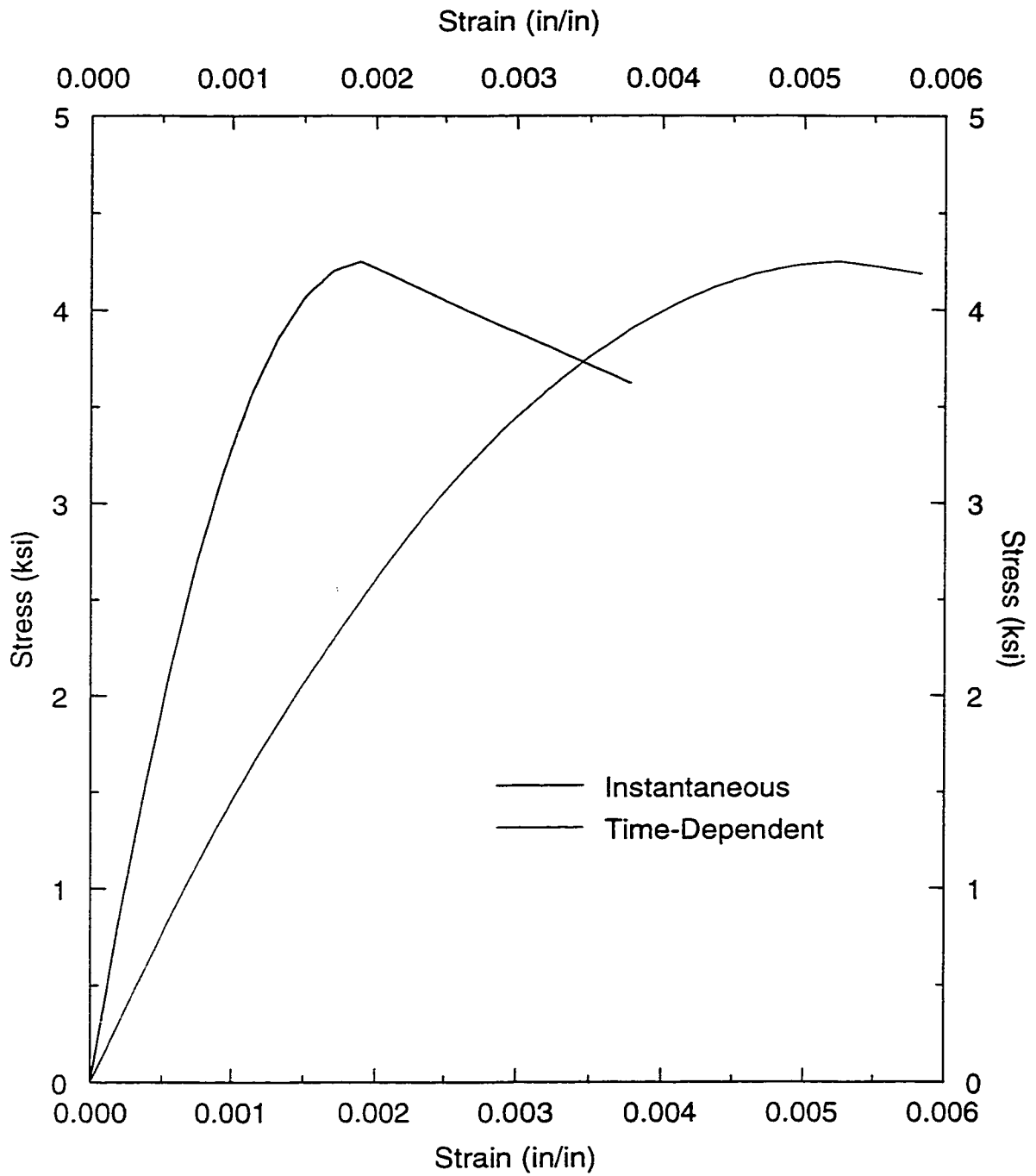


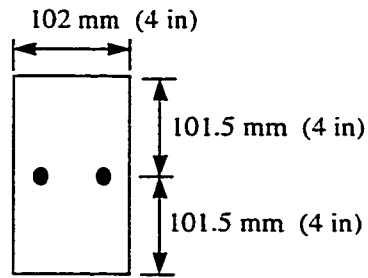
Fig. 5.20 Moment-Curvature Relationship of Mid-span Cross Section
(Case of Fixed Axial Force)

**Stress-Strain Relationship due to N and M
(Instantaneous and Time-Dependent)**

$N = -600 \text{ k}$ (-2669 kN), $M = 41000 \text{ k.in}$ (4633 kN.m)



**Fig. 5.21 Instantaneous and Time-Dependent
Stress-Strain Relationship**



Cross Section of Pretensioned Member

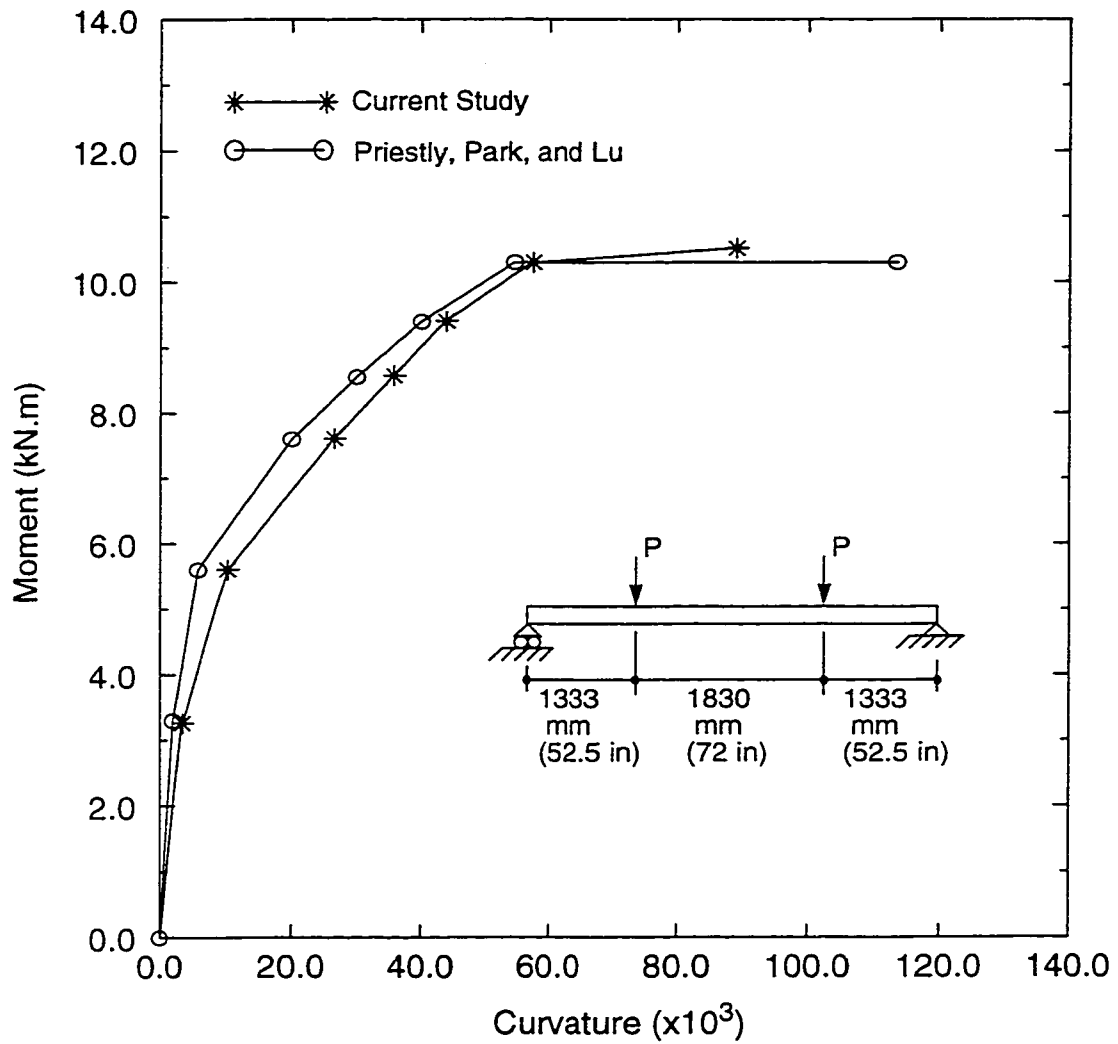


Fig. 5.22 Comparison Between This Study and Experimental Work by Priestley, Park, and Lu

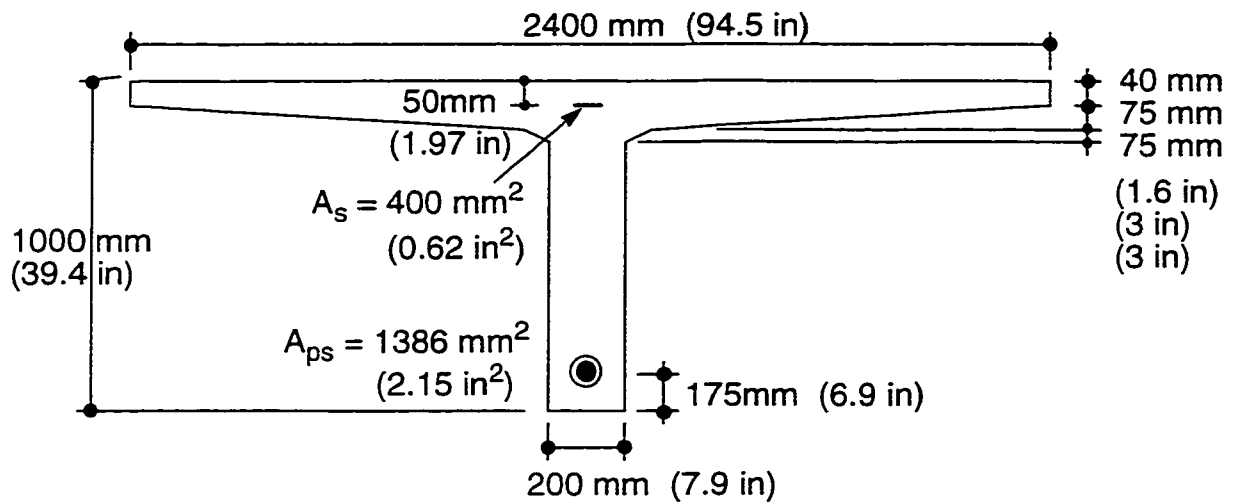


Fig. 5.23(a) Cross Section of a Single-Tee Beam

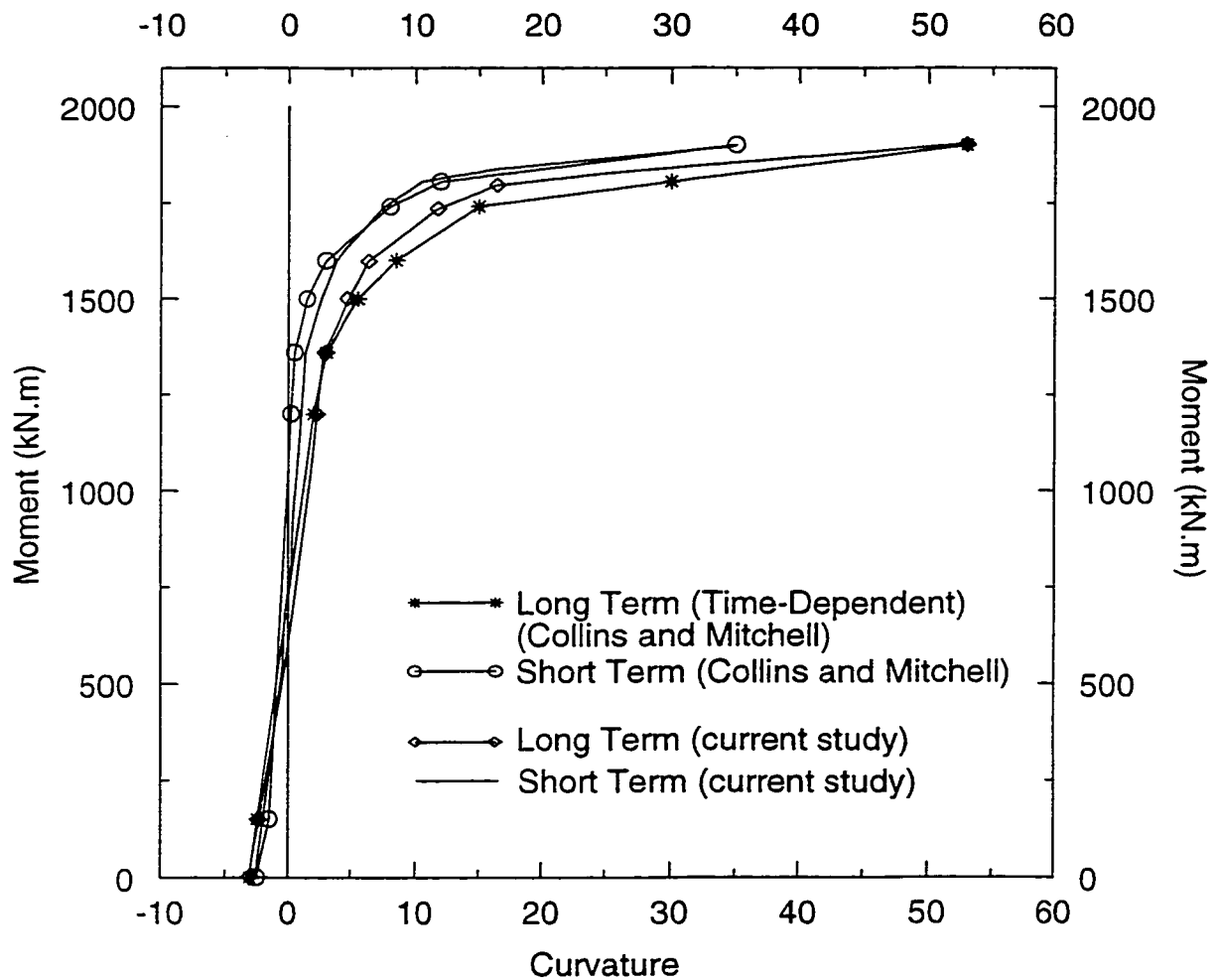


Fig. 5.23(b) Comparison Between this Study and Collins and Mitchell Layer-By-Layer Approach (1987) for M-ψ response

CHAPTER SIX

ANALYSIS OF PRESTRESSED REINFORCED CONCRETE STRUCTURES

6.1 General

A general procedure and equations for the short and long term nonlinear analysis of planar reinforced concrete sections using the mathematical models for the material properties were presented in the preceding chapters. The procedure yields the solution for the changes in stresses and strains due to external loads applied at the section. In the present chapter the changes in the stresses and strains will be used in the analysis of prestressed reinforced concrete members. The time-dependent effects are most significant in structures made up of members of different ages and material properties such as bridges built up of precast prestressed concrete members carrying a cast-in-situ concrete deck. Cracking substantially reduces the flexural rigidity of reinforced concrete members especially under increasing loads.

Depending on the method of applying the prestress, prestressed concrete structures are classified into pre-tensioned and post-tensioned structures. The first step in pretensioning is the stressing of the high strength steel tendons between the abutments of a pretensioning bed. The concrete is then placed in the form and after the desired concrete strength has been reached, the tendons are cut and the member becomes prestressed by transferring the prestress to the concrete. In the posttensioning the prestress is transferred gradually to the concrete while the prestressing steel is tensioned against the hardened

concrete, and anchored against it immediately after the tensioning operation. Depending on whether the prestressing steel is grouted or ungrouted after the tensioning operation or if the tendons are placed outside the concrete section, posttensioned structures are further classified as bonded, unbonded, or externally prestressed structures.

In the analysis of the prestressed reinforced concrete structures, the variation of the stress in the prestressing steel during various stages of loading is an important factor since the behaviour of the structure is dependent largely on the amount of prestress acting on them. In pretensioned structures, the prestress loss takes place before the transfer of the prestress due to shrinkage and creep of concrete and the relaxation of prestressing steel. At the transfer of the prestress, the loss is due to the elastic shortening of the concrete and after the transfer, the loss is due to the relaxation of the prestressing steel and the load history. In posttensioned members, the loss takes place during the tensioning operation due to the friction between the prestressing steel and the duct and the anchorage slip. After the transfer of the prestress, the loss is due to shrinkage and creep of concrete, the relaxation of prestressing steel, and the effects of the load history.

This study aims at finding the displacements, internal forces, stresses and strains of the concrete, reinforcing steel and the prestressing steel of the reinforced member at any time during their service by using a numerical procedure which includes the material nonlinearity and the time-dependent effects of creep and shrinkage of concrete and the relaxation of the prestressing steel. The numerical procedure is based on the displacement method of structural analysis.

6.2 Structural Modeling and Discretization

A typical planar reinforced or prestressed reinforced concrete structure is shown in Fig. 6.1(a). In the analysis by the displacement method, the frame is idealized as an assemblage of straight beam elements connected at the nodes (joints), Fig. 6.1(b). If external tendons are present, these tendons are modeled as truss elements. The external tendons are connected to the structure at the deviator and the anchorage locations (nodes) with one degree of freedom at each node, translation in the longitudinal direction of the tendon. The reinforced concrete member is modeled as a beam element with two nodes and one plane of symmetry in which the external loads are applied. Each node has three degrees of freedom, two translation and one rotation defined with respect to an arbitrarily chosen global system of axes, see Fig. 6.2(a). The global coordinate system is fixed in the space and is common for all elements. Equilibrium equations for the entire structure are derived and solved in this global coordinate system. Since the centroid of the transformed section changes position with time due to varying concrete properties, cracking, and load history, a reference axis is arbitrarily chosen for each member and is kept unchanged through all steps of analysis. The nodes of the member are located at the intersections of the reference axes of the individual members, Fig. 6.1(b). The reinforced concrete member with external tendons must have at least one node at the support (anchorage zone) or at the deviator location.

A local system of axes is defined for each individual member as follows, Fig. 6.2(b). Let O_1 and O_2 be the nodes of the element. O_1 is the origin of this local coordinate system. The axis connecting the two nodes, O_1 and O_2 , is the x^* axis. The axis x^* coincides with the reference axis of the element and is directed from O_1 to O_2 . The y^* and z^* are

perpendicular to the x^* axis with y^* lying in the plane of the frame. For a typical element, a number of sections is defined with the first and the last sections at nodes O_1 and O_2 respectively. The stiffness matrix of the member, the fixed-end forces, and the displacements at its two ends and the internal forces at the various sections are evaluated in the local coordinate system $x^*y^*z^*$ (El-Badry, M.M, 1988).

The concrete element can be of a variable cross section over its length. It can be made up of several concrete types with different material properties. Material properties and ages can also vary from member to member. The geometry of each concrete part is defined by its dimensions and depths from the top fibers. The cross section is assumed to remain plane at all stages of loading and time. A member may contain several prestressing tendons and nonprestressing steel layers. A prestressing tendon may be internal or external, bonded or unbonded. Perfect bond between the concrete and the prestressing steel is assumed for pretensioned structures. The tendon is defined by its profile, cross-sectional area, and its initial tensioning force. A nonprestressing steel layer is defined by its cross-sectional area and its depth from the top fibers. Concrete and the reinforcing steel are assumed to be perfectly bonded together. A steel layer, consisting of prestressing or nonprestressing, may extend over a portion or the full length of the element. Thus the number of steel layers may be different from section to section, see Fig. 6.3 (a). An external tendon is defined by its profile, cross-sectional area, modulus of elasticity, tensile strength, and its initial prestress. The external tendon is considered as an assemblage on truss elements. Each truss element has two nodes and each node has one degree of freedom, axial translation. The truss elements that form the external tendon interconnect at their nodes. These nodes are located at the intersections of the centroidal lines of the truss elements. The

nodes of any truss can be at two consecutive deviators or one node can be at one deviator location and the other node at an anchorage zone, Fig. 6.3(b).

External loads can be in the form of concentrated loads or couples acting at any point on the axis of the member and/or distributed loads.

The time period for which the structure is analyzed is divided in several time intervals. The start or the end of the any interval coincides with the addition of parts of the member, with the application of the loads, or the application of the prestressing. In each interval, the analysis gives the instantaneous and the time-dependent changes in displacements at the nodes, three forces (normal, shearing, and bending moment) at the two ends of individual members, and the reactions at the supports. The changes in stresses and strains of individual sections are calculated using the procedure in Chapter 5.

6.3 Initial Prestressing Force

In pretensioned members, the initial prestressing force required in the analysis is the force in the tendons immediately before transfer. In the case of posttensioning, the initial forces in the tendons are computed from the jacking force at the tendon ends and the instantaneous losses due to friction and anchor setting. Such losses result in a variation in the initial force over the length of the tendon.

6.3.1 Losses Due to Friction

When a tendon is tensioned by a jack, the force produced is not constant along the length of the tendon due to friction between the tendon and the duct. It is customary to consider the frictional losses to be consisting of two components: the curvature and the

wobble frictional losses. Curvature frictional loss results from the intended change of angle of the tendon profile. Wobble friction loss occurs due to imperfection in the tendons as unintentional misalignment of the ducts. This type of friction affects both straight and curved tendons and depends on the friction coefficient and the tendon length. The prestressing force at any point along the tendon after occurrence of friction losses can be calculated by the following (Lin, 1956):

$$P_j = P_i e^{-(\mu\theta_{ij} + ks_{ij})} \quad (6.1)$$

where P_i and P_j are the prestressing forces at two consecutive sections, with section i closer to the jacking end; s_{ij} and θ_{ij} are, respectively, the length of the tendon and the change in its slope, in radians, between section i and j ; μ and k are the curvature and wobble friction coefficients, respectively. A range of values for μ and k has been suggested by the ACI Committee 343 (1977). The angle θ_{ij} is computed from the tendon profile and the length s_{ij} is calculated from the following equation:

$$s = \int_i^j ds = \int_{x_i}^{x_j} \sqrt{1 + (dy/dx)^2} dx \quad (6.2)$$

where dy/dx is the slope of the tendon with y being the depth of the tendon from the reference axis. The integration in Equation (6.2) is performed numerically. Successive application of Equation (6.1) starting from the jacking end gives the variation of the prestressing force along the tendon length.

6.3.2 Losses Due to Anchorage Set

When the jacking force is transmitted from the jack to the anchorage device, a small

slip occurs in the anchor before the tendons can be firmly gripped. The amount of this anchorage slip can be in the range from 2 to 10 mm, depending on the prestressing system, and is usually provide by the suppliers of the anchorage device. The loss of prestress due to anchorage set can be particularly important in short members.

When the anchor sets a distance δ , a sudden drop in the jack force takes place and the friction force reverses direction over a certain length L_s from the jacking end, Fig. 6.4. Beyond the length L_s , the anchor set has no effects and the force in the tendon remains the same as just before the anchoring operation. Since the initial and the reversed friction forces depend on the same friction coefficients, the two curves AC and BC , representing the variation of P with the distance s before and after the anchor set, have equal and opposite slope and are thus symmetric about line EC . Therefore, in order to define the curve BC , it is sufficient to determine the location of point C , i.e., the length L_s .

The total shortening of the tendon over the length L_s is equal to the anchorage set δ . From Fig. 6.4, the change in tendon length due to anchor set is also equal to the area ABC divided by $A_{ps}E_{ps}$, where A_{ps} and E_{ps} are the cross sectional area and the modulus of elasticity of the prestressed tendon, respectively. In the analysis, the prestressing force without considering the anchorage set is first determined at each section of the member by Equation (6.1). Consider any section k at which the prestressing force is P_k . The shaded area A shown in Fig. 6.5 can be calculated as follows:

$$\text{Area}(A) = \sum_{i=1}^{k-1} s_{ij}(P_i + P_j) - 2P_k s_k \quad (6.3)$$

where $j = i + 1$ and s_k is the length of tendon from the anchor to the location of section k .

The location of point C and the variation of the prestressing force after anchor set are determined using the following steps:

1. Set $k = 2$, i.e., the section next to the jacking end.
2. Calculate the shaded area A at section h from Equation (6.3) and compare with the quantity $\delta A_{ps} E_{ps}$.
3. If the area A is less than $\delta A_{ps} E_{ps}$, then the length L_s is larger than the length of the tendon up to the section k , i.e. s_k . Take $k = k + 1$ and go to step 2.
4. If the area A is equal to $\delta A_{ps} E_{ps}$, point C lies at the section k and the length is equal to s_k .
The prestressing force at C is then $P_c = P_k$. Go to step 6.
5. If the area A is greater than $\delta A_{ps} E_{ps}$, then point C lies between sections $(k - 1)$ and k , and L_s has a value between $s_{(k-1)}$ and s_k . In this case, calculation of the area A and comparison with $\delta A_{ps} E_{ps}$ should be repeated for various points between sections $(k - 1)$ and k . Calculate the prestressing force P_c at point C from Equation (6.1).
6. At any section i from the jacking end point C , the loss in prestressing ΔP_i due to anchor set is given by:

$$\Delta P_i = 2(P_i - P_c) \quad (6.4)$$

Thus, calculate the prestressing force after the anchor set as:

$$P'_i = P_i - \Delta P_i = P_i - 2(P_i - P_c) = 2P_c - P_i \quad (6.5)$$

where P_i and P'_i are the prestressing forces at section i before and after the anchor set. The curve BC can thus be defined.

When the tendon is short, the length L_s can be larger than the total tendon length and the anchor set can affect the value of the prestressing force at the other end of the tendon, Fig. 6.6. The unknown value to be determined in this case is the drop ΔP_D in the

prestressing force at the other end of the tendon. The value of ΔP_D can be obtained by equating the area $ABD'D$ in Fig. 6.6 to the quantity $\delta A_{ps} E_{ps}$. Thus:

$$\text{Area}(ABD'D) = \text{Area}(A) + \Delta P_D s_D \quad (6.6)$$

$$\text{Area}(ABD'D) = \sum_{i=1}^{n-1} s_{ij}(P_i + P_j) - 2P_D s_D + \Delta P_D s_D \quad (6.7)$$

$$\text{Area}(ABD'D) = \delta A_{ps} E_{ps} \quad (6.8)$$

where n is the total number of sections in the member, P_D is the force at the other end of tendon before anchor setting and s_D is the total tendon length. From Equations (6.6), (6.7), and (6.8):

$$\Delta P_D = \frac{1}{s_D} \left[\delta A_{ps} E_{ps} - \sum_{i=1}^{n-1} s_{ij}(P_i + P_j) + 2P_D s_D \right] \quad (6.9)$$

The prestressing force P'_i at any section i after anchor set (curve BD') is given by:

$$P'_i = 2P_D - P_i - \Delta P_D \quad (6.10)$$

6.3.3 Effect of Stressing Procedure

One of the technique used frequently in practice in order to reduce losses due to friction and anchor set is to use jacking from the two end of the tendon. When jacking takes place at both ends, the procedure described in the preceding two subsections are applied measuring the parameters q_{ij} and s_{ij} from each end. This gives two values of the prestressing force at each section, only the larger of the two values is of significance. Fig. 6.7 shows a typical variation of the prestressing force after losses due to friction and anchor set along a post tensioned tendon jacked from both ends (curve $BCEC'B'$).

6.4 Member Stiffness Matrix

If a member has variable cross section properties throughout its length, then it has a variable flexural rigidity accordingly. Further variation of stiffness along the length of the member can also be expected after occurrence of cracking. The slope of the moment-curvature diagram of a section represents the flexural rigidity of the section. After cracking, or depending on the stress level, the moment-curvature is nonlinear and its slope at any point depends on the magnitude of the moment applied. Thus, when a member is subjected to high load levels, the flexural rigidity, EI , will vary from section to section according to the variation of the bending moment over the member length. One approach to account for the variation in the stiffness is by dividing the structure into elements of small lengths and assigning uniform axial and bending stiffnesses to each element. Another approach is to use longer elements and account for the variation in the stiffness within the element.

In analyzing a structure by the stiffness (displacement) method, a set of simultaneous equations, that is proportional to the number of the nodes in the structures, must be solved. The stiffness coefficients for a nonprismatic element can be developed in a variety of ways, e.g., column analogy or virtual work.

A more desirable approach in calculating the stiffness of a nonprismatic element is by evaluating the flexibility matrix of the element and then obtaining the stiffness matrix by inversion. The flexibility coefficients at the member ends can be obtained by the unit-load method (Ghali and Neville, 1978). This approach was adopted by El-Badry, M.M. 1988, and is used in this study.

Fig. 6.8 shows a typical plane frame member in its undeformed and deformed states. The member has six degrees of freedom, $\{D'\}$, located at the two ends (nodes) O_1

and O_2 . The total deformations of the member consist of two components: rigid body displacements and deformations due to internal strains. The rigid body displacements do not change the stresses and strains in the member nor the forces at its ends. Such displacements can be excluded from the total deformations by fixing the member at one of its end, i.e. O_1 , as shown in Fig. 6.8. The member in its configuration has at node O_1 three degrees of freedom, $\{d'\}$, which are related to $\{D'\}$ by geometry as follows:

$$\{d'\}_{3 \times 1} = [H]_{3 \times 6} \{D'\}_{6 \times 1} \quad (6.11)$$

where $[H]$ is given by:

$$[H] = \begin{bmatrix} -1 & 0 & 0 & -1 & 0 & 0 \\ 0 & 1 & 0 & 0 & -1 & l \\ 0 & 0 & 1 & 0 & 0 & -1 \end{bmatrix} \quad (6.12)$$

with l being the length of the member. The elements of $\{d'\}$ represent the relative displacements of end O_1 with respect to end O_2 .

Generate the flexibility matrix $[f]$ corresponding to the three displacements at the free end O_1 . According to the unit-load method, any element in the flexibility matrix is given by:

$$f_{ij} = \int_0^l N_{ui} \epsilon_{Oj} dx + \int_0^l M_{ui} \psi_j dx \quad (6.13)$$

where f_{ij} is the displacement at coordinate i due to a unit force applied at coordinate j ; N_{ui} and M_{ui} are the normal force and the bending moment at any section at a distance x for end O_1 due to a unit force at coordinate i , with $i = 1, 2$, or 3 , see Fig. 6.9; ϵ_{Oj} and ψ_j are the strain

at the reference point O and the curvature produced at the same section by a unit force applied at coordinate j , with $j = 1, 2$, or 3 . Recall that the cross section of the member has an axis of symmetry in the plane of the frame. The reference axis O_1O_2 intersects the axis of symmetry at the reference point O. The force N_{ui} acts at O and the moment M_{ui} is about an axis through O in the plane of the cross section.

Thus from Fig. 6.9 and Equation (6.13), the elements of any column j of the matrix $[f]$ are:

$$f_{1j} = -\int_0^l \epsilon_{Oj} dx \quad f_{2j} = -\int_0^l \psi_j x dx \quad f_{3j} = \int_0^l \psi_j dx \quad (6.14)$$

The integrals in the equations are evaluated numerically using the values of ϵ_O and ψ determined as described in Chapter 6 at a number of sections for which the geometry and cross section areas of reinforcements are given as data. For the analysis of the instantaneous effects, use the modulus of elasticity of concrete and the properties of the transformed section at the time of application of the load. When the analysis is for the time-dependent effects during a period t_i to t_{i+1} , the age-adjusted modulus of elasticity and the properties of the age-adjusted transformed section are to be used to give the age-adjusted flexibility matrix.

Inversion of the flexibility matrix will give a 3x3 stiffness matrix corresponding to the coordinates at end O_1 . The forces at end O_2 are obtained by equilibrium and thus the stiffness matrix for the six coordinates is generated:

$$[S] = [H]^T [f]^{-1} [H] \quad (6.15)$$

where $[S']$ is the member stiffness matrix in the local coordinates and $[H]$ is given by Equation (6.12). The stiffness matrix will be expressed in terms of the reference modulus of elasticity, E_{ref} and A , B , and I , the transformed section properties with respect to the reference point O .

In order to generate the structure stiffness matrix, member stiffness matrices must be transformed from local coordinate system to the global system. Such transformation can be performed by the following equation:

$$[S_m] = [T]^T [S']^{-1} [T] \quad (6.16)$$

where $[S_m]$ is the member stiffness matrix in global coordinates, the subscript m refers to the member number; $[T]$ is a transformation matrix given by:

$$[T] = \begin{bmatrix} [t] & [0] \\ [0] & [t] \end{bmatrix} \quad (6.17)$$

with matrix $[t]$ given by:

$$[t] = \begin{bmatrix} c & s & 0 \\ -s & c & 0 \\ 0 & 0 & 1 \end{bmatrix} \quad (6.18)$$

where $c = \cos \alpha$ and $s = \sin \alpha$, with α being the angle between the global and local coordinates, measured from the global x -axis to the local x^* -axis, Fig. 6.2(b).

When external prestressing cables are present, Fig. 6.10(a), then these cable contribute to the stiffness of the beam element. The external tendon is treated as an assemblage of truss elements. Each truss element has two nodes located at the centroidal lines of the individual truss element. Each node has one degree of freedom, axial

translation. The conventional stiffness of a truss element with two degrees of freedom is:

$$[S_t] = \frac{EA}{l} \begin{bmatrix} 1 & -1 \\ -1 & 1 \end{bmatrix} \quad (6.19)$$

The contribution of the external tendon to the stiffness of the element can be computed by transforming the local stiffness matrix of the external tendon (truss element) $[S_t]$ to the local coordinates of the beam element. This transformation is formed by geometrical relationship of displacements as shown in Fig. 6.10(c) (Ghali and Neville, 1989):

$$[S_t]_{transf} = [TR]^T [S_t] [TR] \quad (6.20)$$

where $[TR]$ is a transformation matrix and is given as follows:

$$[TR] = \begin{bmatrix} \cos(\alpha) & -\sin(\alpha) & -a\cos(\alpha) & 0 & 0 & 0 \\ 0 & 0 & 0 & \cos(\alpha) & -\sin(\alpha) & -b\cos(\alpha) \end{bmatrix} \quad (6.21)$$

α is the slope of the external tendon as shown in Fig. 6.10(b) and (c) and a and b are the eccentricities (if any) of the two end of the external tendon, see Fig. 6.10(c).

The transformation of the truss element stiffness matrix to the local coordinates of the element will yield the following truss stiffness matrix at the two nodes of the element as follows, Fig. 6.10(c):

$$[S_t]_{transf} = \frac{EA}{l} \begin{bmatrix} C^2 & -SC & -aC^2 & -C^2 & SC & bC^2 \\ -SC & S^2 & aSC & SC & -S^2 & -bSC \\ -aC^2 & aSC & a^2C^2 & aC^2 & -aSC & -abC^2 \\ -C^2 & SC & aC^2 & C^2 & -SC & -bC^2 \\ SC & -S^2 & -aSC & -SC & S^2 & bSC \\ bC^2 & -bSC & -abC^2 & -bC^2 & bSC & b^2C^2 \end{bmatrix} \quad (6.22)$$

where C is $\cos(\alpha)$, S is $\sin(\alpha)$, and a and b are as before.

The transformed stiffness matrix of the external tendon (truss element) $[S_t]_{transf}$ is then to be added to the element local stiffness matrix $[S']$ to get the local stiffness matrix of an element with external tendons.

6.5 Fixed-End Forces

The fixed-end forces are those forces which when applied at the two ends of a member will lock or suppress the nodal displacements when the member is subjected to non-nodal loading. These restraining forces confine the effects of member loads to within the respective members. When non-nodal loads are applied on the member, the three displacements at the free end, O_1 , of the member, treated as a cantilever, can be obtained by the unit-load method as follows:

$$\Delta d'_1 = -\int_0^l \Delta \epsilon_O dx \quad \Delta d'_2 = -\int_0^l \Delta \psi dx \quad \Delta d'_3 = \int_0^l \Delta \psi dx \quad (6.23)$$

where $\Delta \epsilon_O$ and $\Delta \psi$ are the change in strain at the reference point O and in curvature produced at any section due to the external loads applied on the cantilever.

The change in the fixed-end forces at the three local coordinates at the free end are obtained by the stiffness approach:

$$\{\Delta F'\}_{O1} = -[f]^{-1}\{\Delta d'\} \quad (6.24)$$

The forces at the fixed end, O_2 , can be determined by equilibrium, therefore, the change in the six fixed-end forces are evaluated by:

$$\{\Delta F'\} = [H]^T \{\Delta F'\}_{O1} + \{\Delta R\} \quad (6.25)$$

The first three elements in vector $\{\Delta R\}$ are zero, while the last three are the changes in the three reactions due to the external loads applied on a cantilever fixed at end O_2 . To determine the changes in the time-dependent fixed-end forces during any interval t_i to t_{i+1} , $\Delta \varepsilon_o(t_{i+1}, t_i)$ and $\Delta \psi(t_{i+1}, t_i)$ are calculated at the different sections using the properties of the age-adjusted transformed section and the flexibility matrix is replaced by the age-adjusted flexibility matrix. Using Equations (6.23), (6.24), and (6.25) gives the changes in the time-dependent displacement $\{\Delta d'(t_{i+1}, t_i)\}$, the changes in the fixed-end forces $\{\Delta F'(t_{i+1}, t_i)\}_{O1}$, and the increments $\{\Delta F'(t_{i+1}, t_i)\}$ of the six fixed-end forces at the two ends of the member, respectively. Before assemblage of the overall load vector, the forces $\{\Delta F'\}$ for all member must be transformed from local coordinates to global coordinates as follows:

$$\{\Delta F_m\} = [T]^T \{\Delta F'\} \quad (6.26)$$

where $\{\Delta F_m\}$ is the load vector in global coordinates for member number m and $[T]$ is given by Equation (6.17).

6.6 Calculation of Deformations of a Member

This section concerns with the numerical evaluation of the deformations, i.e. elongation, deflection, and rotation in a frame member. The most suitable technique for the calculation of the deformations is the method of elastic weights (Ghali and Neville, 1978). In this method, the curvature diagram in a beam is treated as a distributed transverse load referred to as the elastic load or weight, acting on a conjugate beam. The length of the conjugate beam is equal to that of the actual beam, but the support conditions are changed. Fixed and free ends in the actual beam are changed respectively to free and fixed in the conjugate beam. A simple support remain unchanged. The deflection and the rotation at any point in the actual beam are calculated respectively as the bending moment and the shearing force due to elastic loads on the conjugate beam. Fig. 6.11(b) shows an example of the curvature diagram in a typical prestressed member, Fig. 6.11(a). This diagram can be obtained from the curvature values determined at a number of selected sections along the member. In the present analysis, the sections need not necessarily be chosen at equal spaces, but two sections with zero distance apart must be selected at the points of abrupt changes in the curvature distribution, i.e. at the location of a sudden change in the cross section dimensions or reinforcement areas or at a point where a concentrated couple is applied. A part of the curvature diagram between any two sudden changes, is approximated by a straight line between each two consecutive sections or by a series of parabolas over each of the three sections. In the latter case, the corresponding length of the member, must be divided into an odd number of sections, i.e. an even number of spaces. By such an approximation, the curvature diagram on the actual member can be replaced by equivalent concentrated elastic loads on the conjugate beam as shown in Fig. 6.11(c).

The equivalent concentrated forces corresponding to a load varying linearly between any two sections i and $(i+1)$ can be obtained. For a parabolic variation over three sections $(i-1)$, i , and $(i+1)$, which are not equally spaced, the equivalent loads are given by (El-Badry, M.M., 1988):

$$\begin{bmatrix} Q_{i-1} \\ Q_i \\ Q_{i+1} \end{bmatrix} = \frac{1}{12} \begin{bmatrix} \frac{s_l(3s_l+4s_r)}{s_l+s_r} & \frac{s_l(s_l+2s_r)}{s_r} & \frac{s_l^3}{s_r(s_l+s_r)} \\ \frac{s_l^3+2s_l^2s_r-s_r^3}{s_l(s_l+s_r)} & \frac{s_l^3+s_r^3+4s_ls_r(s_l+s_r)}{s_ls_r} & \frac{-s_l^3+2s_ls_r^2+s_r^3}{s_r(s_l+s_r)} \\ \frac{s_r^3}{s_l(s_l+s_r)} & \frac{s_r(2s_l+s_r)}{s_l} & \frac{s_r(4s_l+3s_r)}{s_l+s_r} \end{bmatrix} \begin{bmatrix} \psi_{i-1} \\ \psi_i \\ \psi_{i+1} \end{bmatrix} \quad (6.27)$$

where s_l and s_r are the spacing to the left and to the right of section i . When the load on each spacing or on each two consecutive spacings are replaced by equivalent concentrated force, the forces are assembled in a vector $\{Q\}$ and therefore:

$$\{Q\}_{n \times 1} = [A]_{n \times n} \{\psi\}_{n-1} \quad (6.28)$$

where n is the total number of sections in the member and the elements of the matrix $[A]$ are functions of spacings between sections. The elements of the i th column in $[A]$ represent equivalent concentrated loads at all sections when at section i , $\psi_i = 1$, while at all other sections, $\psi = 0$.

The deflection d'_2 and the rotation d'_3 at the free end of a cantilever fixed at end O_2 can now be expressed in terms of $\{\psi\}$ as:

$$d'_2 = - \begin{bmatrix} x'_1 & x'_2 & x'_3 & & x'_n \end{bmatrix} [A] \{\psi\} \quad (6.29)$$

$$d'_3 = - \begin{bmatrix} 1 & 1 & 1 & & 1 \end{bmatrix} [A] \{\psi\} \quad (6.30)$$

The right hand sides of these two equations represent respectively the bending

moment and the shear at end O_1 of a conjugate cantilever fixed at end O_1 and subjected to the equivalent concentrated elastic loads $\{Q\}$.

Equation (6.30) gives the value of the integral $\int \psi dx$ evaluated over the member length. The displacement d'_1 represents the total change in the member length and is equal to $-\int \epsilon_O dx$ evaluated over the total length. The value of this integral can be obtained by Equation (6.30) simply by replacing ψ by ϵ_O , thus

$$d'_1 = -[1 \ 1 \ 1 \quad \quad \quad 1] [A] \{\epsilon_O\} \quad (6.31)$$

Equations (6.29) to (6.30) are employed in the present study to obtain the flexibility coefficients in Equation (6.14) and the displacement components in Equation (6.24). An equation similar to (6.29) can be used to obtain the deflection at any section in a general plane frame member. Fig. 6.12 depicts such a member in its original and deflected shapes. The deflection δ_k at any section k is the sum of two components δ_{1k} and the deflection of the chord, i.e. the straight line joining the two displaced ends of the member (line $O'_1O'_2$ in Fig. 6.12), and δ_{2k} , the deflection measured from the chord. The component δ_{1k} can be obtained from the displacements D'_2 and D'_5 of the ends O_1 and O_2 by linear interpolation; thus

$$\delta_{1k} = \frac{l - x_k}{l} D'_2 + \frac{x_k}{l} D'_5 \quad (6.32)$$

The component δ_{2k} can be expressed in terms of $\{y\}$ as:

$$\delta_{2k} = [\hat{x}_1 \ \hat{x}_2 \ \hat{x}_3 \quad \quad \quad \hat{x}_n] [A] \{\psi\} \quad (6.33)$$

where

$$\hat{x}_i = \frac{x'_i}{l} (l - x'_k) \quad i \leq k \quad (6.34)$$

and

$$\hat{x}_i = \frac{x'_k}{l}(l - x'_i) \quad i > k \quad (6.35)$$

Equation (6.33) represents the bending moment at section k of a conjugate simple beam supported at O'_1 and O'_2 and subjected to the equivalent concentrated elastic load $\{Q\}$.

6.7 Imposition of Support Conditions

There are several methods for incorporating the boundary conditions into the unconstrained structure stiffness equation without rearranging the stiffness matrix. The objective is to modify the structure stiffness equation such that the expected solution will be obtained by the usual way of solving $[K]\{r\}=\{F\}$ where $\{r\}$ remains the solution vector (displacements) and $\{F\}$ the known load vector. The method used here is the penalty method.

Suppose that a nodal displacement r_n along direction n is prescribed to take a value δ , the procedure for imposing this boundary condition is by making some minor adjustments of the n th row of the equation $[K]\{r\}=\{F\}$ as follows:

- 1- The stiffness element k_{nn} is modified to:

$$k_{nn(\text{constraint})} = k_{nn} + H \quad (6.36)$$

where H is calculated as:

$$H = k_{nn} \times 10^{-6} \quad (6.37)$$

- 2- The element F_n of the load vector is modified to:

$$F_{n(\text{constraint})} = F_n + H \times \delta \quad (6.38)$$

The above two steps are repeated for each prescribed displacement. Note that this modification does not disturb the symmetry of $[K]$.

After solving the simultaneous equilibrium equations in the usual way for the nodal displacements $\{r\}$, the reaction R_n , along direction n , can be calculated as:

$$R_n = H \times (\delta - r_n) \quad (6.39)$$

6.8 Analysis Procedure

In a nonlinear problem, the structure stiffness matrix depends on the final deformed shape of the structure and the stress level, i.e. on the displacements and forces. The final deformed shape of the structure is not known in advance and therefore iterative techniques have to be employed. Two iterative techniques are commonly used: initial stiffness procedure and tangent stiffness procedure.

In this study, the initial stiffness procedure is used where for each construction stage, load application, or time interval, the total load is applied, the stiffness is kept constant, and iterations are performed until equilibrium conditions are satisfied to an acceptable degree of accuracy. In each iteration, equilibrium is violated because an approximate structure stiffness is used. For each iteration, a linear conventional analysis is performed, as discussed below, using an approximate stiffness to obtain the instantaneous and time-dependent displacements at the nodes, reactions at the supports, internal forces in the members, and strains at the various sections. Using the strains obtained, the stresses are computed from the material stress-strain relationships. From the stresses, the forces in each member are calculated. The calculated forces are different from the applied forces. This difference represents unbalanced forces which are applied on the structure in the next

iteration to compute additional displacements, reactions, internal forces, and strains. These additional values are added to the previous values to obtain the total values. Iterations are stopped when the unbalanced forces are less by a predetermined level of accuracy. If unbonded tendons are present, the change in the length of the member is computed from the final nodal axial and rotational displacements in the member local coordinates. Dividing this change in length by the original length of the member yields the average change in strain which is considered the same as for the unbonded tendons. Therefore, the change in the prestressing force can be obtained. The unbalanced force of the unbonded tendon is applied and the iterative procedure is repeated until the change in the member length is less than a specific tolerance. A newly calculated prestressing force in the unbonded tendons is to be used in the next time interval. When the analysis is for the time-dependent changes, the stiffness to be used in the respective time interval is the age-adjusted stiffness.

For each iteration within a construction stage, load application or time interval, the linear stiffness analysis is used as follows to determine the increments of nodal displacements and member end forces:

- 1) The structure is idealized to a set of elements connected together at the joints (nodes).
- 2) The global structure coordinates and the local coordinates for each member are set.
- 3) For each member, the stiffness matrix is generated, rotated into structure coordinates and positioned in the global structure stiffness matrix $[K]$. When the analysis is for the time-dependent changes, the stiffness to be used in this step is the age-adjusted stiffness.
- 4) Loads applied directly at the nodes, in global coordinates are placed directly in the load

- vector $\{F\}$. Loads equivalent to loads applied on the members are calculated at the end nodes, negatives of fixed-end actions, then rotated into structure coordinates and placed into the load vector $\{F\}$.
- 5) The global structure stiffness matrix $[K]$ and the load vector $\{F\}$ are corrected for the known support conditions.
 - 6) Joint displacement are found by solving a set of equilibrium equations $\{D\} = [K]^{-1}\{F\}$.
 - 7) The displacement corresponding to each member is extracted from $\{D\}$ and then rotated into member coordinates. The final member end actions can be found by multiplying the member stiffness matrix by its end joint displacements, and then adding the resulting vector to the member fixed end actions.

It is worth noting that the analysis presented in this chapter has an advantage over the standard finite element techniques, particularly when nonprismatic members are involved. The essential feature of the present analysis is that the actual deflected shape of a member is obtained by integrating the actual strains and curvatures. In the finite element method, the deflected shape of a member is usually assumed as a function of the displacements at the nodes and equilibrium between the external and internal forces is satisfied only at the nodes. A large number of elements is usually needed to overcome this drawback especially for cases where nonlinear behaviour is expected.

6.9 Verification of the Procedure

The current analysis was performed using the program CPF, developed by El-Badry, M.M., 1989, after modifications to include the instantaneous and time-dependent nonlinear analysis of prestressed reinforced concrete beams and to include internal

unbonded and external tendons in the analysis. A series of studies were undertaken to verify the program satisfactorily modeling the nonlinear behaviour of a variety of concrete structures. The results of some of these verification studies are reported in the following sections.

Externally and internally prestressed beams with the same cross section configurations but different tendon profiles and different span-to-depth ratios are studied. Also beams with internal unbonded tendons are examined. These studies were performed to show that the nonlinear response of the concrete is modeled satisfactorily

6.9.1 Reinforced Concrete Beam Analysis

A simple reinforced beam tested analyzed by Kang (1977) and Lin (1973) was selected for comparison and is shown in Fig. 6.13. The results of the current analysis on the same beam were compared with experimental values as well as with Kang's and Lin's analytical results. The beam has a rectangular cross section throughout its length. It has two #4 compression steel bars and 5 #9 tension steel bars. The concrete has a compressive strength of 5.62 ksi (39 MPa), tensile strength of 0.611 ksi (4.21 MPa), and a maximum compressive strain of 0.0038. The #4 steel bars has a modulus of elasticity of 29200 ksi (201000 MPa), a yielding strength of 50.1 ksi (345.4 MPa), a strain hardening modulus of 144 ksi (993 MPa), and a rupture strain of 0.2. The #9 steel bars has a modulus of elasticity of 30700 ksi (212000 MPa), a yielding strength of 80.1 ksi (552 MPa), a strain hardening modulus of 418 ksi (2882 MPa), and a rupture strain of 0.139. Geometric nonlinearity was neglected in both Kang's and Lin's analysis.

In Fig. 6.13, load-deflection curves at midspan are plotted. Experimental and

analytical results by Kang's analysis, Lin's analysis, and the current analysis are shown together for comparison. In the experiment, about 30% of the ultimate load was first applied and removed. The beam was then loaded again up to the ultimate load. The load-deflection curve shown in Fig. 6.13 corresponds to the second cycle of loading. In the three analyses, the midspan load was applied in one cycle. The difference between the experimental and the analytical results in the lower load level can be attributed to the effects of load reversal. The three analyses predict the ultimate load same as that of the experimental value. It can be seen that the load-deflection curve of the current analysis is closer to that for the experiment than those of Kang's and Lin's analyses especially at the ultimate load level. This can be attributed to the fact that in Kang's analysis the section is divided into a number of concrete layers as opposed to a closed form solution in the current study and that the stress-strain curve for concrete in Lin's analysis is assumed elastic-perfectly plastic as opposed to a concrete stress-strain curve with a parabola in the current study.

6.9.2 Analysis of Pretensioned Column

A pretensioned column was tested and analyzed by Aroni (1968) and Kang (1977) was used for comparison and is shown in Fig. 6.14. The 60 in. (1524 mm) long column was axially pretensioned with four 0.198 in. (5 mm) diameter high tensile steel wires. The prestress was released at 14 days after casting of concrete and cured under water until 28 days after casting, when the eccentric load was applied up to failure. The initial prestressing force was 15600 lbs (69.4 kN). The geometric nonlinearity was neglected.

The eccentric compression is simulated by an equivalent concentric compression

and a moment. It can be seen from Fig. 6.14 that a good agreement was obtained between the experimental results and the analytical results for Aroni, Kang, and the present study.

6.9.3 Simply Supported Prestressed Beam

Fig. 6.15(a) shows a pretensioned partially prestressed simple beam. The midspan cross section of the beam is shown in Fig. 6.15(b). The section is constant over the span with the exception of the location of the prestressed steel. The beam is pretensioned with a tendon depressed at points B and C with the profile shown in Fig. 6.15(a). The beam carries a uniform dead load of intensity 14 kN/m (0.96 k/ft) introduced at age t_o at the same time as the prestress transfer. At time t , long after t_o , a uniformly distributed live load is introduced. It is required to determine the response of the beam.

Tension in prestress tendon just before transfer = 1250 kN (281 kip), moduli of elasticity of concrete at age t_o and t are $E_c(t_o) = 24$ GPa (3481 ksi) and $E_c(t) = 30$ GPa (4350 ksi), $E_s = 200$ GPa (29000 ksi) for all reinforcement, $\phi(t, t_o) = 2$, $\chi(t, t_o) = 0.8$, $f_{pu} = 1860$ MPa (270 ksi), reduced relaxation for the period $(t - t_o) = -90$ MPa (-13 ksi), shrinkage for the same period $\epsilon_{cs}(t, t_o) = -300 \times 10^{-6}$. Assume high-bond quality of reinforcement and tensile strength of concrete $f_{ct} = 2.5$ MPa (0.36 ksi). Cracking is considered in this example.

The same beam is now posttensioned with external tendons with three different profiles, see Fig. 6.16. Material properties are the same as above. It is required to study the instantaneous and long-term response of the beam and evaluate the different parameters that affect the behaviour such as span-to-depth ratio and eccentricity changes.

It can be seen from Figs. 6.17 to 6.29 that the deflection of the beams is affected by the time-dependent effects of creep, shrinkage, and relaxation. The time-dependent effects

increase with the span; i.e. the span-to-depth ratio. These figures also show that the deflections are smaller in beams with external tendon than those in beams with internal tendons. The deflection of the external tendon is restricted to the deflection of the beam at the deviator locations, and it is different from the deflection of the beam at any other location. Also, the eccentricity variations were found to be affected by the time-dependent material properties and the span-to-depth ratios, Figs. 6.30 to 6.35. The ratio of the eccentricity after time-dependent effects to the corresponding eccentricity at the initial loading for the same section, $e(t)/e(t_0)$, was plotted versus the ratio of distance between the support and the section to the beam span, X/S , for different span-to-depth ratios, S/d_p . It can be seen that the ratio $e(t)/e(t_0)$ is equal to unity over the supports and at the deviators. At all other locations, the eccentricity considering the time-dependent effects become smaller than the initial eccentricities. The ratio $e(t)/e(t_0)$ decreases with the increase in span-to-depth ratio. Therefore, the change in eccentricity becomes significant when the span-to-depth ratio increases and has to be considered.

Fig. 6.36 shows the instantaneous and long-term deflections of the simply supported beams. It can be seen from these graphs that the time-dependent effects yield deflections much larger than those due to instantaneous effects. These deflections may even be larger than the deflections specified for serviceability requirements. The graphs also indicate that the profile of the external tendons has no effects on reducing the time-dependent deflections. It can be concluded that the time-dependent effects may significantly affect the response of the member regardless of the tendon profile.

Figs. 6.37 (a) and (b) show the load-deflection and the moment-deflection behaviour of the analyzed simple beam of 10 m (33 ft) span respectively. The external

prestressing was applied after time-dependent effects took place under the self-weight of the beam. The curves shown in these figures are similar to the load-deflection and the moment-deflection response of flexural concrete members observed in many experimental studies. The graph in Fig. 6.37 (a) indicates that the load-deflection response of the strengthened beam was improved. This is indicated by the increase in the stiffness of the concrete member (expressed as the slope of the load-deflection response) after strengthening and applying live load. As shown in Fig. 6.37 (a), external prestressing led to a stiffer load-deflection response. Fig. 6.37 (b) shows the residual deflection in the beam after prestressing and it can be observed that the time-dependent effects are an important factor in the analysis and can yield members with residual deflection even after strengthening.

Fig. 6.38 shows the moment-deflection curve for the analyzed beams. It can be seen that a reduction in the flexural stiffness of the beam occurs due to the loss in the prestressing force. The instantaneous behaviour of the beams yields small deflection associated with a relatively large bending moment. After the transfer of the prestress, beams with high span-to-depth ratios exhibit large deflections associated with relatively small increase in bending moment. This is due to a reduction in the flexural stiffness which results in a reduced prestressing force and continuous change in the eccentricity between the external cables and the beam. Therefore members with high span-to-depth ratios may reach high and unacceptable deflections due to the time-dependent effects only and well before the application of live loads.

Figs. 6.39 (a) and (b) show the variation of the stress increase in external tendons Δf_{ps} versus midspan deflection. Fig. 6.39 (a) shows that the rate of the stress increase, Δf_{ps} ,

decreases with increasing the span-to-depth ratio. Fig. 6.39 (b) shows a continuing decrease in Δf_{ps} and this can be attributed to the high deformations within the maximum moment region compared to the deformations elsewhere along the beam. The curves in the Figs. 6.39 (a) and (b) follow the same trend shown in most of the literature (i.e. Naaman, 1990, Naaman and Alkhairi, 1991, Alkhairi and Naaman, 1993, and Harajli, 1993).

Fig. 6.40 (a) shows the distribution of top and bottom fiber stresses against one half of the span of the beam. It can be seen from Fig. 6.40 (a) that sudden change in the stresses occur at the location of the external tendon deviators. It can also be noticed that the time-dependent effects do not have significant influence on the top stresses. The largest change in the top stress occurs at the location of the deviators. This is due to the loss in prestressing taking place between the initial loading and the end of the time-dependent effects. It can also be seen that the time-dependent effects significantly increase the bottom fibre stresses. This may lead to cracking of the beam before the application of the live loads. This is due to the non-existence bond between the concrete and the external tendons. Fig. 6.40 (b) shows the compressive stress at concrete top fiber versus time. It can be seen from this figure that the relation is nonlinear during a period of 1400 days despite the fact that the stress distribution at initial loading is linear. This can be attributed to the nonlinear creep effects resulting from the sustained compressive stress on concrete which in turn affects the time-dependent behaviour of the beam.

Fig. 6.41 shows that the relation between the strain in the external cables and the beam deflection due to the instantaneous and time-dependent effects can be considered linear. This agrees with Harajli (1993).

The live load was applied on the beam after the time-dependent effects have taken

place. Fig. 6.42 shows the relation between the live load and the ratio of the maximum stress to the initial stress in the external tendons. It can be seen from Fig. 6.42 that this relation is linear, which agrees with Harajli (1993). Fig. 6.42 also shows that for beams with low span-to-depth ratios, the stress in the external tendon increases at a low rate as the live load increases as opposed to beams with high span-to-depth ratios. It is also worth noting that after the time-dependent effects have taken place the stress ratio in beams with high span-to-depth ratios is less than the stress ratio in beams with low span-to-depth ratios. This is due to the loss in prestressing resulted from large deflections due to time-dependent effect in beams with high span-to-depth ratios. Large deflections result in a decrease in eccentricity between the tendons and the beam and hence, a decrease in the bending moment from external tendons. It has to be mentioned that the ratio of the prestressing stress to initial stress varies nonlinearly with the span as shown in Fig. 6.43. This nonlinear variation in the stress is due to the loss in prestressing after time-dependent effects, variations in the eccentricity, and crack development in the beam which all occur at an increasing pace as the span-to-depth ratio increases.

6.9.4 Simply Supported Beams with Internal unbonded Tendons Tested by Harajli and Compared With The Current Study

This verification is used to check the moment-deflection response of beam specimens with internal unbonded prestressing tendons and tensile reinforcing steel loaded to flexural failure. Harajli (1995) tested a total of 26 simply supported beam specimens with internal unbonded tendons. Four of these beam specimens are used for comparison with the current procedure. These beams have rectangular cross section whose dimensions are 5"x9"

(127mmx229mm). The span of the beams is 120" (3048 mm). The depths of the reinforcing tensile steel and the prestressed wires from the top fiber are 8" (203 mm) and 6.3" (160 mm), respectively, see Fig. 6.44. The ducts for the prestressing wires were 2mm thick smooth plastic tubes with a 12 mm (0.47 in) internal diameter. A summary of reinforcement and strength parameters of the various beam specimen is given in the following table:

Beam designation	Type of loading	P/steel A_{ps} in ²	R/steel A_s in ²	Concrete Strength, f'_c (ksi)	Grade of P/ steel f_{pu} (ksi)	Effective prestress f_{pe} (ksi)	Yield stress of R/steel f_y (ksi)
P2R3-3	2-1/3 point load	2 (7 mm) 0.12	2 (6 mm) plain bars	6.8 (46.9 MPa)	215 (1482 MPa)	125 (862 MPa)	40 (276 MPa)
P2R3-0	2-1/3 point load	2 (7 mm) 0.12	2 (6 mm) plain bars	5.6 (38.6 MPa)	207 (1427 MPa)	127 (876 MPa)	40 (276 MPa)
P3R3-3	2-1/3 point load	3 (7 mm) 0.18	2 (6 mm) plain bars	6.75 (46.5 MPa)	207 (1427 MPa)	128 (882.6 MPa)	40 (276 MPa)
P3R3-0	2-1/3 point load	3 (7 mm) 0.18	2 (6 mm) plain bars	5.98 (41.2 MPa)	207 (1427 MPa)	123 (848 MPa)	40 (276 MPa)

It can be seen from Figs. 6.45 to 6.48 that there is a good agreement between the current procedure and the experimentally observed applied midspan moment versus deflection. The maximum deflections at the collapse load are in close agreement. The slight differences in deflection are partly due to stress-strain model of the prestressing steel and the shear effects which are neglected in the nonlinear analysis.

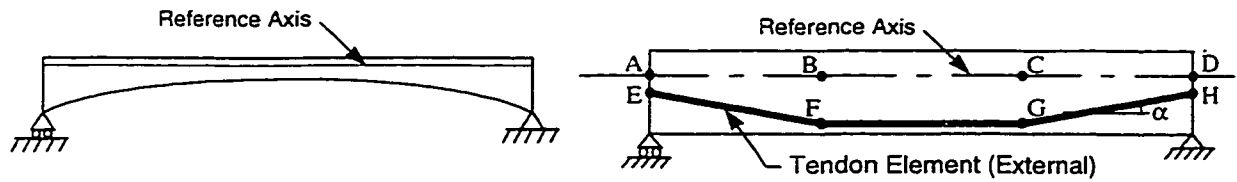


Fig. 6.1(a) Typical Reinforced or Prestressed Plane Structure

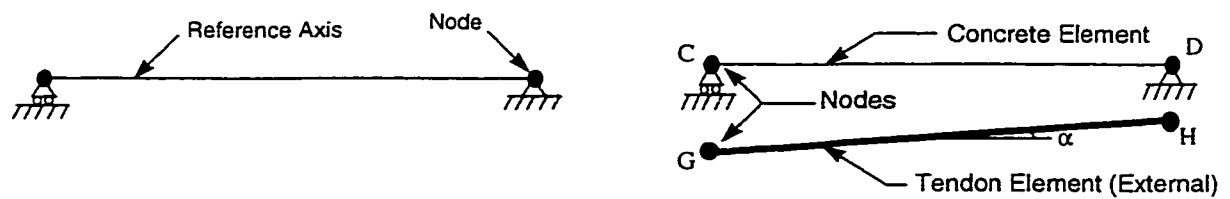


Fig. 6.1(b) Idealization of a Plane Structure

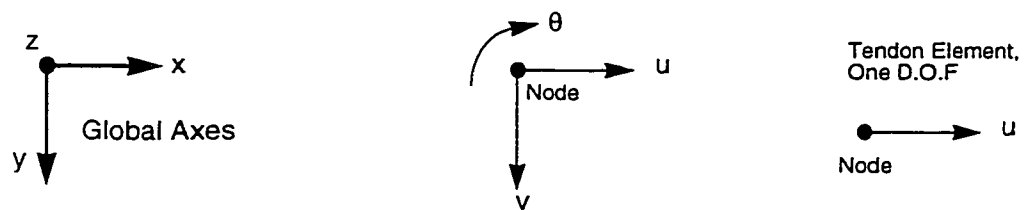


Fig. 6.2(a) Displacement Components at a Typical Node

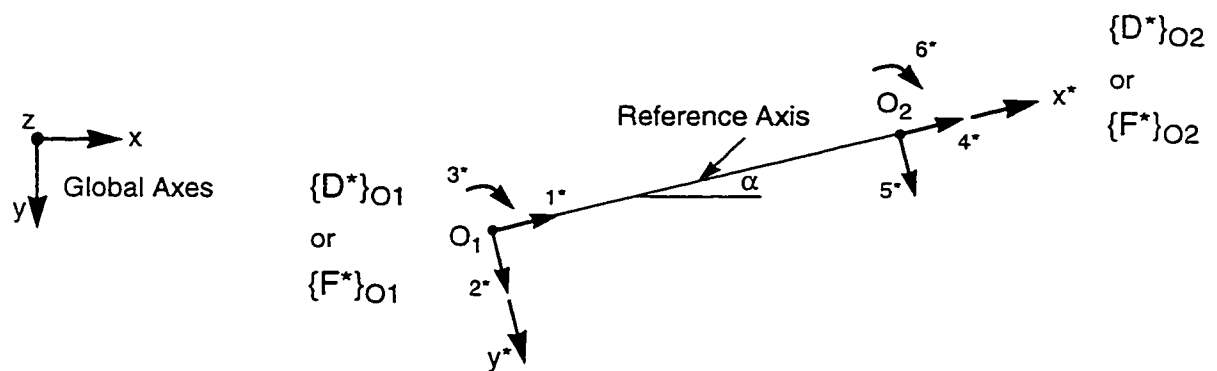


Fig. 6.2(b) Local Axes and Positive Directions of Member End Forces and Displacements

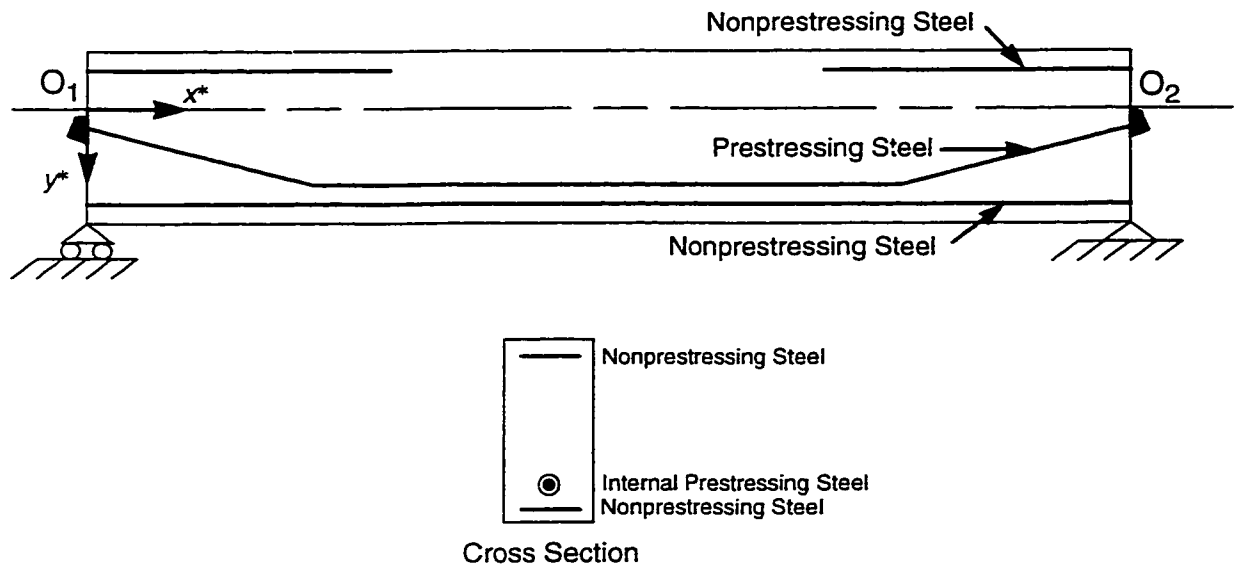


Fig. 6.3(a) A Plane Frame Member with Internal Tendons

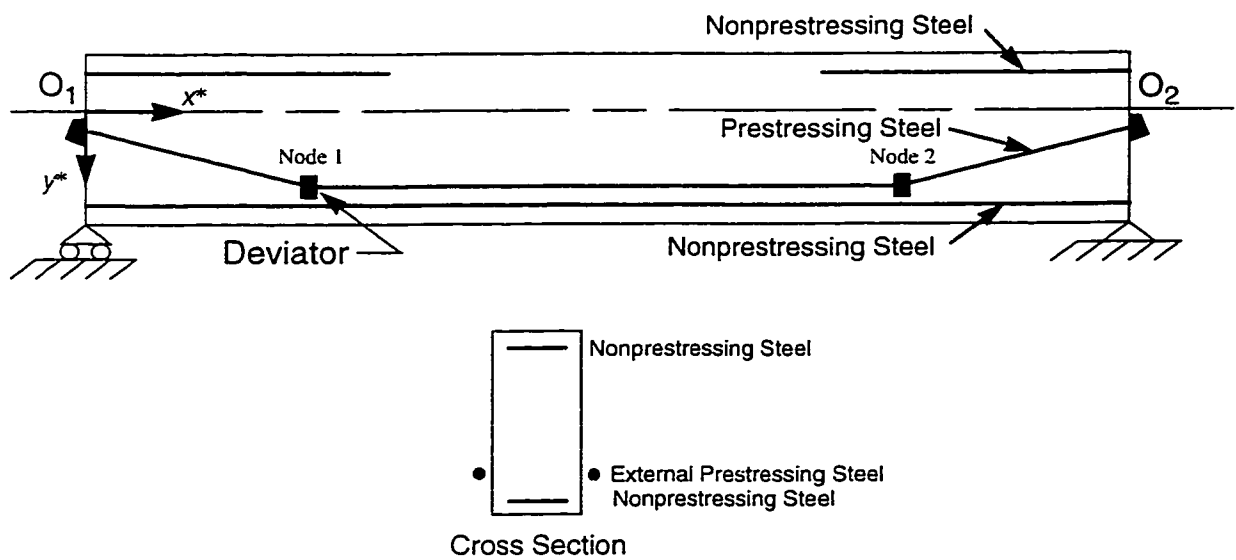


Fig. 6.3(b) A Plane Frame Member with External Tendons

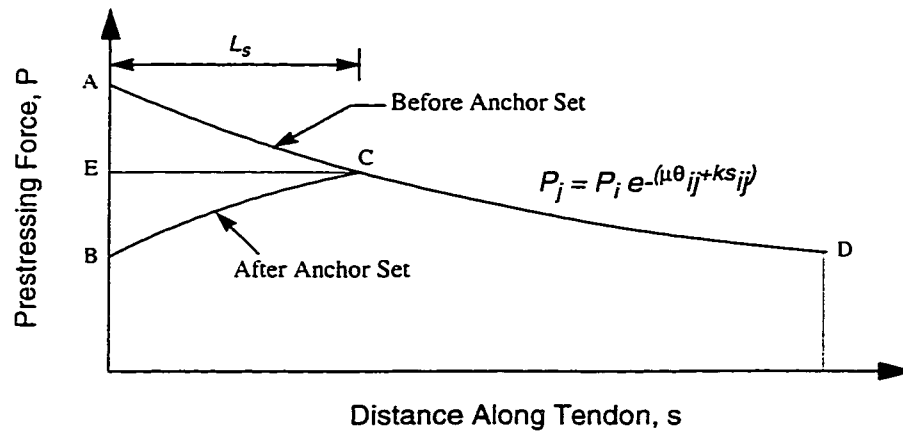


Fig. 6.4 Variation of Prestressing Force Along a Tendon Before and After Anchor Set (El-Badry, M.M., 1988)

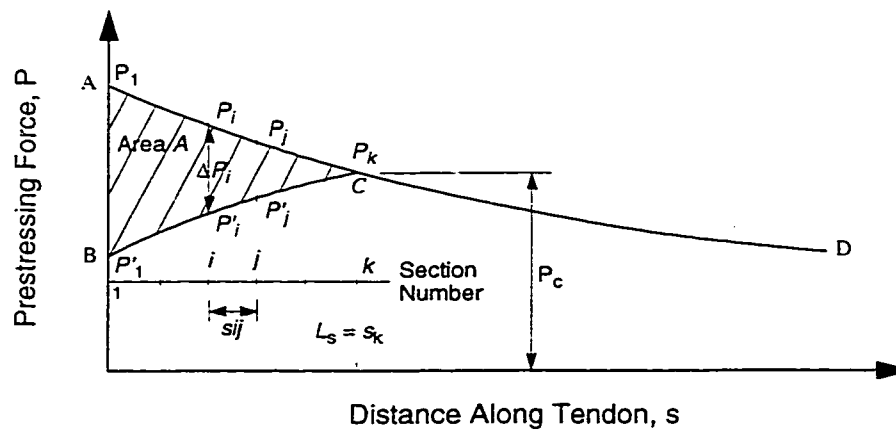


Fig. 6.5 Calculation of Area A (Case of C at Section k) (El-Badry, M.M., 1988)

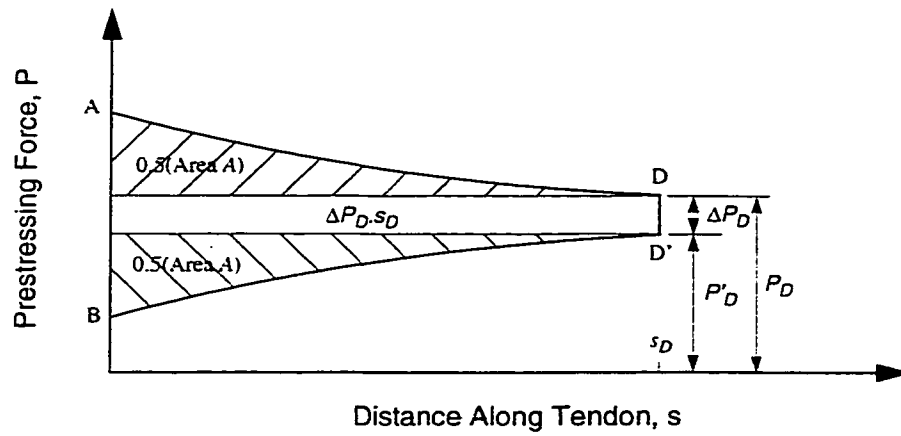


Fig. 6.6 Calculation of Area A ($L_s >$ Tendon Length)
(El-Badry, M.M., 1988)

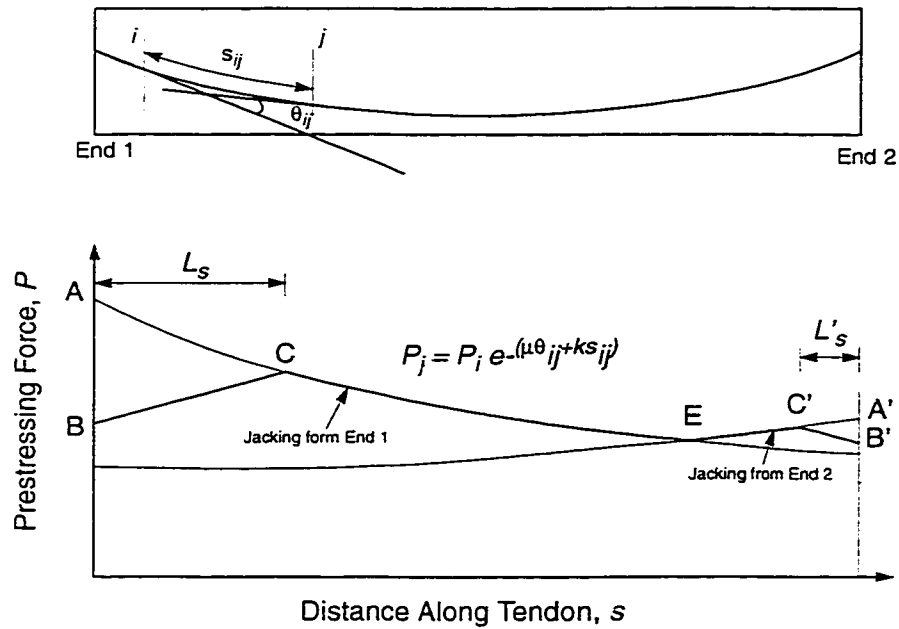


Fig. 6.7 Typical Variation of Prestressing Force (Jacking from Both Ends)
(El-Badry, M.M., 1988)

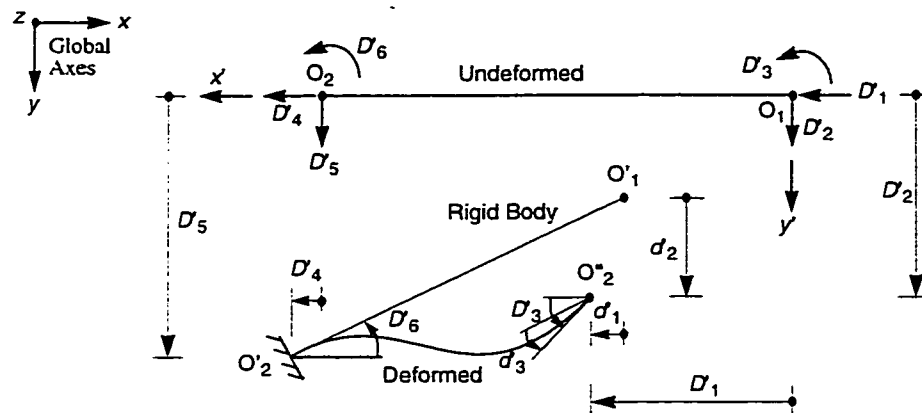


Fig. 6.8 Displacements $\{D'\}$ and $\{d'\}$ in a typical Plane Frame Member

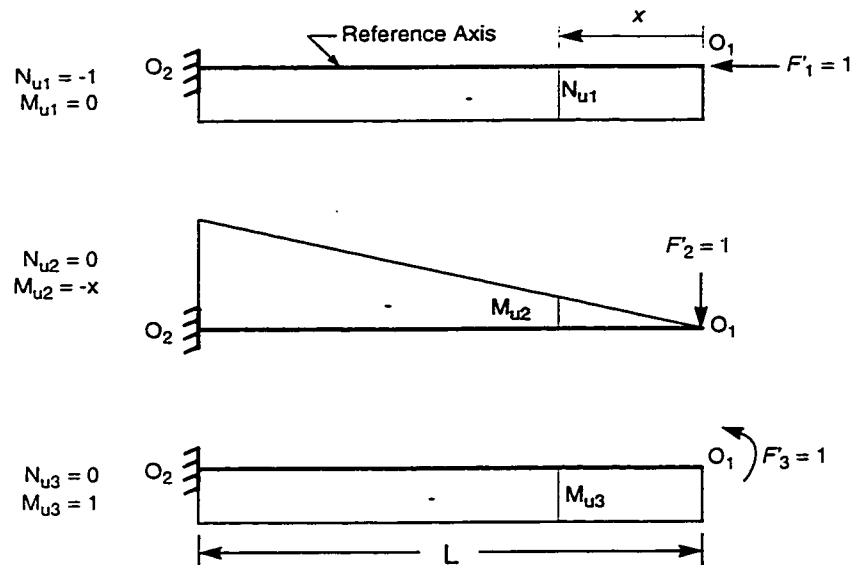
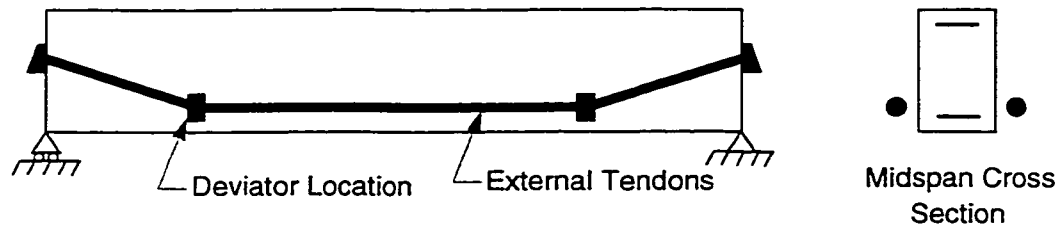
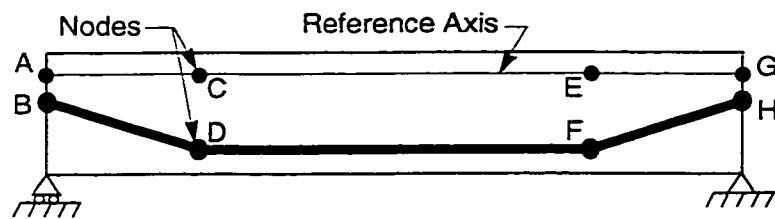


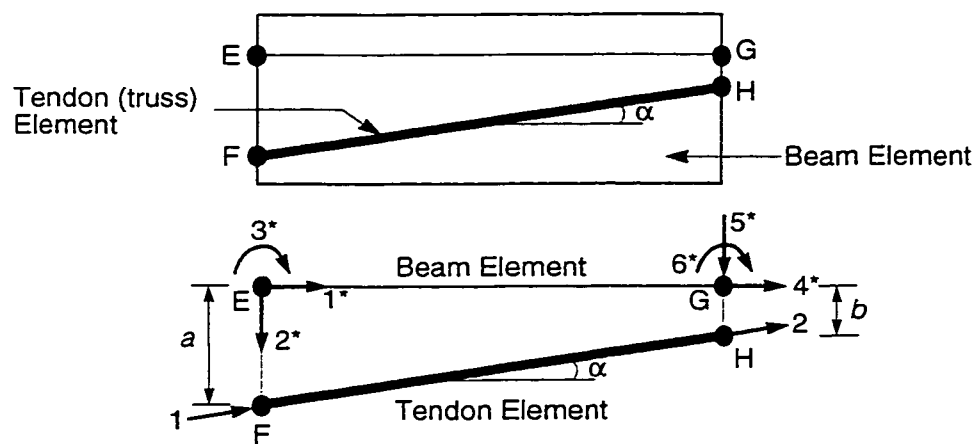
Fig. 6.9 Normal Force and Bending Moment Diagrams Due to Unit Forces at the Three Coordinates at End O_1



(a) Typical Beam with External tendons

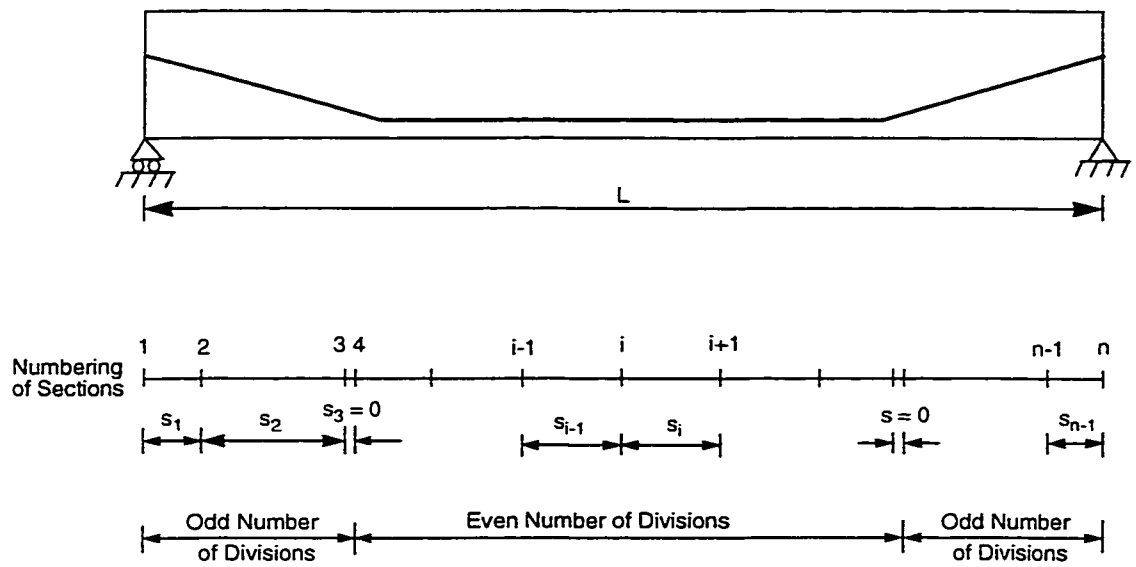


(b) External Tendons Treated as Assemblage of Truss Elements

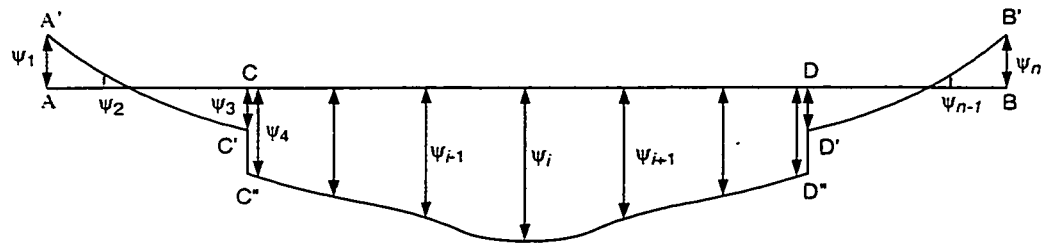


(c) Idealization of a Beam Element with External Tendons

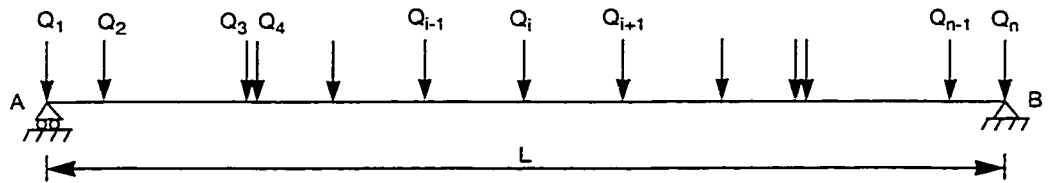
Fig. 6.10 Structural Model With Eccentricity at the Ends



(a) Division of Member into Sections



(b) Curvature Diagram



(b) Equivalent Concentrated Elastic Loads on a Conjugate Beam

Fig. 6.11 Division of a Member into Sections and Calculation of Elastic Loads for Calculating the Deformations (El-Badry, M.M., 1988)

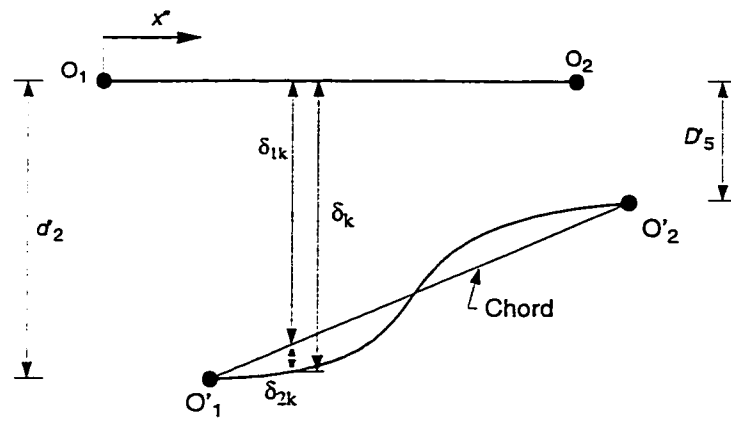


Fig. 6.12 Original and Deflected Shape of a Typical Plane Frame Member

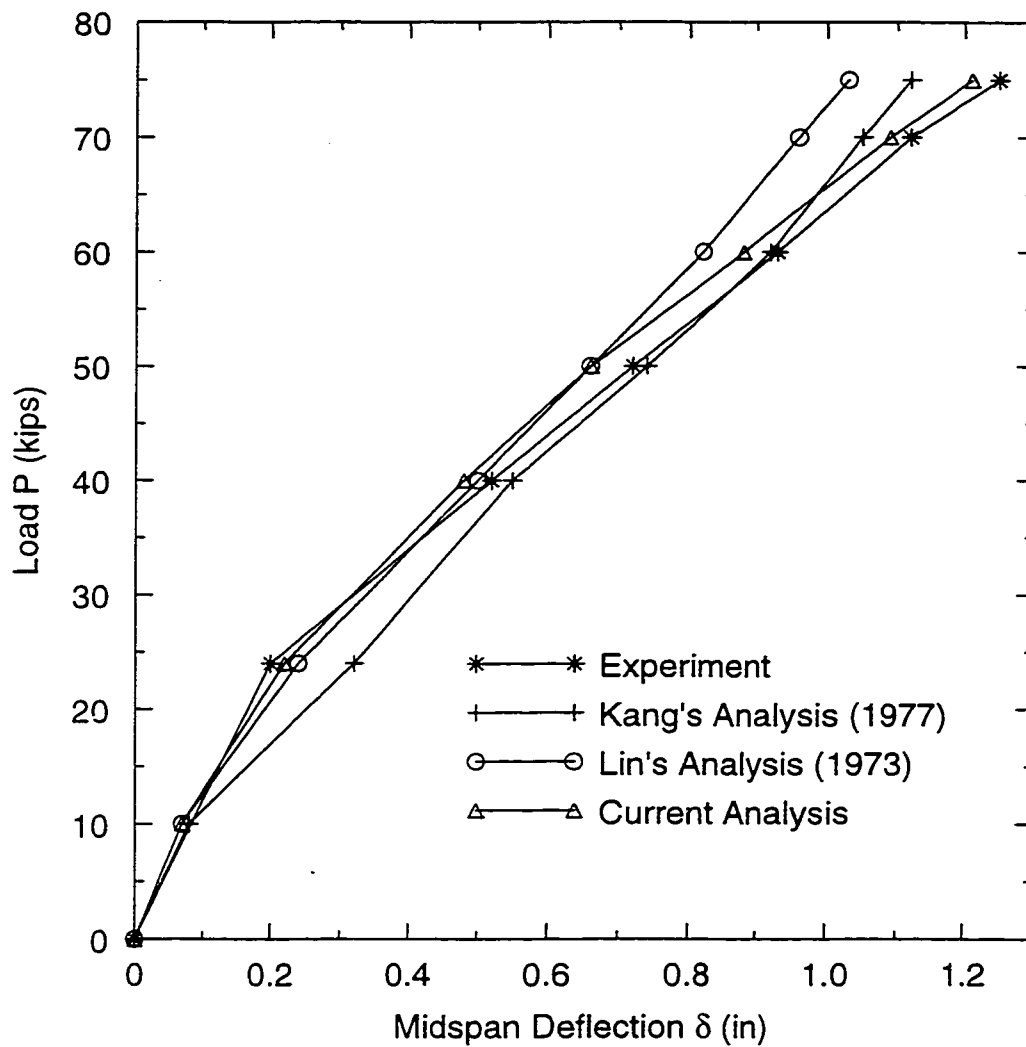
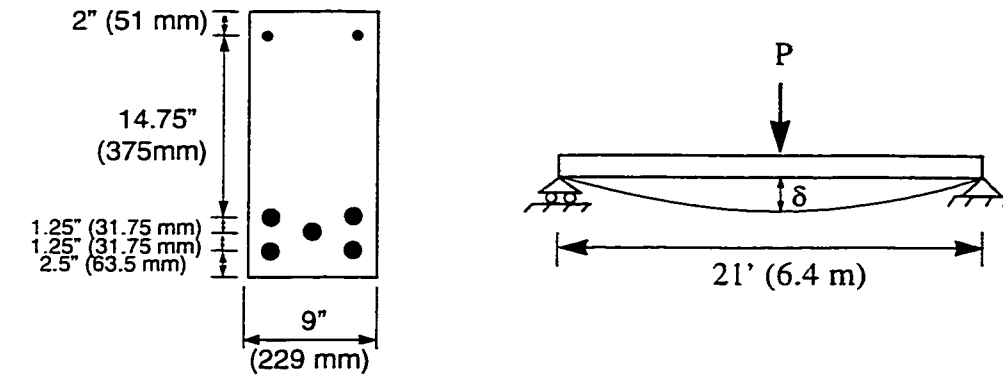


Fig. 6.13 Comparison Between this Study and experiment, Kang (1977), and Lin (1973) for the Midspan Deflection

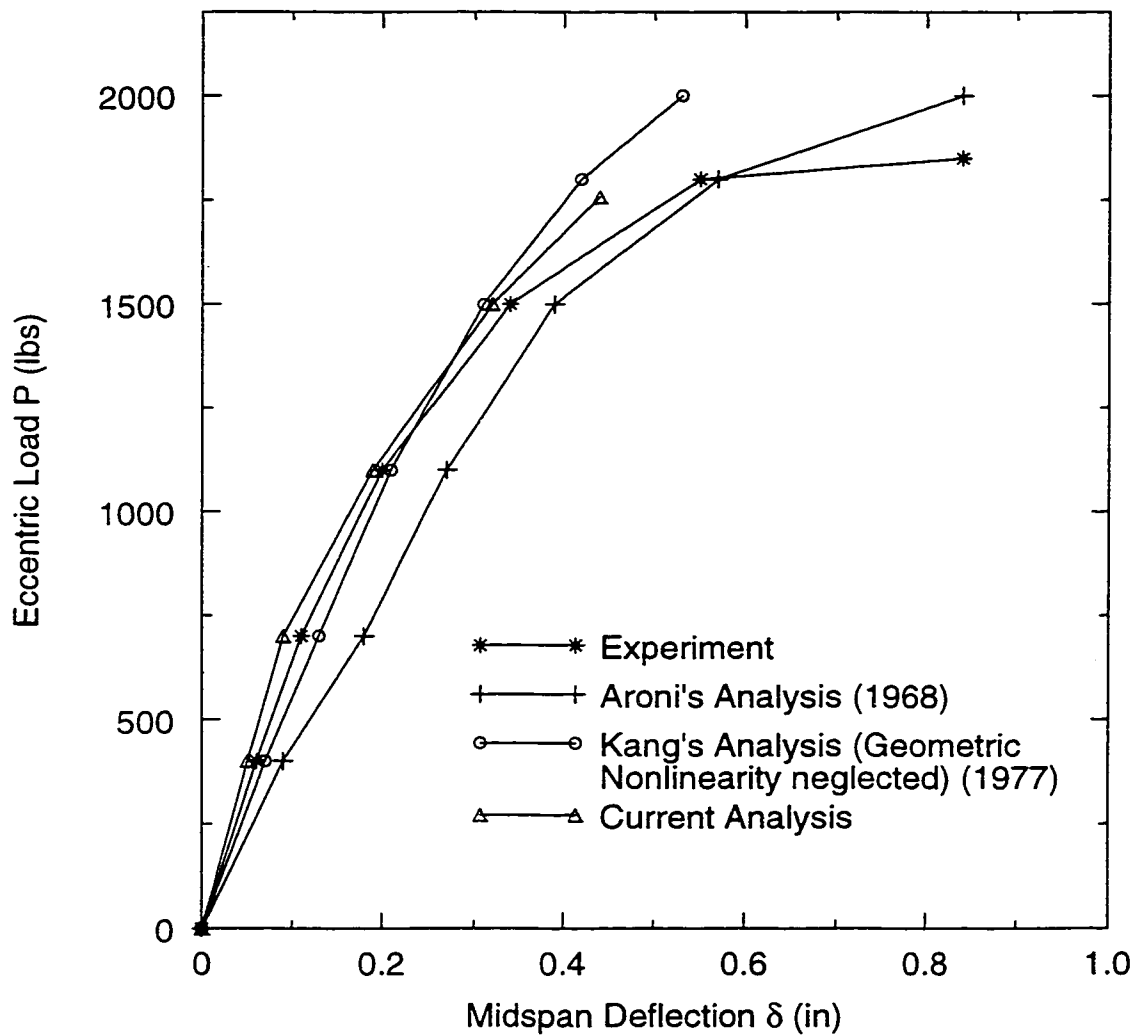
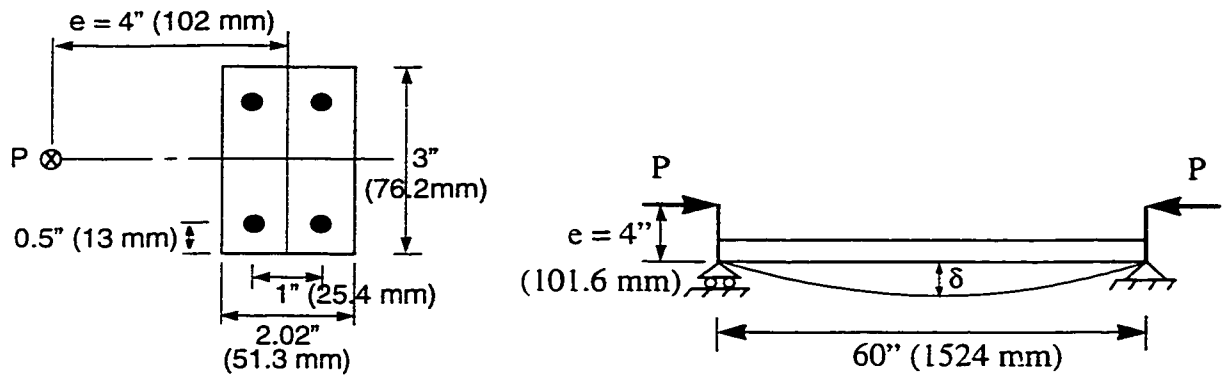
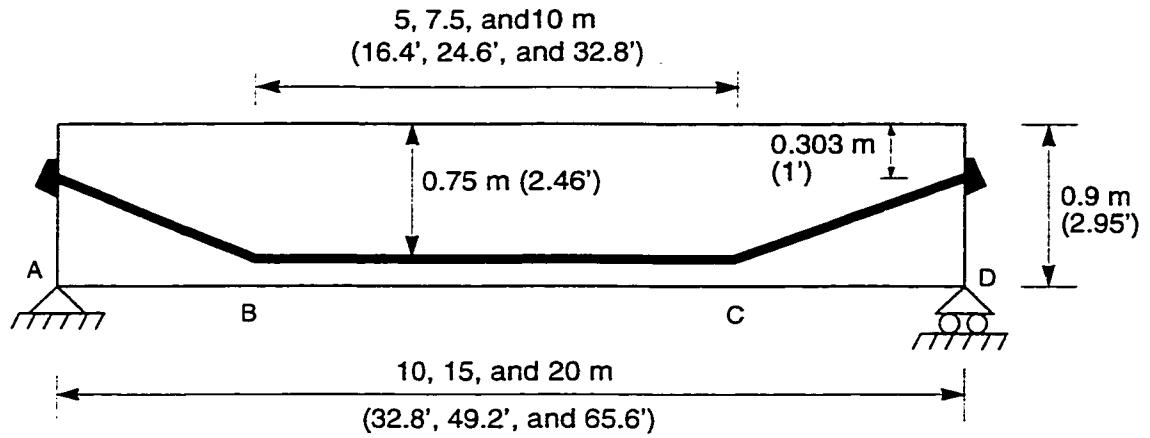
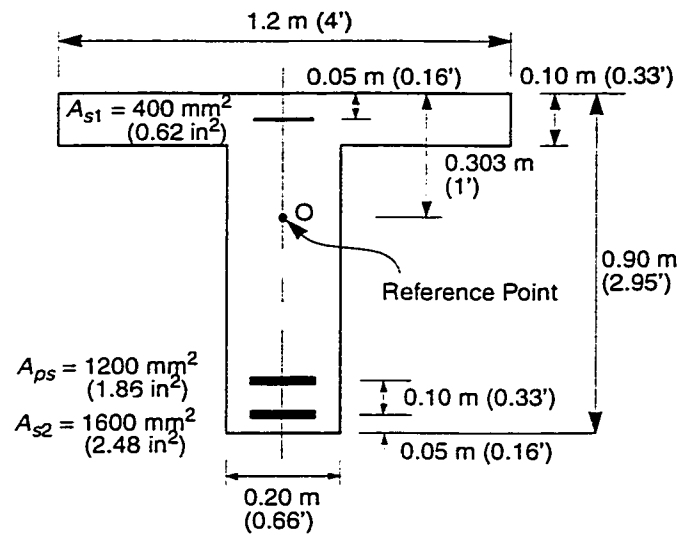


Fig. 6.14 Comparison Between this Study and experiment, Aroni (1968), and Kang (1977) for the Midspan Deflection



(a) Internal Tendon Profile



(b) Midspan Cross Section Dimensions

Fig. 6.15 Pretensioned Partially Prestressed Beam

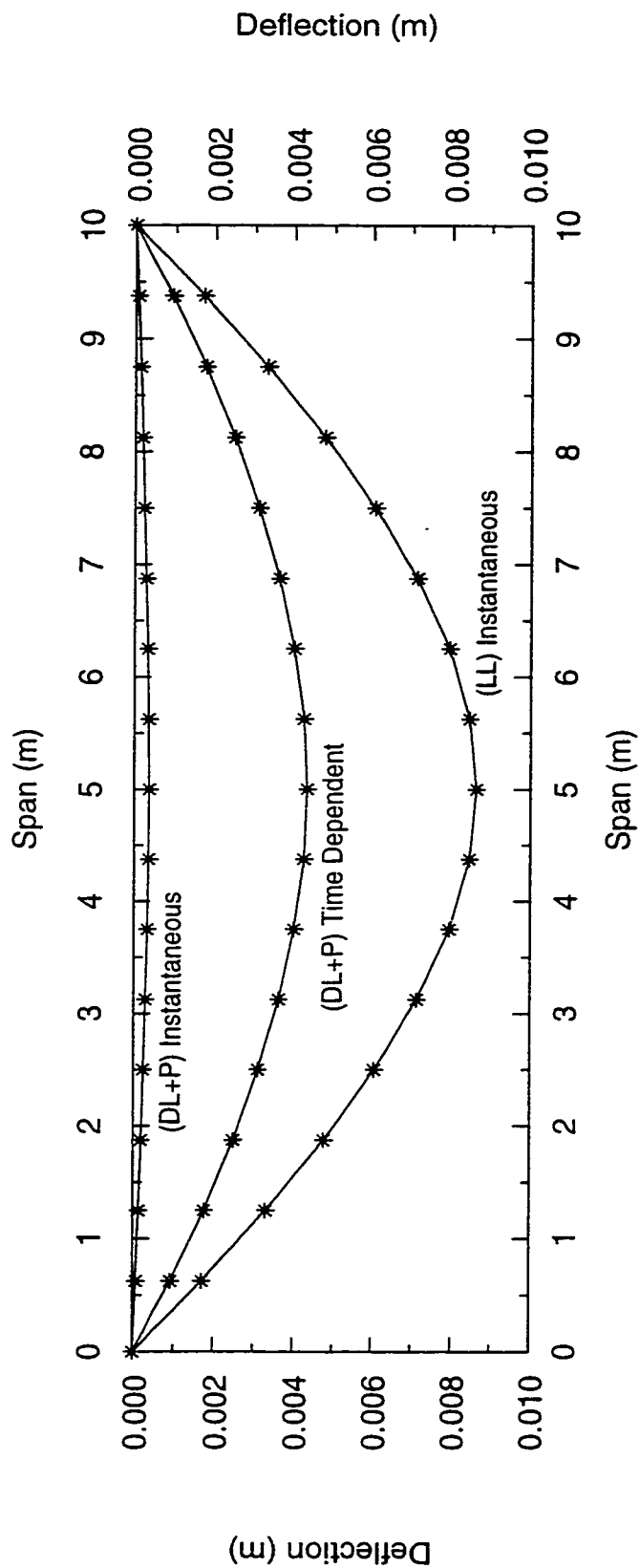
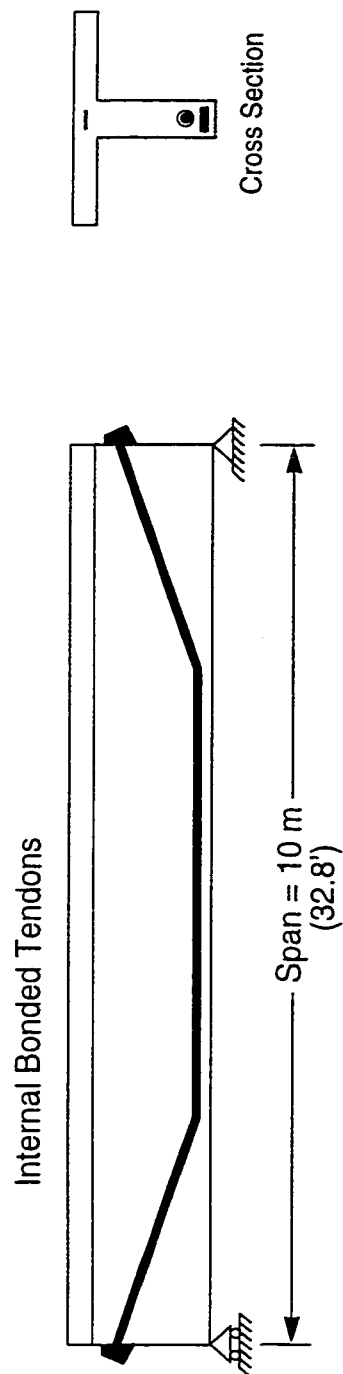


Fig. 6.17 Deflection Due to Instantaneous, Time-Dependent Effects, and L.L.

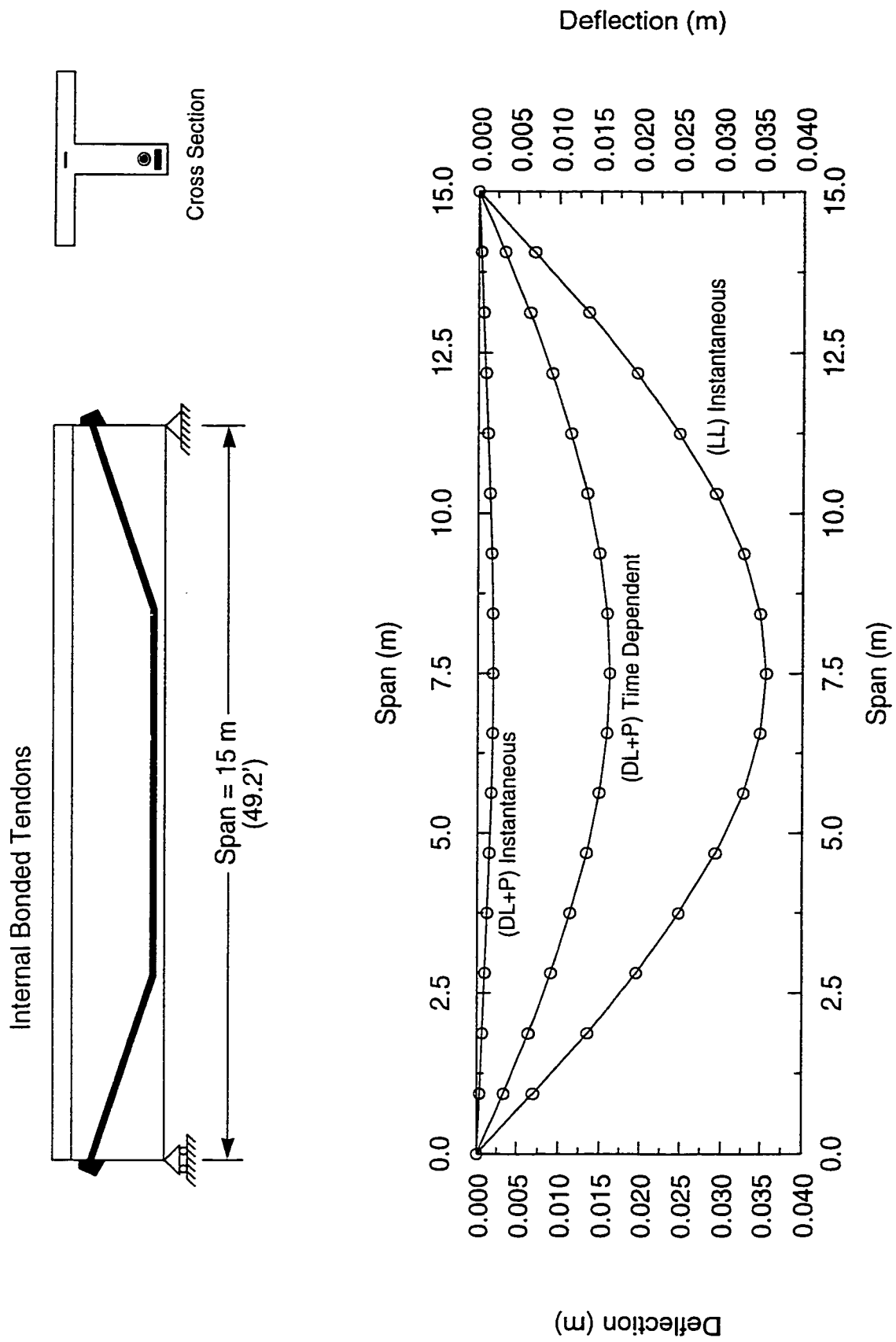


Fig. 6.18 Deflection Due to Instantaneous, Time-Dependent Effects, and L.L.

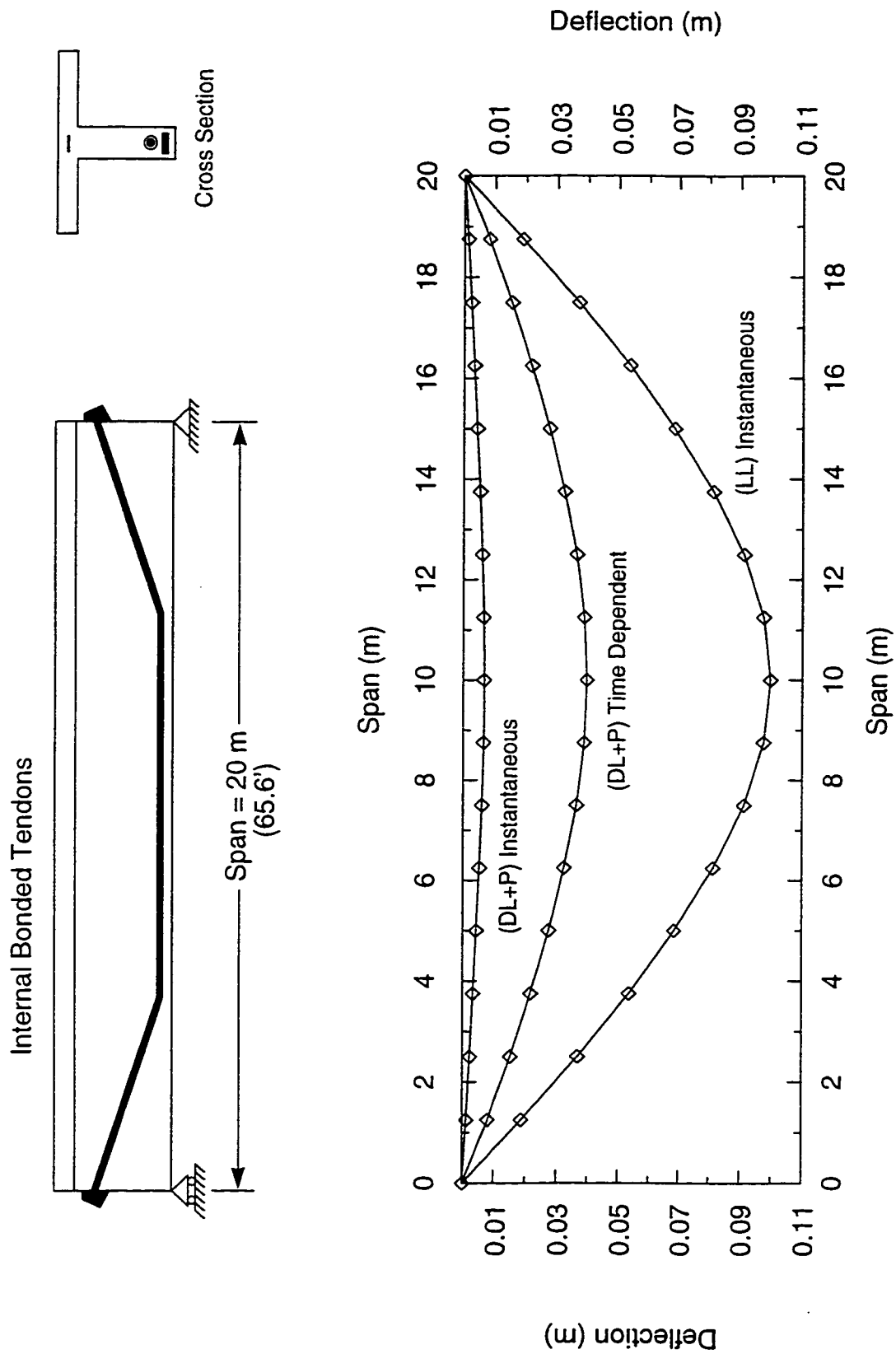


Fig. 6.19 Deflection Due to Instantaneous, Time-Dependent Effects, and L.L.

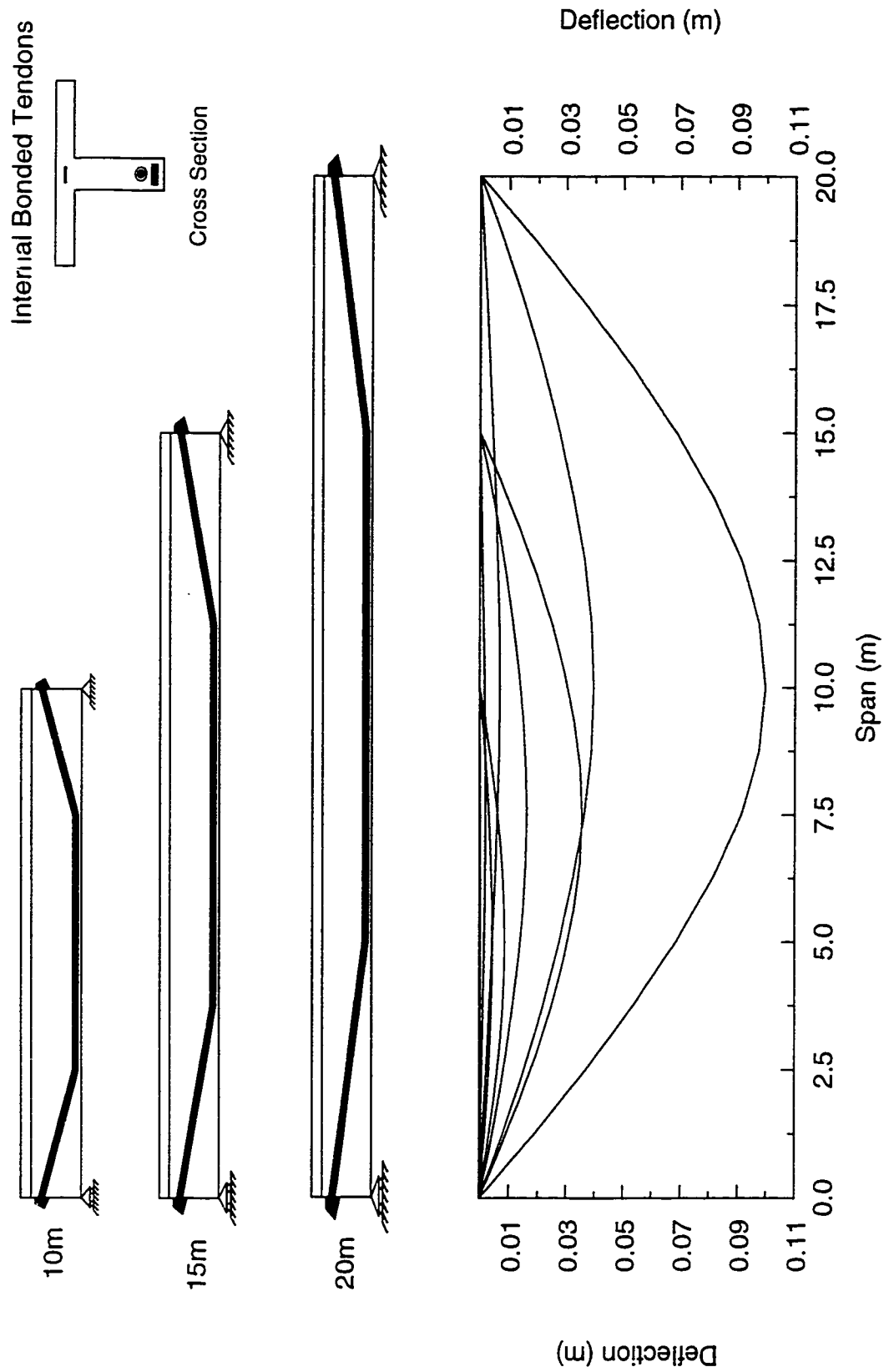


Fig. 6.20 Deflection Due to Instantaneous, Time-Dependent Effects, and L.L.
for 3 Different Span-to-Depth ratios

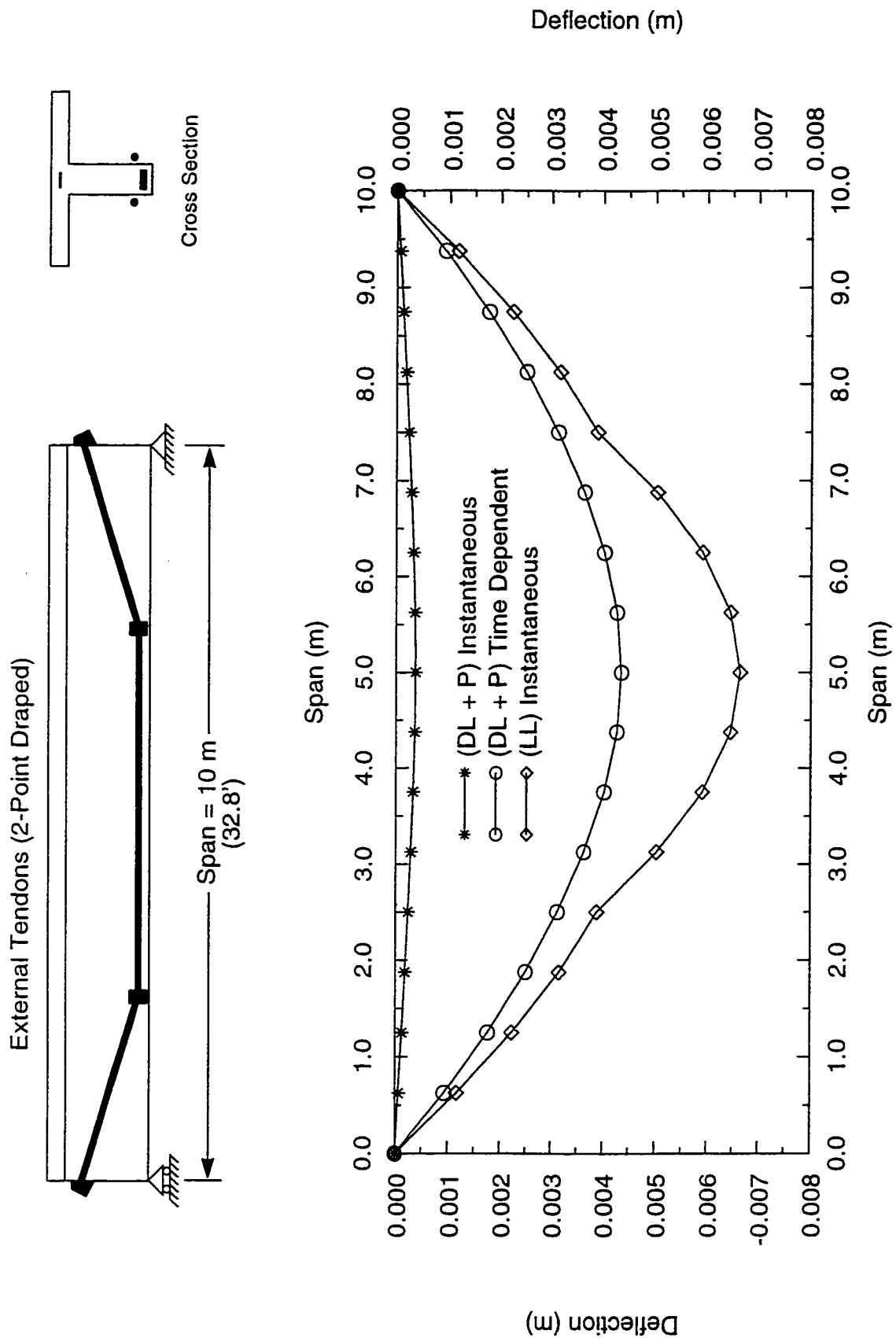


Fig. 6.21 Deflection Due to Instantaneous, Time-Dependent Effects, and L.L.

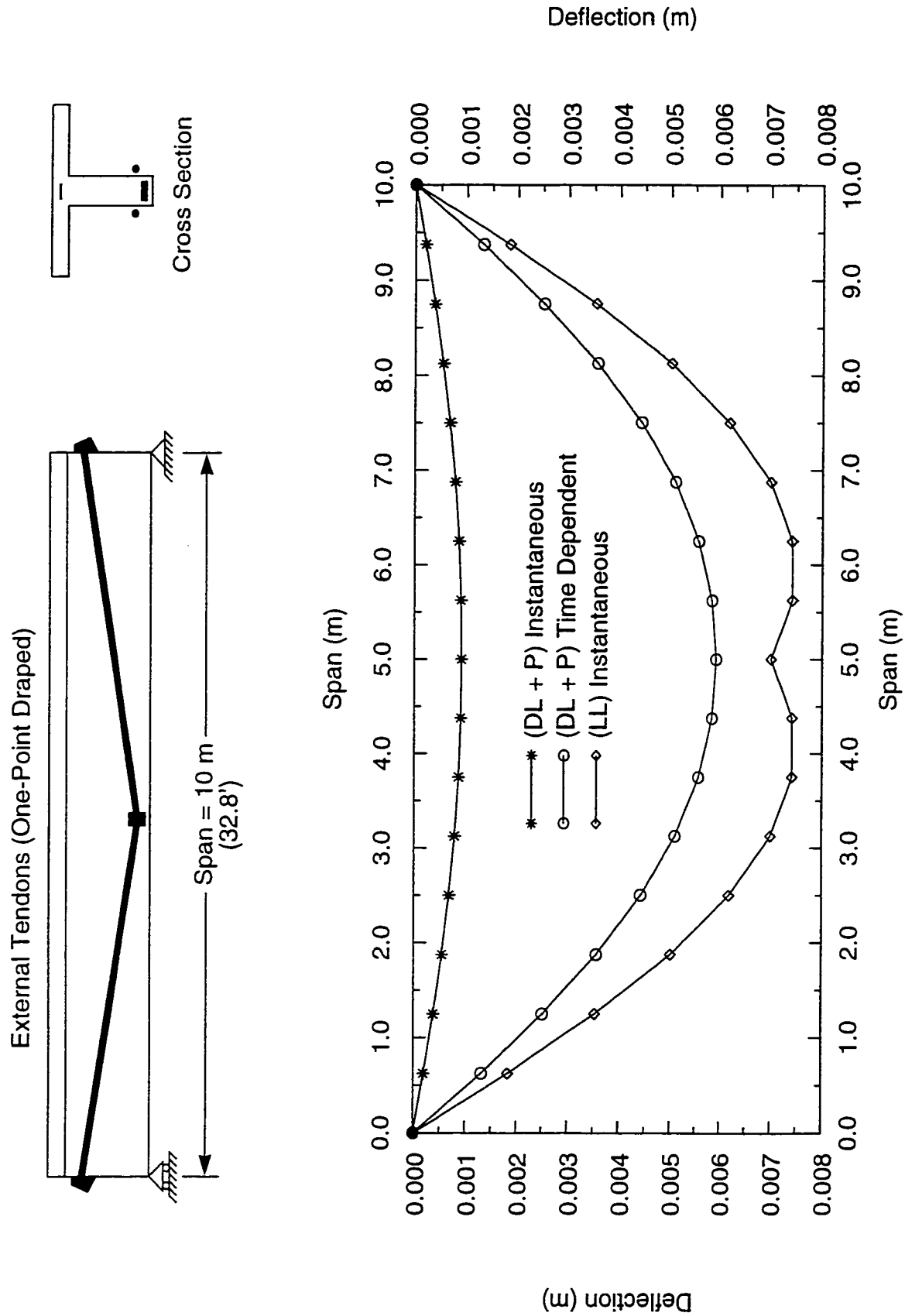


Fig. 6.22 Deflection Due to Instantaneous, Time-Dependent Effects, and L.L.

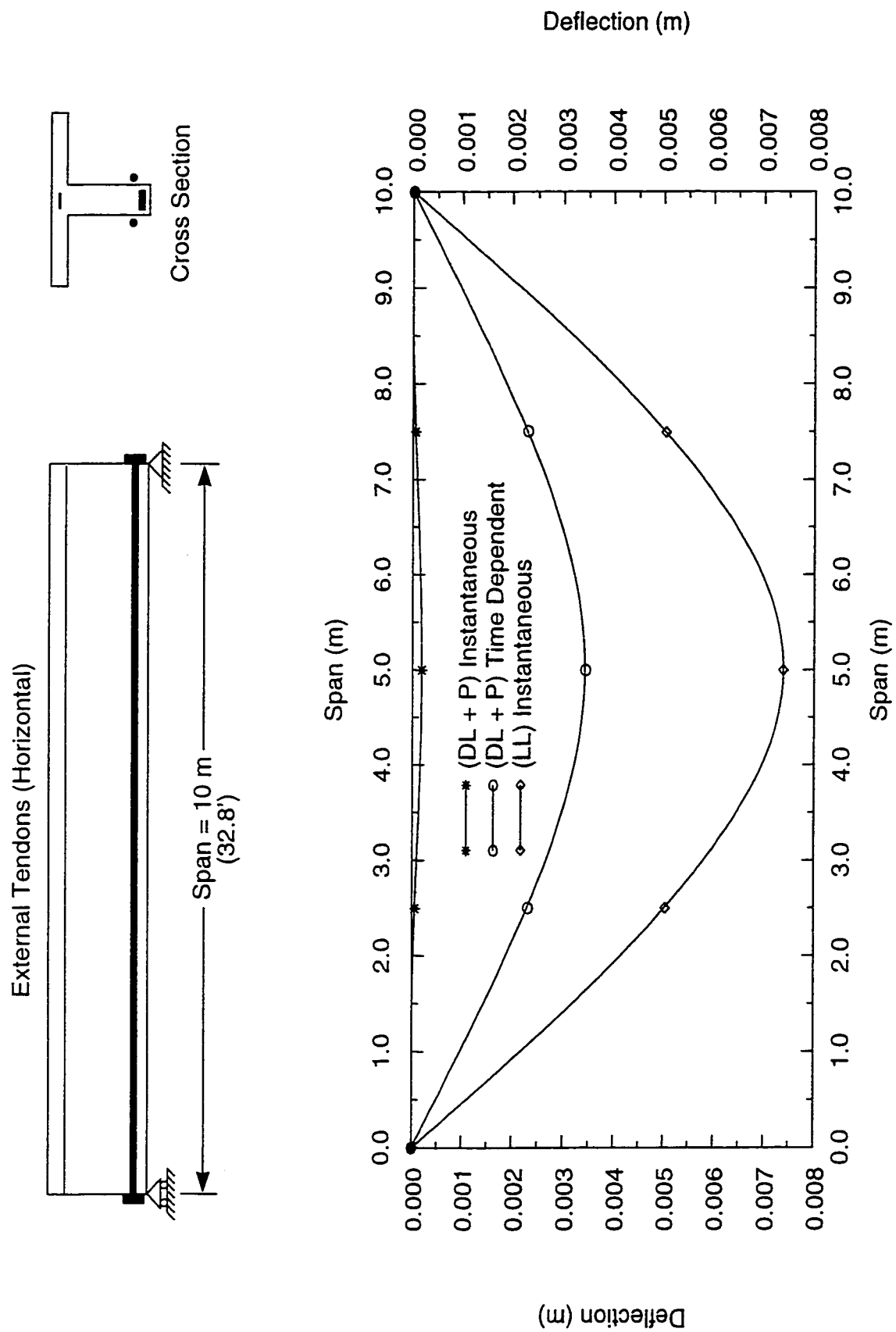


Fig. 6.23 Deflection Due to Instantaneous, Time-Dependent Effects, and L.L.

External Tendons (2-Point Draped)

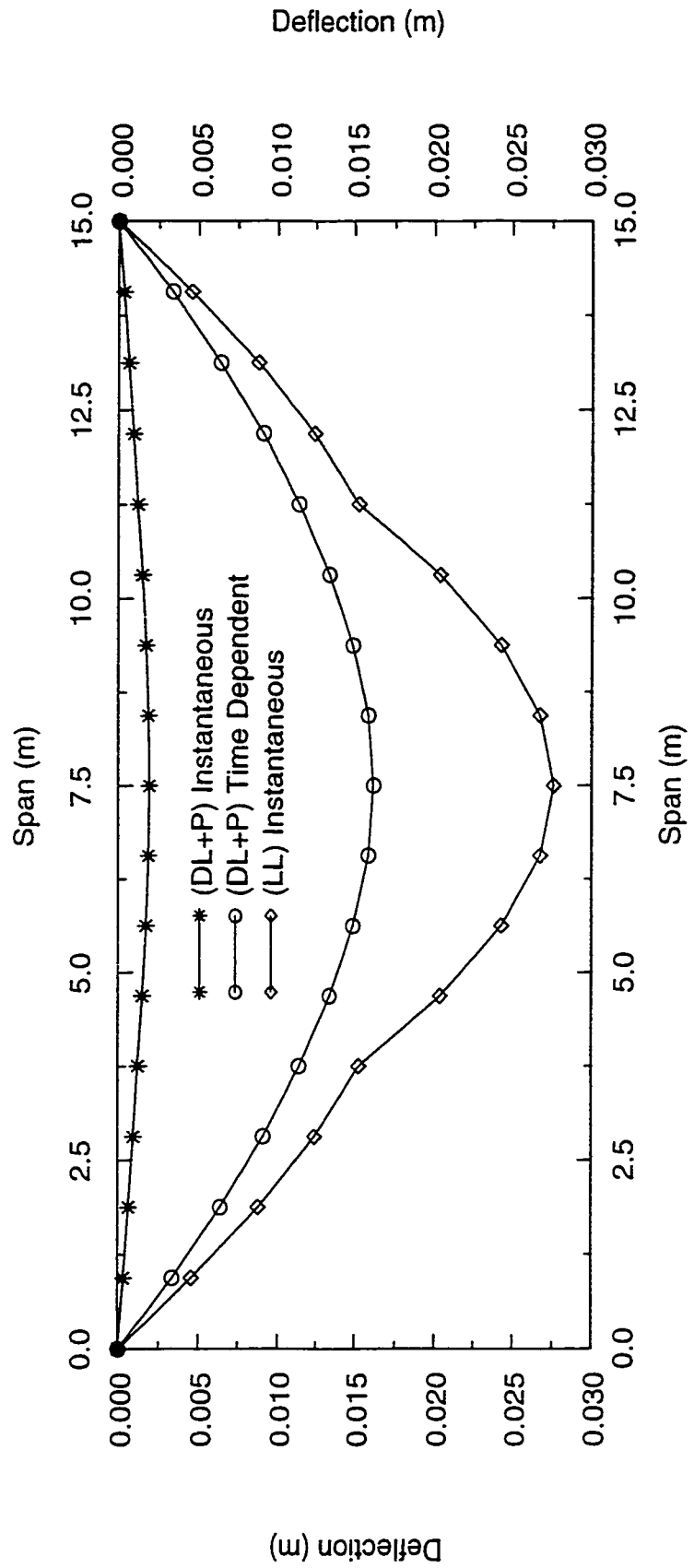
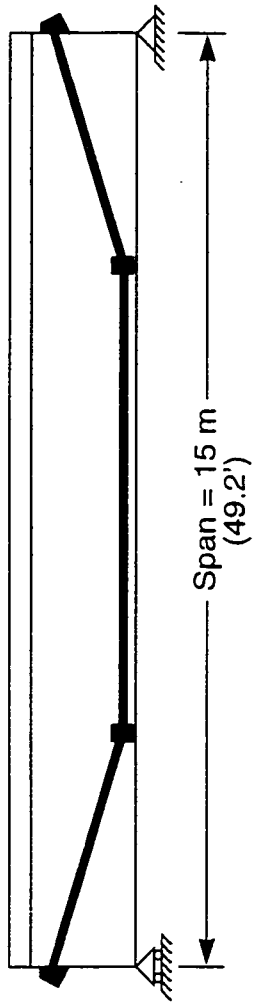
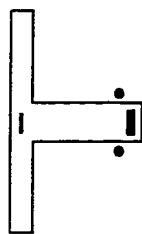
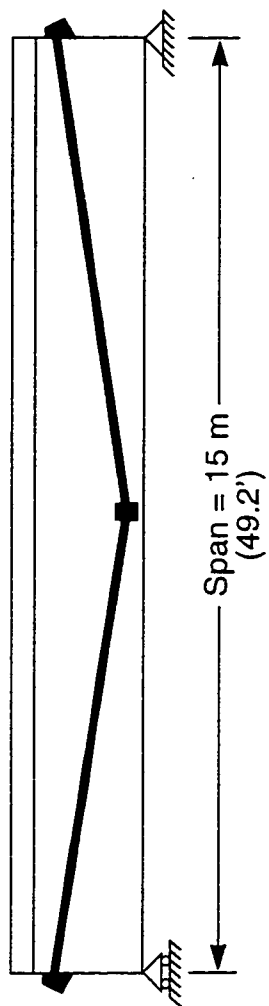


Fig. 6.24 Deflection Due to Instantaneous, Time-Dependent Effects, and L.L.

External Tendons (One-Point Draped)



Cross Section

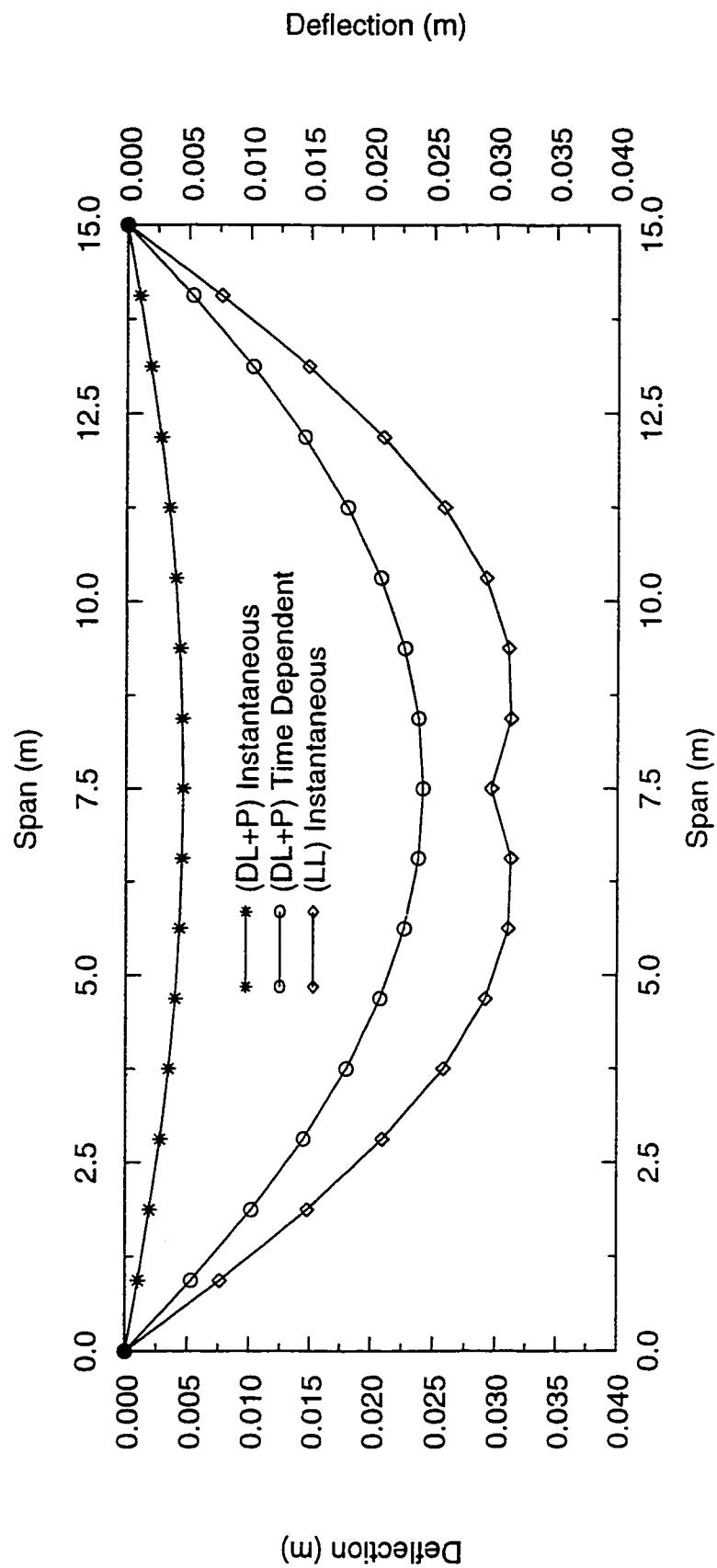


Fig. 6.25 Deflection Due to Instantaneous, Time-Dependent Effects, and L.L.

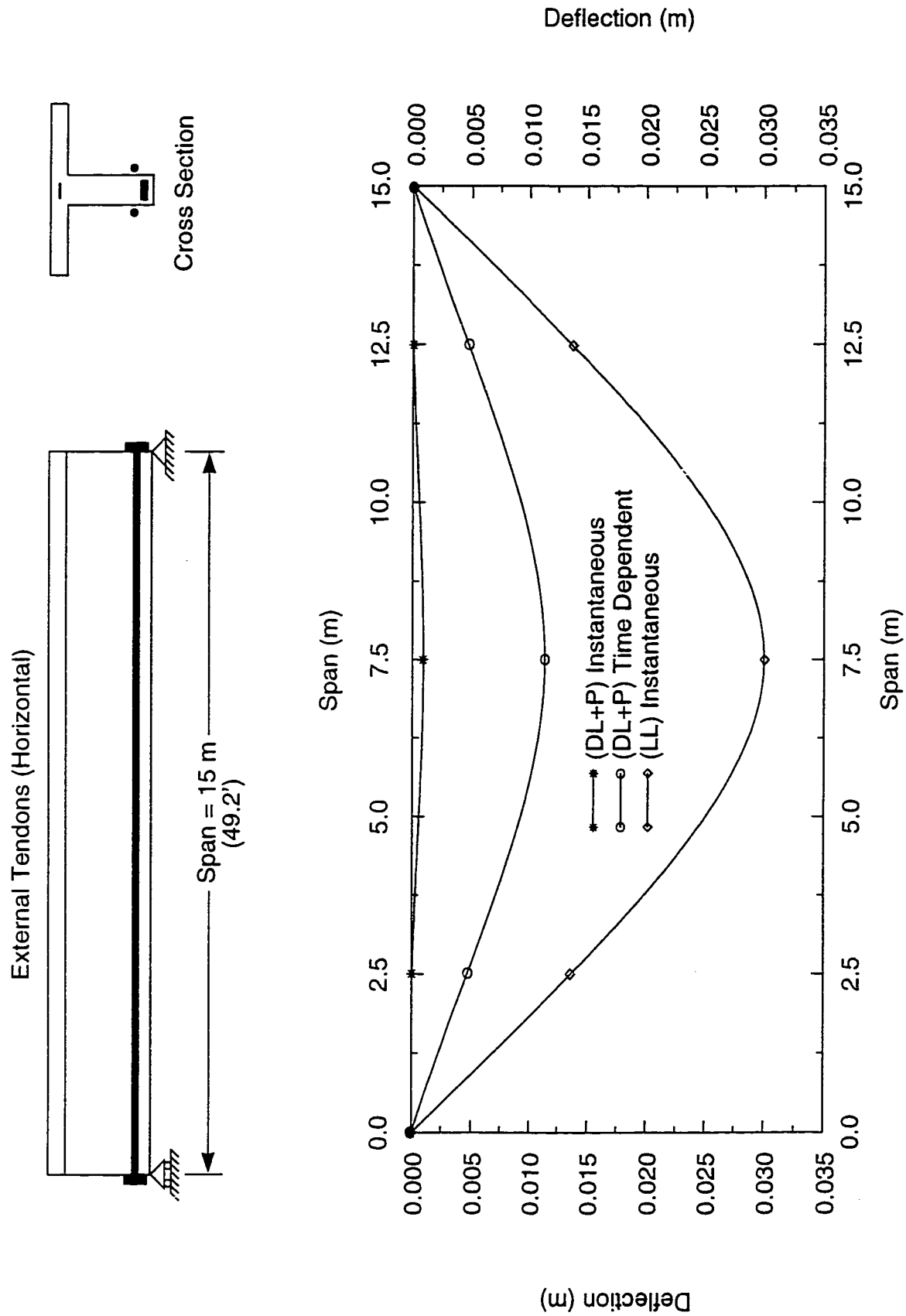


Fig. 6.26 Deflection Due to Instantaneous, Time-Dependent Effects, and L.L.

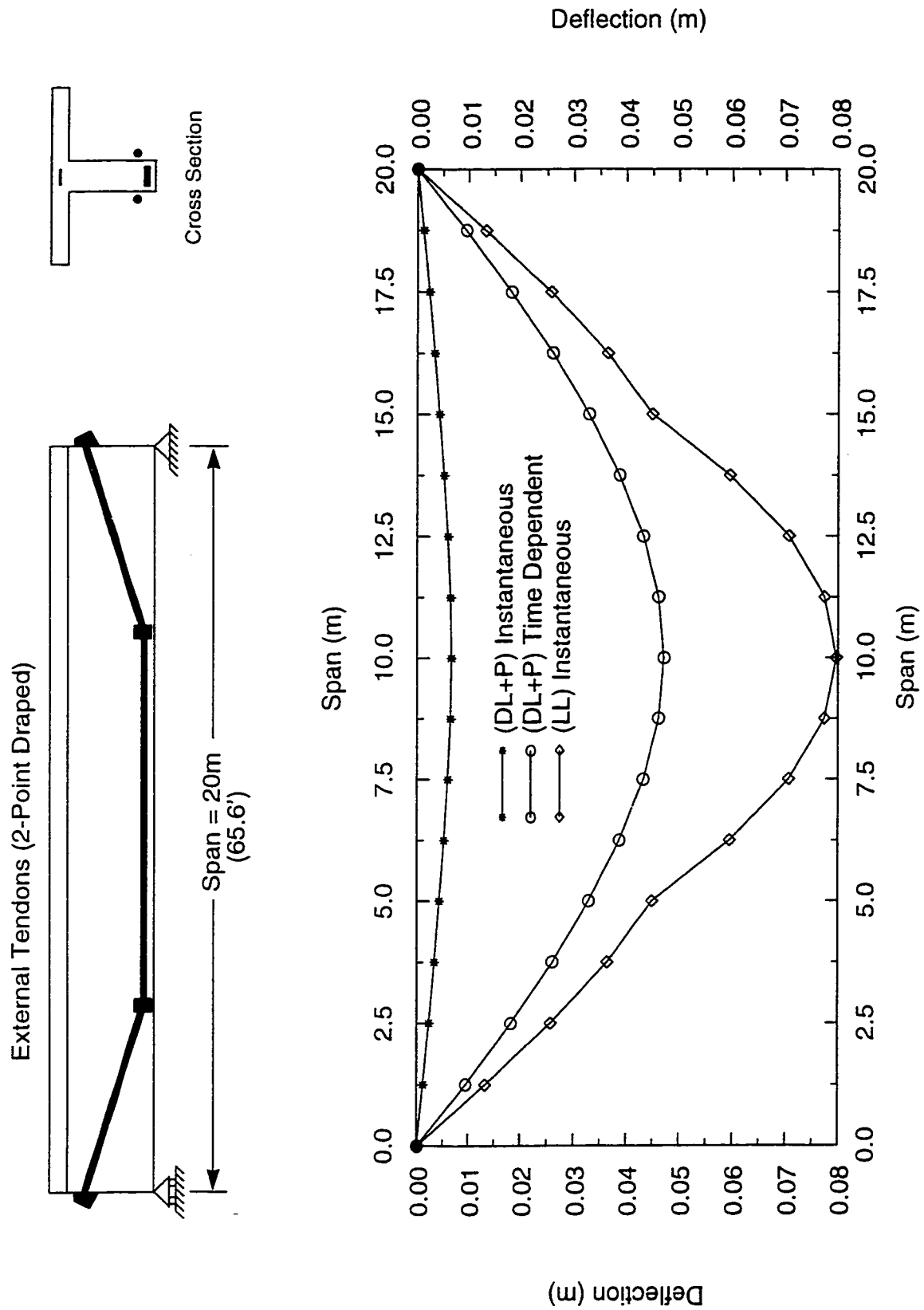


Fig. 6.27 Deflection Due to Instantaneous, Time-Dependent Effects, and L.L.

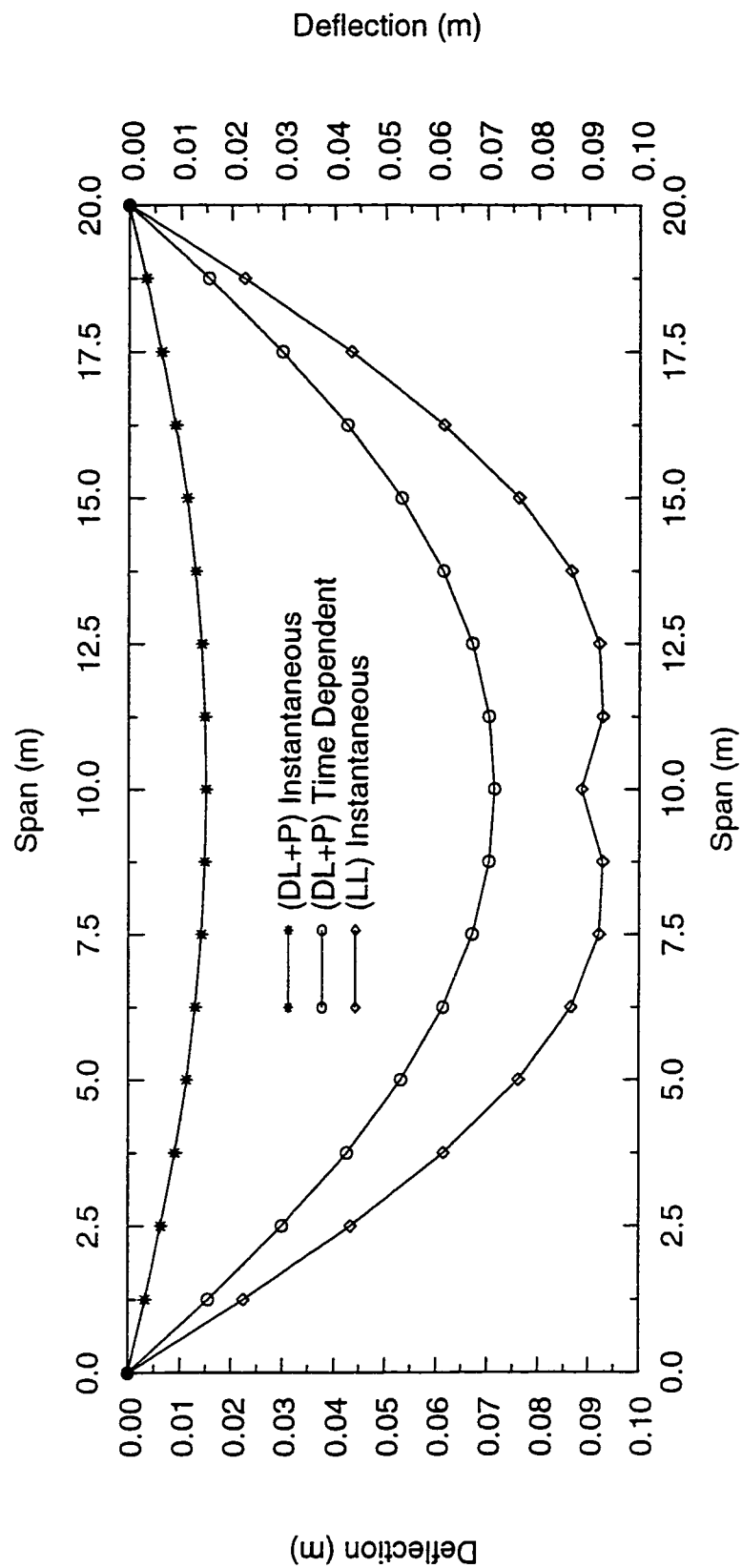
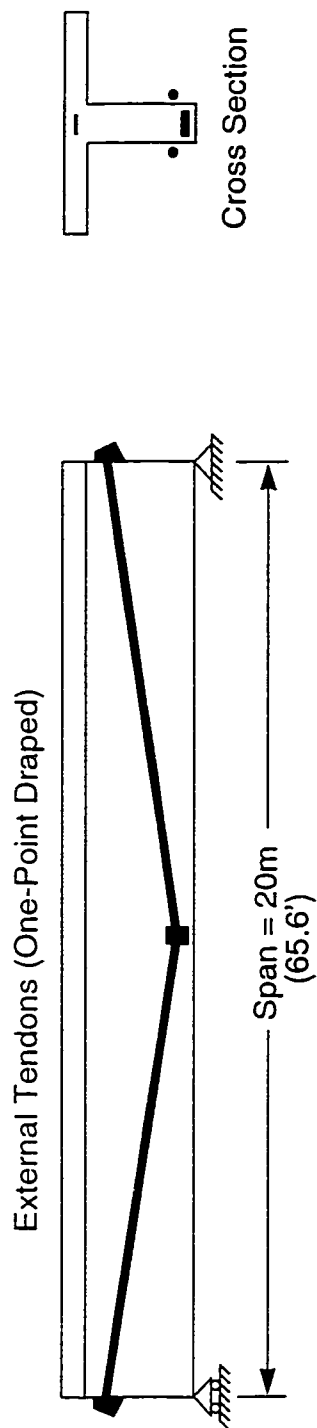


Fig. 6.28 Deflection Due to Instantaneous, Time-Dependent Effects, and L.L.

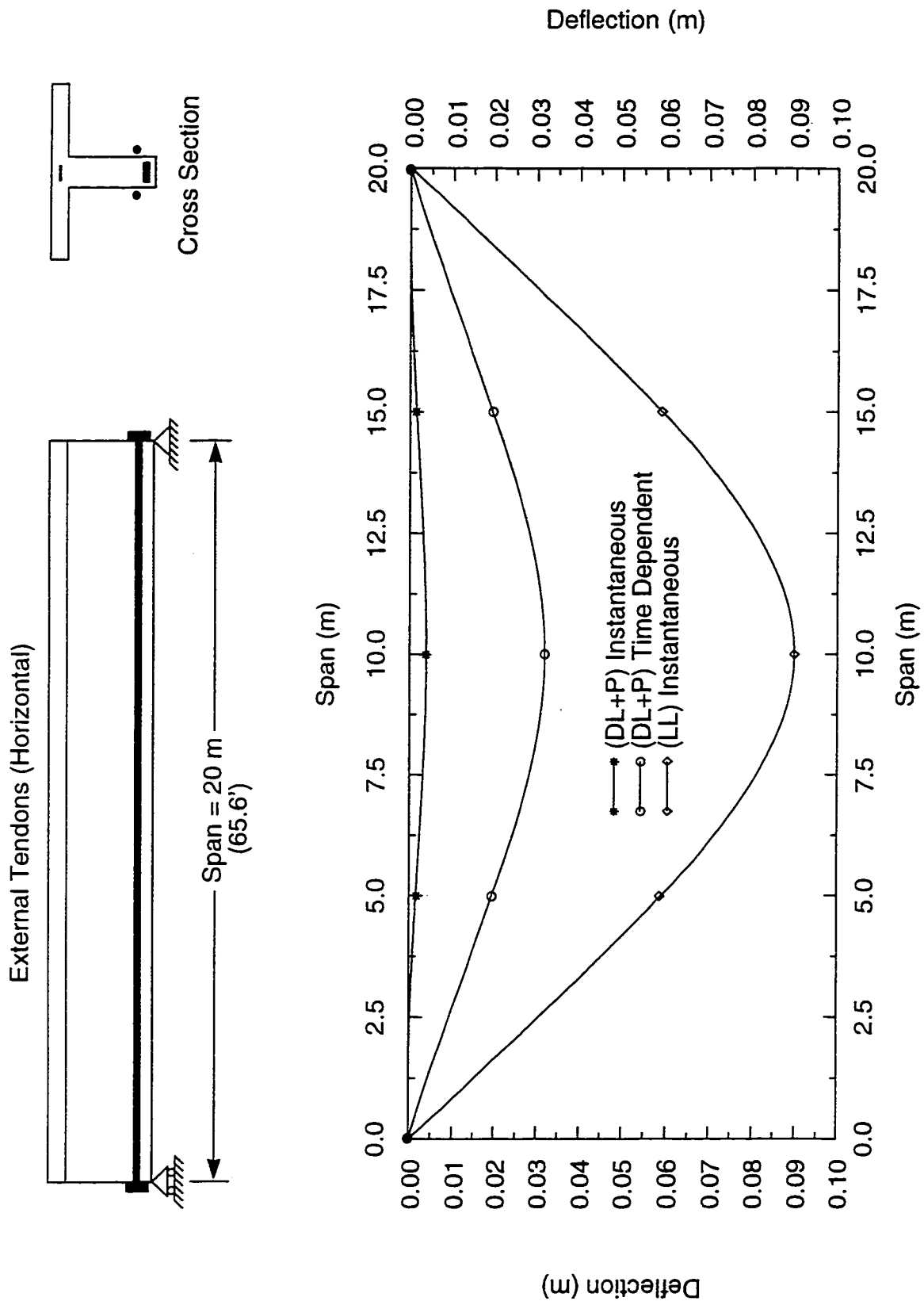


Fig. 6.29 Deflection Due to Instantaneous, Time-Dependent Effects, and L.L.

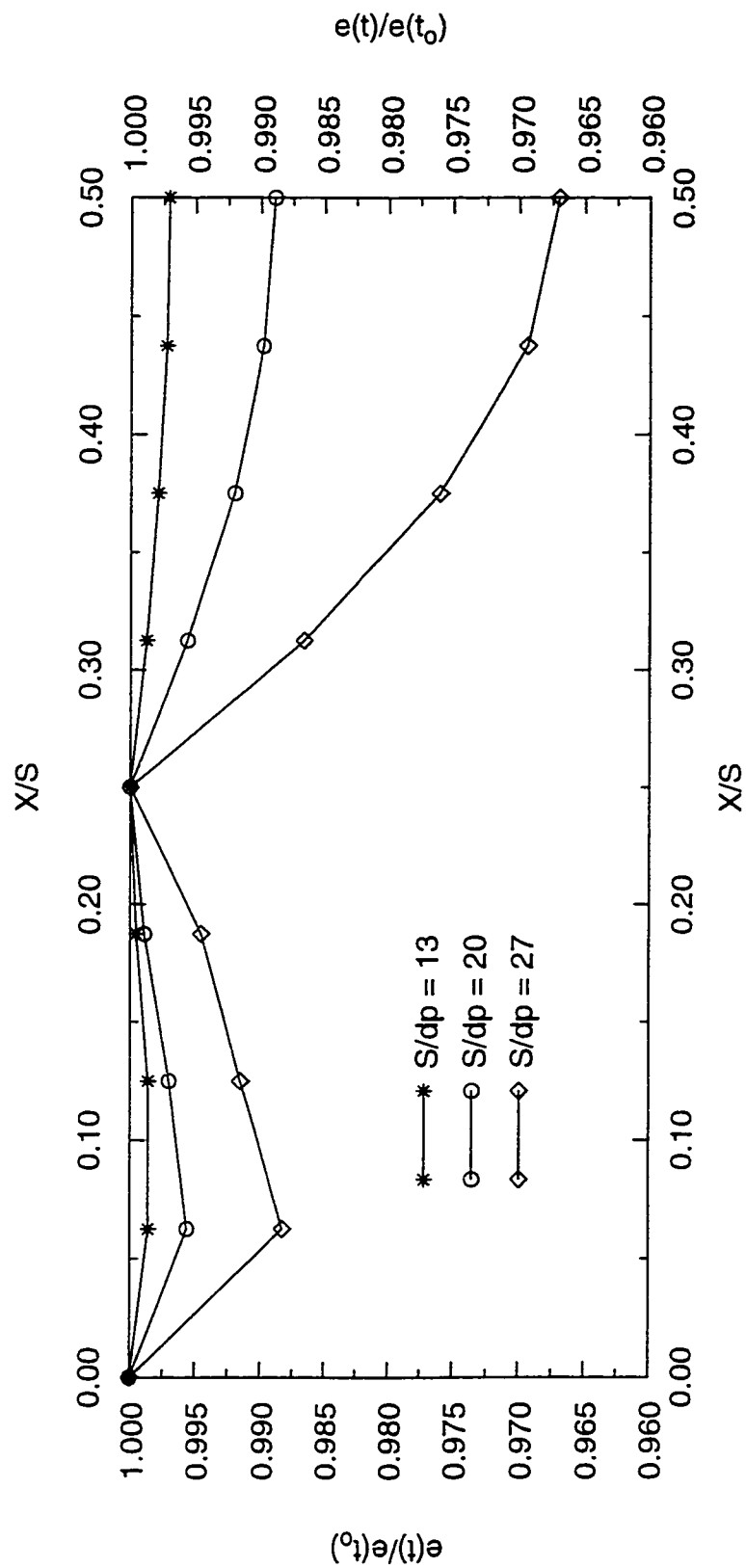
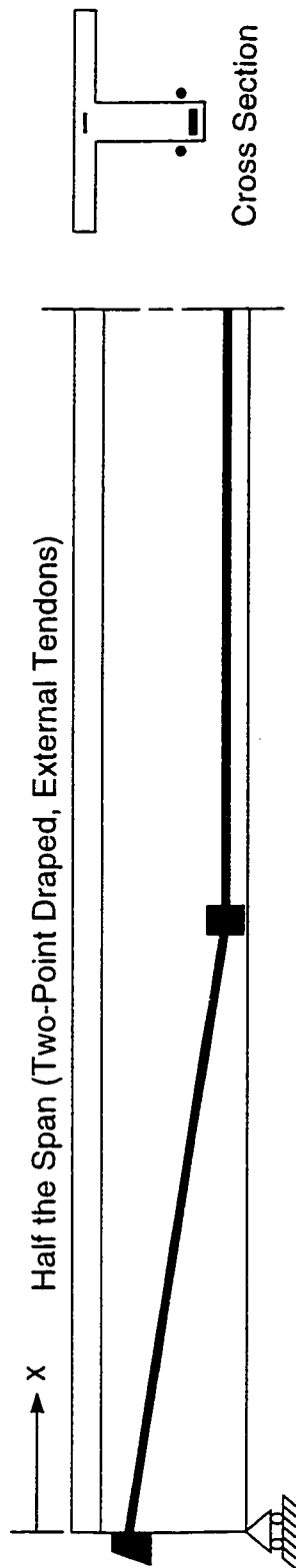


Fig. 6.30 Eccentricity Variation along the Span Due to Time-Dependent Effects

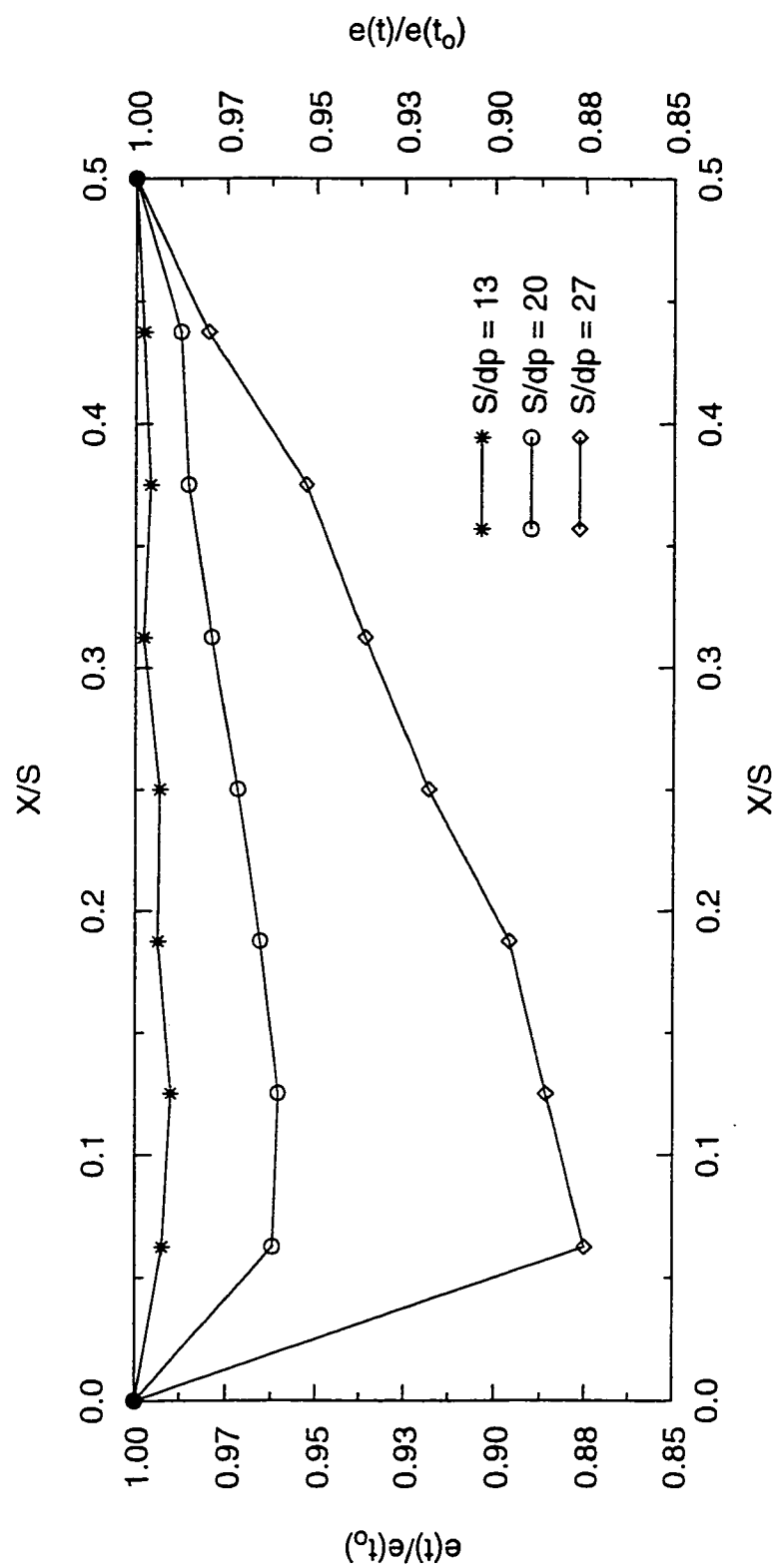
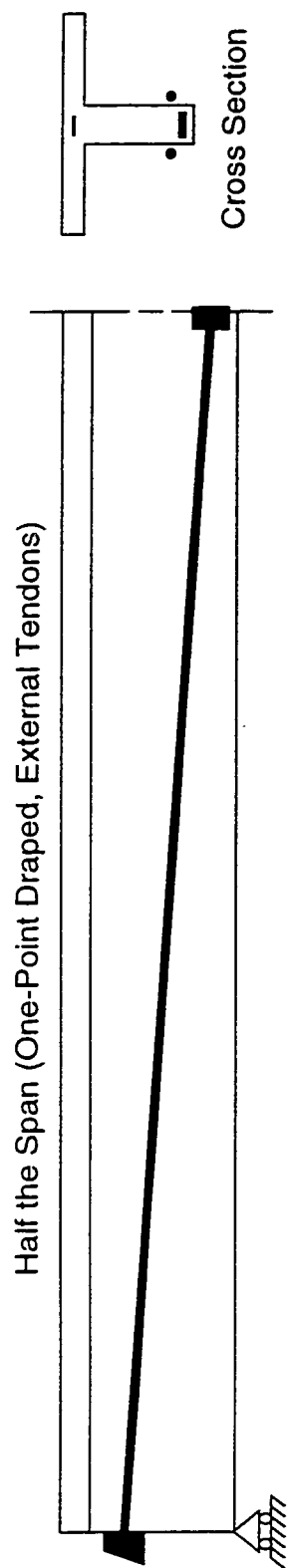


Fig. 6.31 Eccentricity Variation along the Span Due to Time-Dependent Effects

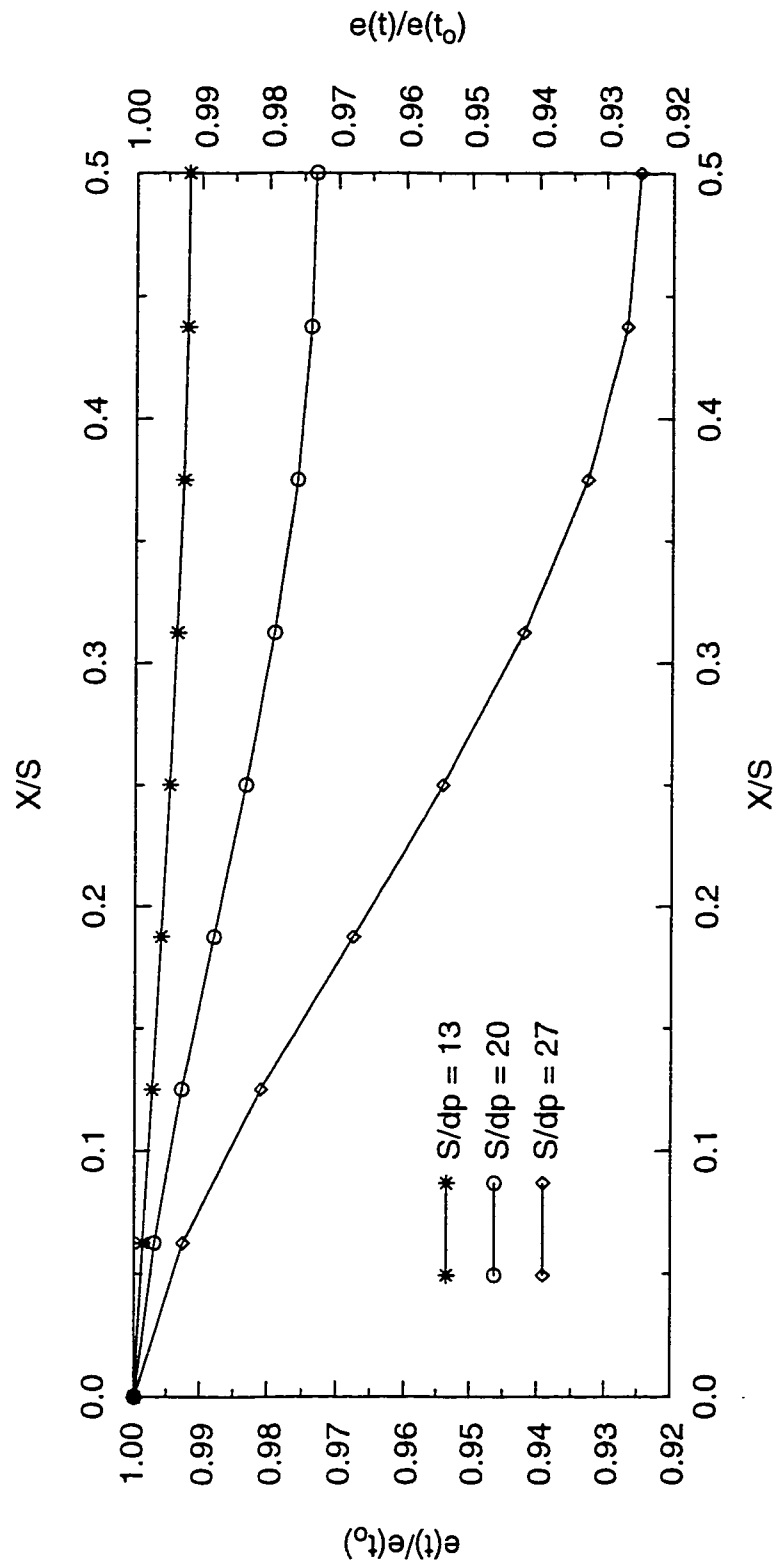
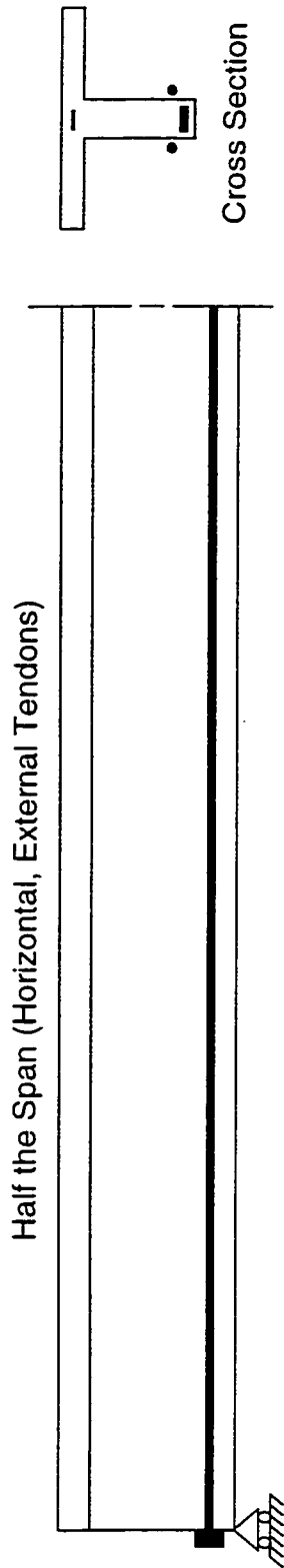


Fig. 6.32 Eccentricity Variation along the Span Due to Time-Dependent Effects

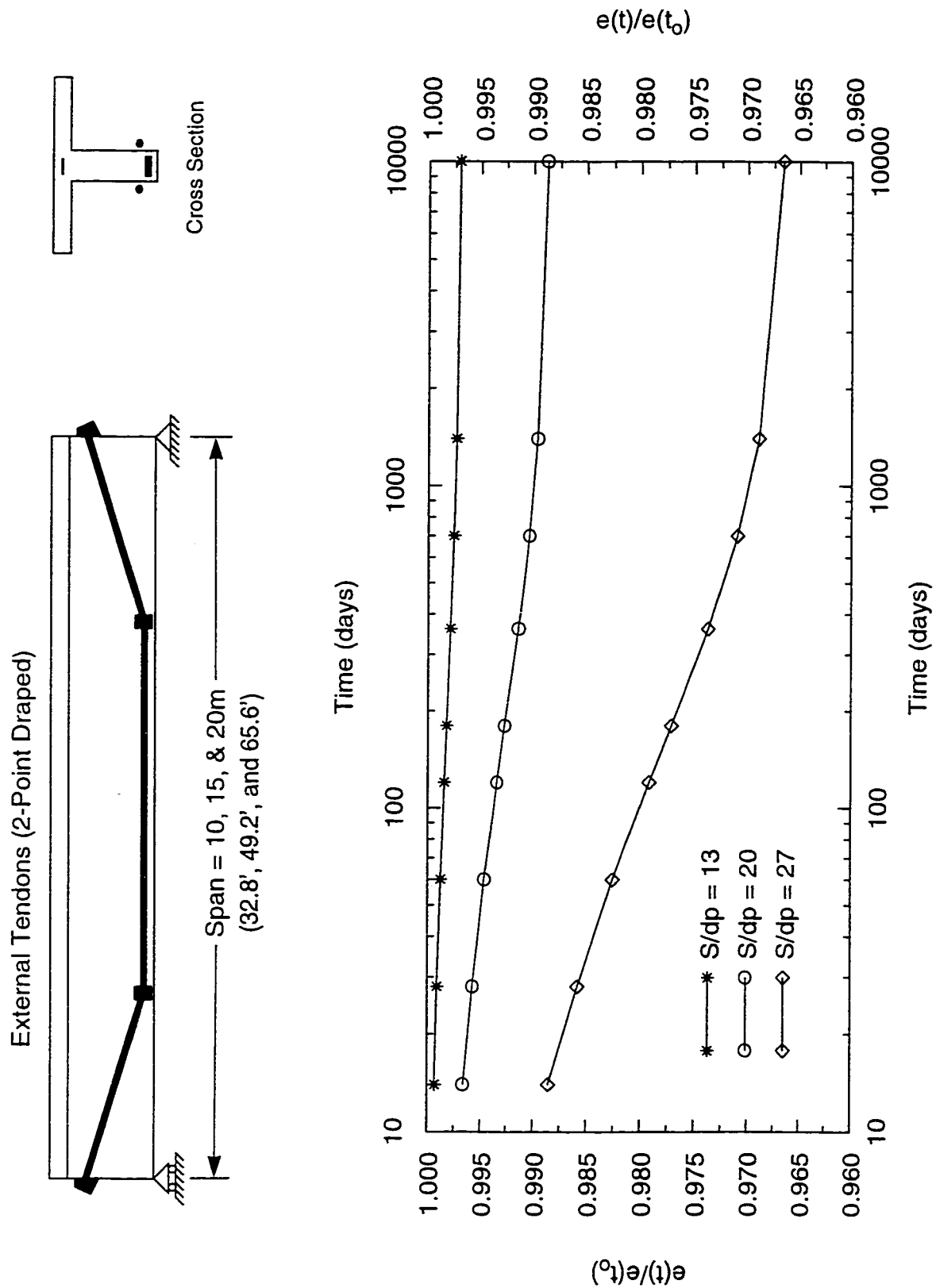


Fig. 6.33 Eccentricity Variation with Time (Time-Dependent Effects)

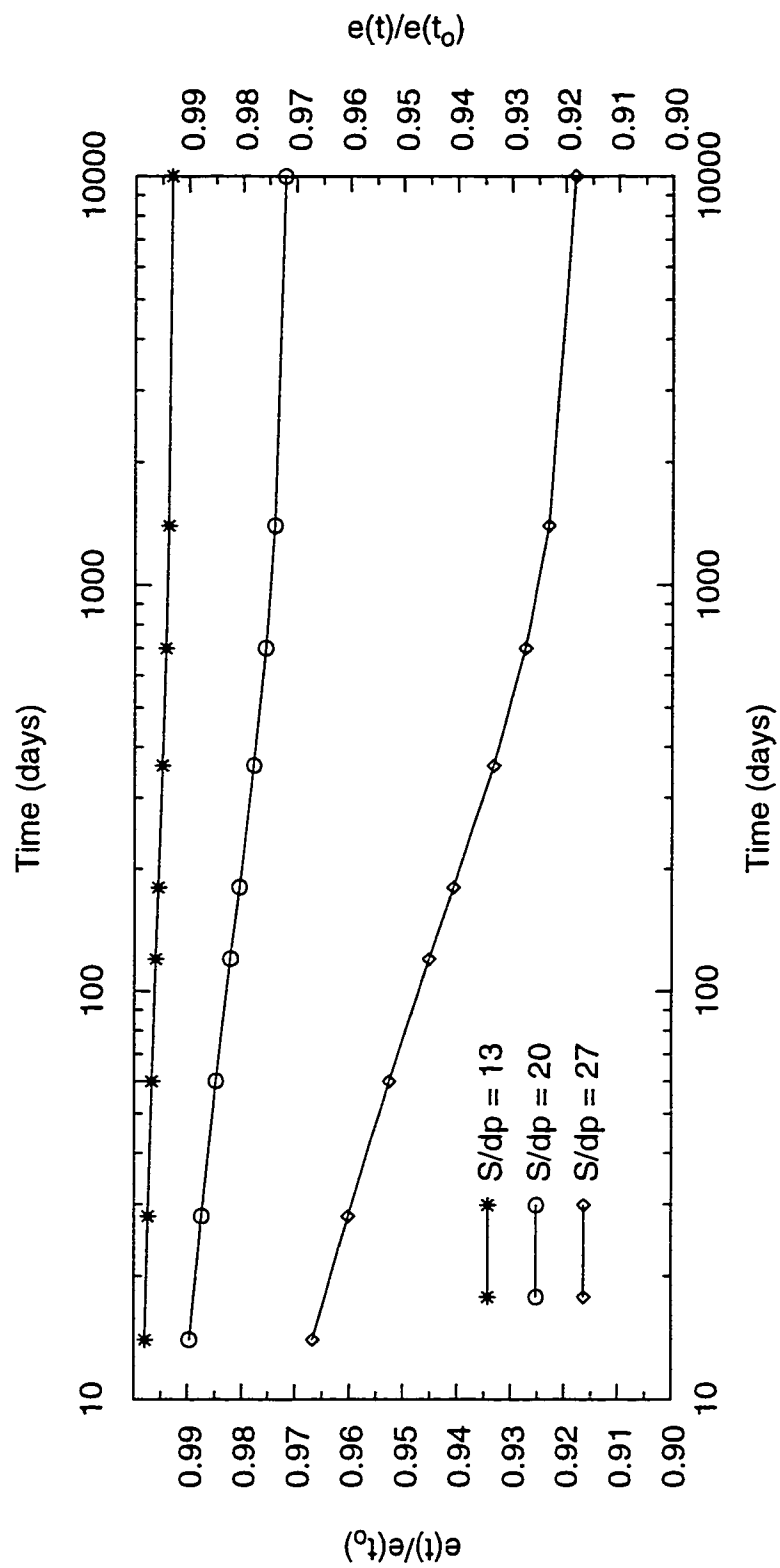
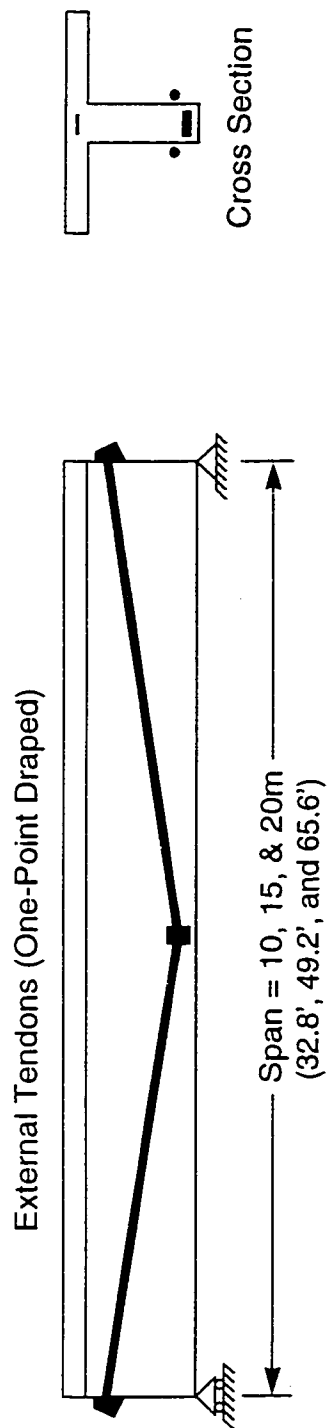


Fig. 6.34 Eccentricity Variation with Time (Time-Dependent Effects)

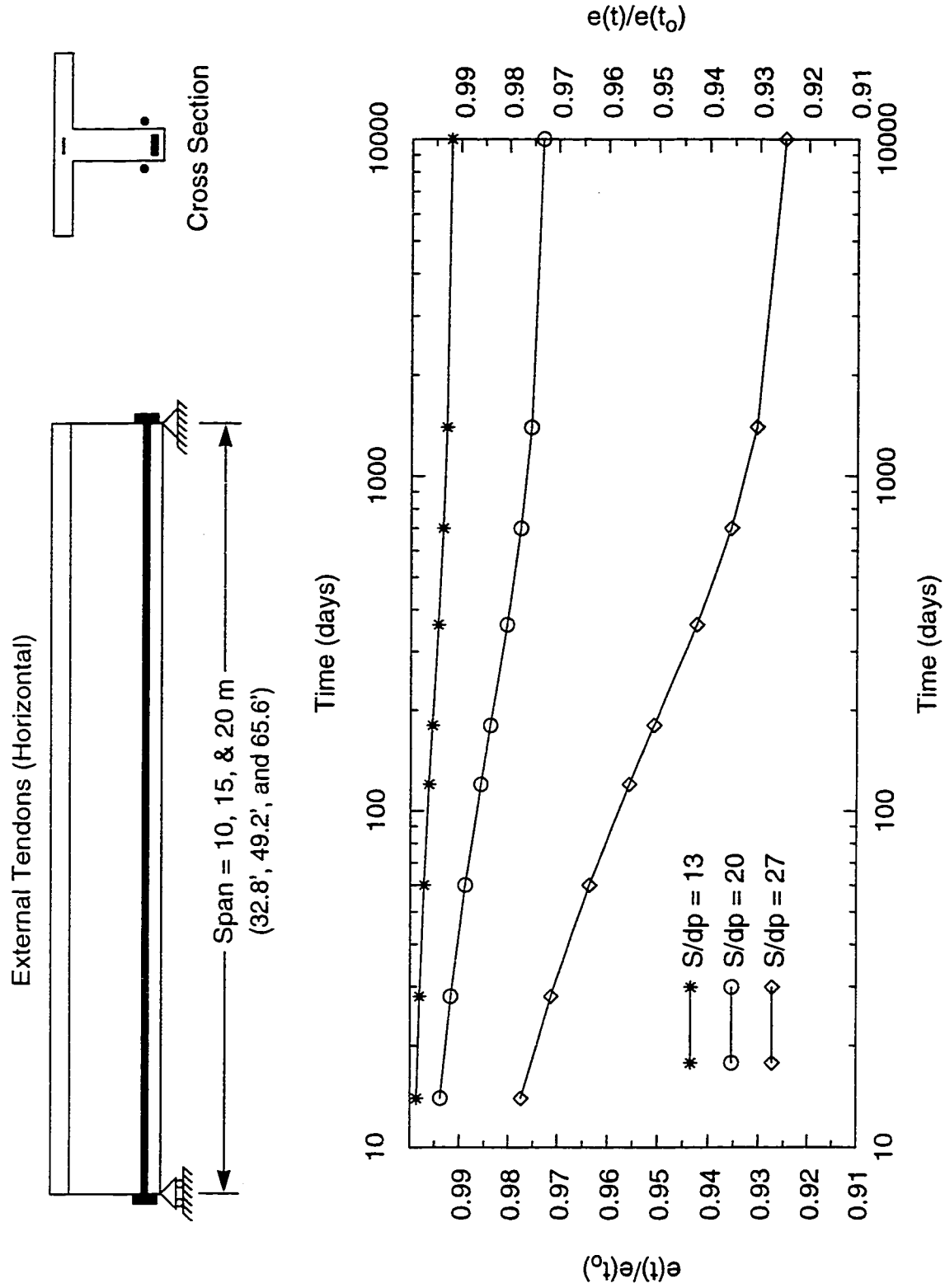


Fig. 6.35 Eccentricity Variation with Time (Time-Dependent Effects)

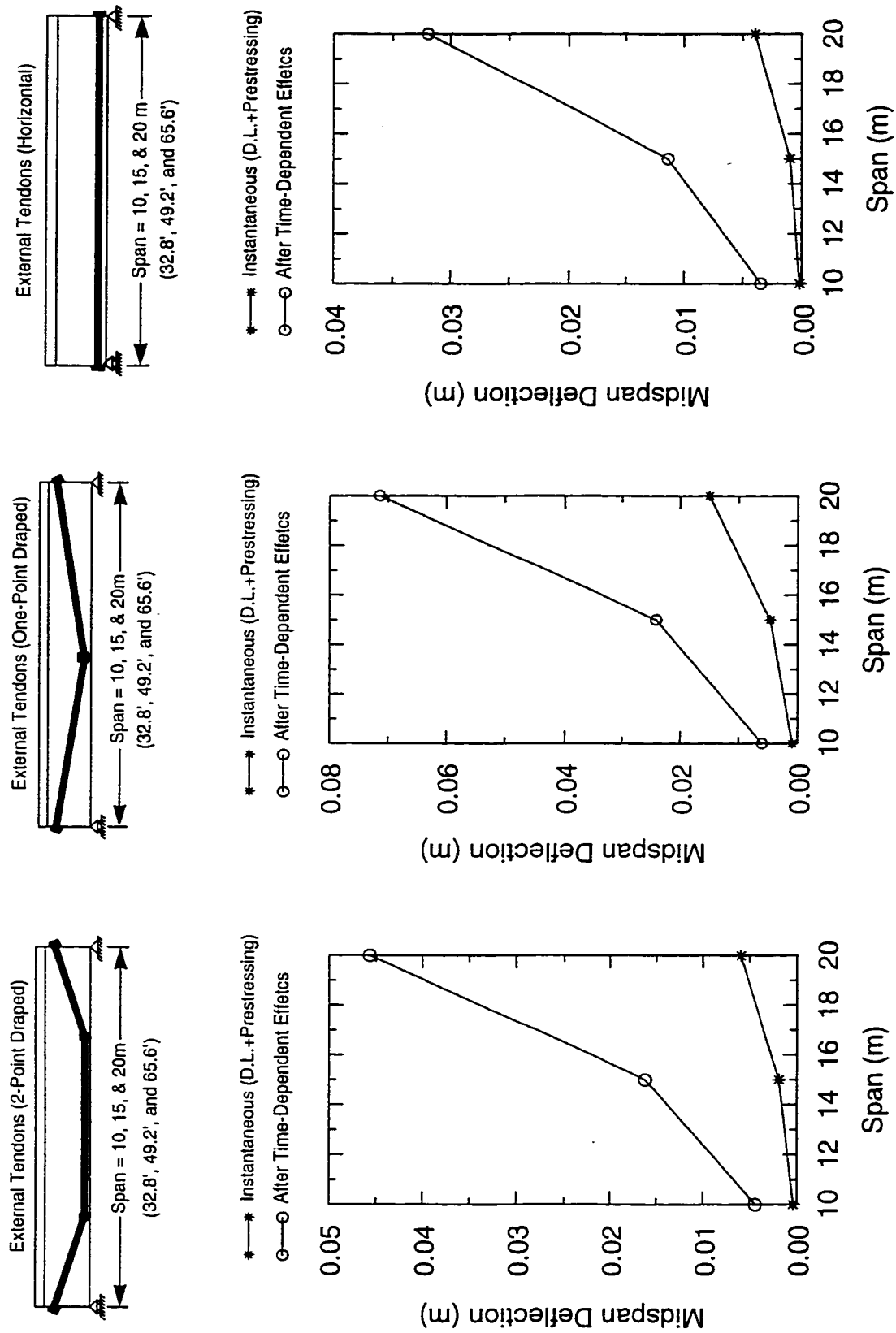


Fig. 6.36 Midspan Instantaneous and Time-Dependent Deflections

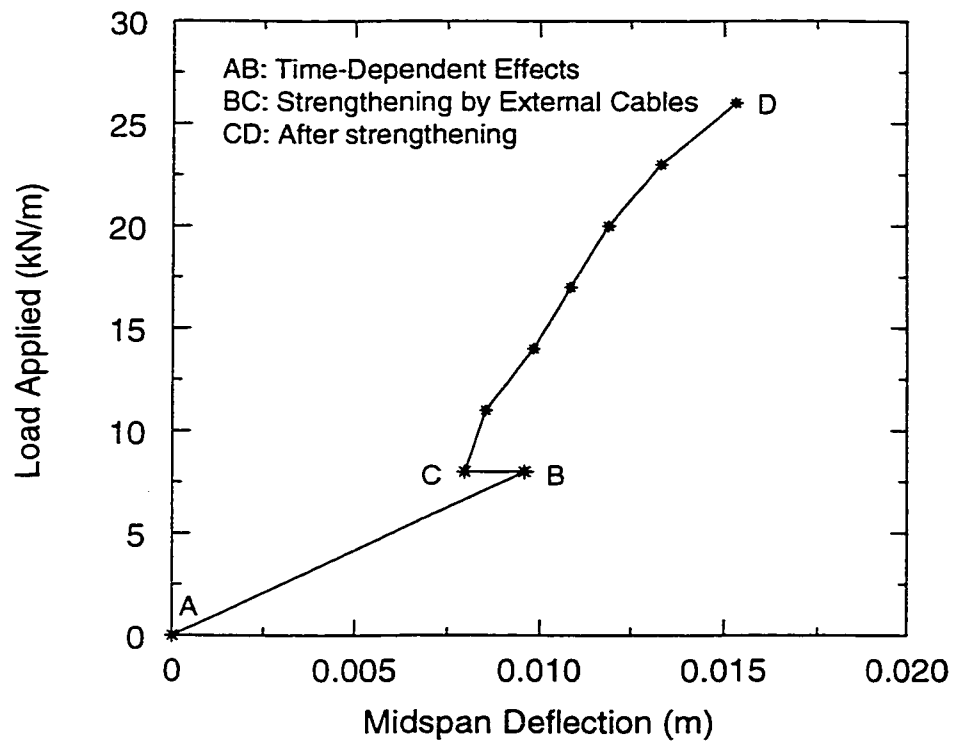


Fig. 6.37 (a) Load versus Deflection for Beam of Span 10m

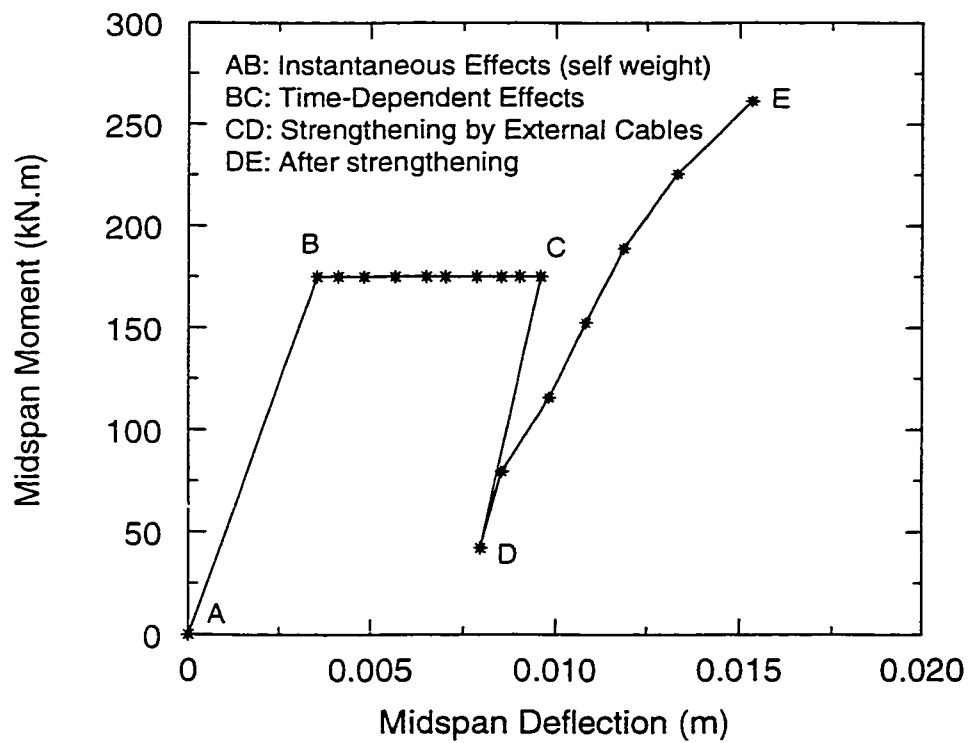


Fig. 6.37 (b) Moment versus Deflection for Beam of Span 10m

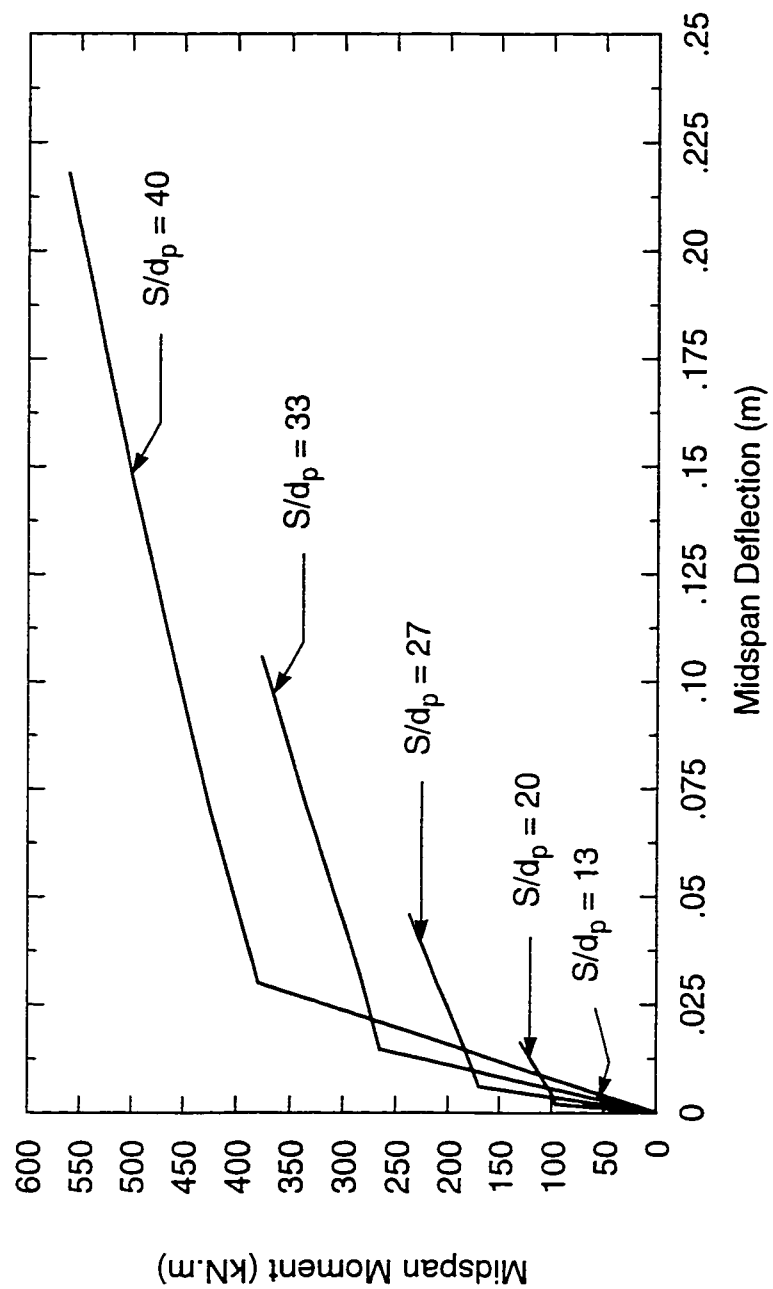
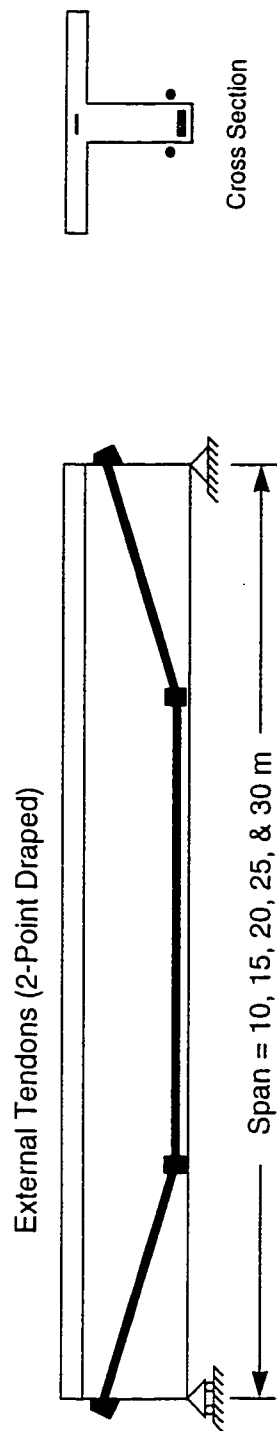


Fig. 6.38 Moment-Deflection of the Beam (due to prestressing, self weight, and time-dependent effects)

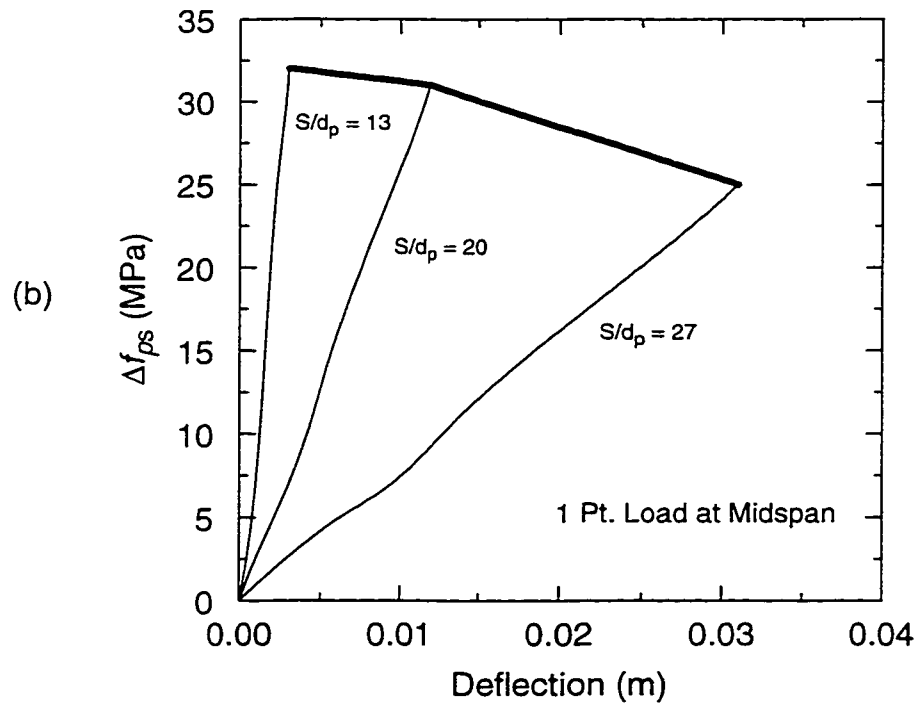
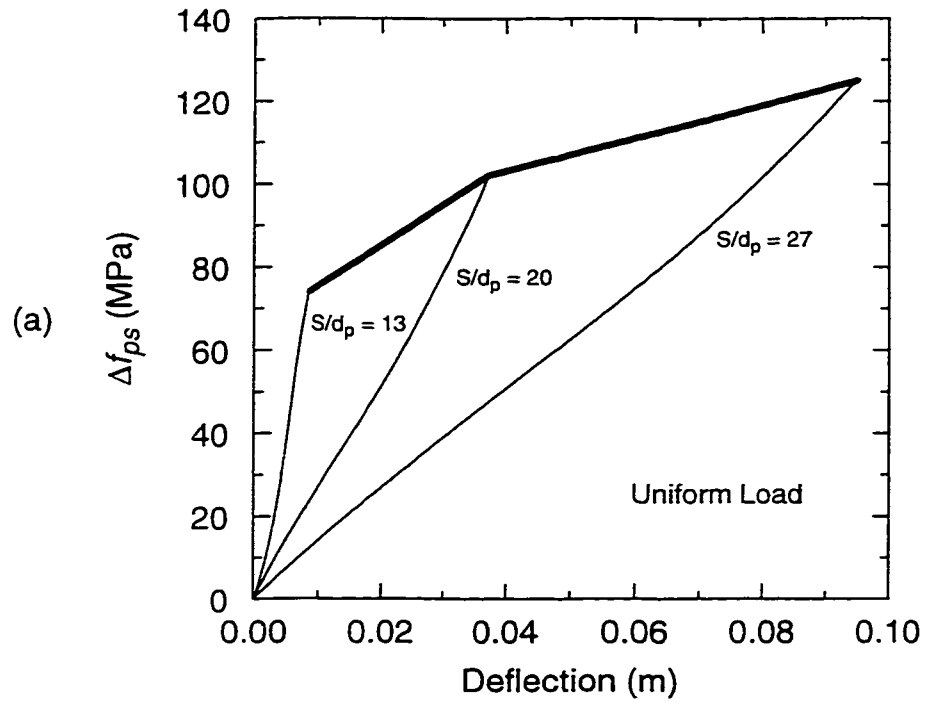


Fig. 6.39 Δf_{ps} vs. Deflection (Various Span-to-Depth Ratios)

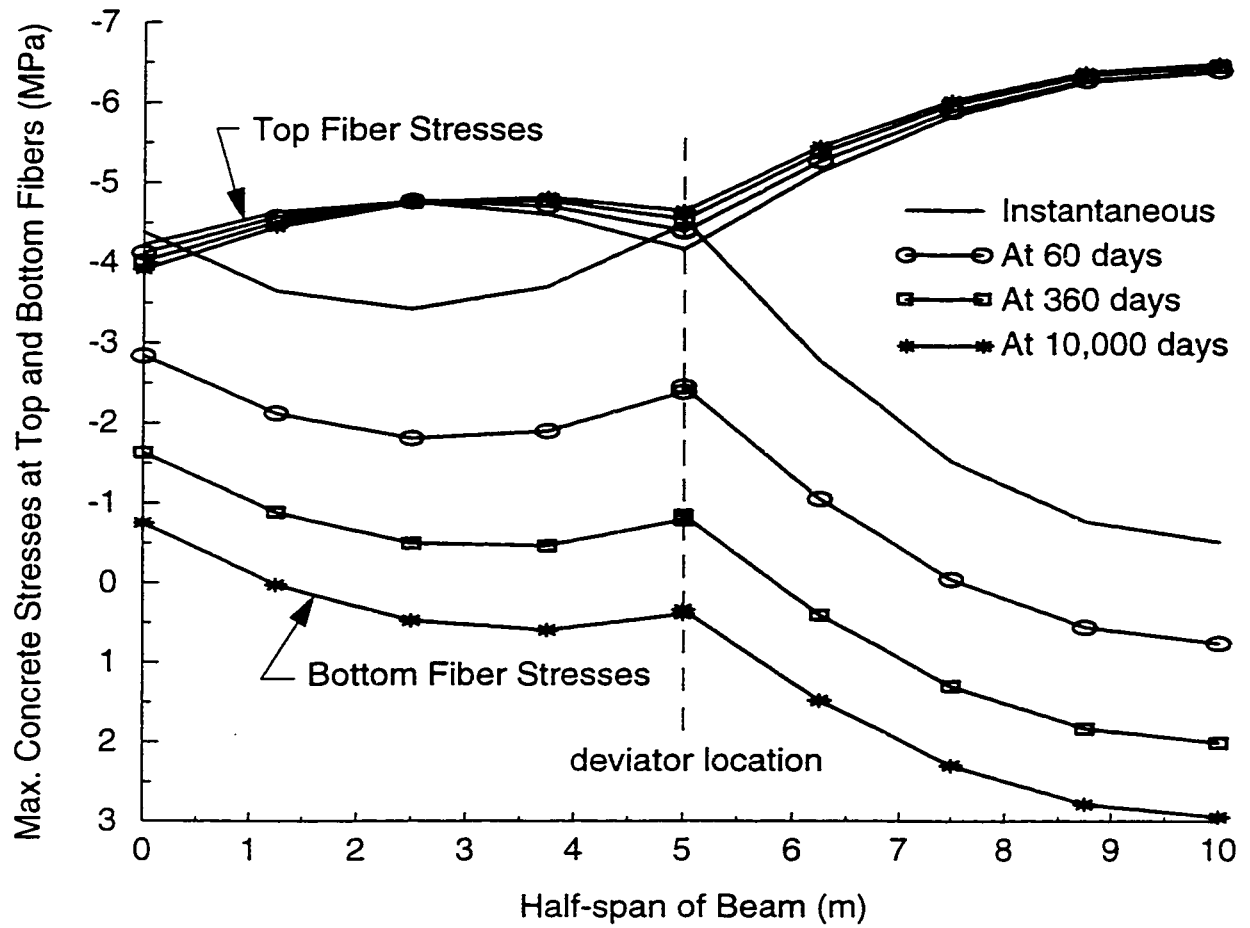


Fig. 6.40 (a) Distribution of Top and Bottom Stresses in Concrete along the Span

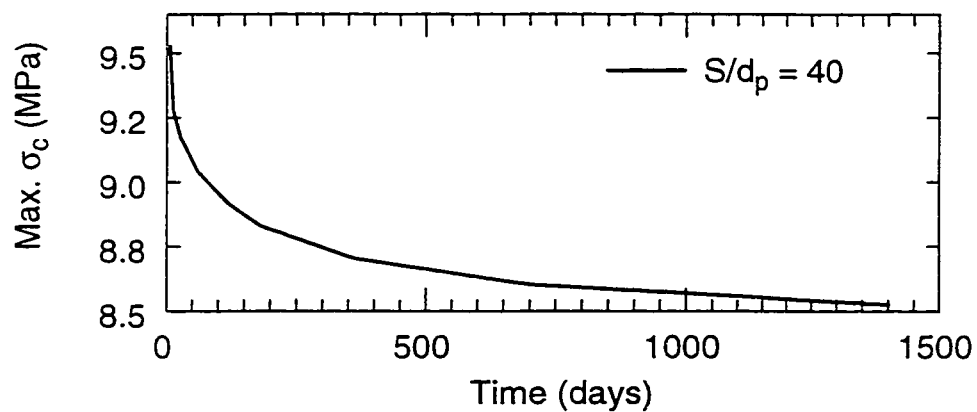


Fig. 6.40 (b) Variation of Maximum Compressive Stress in Concrete with Time

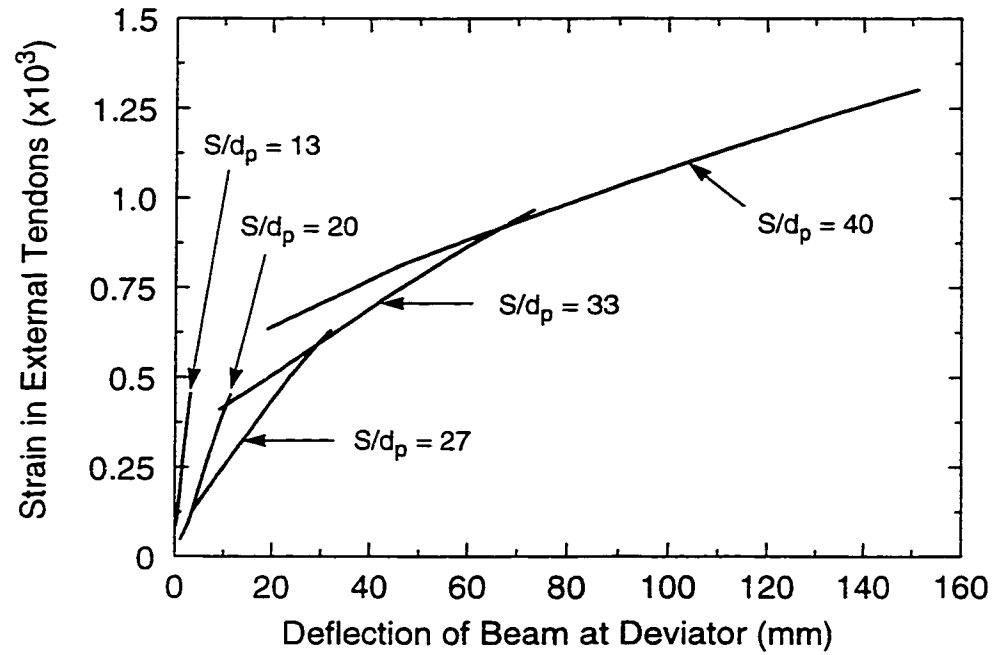


Fig. 6.41 Strain-Deflection Relation at Deviator (due to time-dependent effects)

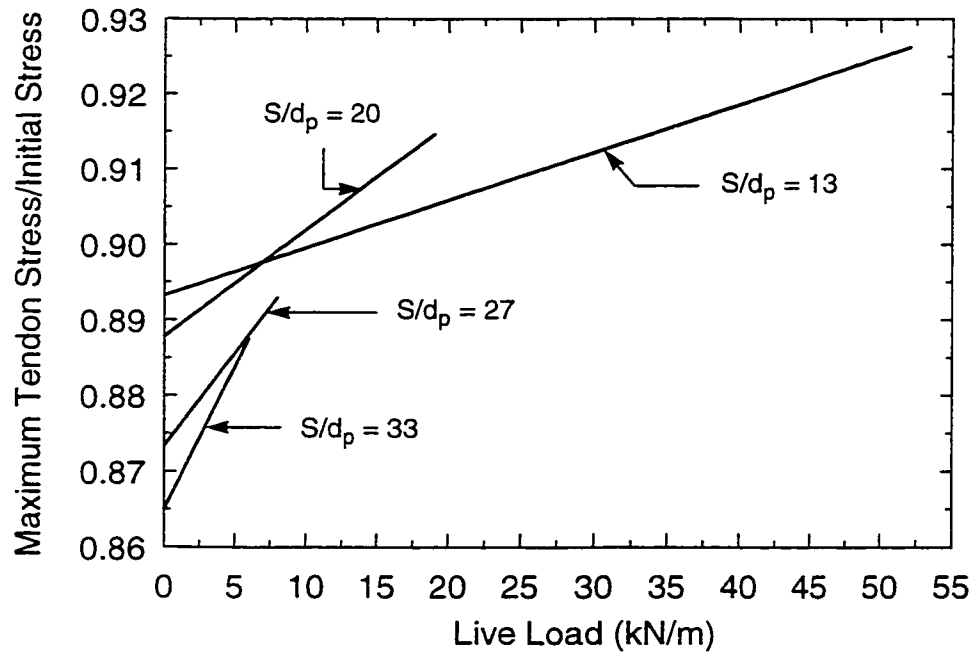


Fig. 6.42 Stress in External Tendons due to Live Loads

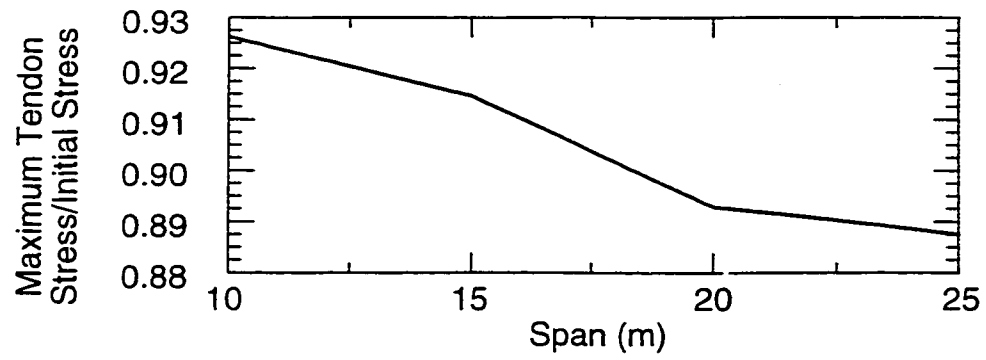


Fig. 6.43 Variations of the Stress in External Tendons With Different Spans

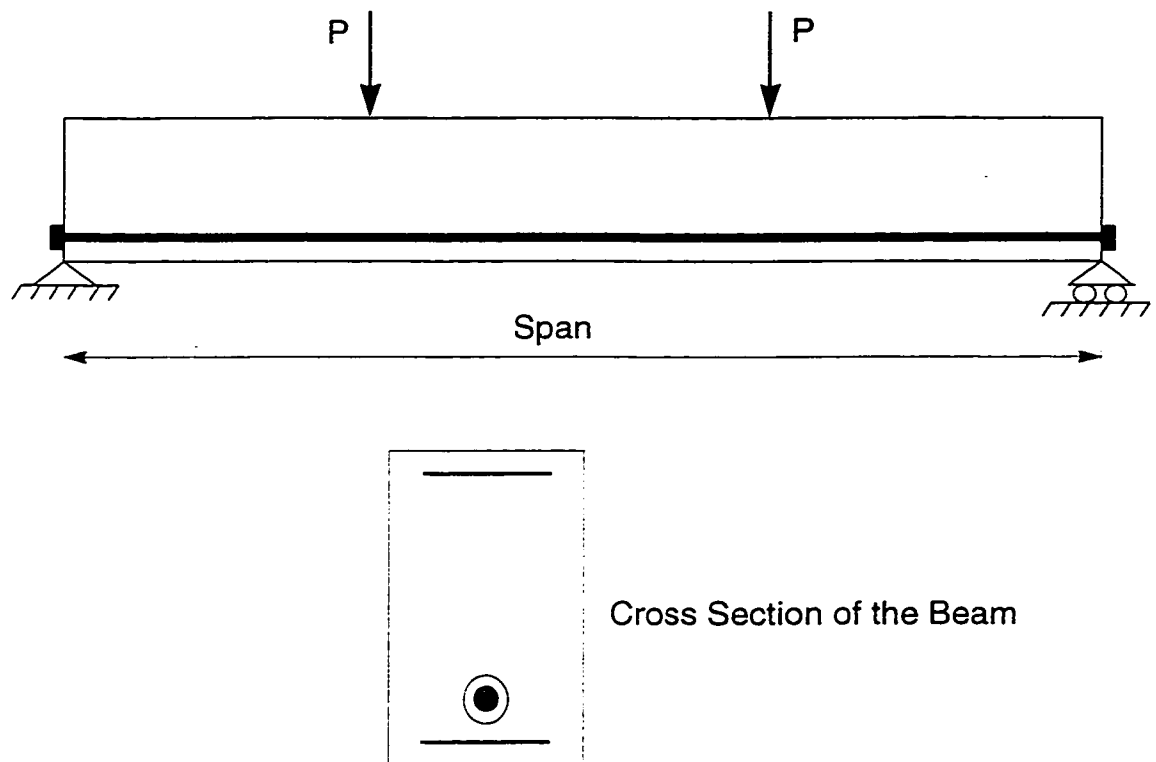


Fig. 6.44 Simple Beam Prestressed with internal unbonded Tendons
(Tested by Harajli Experimentally)

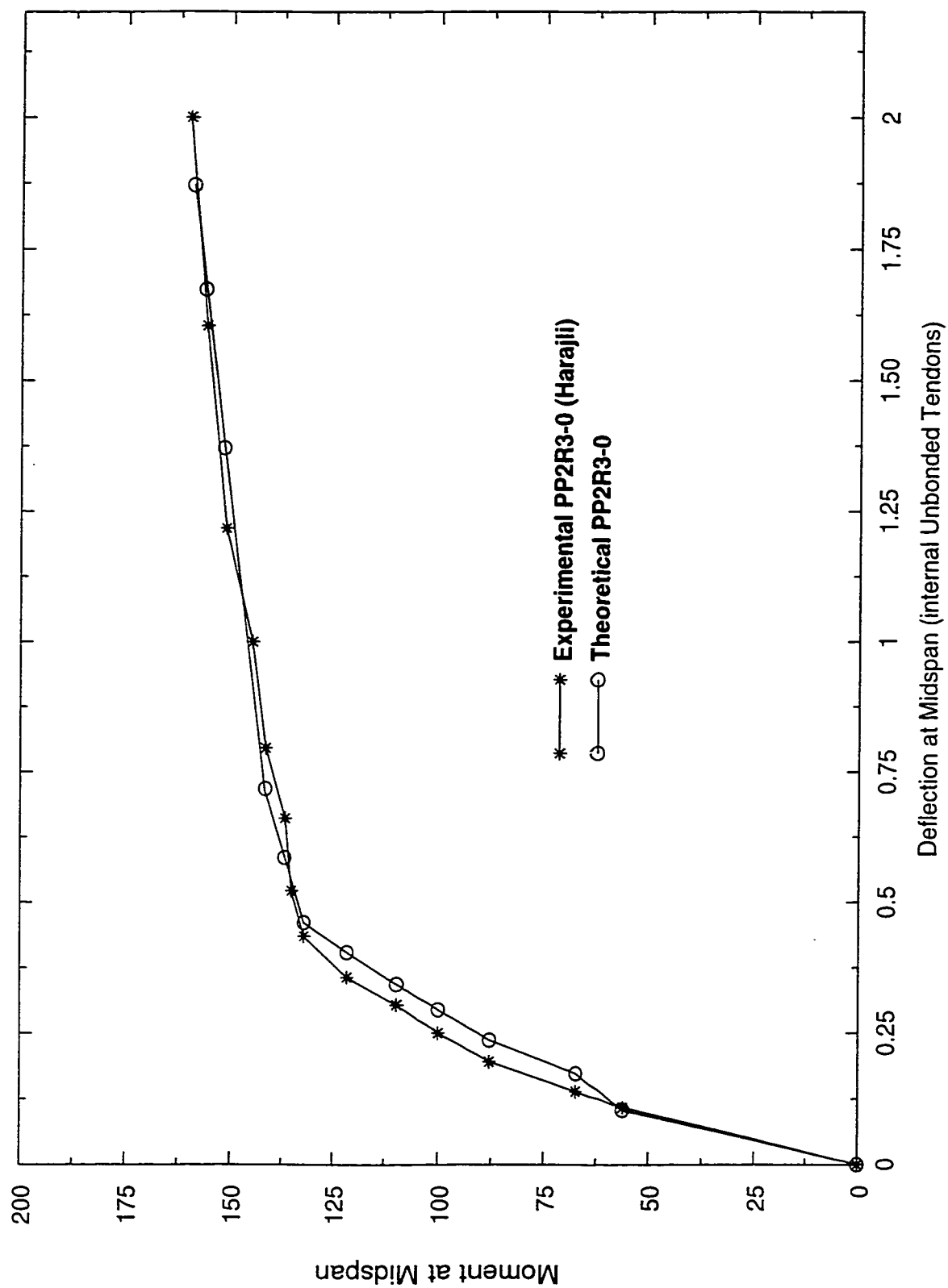


Fig. 6.45 Comparison Between the Current Study and Experimental Work By Harajli

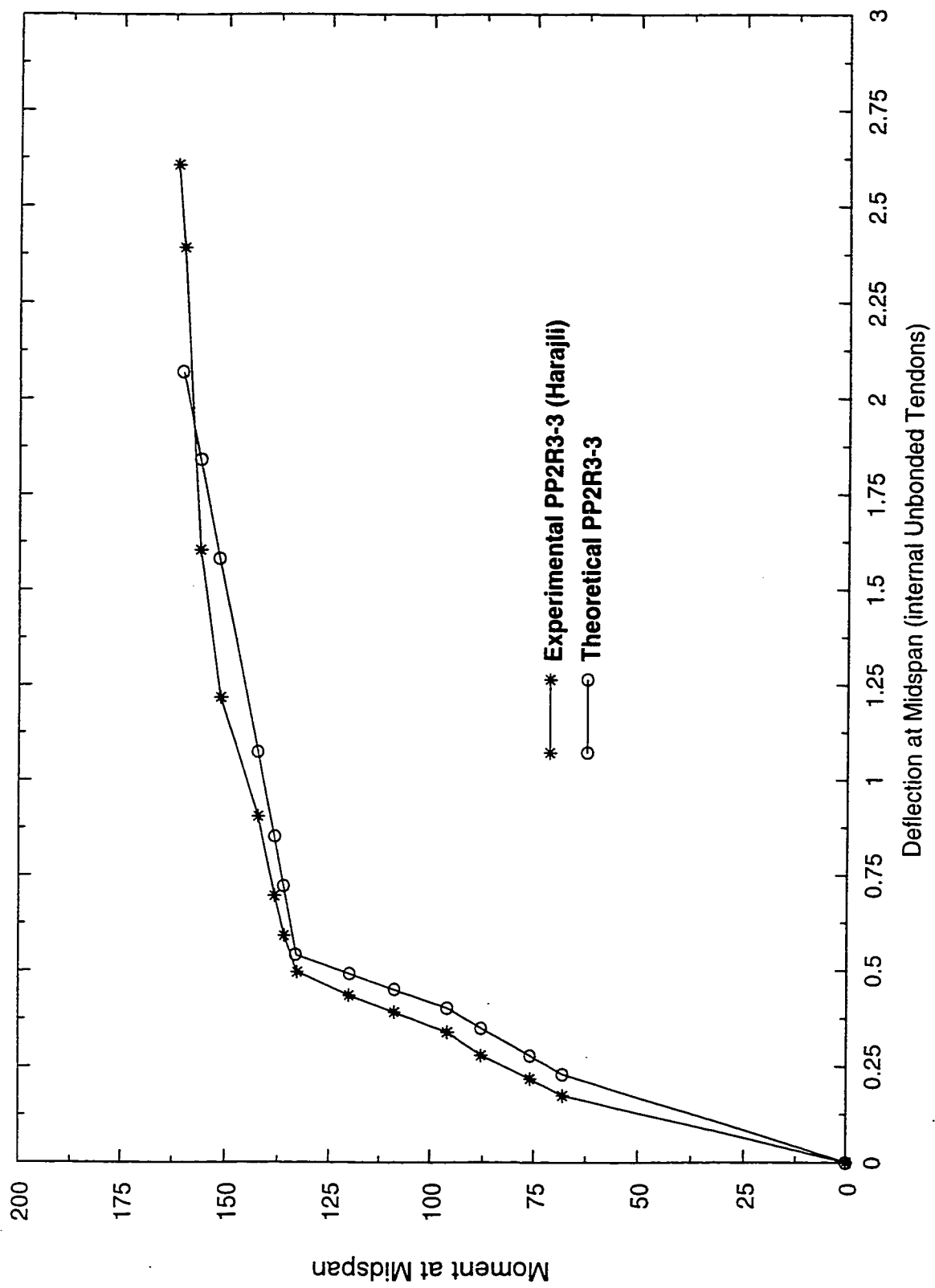


Fig. 6.46 Comparison Between the Current Study and Experimental Work By Harajli

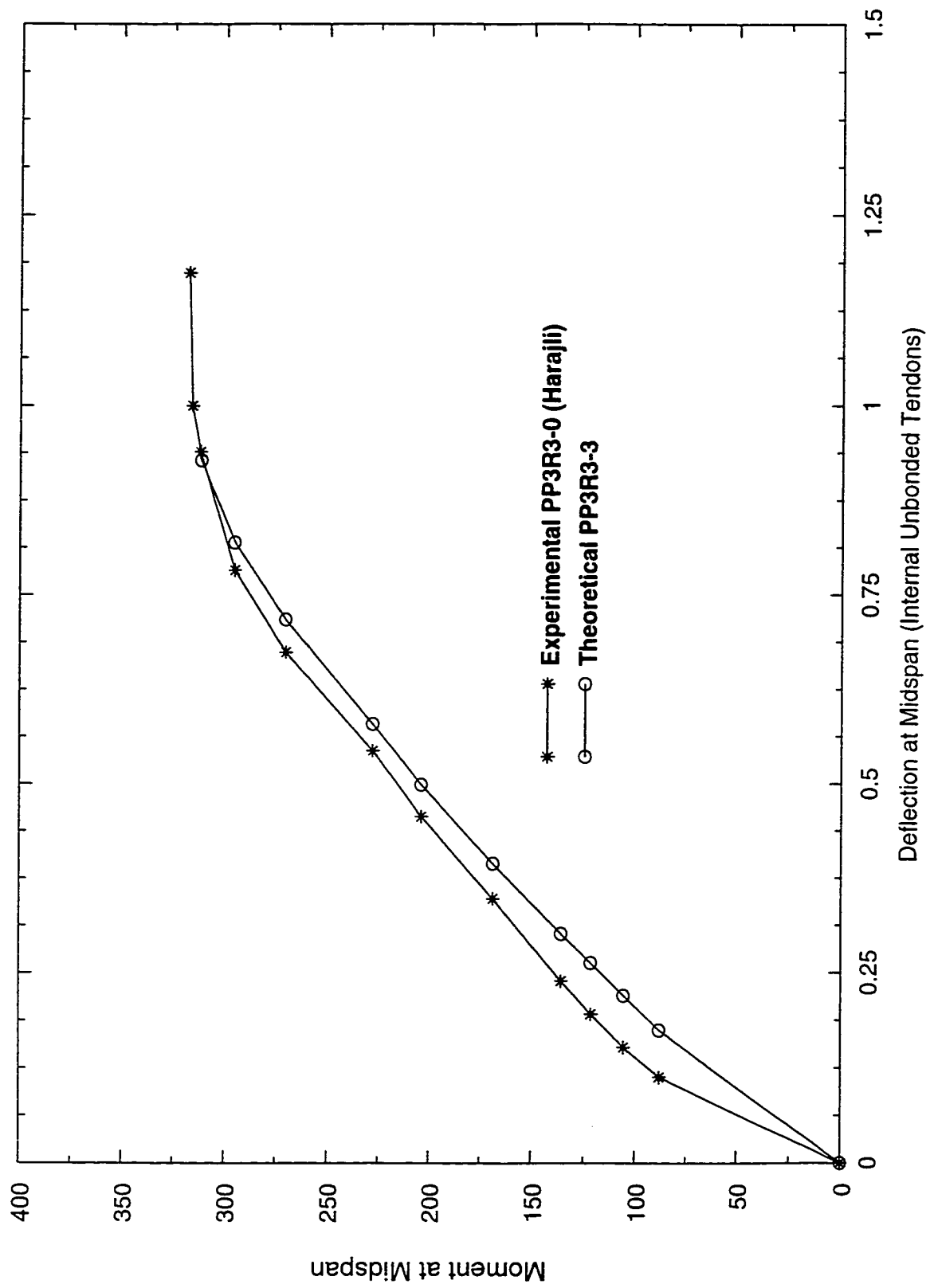


Fig. 6.47 Comparison Between the Current Study and Experimental Work By Harajli

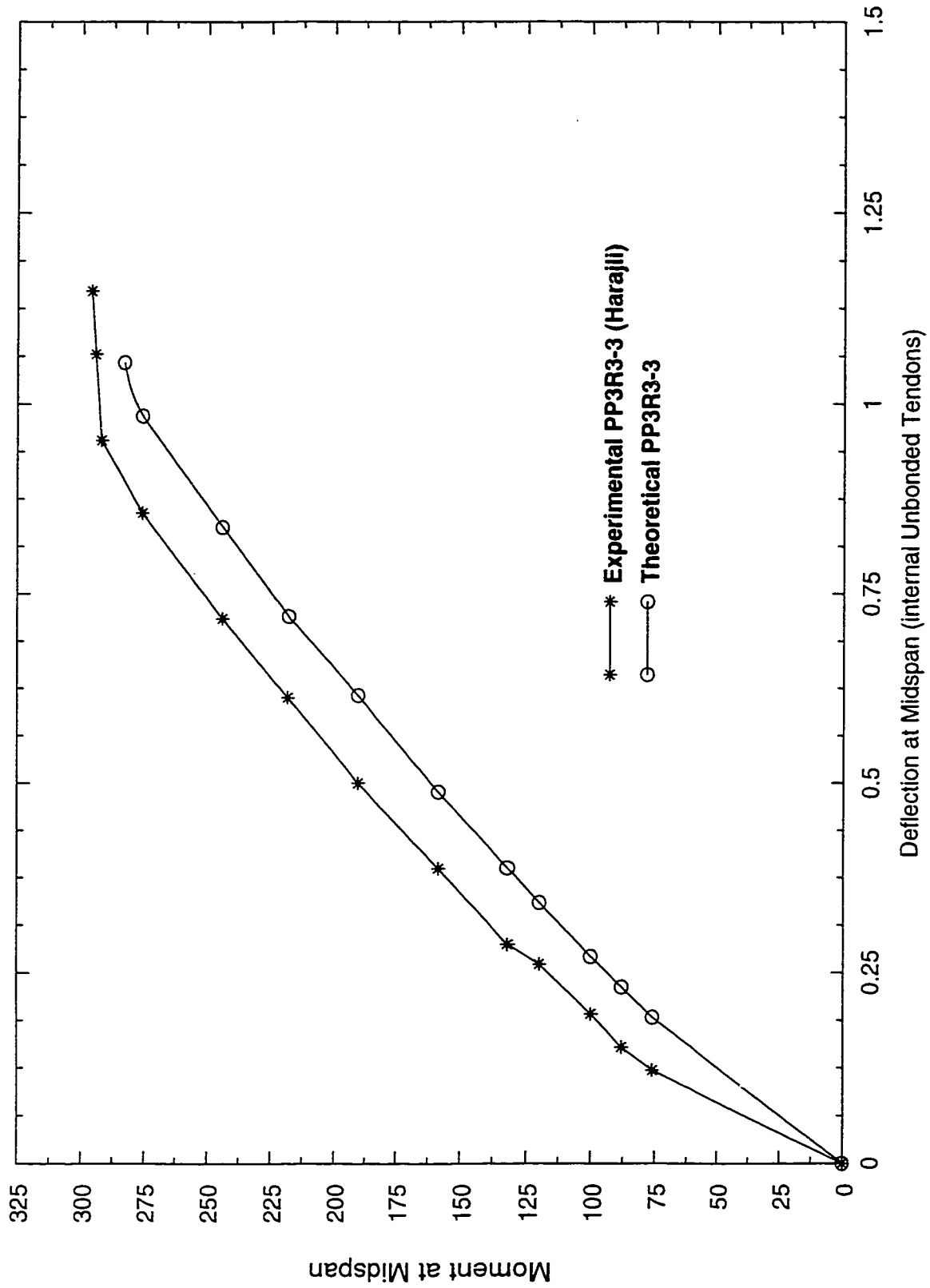


Fig. 6.48 Comparison Between the Current Study and Experimental Work By Harajli

CHAPTER SEVEN

SUMMARY AND CONCLUSIONS

7.1 Summary

An efficient numerical procedure for the material nonlinear analysis of planar reinforced and externally and/or internally prestressed concrete frames including the time-dependent effects due to creep and shrinkage of concrete and relaxation of the tendons has been presented. The method is capable of predicting the displacements, internal forces, stresses and strains of these structures throughout their service load history, as well as throughout elastic, inelastic, and ultimate load ranges.

The stress-strain relationship of concrete has long been recognized as being nonlinear. In accounting for this nonlinearity, concrete, reinforcing steel, and the prestressing steel are assumed in this study to be in states of uniaxial stress. Their strain states are traced throughout the analysis. For concrete, the material is modeled as a parabola and a linear descending part in the compression and a linear relation in the tension. For the reinforcing and prestressing steel, the relation is bilinear and multilinear, respectively.

The time-dependent effects of creep and shrinkage become significant parts of the long term behaviour of reinforced concrete beams. Nonlinear analyses of reinforced concrete structures in which these strains are not included, will give incorrect distribution of stresses.

In the time-dependent analysis, the time domain is divided into a number of time intervals. For each time interval, nonlinear equilibrium equations are set up and solved by

the stiffness method. Iterative technique is used for the solution of the nonlinear equilibrium equations. At any instant t_i , the instantaneous changes in stresses and deformations are calculated and added to the existing values. Also for any time interval, i , the time-dependent change in stresses and deformations taking place between t_i and t_{i+1} are determined and added to update the existing values. In this study, creep and shrinkage of concrete and steel relaxation are included and recognized in every time interval.

In order to account for the varied material properties within a reinforced concrete element, the element is divided into a discrete number of concrete parts and steel layers of different properties.

Finally, a series of numerical examples are analyzed by the current study to investigate the validity of the present procedure. The results are compared with experimental data and other theoretical results.

7.2 Feature of The Current Study

This study addresses and combines into a single package various issues involving the use of unbonded tendons in flexural members. To the best of the author's knowledge, none of the studies to date dealt with these issues in a simultaneous manner. These issues include: 1) the time-dependent effects of creep and shrinkage of the concrete and relaxation of the prestressing steel on the flexural behaviour of beams prestressed with bonded and/or unbonded internal and /or external tendons from zero load up to failure, 2) the difference in flexural behaviour between beams prestressed with bonded/unbonded internal versus external tendons and the time-dependent effects on the loss of eccentricity associated with the use of external tendons, 3) the calculation of the instantaneous and time-dependent

deflections at any section from the real strains and curvatures at the various sections throughout the span of the beam, 3) the effect of varying of the tendon profile geometry and the effects of the span-to-depth ratios on the flexural behaviour of beams, and 4) the instantaneous and time-dependent analysis of beams with different concrete types and different steel types subjected to various loading types.

7.3 Conclusions

The following conclusions can be drawn from the studies performed in the current analytical work:

- 1) For beams with low span-to-depth ratios (from 13 to 20) and subject to instantaneous (self weight and prestressing) and time-dependent effects, the deflection of a beam with internal tendons is almost similar to that of beam with external tendons and having the same profile. This is because beams with low span-to-depth ratios are characterized as being very stiff, thus produce very small vertical deflections. Therefore, beams with external tendons and having low-span-to-depth ratios can be analyzed the same way as beams prestressed with internal bonded tendons.
- 2) Time-dependent effects have proven to decrease the eccentricity between the external tendons and the beam. The ratio of the eccentricity after time-dependent effects to the corresponding eccentricity at the initial loading for the same section, $e_{(t)}/e_{(t_0)}$ is equal to unity over the support and at the deviators. At all other locations the eccentricities considering the time-dependent effects become smaller than the initial eccentricities, Figs. 6.30-6.35. This will lead to large deflections and deformations and therefore lead to a reduced stiffness of the member.

- 3) The time-dependent effects have yielded deflections about five times those of the instantaneous effects regardless of the external tendon profile geometry and regardless of the span-to-depth ratios, Fig. 6.36. Therefore, the aim of the external prestressing, which is generally to reduce the stresses in the reinforced concrete and hence to allow the structure to support additional live load, may be weakened if time-dependent effects are not considered.
- 4) Beams with high span-to-depth ratios exhibit large deflections associated with relatively small increase in the bending moments. This is due to a reduction in the flexural stiffness which is a result of a reduced prestressing force and continuous change in eccentricity between the external cables and the beam at the section of maximum bending moment. Therefore, members with high span-to-depth ratios may reach high and unacceptable deflections due to the time-dependent effects only and well before the application of live loads.
- 5) The rate of the stress increase, Δf_{ps} , in the external tendons decreases with increasing the span-to-depth ratio, Figs. 6.39 (a) and (b). This is due to the loss in prestressing resulting from large deflections due to time-dependent effects and the eccentricity variations of the cables.
- 6) The relation of the compressive stress at concrete top fiber versus time is nonlinear during a period exceeding 4 years, Fig. 6.40 (b), despite the fact that the stress distribution at initial loading is linear. This can be attributed to the nonlinear creep effects resulted from the sustained compressive stress on concrete which in turn affects the time-dependent behaviour of the beam.
- 7) For the same span-to-depth ratio, external tendons with horizontal profile have

proven to yield beams with instantaneous and long-term deflections smaller than those of beams with one point or two-point draped tendon profiles. This is because beams with horizontal external tendons have constant eccentricity throughout their spans whereas beams with draped external tendon profiles have decreasing eccentricity between the deviator and the anchorage zones, see Figs. 6.19-6.27. Therefore, the instantaneous (self-weight and prestressing) and time-dependent effects are more significant in beams with draped external tendon profiles than those with horizontal tendon profiles. But when live load is applied, beams with horizontal tendons exhibit more deflections (at midspan section) than those of beams with one or two-point draped tendons. This can be attributed to the section of maximum moment of the beam with horizontal tendon profile losing eccentricity at a faster rate under live load, Figs. 6.19-6.27. This will yield higher deflections.

- 8) The load-deflection response may be improved after strengthening, Fig. 6.37 (a). This was caused by an increase in the stiffness of the concrete member, expressed as the slope of the load-deflection response, after strengthening and loading. This increase in the load-deflection slope has slowed down the rate of the deflection resulting in an improved flexural behaviour of the member. Therefore, external prestressing improves the flexural resistance of the concrete members.

7.4 Recommendations for future study

The following possible avenues can be pursued as an extension of the current analytical investigation:

- 1) In Chapter 5, a methodology was presented to model the effects of shear deformations

on the behaviour of homogeneous noncracked members. This methodology combines the effects of shear, axial force, and flexure and provides an accurate modeling of the strain and curvature for elastic analysis. An analytical investigation can be carried out using this methodology to accommodate nonlinear analysis of nonhomogeneous cracked members and therefore to study the effects of shear deformations on the behaviour of prestressed concrete members. In these members, the dowel action contributed by internal strands and normal steel and the aggregate interlock can be studied analytically.

- 2) Slippage of the external tendons at deviator locations can be examined closely with special attention given to the frictional losses at these locations.
- 3) This study can be extended to include continuous beams to study the effect of loading one or more spans on the stress in unbonded tendons. Harajli and Kanj (1990) concluded that the ratio of loaded spans to the total number of spans between the anchorage ends is more important than the factor of span-to-depth ratio.
- 4) Analysis of segmentally erected prestressed concrete elements with joints can be explored. Limited work has been done addressing this issue, El-Habr (1988) and MacGregor et al. (1989).
- 5) The use of fiber reinforced concrete can be examined and compared to concrete beams with normal reinforcement. The ductility of beams prestressed with fiber reinforced plastic (FRP) tendons can also be studied and compared to that of beams prestressed with conventional steel tendons.
- 6) Geometric nonlinearity, $P-\Delta$ effects, resulting from large deflections can be examined to study its effect on the flexural behaviour of externally prestressed reinforced

concrete members. Iterative analysis has to be performed to account for geometric nonlinearity since the deformed geometry of the member is not known in advance.

- 7) Experimental work on the subject including all or some of the parameters mentioned above will be helpful and complementary to the analytical work.

REFERENCES

Aas-Jackobsen, K., "Design of Slender Reinforced Concrete Frames," Bericht Nr. 48, Institu Für Baustatik, Eth, Zürich, 1973.

Abdel Karim, A.M., "Analysis and Design of Precast/Prestressed Concrete Sliced-Girder Bridges," Ph.D. Dissertation, University of Nebraska at Lincoln, Nebraska, November, 1991.

ACI Committee 343, "Analysis and Design of Reinforced Concrete Bridge Structures," *ACI Report 343-77*, American Concrete Institute, Detroit, 1977.

ACI Committee 318, "Building Code Requirements for Reinforced Concrete (ACI 318-83)," American Concrete Institute, Detroit, Michigan, 1983.

ACI Committee 209, "Prediction of Creep, Shrinkage, and Temperature effects in Concrete Structures," *Designing for Creep and Shrinkage in Concrete Structures*, Special Publication, No. SP-76, American Concrete Institute, Detroit, 1990.

ACI Committee 209, "Prediction of Creep, Shrinkage, and Temperature effects in Concrete Structures," American Concrete Institute, Detroit, 1990.

Aldstedt, E., "Nonlinear Analysis of Reinforced Concrete Frames," Division of Structural Mechanics Institute of Technology, University of Trondheim, Norway, 1975.

Alkhairi, F. M. and Naaman, A. E., "Analysis of Beams Prestressed with Unbonded Internal or External Tendons," *ASCE, Journal of Structural Engineering*, Vol. 119, No. 9, September 1993.

Argyris, J.H., et al., "Recent Developments in the Finite Element Analysis of Prestressed

Concrete Reactor Vessels," Paper H1/1, 2nd International Conference on Structural Mechanics in Reactor Technology, Berlin, West Germany, September, 1973.

Aroni, S., "Slender Prestressed Concrete Columns," UC-SESM Report No. 67-10, Division of Structural Mechanics, University of California, Berkeley, 1967.

Bazant, Z.P., "Prediction of Concrete Creep Effects Using Age-Adjusted Effective Modulus Method," Journal of the American Concrete Institute, ACI Proceedings, Vol. 69, No. 4, April 1972.

Bazant, Z.P., and El-Nimeiri, M., "Stiffness Method for Curved Box Girders at Initial Stress," Journal of Structural Division, ASCE Proceedings, Vol. 100, No. ST10, October 1973, pp. 1851-1874.

Bazant, Z.P., and Najjar, L.T., "Comparison of Approximate Linear Methods for Concrete Creep," Journal of the Structural Division, ASCE Proceedings, Vol. 99, No. ST9, September 1973.

Bazant, Z. P. and Oh, B. H., "Deformation of Progressively Cracking Reinforced Concrete Beams," ACI Journal, V. 81, No. 3, May-June 1984, pp. 268-278

Branson, D. E. and Christian, M.L., "Time-Dependent Concrete Properties Related to Design Strength and Elastic Properties, Creep and Shrinkage," Special Publication, No. SP-27, American Concrete Institute, Detroit, pp. 257-267.

Branson, D. E. and Trost, H., "Unified procedures for Predicting the Deflection and Centroidal Axis Location of Partially Cracked Nonprestressed Concrete Members," ACI Journal, Proceedings, V. 79, No. 2, March-April 1982, pp. 119-130.

Brøndum-Nielsen, T., "Ultimate Limit States of Cracked Arbitrary Concrete Sections

Under Axial Load and Biaxial Bending," Concrete International: Design & Construction, V. 4, No. 11, Nov. 1982, pp. 51-55.

Brøndum-Nielsen, T., "Ultimate Flexural Capacity of Partially or Fully Prestressed Cracked Arbitrary Concrete Sections Under Axial Load Combined with Biaxial Bending," Concrete International: Design & Construction, V. 5, No. 1, Jan. 1983, pp. 77-78.

Brøndum-Nielsen, T., "Ultimate Flexural Capacity of Fully Prestressed, Partially Prestressed, and Nonprestressed Arbitrary Concrete Sections under Symmetric Bending," ACI Journal, January-February 1986.

Brown, R.C., Jr., Burns, N.H., and Breen, J.E., (1974), "Computer Analysis of Segmentally Erected Precast Prestressed Box Girder Bridges," Centre of Highway Research, University of Texas at Austin, Austin, Texas.

Burns, N. H., Helwig, T., and Tsujimoto, T., "Effective Prestress Force in Continuous Post-Tensioned Beams with Unbonded Tendons," ACI Structural Journal, January-February 1991.

Campbell, T. I and Kodur, V. K., "Deformation Controlled Nonlinear Analysis Prestressed Concrete Continuous Beams," PCI Journal, September-October 1990.

CEB-FIP, Model Code for Concrete Structures, Comite Euro-International du Beton - Federation International de la Precontrainte, Paris, 348 pp., 1978.

CEB-FIP, Evaluation of Time dependent Behavior of Concrete, Comite Euro-International du Beton, Bulletin d'information No. 199, Paris, Aout 1990.

Chan, E.C., "Nonlinear Geometric, Material, and Time Dependent Analysis of Reinforced and Prestressed Concrete Shells with Edge Beams," UC-SESM Report No. 82-08,

Division of Structural Engineering and Structural Mechanics, University of California, Berkley, California, December 1982.

Chen, J., You, C., Bazant, Z. P., "Deformation of Progressively Cracking Partially Prestressed Concrete Beams," *PCI Journal*, January-February 1992.

Collins, M.P., "Towards a Rational Theory for RC Members in Shear," *Journal of the Structural Division, ASCE*, Vol. 104, pp. 649-666, April 1978.

Collins, M.P. and Mitchell, D., "Shear and Torsion Design of Prestressed and Non-Prestressed Concrete Beams," *Journal of the Prestressed Concrete Institute*, Vol. 25, No. 5, Sept.-Oct. 1980, Discussion and Closure *PCI Journal*, Vol. 26, No. 60, Nov.-Dec. 1981.

Collins, M.P. and Mitchell, D., "Evaluating Existing Bridge Structures Using the Modified Compression Field Theory," American Concrete Institute Publication, "*Strength Evaluation of Existing Concrete Bridges*," PCI SP-88, pp. 109-141, 1985.

Collins, M.P. and Mitchell, D., *Prestressed Concrete Basics*, First Edition, Canadian Prestressed Concrete Institute, 1987.

Connor, J.J, and Sarne, Y., "Nonlinear Analysis of Prestressed Concrete Reactor Pressure Vessels," Paper H2/2, 3rd International Conference on Structural Mechanics in Reactor Technology, London, September 1975.

Davis, R.E., and Davis, H.E., "Flow of Concrete under Sustained Compressive Stress." *Proceedings American Society for testing and Materials*, part II, Vol. 30, pp. 707-730, 1930.

Davis, R.E., and Davis, H.E., and Brown, E.H., "Plastic Flow and Volume Changes in Concrete," *Proceedings American Society for testing and Materials*, part II, Vol. 37, pp.

317-330, 1937.

El-Ariss, B. and El-Badry, M.M., "Serviceability and Strength of Externally Prestressed Concrete Structures," published in the CSCE 1996 Annual Conference, Structural Specialty, May 29-June 01, Edmonton, Alberta, Canada. 1996.

El-Badry, M.M., "Serviceability of Concrete Structures," Ph.D. Dissertation, Department of Civil Engineering, The University of Calgary, Calgary, Alberta, November 1988.

El-Badry, M.M. and Ghali, A., User's Manuel and Computer Program CRACK, Research Report No. CE85-1, Department of Civil Engineering, The University of Calgary, Calgary, Alberta, Canada, January 1985, (Revised February 1986).

El-Badry, M.M. and Ghali, A., User's Manuel and Computer Program CPF: Cracked Plane Frames in Prestressed Concrete, Research Report No. CE85-2, Department of Civil Engineering, The University of Calgary, Calgary, Alberta, Canada, January 1985, (Revised March 1989).

El-Badry, M.M., and Ghali, A., "Serviceability Design of Continuous Prestressed Concrete Structures," Prestressed Concrete Institute, PCI Journal, Vol. 34, No. 1, January-February 1989.

El-Habr, K.C., "Finite Element Analysis of Externally Prestressed Segmental Construction," MS Thesis, University of Texas at Austin, Texas.

England, G.L. and Illiston, J.M., "Method of Computing Stress in Concrete from a History of Measured Strain," Civil Engineering and Public Works Review, London, Vol. 60, pp. 692-694, April 1965.

Faber, O., "Plastic Yield, Shrinkage and Other Problems of Concrete and Their Effects on

Design," Minutes of Proceedings of Institute of Civil Engineers, Vol. 225, Part I, London, 1927.

Franklin, H.A., "Nonlinear Analysis of Reinforced Concrete Frames and Panels," Ph.D. Dissertation, Division of Structural Engineering and Structural Mechanics, University of California, Berkeley, UC-SESM Report No. 70-5, March 1970.

Ghali, A. and Favre, R., "Concrete Structures: Stresses and Deformations," London, New York: Chapman and Hall, 1986 and 1994.

Ghali, A. and Neville, A.M., *Structural Analysis: a Unified classical and Matrix Approach*, 3rd. Edition, London, New York, Chapman and Hall, 1989.

Ghali, A. Sisodiya, R.G., and Tadros, G.S., "Displacements and Losses in Multistage Prestressed Members," Journal of the Structural Division, ASCE, Vol. 100, No. ST11, November 1974.

Ghali, A. and Trevino, J., "Relaxation of Steel in Prestresses Concrete," PCI Journal, V. 30, No. 5, September-October 1985, pp. 82-94.

Gilbert, R.I., and Warne, R.F., "Nonlinear Analysis of reinforced Concrete Slabs with Tension Stiffening," UNICIV Report No. r-167, University of New South Wales, Kensington, N.S.W., Australia, January 1977.

Glanville, W.H., "The creep or Flow of Concrete Under Load," Department of Scientific and Industrial Research, building Research Technical Paper, No. 12, 1930.

Greunen, J.V., "Nonlinear Geometric, Material, and Time Dependent Analysis of Reinforced and Prestressed Concrete Slabs and Panels," UC-SESM Report No. 79-3, Division of Structural Engineering and Structural Mechanics, University of California,

Berkley, California, October 1979.

Guyon, Y., "Prestressed concrete," Edited by W. M. Johns, London, Contractors Record and Municipal Engineering, 543 pp., 1960.

Harajli, M.H., "Effect of Span-Depth Ratio on the Ultimate Steel Stress in Unbonded Prestressed Concrete Members," ACI Structural Journal, Vol. 87, No.3, May-June 1990.

Harajli, M.H., "Effect of Span-Depth Ratio on the Ultimate Steel Stress in Unbonded Prestressed Concrete Members," ACI Structural Journal, May-June 1990.

Harajli, M.H., "Strengthening of Concrete Beams by External Prestressing," PCI Journal, Vol. 38, No. 6, November-December 1993.

Harajli, M.H. and Hijazi, S.A., "Evaluation of the Ultimate Steel Stress in Partially Prestressed Concrete Members," PCI Journal, January-February 1991.

Harajli, M.H. and Kanj, M.Y., "Experimental Study of the Behaviour of Unbonded Partially Prestressed Beams in Flexure," Report Published in 1990, The American University of Beirut, Beirut, Lebanon, 1990.

Harajli, M.H. and Kanj, M.Y., "Ultimate Flexural Strength of Concrete Members Prestressed with Unbonded Tendons," ACI Structural Journal, November-December 1991.

Harajli, M.H., and Wehbe, I.A., "Analysis of Flexural Concrete Members Strengthened using External Prestressing," American Society of Civil Engineering, ASCE-SAS, Proceedings of the First Regional Conference and Exhibition-Advanced Technology in Civil Engineering, Manama, Bahrain, pp. 219-232, September 18-20, 1994.

Hognestad, E., "A Study of Combined and Axial Load in Reinforced Concrete Members," University of Illinois Engineering Experiment Station, Bulletin Series No. 399, Bulletin

No. 1, November 1951.

Kang, Y.J., "Nonlinear Geometric, Material and Time Dependent Analysis of Reinforced and Prestressed Concrete Frames," UC-SESN Report No. 77-1, Division of Structural Engineering and Structural Mechanics, University of California, Berkley, California, January 1977.

Kang, Y.J., and Scordelis, A.C., "Nonlinear Analysis of Prestressed Concrete Frames," Journal of the Structural Division, ASCE, Vol. 106, No. ST2, Pro. Paper 15191, February, 1980, pp. 445-462.

Kashima, S. and Breen, J.E., "Construction and Load Tests of Segmental Precast Box Girder Bridge Model," Center of Highway Research, University of Texas at Austin, Austin, Texas, pp. 261, 1975.

Ketchum, M.A., "Redistribution of Stresses in Segmentally Erected Prestressed Concrete Bridges," UC-SESM Report No. 86-07, Division of Structural Engineering and Structural Mechanics, University of California, Berkeley, California, May 1986.

Khalil, M.S., "Time Dependent Non-Linear Analysis of Prestressed Concrete Cable-Stayed Girders and Other Concrete Structures," Ph.D. Dissertation, Department of Civil Engineering, University of Calgary, Calgary, Alberta, April 1979.

Kim, J.K., "Prediction of Time-Dependent Deformations of Concrete and Bridge Deflection Probability," Ph.D. Dissertation, Department of Civil Engineering, Northwestern University, Evanston, Illinois, December 1990.

Kline, T.R., "Strengthening a Prestressed Double Tee Beam," Concrete Repair Digest Journal, Aberdeen Group, December 1995 - January 1996.

Lin, C.S., "Nonlinear Analysis of Reinforced Concrete Slabs and Shells," Ph.D. Dissertation, Division of Structural Engineering and Structural Mechanics, University of California, Berkley, California, UC-SESM Report No. 73-7, April 1973.

Lin, C.S., "Nonlinear Analysis of Reinforced Concrete Shells of General Form," Journal of the Structural Division, ASCE, Vol. 101. No. ST3, March, 1975.

Loov, R., "Flexural Strength of Prestressed Beams with Unbonded Tendons," Lecture presented to the North East Forestry University, Harbin, China, June 1987.

MacGregor, R.G, Kreger, M.E., and Breen, J.E., "Strength and Ductility of a Three-Span Externally Post-Tensioned Segmental Box Girder Model," A Preliminary Review Copy Submitted to Texas State Department of Highways and Public Transportation, Report No. 365-3F, 279 pp., January 1989.

Mattock, Alan H., Yamazaki, Jun, and Kattula, Basil T., "Comparative Study of Prestressed Concrete Beams, With and Without Bond," ACI Journal, Proceedings V. 68. No. 2, February 1971, pp. 116-125.

Mengotto, M. and Pinto, P. E., "Method of Analysis for Cyclically Loaded R.C. Plane Frames, Including Changes in Geometry and Non-Elastic Behaviour of Elements Under Combined Normal Force and Bending," IABSE Preliminary Report for Symposium on Resistance and Ultimate Deformability of Structures Acted on by Well-Defined Repeated Loads, Lisbon, 1973, pp. 15-22.

Mitchell, D. and Collins, M.P., "Diagonal Compression Field Theory - A Rational Model for Structural Concrete in Pure Torsion," *ACI Journal*, Vol. 71, pp. 396-408, Aug. 1974.

Morsch, E., "Concrete-Steel Construction," McGraw Hill, New York, 1909, pp. 368, (English translation by E.P. Goodrich of third edition of *Der Eisenbetonbau*, first edition

1902).

Muller, J., and Gauthier, Y., "Ultimate Behaviour of Precast Segmental Box-girders with External Tendons," *External Prestressing in Bridges; ACI SP 120-17, Proc., Int. Symp.*, A. E. Naaman and J. E. Breen, eds., American Concrete Institute (ACI), Detroit, Michigan, 355-373.

Naaman, A. E., "Partially Prestressed Concrete: Review and Recommendations," *PCI Journal*, V. 30, No. 6, November-December 1985. pp. 31-71.

Naaman, A. E., "New Methodology for the Analysis of Beams Prestressed with External or Unbonded Tendons," *External Prestressing in Bridges, SP-120*, American Concrete Institute, Detroit, 1990, pp. 339-354.

Naaman, A.E., "External Prestressing for Rehabilitation-Analysis and Design Implications," *Proceeding of the 3rd International Workshop on Bridge Rehabilitation, Bridge Rehabilitation*. Andrzej S. Nowak and Balthasar Novak (Editors), organized by The technical University Darmstadt and The University of Michigan, June 1992.

Naaman, A. E. and F. M. Alkhairi, "Stress at Ultimate in Unbonded Post-Tensioning Tendons - Part I: Evaluation of the State-of-the-Art, Part 2: Proposed Methodology," *ACI Structural Journal*, Vol. 88, No. 6, September-October 1991, pp. 641-651.

Naaman, A. E. and F. M. Alkhairi, "Stress at Ultimate in Unbonded Post-Tensioning Tendons - Part II: Proposed Methodology," *ACI Structural Journal*, Vol. 88, No. 6, pp. 683-692, November-December 1991.

Naaman, A.E., and Breen, J.E., (Editors), *External Prestressing in Bridges*, ACI Publication SP-120, Proceedings of an International Symposium, American Concrete Institute, Detroit, Michigan, USA, 1990.

Neville, A.M., "Properties of Concrete," Pittman Publishing, Second Edition, 1973.

Neville, A.M., Dilger, W.H., and Brooks, J.J, Creep of Plain and Structural Concrete, Construction Press, London and New York, 361 pp., 1983.

Ngo, D., and Scordelis, A.C., "Finite Element Analysis of Reinforced Concrete Beams," ACI Journal, Vol. 64, No. 3, March 1967.

Ngo, D., Scordelis, A.C., and Franklin, H.A., "Finite Element Study of Reinforced Concrete Beams with Diagonal Tension Cracks," UC-SESM Report No. 70-19, Division of Structural Engineering and Structural Mechanics, University of California, Berkeley, December 1970.

Nilson, A.H., "Finite Element Analysis of Reinforced Concrete," Ph.D. Dissertation, Division of Structural Engineering and Structural Mechanics, University of California, Berkeley, March 1967.

Nilson, A.H., "Nonlinear Analysis of Reinforced Concrete by Finite Element Method," ACI Journal, Vol. 65, No. 9, September 1968.

Park, R. and Paulay, T., "Reinforced Concrete Structures," A Wiley-interscience publication, New York, 1975.

Priestely, M.J.N, Park, R., and Lu, F., "Moment Curvature Relationship for Prestressed Concrete in Constant Zones," Magazine of Concrete Research, Vol. 23, No. 75-76, pp.69-78, June-September 1971.

Proceedings of the First International Conference: "Deterioration and repair of Reinforced Concrete in the Arabian Gulf, The Bahrain Society of Engineers, Vol. 1, 529 pp., Vol. 2, 250 pp., Bahrain, October 26-29, 1985.

Proceedings of the Third International Conference: "Deterioration and repair of Reinforced Concrete in the Arabian Gulf, The Bahrain Society of Engineers, Vol. 1, 733 pp., Vol. 2, 339 pp., Bahrain, October 22-24, 1989.

Rashid, Y.R., "Ultimate Strength Analysis of Prestressed Concrete Pressure Vessels," Nuclear Engineering Design, Vol. 7. 1968

Rashid, Y.R., and Reckenhauer, W. "Pressure Vessel Analysis by Finite Element Techniques," Conference on Prestressed Concrete Vessels, Institute of Civil Engineer, London, 1968.

Rashid, Y.R., "Nonlinear Analysis of Two-Dimensional Problems in Concrete Creep," Journal of Applied Mechanics, Transactions of ASME, Paper No. 71-APNW-25, 1971.

Ritter, W., "Die Bauweise Hennebique," (Construction Techniques of Hennebique), *Schweizerische Bauzeitung*, Zurich, Feb. 1899.

Rusch, H., Jungwirth, D., and Hilsdorf, H., "Kritische Sichtung der Einflüsse von Kriechen und Schwinden des betons auf das Verhalten der Tragwerke," Beton and Stahlbetonbau, Vol. 68, Nos. 3, 4, and 5, 1973.

Same, Y., "Material Nonlinear Time-Dependent Three-Dimensional Finite Element Analysis for Reinforced and Prestressed Concrete Structures, Ph.D. Dissertation, Department of Civil Engineering, Massachusetts Institute of Technology, Cambridge, 1975.

Sandhu, R.S., Wilson, E.L., and Raphael, J.M., "Two-Dimensional Stress Analysis with Incremental Construction and Creep," UC-SESM Report No. 67-34, Division of Structural Engineering and Structural Mechanics, University of California, Berkeley, December 1967.

Scanlon, A., "Time Dependent Deflections of Reinforced Concrete Slabs," Ph.D. Dissertation, Department of Civil Engineering, University of Alberta, Edmonton, Canada, December 1971.

Scanlon, A., and Murray, D.W., "Time Dependent Reinforced Concrete Slab Deflections," Journal of the Structural Division, ASCE, Vol. 100, No. ST9, September 1974.

Schnobrich, W.C., "Finite Element Determination of Nonlinear Behaviour of Reinforced Concrete Plates and Shells," Proceedings of the Symposium on Nonlinear Techniques and Behaviour in Structural Analysis, Transport and Road Research Laboratory, Department of Environment, England, 1974.

Schnobrich, W.C., "Behaviour of Reinforced Concrete Predicted by Finite Element Method," Proceedings of the Second National Symposium on Computerized Structural Analysis and design, George Washington University, Washington D.C., March 1976.

Scordelis, A.C., "Finite Element Analysis of Reinforced Concrete Structures," Proceedings of the specialty Conference on Finite Element Methods in Civil Engineering, Montreal, June 1972.

Scordelis, A. C., "Computer Models for Nonlinear Analysis of Reinforced and Prestressed Concrete Structures," PCI Journal, November-December 1984.

Seible, F., Priestley, M., and Kirshnan, K., "Strengthening Techniques of Reinforced Concrete Bridges Superstructures," Research Report No. SSRP-90/06, Department of Applied Mechanics and Engineering Sciences, University of California, San Diego, USA, pp. 165, December 1990.

Selna, L.G., "Time-Dependent Behaviour of Reinforced Concrete Structures," UC-SESM Report No. 67-19, Division of Structural Engineering and Structural Mechanics,

University of California, Berkeley, 1967.

Selna, L.G., "Creep, Cracking and Shrinkage in Concrete Frame Structures," *Journal of the Structural Division, ASCE*, Vol. 95, No. ST12, December 1969.

Suidan, M.T., and Schnobrich, W.C., "Finite Element Analysis of Reinforced Concrete," *Journal of the Structural Division, ASCE*, Vol. 99, No. ST10, October 1973.

Tan, K. H. and Naaman, A. E., "Strut-and-Tie Model for Externally Prestressed Concrete Beams," *ACI Structural Journal*, November-December 1993.

Tao, X. and Du, G., "Ultimate Stress of Unbonded Tendons in Partially Prestressed Concrete Beams," *PCI Journal*, V. 30, No. 6, pp. 72-91, November-December 1985.

Troxell, G.E, Raphael, J.M., and Davis, R.E., "Long-Time Creep and Shrinkage Tests of Plain and Reinforced Concrete," *Proceeding ASTM*, Vol. 58, pp. 1101-1120, 1958.

Van Zyle, S.F., "Analysis of curved Segmentally Erected Prestressed Concrete Box Girder Bridges," Ph.D. Thesis, SESM Report No. 78-2, University of California at Berkeley, Berkeley, California, 1978.

Vecchio, F.J. and Collins, M.P., "The Modified Compression Field Theory for Reinforced Concrete Elements Subjected to Shear," *Journal of the American Concrete Institute*, Vol. 83, No. 2, pp. 219-231, March-April 1986.

Wahl, H.W., and Kasiba, R.J., "Design and Construction Aspects of Large Prestressed Concrete (PWR) Containment Vessel," *ACI Journal*, Vol 77, No. 5, May 1969.

Wegner, R. "Finite Element Models of Reinforced Concrete," Preprint, Proceedings of the U.S. - Germany Symposium on Formulation and Computational Methods in Finite

Element Analysis, Massachusetts Institute of Technology, Cambridge, August 1976.

Ziadat, G., "Time-Dependent Analysis of Prestressed Concrete Segmental Bridges," Ph.D. Dissertation, University of Bristol, Bristol, U.K., November 1988.

Zienkiewicz, O.C., Owen, D.R.J., Phillips, D.V., and Nayak, G.C., "Finite Element Methods in the Analysis of Reactor Vessels," Paper M5/1, 1st International Conference on Structural Mechanics in Reactor Technology, Berlin, West Germany, September, 1977.

Xanthakos, P.P., (Editor), *Bridge Strengthening and Rehabilitation*, Printice Hall PTR, 1996.